

Towards the Development of a
Multicomponent, Nanoscale Oral Vaccine
Delivery System Targeting Infectious
Bursal Disease (IBD)

By

Marie W. Pettit [B.Sc. (Hons)]

A thesis submitted in partial fulfilment of the requirements of the University of
Greenwich for the Degree of Doctor of Philosophy

July 2013

Faculty of Engineering and Science
University of Greenwich, Medway Campus
Central Avenue, Chatham Maritime
Kent
ME4 4TB



DECLARATION

“I certify that this work has not been accepted in substance for any degree, and is not concurrently being submitted for any degree other than that of Doctor of Philosophy being studied at the University of Greenwich. I also declare that this work is the result of my own investigations except where otherwise identified by references and that I have not plagiarised the work of others”.

Marie Pettit (Candidate)

.....

PhD Supervisors

Dr Simon Richardson (1st Supervisor)

Prof. John Mitchell (2nd Supervisor)

July, 2013

ACKNOWLEDGEMENTS

Firstly, I would like to thank my supervisor Dr Simon Richardson, for his help and support throughout the duration of my studies. He has always remained patient and offered assistance whenever required. Additional thanks goes to Mr Paul Dyer, for his help and guidance throughout my studies.

I would like to thank the School of Science for funding my PhD, without which I would not be able to be researching such an interesting area. Further, I would like to thank other academics who have assisted in my studies, Professor John Mitchell my second supervisor but who has provided a vast amount of support, Professor Frank Pullen, assisting with mass spectroscopy, Dr Bruce Alexandra for assistance with circular dichroism, Professor Peter Griffiths for his help undertaking and analysing Small Angle Neutron Scattering data produced at ILL (Grenoble, France) and Professor Babur Chowdhry for assistance with HSDSC data collection and analysis.

Finally, I would like to thank Christine Pettit (my mother) and Robert Pettit (my father) for their support as always, both financial and regarding childcare, without which I would not be able to continue my studies. Additionally I would like to thank David Marton, my partner for his patience whilst I complete my research and also his contribution towards family life.

ABSTRACT

As the global population increases, estimated to reach 9 billion by the year 2050, global food security becomes a priority. A prominent disease implicated in financial loss to the poultry industry, on a global scale, is infectious bursal disease virus (IBDV). Vaccination against IBDV is sub-optimal and difficult to deliver. Therefore it has been highlighted as a key area for the development of an oral vaccine. A highly conserved capsid protein from IBDV (VP2) was identified, and sub-cloned into a bacterial expression cassette. This protein was fused to a potential carrier protein (cholera toxin B chain), previously shown to mediate the exit from the gut lumen into the *lamina propria*. However, to allow this antigen to reach the mucosal associated lymphoid tissue, the protein antigen must remain in its native conformation through the stomach. This work developed a delivery system to meet this end. By encapsulation within a fatty acid coated, protein adsorbed-solid core drug delivery system (SCDDS), it was shown that a model protein antigen (GST-GFP) could be protected from low pH (*i.e.* pH 2.0) and proteases. Protease protection was demonstrated against the exposure of myristic acid coated, GST-GFP adsorbed silica, to both protease K (100 μ U, 1hour (100% protection)) as well as a simulated *in vitro* stomach environment (pepsin (0.2 mg) (100% protection)). Having demonstrated protection from proteases at pH 2.0 and pH7.4, it was then shown that GST-GFP could be released from the myristic acid coated silica at pH 8.8 (consistent with the small intestine). As much as ~15% (15 μ g) (w/w) GST-GFP was released from the aforementioned system. The evidence supporting this conclusion was drawn from molar ellipticity calculations that showed the proportion of helical structure in relation to regions of beta sheet remained constant, pre-adsorption and post-release (16.9% α -helix, 20.8% β -sheet, 43.3% random coil). Finally, this work has shown that if a recombinant antigen was fused to cholera toxin B chain (but not shiga toxin B chain), it was capable of mediating transcytotic passage across, differentiated, polarised Caco-2 cells (1/1000th input (10 ng)).

In conclusion and based upon the evidence provided above, this system warrants further optimisation and investigation to serve as an oral vaccine delivery system to treat IBDV.

CONTENTS PAGE

Contents	Page Number
Declaration	ii
Acknowledgements	iii
Abstract	iv
Contents	v
List of Tables	xii
List of Figures	xiii
Abbreviations	xviii
Research Outputs	xx
Chapter 1: Introduction	1
1.1 The Problem: Global Food Security	1
1.2 The Need for Oral Veterinary Vaccines	3
1.3 Infectious Bursal Disease	4
1.3.1 Pathogenesis of Infectious Bursal Disease	5
1.3.2 Viral Structure and Viral Proteins	7
1.3.3 Serotypes of Infectious Bursal Disease	10
1.3.4 Immune Development in the Chick	11
1.4 Chicken Gastrointestinal Anatomy	13
1.4.1 Proximal Gastrointestinal Anatomy	13
1.4.2 Intestinal Epithelium	14
1.4.3 The Distal GI and the Avian Bursa of Fabricius	14
1.4.4 Current Vaccination for Infectious Bursal Disease Virus	15
1.5 Vaccination Models	16
1.5.1 Attenuated Viral Vaccines	16
1.5.2 DNA Vaccination	16
1.5.2.1 DNA Vaccination via Recombinant Bacterial Vectors	17
1.5.4 <i>In Ovo</i> DNA Vaccination	19
1.6 Oral Vaccination Delivery for IBDV	20
1.6.1 Polymeric Nanoparticles	21

1.6.2	Lipid Based Oral Vaccine Delivery	23
1.6.2.1	Bilosomes	23
1.6.2.2	Archaeosomes	24
1.6.2.3	Virosomes	24
1.7	Adjuvants and Immunomodulators	25
1.8	The Biology of Toxin Adjuvants	27
1.8.1	Shiga Toxin	27
1.8.2	Cholera Toxin	29
1.8.2.1	Cholera Toxin Transcytosis	33
1.8.3	The Proposed Enteric Protein Delivery System	36
1.9	Aims of This Thesis	38
Chapter 2:	Materials and Methods	39
2.1	Materials	39
2.1.1	Equipment	39
2.1.2	Reagents	39
2.1.2.1	Specialised Reagents	40
2.1.2.2	Antibodies	41
2.1.3	Organisms and Cell Lines	42
2.1.4	Stock Solutions	42
2.2	Methods	44
2.2.1	Cell Culture and Viability Techniques	44
2.2.2	Cell Bank	45
2.2.3	Evaluation of Cell Viability by Trypan Blue Exclusion	45
2.2.4	MTT Assay to Asses Cell Viability	46
2.2.5	Preparation, Maintenance and Thawing of Frozen “Stock” Cultures	46
2.2.6	Growth of Transformed <i>E.coli</i>	47
2.2.6.1	Growth of <i>E.coli</i> Using Heat Shock Protocol	47
2.2.6.2	Mini-Scale Protein Production From <i>E.coli</i>	47
2.2.7	Isolation of Plasmid DNA from <i>E.coli</i> Cultures	48
2.2.8	Polymerase Chain Reaction (PCR)	48
2.2.8.1	Gel Electrophoresis	48

2.2.8.2 Recombinant PCR	49
2.2.8.3 Sub-cloning into pET151 Expression Cassette	49
2.2.8.4 Evaluation of <i>E.coli</i> Clones for Plasmid Insertion	50
2.2.9 DNA Sequencing	50
2.2.9.1 Analysis of Sequence Data	50
2.3 Production of GST and GST-GFP Proteins	50
2.3.1 Lysis of Bacteria	51
2.3.2 Sedimentation of Lysed Bacteria to Remove Membrane and Chromatin	51
2.3.3 Purification of Recombinant GST Containing Proteins	51
2.3.3.1 Protein Dialysis	52
2.4 Protein Characterisation by SDS-PAGE	52
2.4.1 Coomassie Staining	52
2.4.2 Western Immunoblot	53
2.4.2.1 Developing the Western Immunoblot	53
2.4.2.2 Densitometry to Quantify Protein Concentration	54
2.4.3 Characterisation of GST-GFP by Mass Spectroscopy	54
2.4.4 Evaluation of GST-GFP Stability by Affinity Isolation	54
2.5 Trichloroacetic Acid (TCA) Precipitation	54
2.6 Transcytosis of Recombinant Proteins	55
2.6.1 Analysis of Protein Trafficking in Mammalian Cells Using Immunofluorescence Microscopy	55
2.6.2 Mounting of Coverslips	56
2.7 Protein Absorption onto Silica Beads	56
2.7.1 Fatty Acid Coating of Protein Adsorbed Silica Beads	56
2.7.2 Freeze Drying of Fatty Acid Coated, Protein Adsorbed Silica Beads	57
2.7.3 Release of GST-GFP from Fatty Acid Coated Silica Beads	57
2.8 <i>In Vitro</i> Digestion Assay	58
2.9 Circular Dichroism of Released Protein from Drug Delivery System	58

Chapter 3: Characterisation of GST-GFP	59
3.1 Characterisation of GST-GFP	59
3.1.1 Glutathione <i>S</i> -transferase (GST)	59
3.1.2 Green Fluorescent Protein (GFP)	60
3.2 Materials and Methods	61
3.2.1 Materials	61
3.2.2 Methods	61
3.2.2.1 Analysis of Clonal Colony Growth	61
3.2.2.2 Optimisation of Bacterial Growth to Increase Protein Yield	61
3.2.2.3 Calibration Curve of GST-GFP to Accurately Quantify Protein Concentration	62
3.2.2.4 Absorption Spectra of GST-GFP	62
3.2.2.5 Emission Spectra of GST-GFP	62
3.2.2.6 Analysis of Secondary Structure by Circular Dichroism	62
3.2.2.7 Protein Stability Analysis via GST Purification	62
3.3 Results	63
3.3.1 Production of GST-GFP	63
3.3.2 Optimisation of <i>E.coli</i> Growth Conditions	72
3.3.3 GST-GFP Characterisation	75
3.3.3.1 Mass Spectroscopy	75
3.3.3.2 Characterisation of GST-GFP by Spectroscopy	78
3.3.3.3 Characterisation of GST-GFP by Circular Dichroism Spectroscopy	79
3.3.4 GST-GFP Stability in Relation to Specific Proteases	83
3.3.5 <i>In Vitro</i> Toxicity of GST-GFP Measured Using a Cell Culture Model	88
3.4 Discussion	92
3.4.1 Production of Model Protein (GST-GFP)	92
3.4.2 Characterisation of GST-GFP	97
3.4.3 GST-GFP Stability and Toxicity	99

3.5	Conclusions	101
Chapter 4:	Characterisation of Solid Core Drug Delivery System (SCDDS)	103
4.1	Introduction	103
4.1.1	Aims of this chapter	105
4.2	Materials and Methods	106
4.2.1	Materials	106
4.2.2	Methods	106
4.2.2.1	Analysis of Silica Beads Using SEM	106
4.2.2.2	GST-GFP Immobilisation on Silica Beads	106
4.2.2.3	Characterisation of Protein Immobilised Silica Beads	106
4.2.2.3.1	Quantification of Protein Mass Using the BCA Assay	107
4.2.2.3.2	Quantification of Protein Mass Using Densitometry	107
4.2.2.3.3	Production of Deuterated GST-GFP	107
4.2.2.4	Characterisation of Silica Beads and Protein Immobilised Silica Beads by SANS	107
4.2.2.5	Fatty Acid Coating of GST-GFP Immobilised Silica Beads	108
4.2.3	Assessing the Degree of Protein Protection Afforded by Fatty Acid Coating Using the <i>In Vitro</i> Digestion Assay	108
4.2.4	GST-GFP Release From Fatty Acid Coated Silica Beads	108
4.2.5	Analysis of Released GST-GFP Secondary Structure by Circular Dichroism	109
4.3	Results	110
4.4	Discussion	121
4.5	Conclusions	126

Chapter 5: Cloning and Expression of Recombinant Proteins to Facilitate Transcytosis Across Polarised Caco-2 Monolayers 127

5.1	Introduction	127
5.1.1	Toxins and Membrane Trafficking	127
5.1.2	Understanding the Mechanisms of Transcytosis	131
5.1.3	Characterisation of Tight Junctions	133
5.1.4	Intracellular Markers for Endocytosis and Transcytosis	134
5.1.5	Analysing Cellular Toxicity	136
5.1.6	<i>In Vitro</i> Cell Models	137
5.2	Materials and Methods	138
5.2.1	Primer Design for Recombinant PCR	138
5.2.2	Polymerase Chain Reaction (PCR) for Amplifying Regions of Gene Interest	139
5.2.3	Gel Electrophoresis to Analyse Amplified Gene Products	139
5.2.4	Sub-Cloning in pET151 Plasmid Vector	139
5.2.5	Sequencing of Sub-Cloned Constructs	140
5.2.6	Sequencing Analysis Using DNASTar	140
5.2.7	Plasmid Transformation into <i>E.coli</i> for Protein Expression	140
5.2.8	Protein Production	141
5.2.9	Caco-2 Growth Curves by MTT Assay	142
5.2.9.1	Caco-2 Cell Viability by Trypan Blue Assay	142
5.2.9.2	Characterisation of TER	142
5.2.9.3	Characterisation of Caco-2 Cell Differentiation by Analysing Increase in Villin Production	142
5.2.9.4	Analysis of Tight Junction Integrity by Inulin Diffusion	143
5.2.9.5	Analysis of Recombinant Protein Trafficking by Immunofluorescent Microscopy	143
5.2.9.6	Mounting Coverslips onto Microscope Slides for Cell Imaging	144
5.2.9.7	Investigation of Recombinant Protein Trafficking in Vero Cells	144
5.2.9.8	Analysis of Recombinant Protein Ability to	144

	Translocate Across Monolayers of Caco-2 Cells	
5.3	Results	145
	5.3.1 Analysis of Shiga Toxin Clones From the Database	145
	5.3.2 Cholera Toxin	148
	5.3.3 VP2 Antigen	150
	5.3.4 Recombinant Protein Expression and Characterisation	162
	5.3.5 Characterisation of Caco-2 Cells	164
	5.3.6 Characterisation of Cellular Trafficking in Vero Cells	170
	5.3.7 Analysis of Recombinant Proteins Ability to Traffic Across Monolayers of Polarised Caco-2 Cells	176
5.4	Discussion	179
	Chapter 6: General Discussion	187
	Chapter 7: References	191

LIST OF TABLES

Table Number	Table Title	Page Number
1	Sample of List A and List B animal diseases from OIE	3
2	Mucosal versus parental vaccination pros and cons	21
3	Review of current strategies for mucosal vaccination	22
4	Selected liposomal formulations for vaccine delivery that are either licensed or in clinical trails	24
5	List of antibodies and suppliers	41
6	Thermal cycles for freeze drying of fatty acid coated protein adsorbed silica	57
7	List of primers used for PCR and sequencing	65
8	Truncations of GST-GFP omitting amino acids to achieve the observed mass from MALDI-TOF MS	77
9	Apparent versus observed molecular weight of GST-GFP	93
10	Fatty acids tested and their corresponding properties	105
11	Analysis of SCDDS size and charge	112
12	Genes required for cloning and their specific uses	129
13	Examples of molecules capable of transcytosis	132
14	Recombinant proteins, their purpose and protein expression	161
15	Analysis of transcytosis by the recombinant proteins	178

LIST OF FIGURES

Figure Number	Title	Page Number
1	IBDV icosahedral structure, taken from PDB – 2GSY	9
2	Structure of VP2, PBD – 2DF7	10
3	Proposed vaccination strategies for viral diseases	18
4	Shiga toxin, PDB – 1DM0	32
5	Toxin factors involved in endocytosis and transcytosis in polarised epithelial cells	35
6	Proposed action of SCDDS	37
7	Plasmid map of GST-GFP encoded in pGEX 3X vector	64
8	Contiguous, strategic view of sequenced data showing depth of coverage over GST-GFP ORF	66
9	<ul style="list-style-type: none"> a) Coomassie stained SDS-PAGE gel showing protein production of heat shocked and normal <i>E.coli</i> MC1061 cultures b) Westernblot followed by immunodetection of HS / N GST-GFP recognized by α-GFP c) Theoretical representation of GST-GFP produced <i>in silico</i> by I-TASSER 	67
10	Comparison between GST-GFP plasmids and protein production	68
11	Agarose gel of clonal PCR products of GST-GFP plasmids	69
12	Coomassie stained SDS-PAGE gel using 6M guanidine Lamealle buffer versus normal Lamealle to reduce residual secondary conformation	70
13	Westernblot followed by immunodetection of small scale protein production of clonal colonies	71
14	GST-GFP production from the 210 plasmid. Coomassie stain and westernblot followed by immunodetection using α -GST and α -GFP antibodies	71
15	Optimization of bacterial growth time pre IPTG induction in <i>E.coli</i> TOP10 bacteria	72
16	Analysis between <i>E.coli</i> TOP10 and MC1061 pre IPTG induction	73
17	Analysis of bacterial growth post IPTG induction for	73

	protein expression	
18	Calibration curve of GST-GFP at known concentrations	74
19	Deconvolved MALDI-TOF MS of GST-GFP	76
20	Analysis of GST-GFP protein sequence by trypsin digest	77
21	Plasmid map of 210 with MALDI-TOF post translational modifications	78
22	Excitation and emission spectra comparison between eGFP and GST-GFP	79
23	CD spectra of GST-GFP in sodium acetate buffer at a range of pH values	80
24	CD spectra of GST-GFP in phosphate buffer at a range of pH values	80
25	CD spectra of GST in phosphate buffer at a range of pH values	81
26	CD spectra of GST in sodium acetate buffer at a range of pH values	81
27	Cd spectra of GST and GST-GFP in phosphate buffer at pH7.7	82
28	CD spectra of native versus denatured GST	82
29	CD spectra of native versus denatured GST-GFP	83
30	Analysis of GST-GFP by western blot followed by immunodetection	84
31	Emission profile of GST-GFP post addition of protease K (10U)	85
32	Decrease in absorbance of GST-GFP following GST isolation on beads	87
33	Percentage degradation of GST-GFP following addition of varying units of protease K	87
34	Stability of GST-GFP over one hour at various concentrations of protease K	88
35	Toxicity of GST-GFP in Vero cells	89
36	Toxicity of GST-GFP in B16 cells	90
37	Toxicity of GST-GFP in Caco-2 cells	91
38	Far UV circular dichroism spectra associated with various types of protein secondary structure	100
39	FEG-SEM image of silica beads	111

40	Protein absorption to silica beads measured by BCA assay	111
41	Cartoon depicting the series of contrast matching techniques used to visualize the protein corona	113
42	SANS data obtained by series of contrast matching techniques	114
43	Fatty acid coating and protein protection from protease K	115
44	Dilutions of fatty acid to analyse coverage required for GST-GFP protection from proteases	117
45	Protection of GST-GFP following myristic acid coating, against protease K and <i>in vitro</i> digestion assay	117
46	GST-GFP release from fatty acid coated silica beads in a pH responsive manner	118
47	Protein release from silica beads	118
48	Circular dichroism of released GST-GFP from silica beads, before and after fatty acid coating	119
49	Protein release as a function of ionic strength	120
50	Protein release form silica beads as a function of volume	120
51	Schematic of SCDDS showing silica core, adsorbed model protein and fatty acid corona	123
52	The Hofmeister series: the effect of salts	125
53	Cholera and Shiga toxin structure	128
54	Cartoon depicting the process of recombinant PCR, using CTBC-GFP as an example	130
55	Regulation of paracellular transport	134
56	SNARE assembly and disassembly	136
57	Schematic representation of Caco-2 cells grown on a transwell filter	138
58	Sequenced plasmid map of STBC (230) in pGEM vector	146
59	Sequenced plasmid map of STBC (231) in pGEM vector	146
60	Sequenced plasmid map of STBC (232) in pET11a vector	147
61	Sequenced plasmid map of STBC fused in frame with GFP	148
62	Sequenced plasmid map of CTBC in pET151 vector	150
63	Analysis of bacterial colonies following TOPO cloning	151
64	Agarose gel of TOPO cloned colonies	152
65	Sequenced plasmid map of CTBC fused in frame to GFP	153

66	Plasmid map of the whole VP2 gene	154
67	Phylogenic tree of various VP2 sequences	154
68	Alignment of VP2 sequences to locate areas of conservation	155
69	Plasmid map of VP2 (<i>Acce I-Spe I</i>)	155
70	Successful VP2 insert into pET151 plasmid	157
71	Sequenced plasmid map of VP2 (<i>Smo I-Xho I</i>)	157
72	VP2 antigen fused in frame to CTBC	158
73	VP2 antigen (<i>Acce I-Spe I</i>) fused in frame to CTBC	159
74	VP2 (<i>Acce I-Spe I</i>) antigen fused to GFP	160
75	Successful cloning of VP2-GFP	160
76	Mature GFP cloned and sequenced in pET151 plasmid	161
77	Toxicity of recombinant proteins in Vero cells	163
78	Toxicity of recombinant proteins in Caco-2 cells	163
79	Growth curve of Caco-2 cells using MTT assay	165
80	Caco-2 cell viability using the trypan blue assay	165
81	Increase in villin production over 21 days with a loading control, α -actin	167
82	TER increase over time (30 days) in Caco-2 cells	168
83	Confluent, non-differentiated Caco-2 cells imaged for tight junction integrity by immune fluorescence	169
84	Confluent, differentiated Caco-2 cells imaged for tight junction integrity by immune fluorescence	170
85	Characterisation of tight junction effects in the presence of VP2	171
86	Characterisation of tight junction effects in the presence of STBC	172
87	Characterisation of tight junction effects in the presence of CTBC	173
88	Immunofluorescent microscopy of Vero cells pulsed with CTBC for one-hour followed by a three-hour chase	175
89	Immunofluorescent microscopy of Vero cells pulsed with CTBC-VP2 for one-hour followed by a three-hour chase	175
90	Immunofluorescent microscopy of Vero cells pulsed with VP2 for one-hour followed by a three-hour chase	176
91	Immunofluorescent microscopy of Vero cells pulsed with	177

	STBC for one-hour followed by a three-hour chase	
92	TER measurements over 240 minutes during transcytosis investigations	178
93	Inulin measurements over 240 minutes during transcytosis investigation	179

ABBREVIATIONS

Abbreviation	Meaning
AC	Adenylate Cyclase
BF	Bursa of Fabricius
BFA	Brefeldin A
BSE	Bovine Spongiform Encephalopathy
cAMP	Cyclic Adenosine Monophosphate
CEF	Chicken Embryonic Fibroblasts
CFTR	Cystic Fibrosis Transmembrane Conductance Regulator
CFU	Colony Forming Units
COPI	Cytoplasmic Coat Protein
CT	Cholera Toxin
CTAC	Cholera Toxin A Chain
CTBC	Cholera Toxin B Chain
DI	Days of Incubation
DMRS	Detergent Resistant Membrane Fractions
dsRNA	Double Stranded RNA
EEA1	Early Endosomal Antigen 1
EF	Oedema Factor
EID ₅₀	Egg Infective Dose
ER	Endoplasmic Reticulum
ERAD	ER Associated Degradation
Fc	Fraction Crystallizable
GALT	Gut Associated Lymphoid Tissue
Gb3	Globotriaosylceramide
GFP	Green Florescent Protein
GM1	Monosialoganglioside
GM130	<i>cis</i> -Golgi matrix protein of 130 KDa
GSH	Glutathione
GST	Glutathione-S-Transferase
HPAI	Highly Pathogenic Avian Influenza Encephalopathy
HUS	Haemolytic Uremic Syndrome
IBDV	Infectious Bursal Disease Virus

IFN	Interferon
IL	Interleukin
IM	Irwin Moulthrop
IMPACT	International Model for Policy for Analysis of Agricultural Commodities and Trade
iNOS	Inducible Nitric Oxide Synthase
ISCOMs	Immune Stimulating Complexes
LF	Lethal Factor
LPS	Lipopolysaccharide
MA	Myristic Acid
MHC	Major Histocompatibility Complex
Mw	Molecular Weight
NISV	Non-Ionic Surfactant Vesicles
OIE	The Office International des Epizooties
O-MALT	Organised Mucosa Associated Lymphoid Tissue
ORF	Open Reading Frame
PA	Protective Antigen
PEG	Poly(ethylene glycol)
PEI	Poly(ethyleneimine)
pIgA	Polymeric IgA
PT	Pertussis Toxin
SANS	Small-Angle Neutron Scattering
SCDDS	Solid Core Drug Delivery System
sIgA	Secretory IgA
SPF	Specific Pathogen Free
STBC	Shiga Toxin B Chain
STx	Shiga Toxin
TCP	Toxin Co-regulated Pilus
TGN46	Trans Golgi Network of 46 KDa
V5	C-terminal sequence of the P and V proteins of Simian Virus 5
vvIBDV	Very Virulent IBDV

SCIENTIFIC OUTPUTS

Authors: Marie W Pettit, Peter Griffiths, Paolo Ferruti, and Simon CW Richardson.

Title: ‘Poly(amidoamine) polymers: soluble linear amphiphilic drug-delivery systems for genes, proteins and oligonucleotides’

Journal: Therapeutic Delivery (2011) **2** (7): 907–917

Authors: Paul D. R. Dyer, Arun K. Kotha, Marie W. Pettit and Simon C. W. Richardson

Title: ‘Imaging Select Mammalian Organelles Using Fluorescent Microscopy: Application to Drug Delivery.’

Book: Cellular and Subcellular Nanotechnology (2013)

Authors: Marie W Pettit, Susan Shorter, Paul Dyer, Simon C. W. Richardson

Poster title: ‘Characterisation of a novel oral vaccine delivery system’

Conference: UK Neutron and Muon Users Meeting (NMUM) 8-9 April 2013 | Warwick, UK

Authors: Marie W Pettit., Simon C. W. Richardson

Workshop: Viral expression vectors for basic and applied studies 24 April to 5 May 2011 | Tartu, Estonia

Authors: Marie W Pettit, Susan Shorter, Paul Dyer, Simon C. W. Richardson

Poster title: ‘Characterisation of a novel oral vaccine delivery system’

Conference: Small angle neutron and X-ray scattering from proteins in solution
6 – 10 May 2013 | Grenoble, France

Authors: Marie W Pettit, Paul Dyer, Simon C. W. Richardson

Poster title: ‘Characterisation of an oral antigen delievry system’

Conference: 9th International Symposium on Polymer Therapeutics: From Laboratory to Clinical Practice 28th-30th May 2012 | Valencia, Spain

Authors: Marie W Pettit, Paul Dyer, Simon C. W. Richardson

Poster title: 'Development of an oral vaccine delivery system'

Conference: The International Conference on Bacillus anthracis, B. cereus and B. thuringiensis. August 7-11, 2011 | Bruges, Belgium,

1.0 Introduction

1.1 The Problem: Global Food Security

The substantial global growth of the human population, (estimated to reach 9.3 billion by 2050 (Cohen 2003)), urbanisation, higher income levels and population growth, puts an ever increasing burden on the food production industry, especially that of meat production (Arinaminpathy *et al.*, 2009). The need to supply enough nutritious food to this large population, whilst land resources continue to diminish, is a major social-economic problem. Since global production of meat has almost doubled over the last generation (25% gain per capita supply) (Smil 2003), the control of animal disease is becoming an ever-burdening concern. More recently, three livestock diseases: Foot and Mouth Disease (FMD), Highly Pathogenic Avian Influenza (HPAI) and Bovine Spongiform Encephalopathy (BSE) have caused major economic, social and animal welfare problems in the United Kingdom (UK) alone (Heffernan *et al.*, 2008).

The outbreak of BSE in the UK, along with the zoonotic transmission to humans (as Creutzfeldt-Jacob disease (CJD)) caused major reduction in beef consumption in Europe between 1986 and 1996, (van der Zijpp 1999) causing loss of human life and inflicting major economic damage (£1.5 billion cost to the UK government) (Caskie *et al.*, 1998). The foot and mouth outbreak of 2001 illustrated the role of trade in live animals, and how this triggered the spread of infection. Overall, the outbreak cost over £9 billion (Arinaminpathy *et al.*, 2009). Zoonotic infections such as HPAI and Anthrax cause concern not only for animal health and social-economic losses but also for human health. Other livestock diseases are derived from wildlife. Bovine tuberculosis is an important disease of cattle in the UK and has a natural reservoir within the wild badger population. This has led to the long run controversy over the culling of badgers as opposed to a vaccination programme for wildlife (Jenkins *et al.*, 2008).

The International Model for Policy Analysis of Agricultural Commodities and Trade (IMPACT) suggest that by 2020, developing countries will consume 70% more meat than developed countries (Heffernan *et al.*, 2008). In concentrated production areas, the control of zoonoses such as salmonellosis and tuberculosis will become more important (Chomel 1998). Economic losses caused by disease are generated from loss in production, human and animal mortality, cost of veterinary treatment, preventative action such as vaccination, hygienic measures and policies such as those for stamping out disease *e.g.* foot and mouth (van der Zijpp 1999).

The Office International des Epizooties (OIE) now known as the World Organisation for Animal Health has classified transmissible animal diseases into List A and List B. List A diseases are to be reported immediately, in order to inform both “at risk” neighbouring countries and international trade partners. List B diseases are considered to have socio-economic and / or public health importance within countries and are significant to the international trade of animals and animal products (Table 1).

Over the last 20 years food borne disease in humans caused by bacteria, parasites, viruses and prions have significantly moved up the political agenda and generated, on occasions, substantial media attention (Newell *et al.*, 2010). Preventative measures such as the vaccination of livestock and wildlife are considered worthy of national news (Black 2011). Vaccination could prevent epidemics such as those seen in recent years from occurring, thus protecting livestock and preventing the spread of zoonoses to humans. This project focuses upon infectious bursal disease virus (IBDV) an immunosuppressive disease affecting the poultry industry worldwide.

Table 1. Sample of List A and List B animal diseases from OIE.

List A	List B
Foot and mouth	<i>Cattle diseases</i>
Vesicular Stomatitis	Anaplasmosis
Swine vesicular disease	Bovine brucellosis
Rinderpest	Bovine genital compylbacteriosis
Contagious bovine pleuropneumonia	Cysticerosis
Lumpy skin disease	Trichromoniasis
Rift valley fever	Bovine spongiform encephalopathy (BSE)
Blue tongue	
Sheep / goat pox	<i>Multiple species</i>
African horse sickness	Anthrax
African swine fever	Aujeszkey disease
Classical swine fever	Q fever
Newcastle disease	Rabies
	<i>Pig diseases</i>
	Atrophic rhinitis
	Porcine brucellosis
	<i>Poultry</i>
	Avian infectious bronchitis
	Avian tuberculosis
	Infectious bursal disease (IBD)
	Fowl cholera

1.2 The Need for Oral Veterinary Vaccination

Since surveillance, biosecurity, culling and movement restrictions are the first line of defence against infectious diseases, it seems that a vaccination strategy, in both wildlife and domesticated animals should be revisited (van der Zijpp 1999). Prerequisites for veterinary vaccines are low immediate economic cost, ease of mass administration, safety and efficacy. For farm animals, the preferred method of

vaccination and in fact medication, is orally (via drinking water or feed) (Ganapathy *et al.*, 2010). Using this methodology, a large number of animals can be medicated at the same time, with a low cost of administration and low workload. However, the main disadvantage is dose control giving rise to variations of dose between animals as well as possible stability and solubility problems (Ganapathy *et al.*, 2010). The licensed CEVAC® TRANSMUNE IBD vaccination (Intervet UK Ltd.) is a live attenuated viral vaccine available for immunisation against IBDV (see section 1.4.4) that has limited stability. CEVAC® stability has been shown to cause a loss of vaccine efficacy due to chlorine, aminic compounds or acidifiers within animal drinking water, as well as requiring storage and transportation in liquid nitrogen, therefore increasing the cost of vaccination (Vermeulen *et al.*, 2002).

Medication or vaccination via feed is generally accepted to be reliable when administered to birds (Zhang-Barber *et al.*, 1999). This is usually performed using premixed formulations. However, careful design is required to ensure the stability of the active ingredient, whilst maintaining homogeneity throughout the mix. Dust production and the subsequent wastage of active component in dust, has been known to cause problems causing economic loss, however the addition of oils has been suggested to reduce this problem (Vermeulen *et al.*, 2002).

Parenteral vaccination or medication within the poultry industry is estimated to be only 1% (per capita) of the total veterinary preventative treatment for disease in birds. This is primarily due to time consumption and stress placed on the birds. Intramuscular injection into birds causes muscular damage. This is due to the relatively large volume injected and irritating components (Vermeulen *et al.*, 2002). Thus an alternative vaccination strategy is required. One disease that results in major economic cost to the poultry industry and requires a more suitable, cost effective and stable delivery system is Infectious Bursal Disease (IBD).

1.3 Infectious Bursal Disease

IBD is a list B OIE infectious disease. The causative agent of infectious bursal disease virus (IBDV) belongs to the genus *Avibirnavirus* of the family *Birnaviridae* (Carlos Rodriguez-Lecompte *et al.*, 2005). IBDV is a highly infectious, acute disease of

sexually immature chickens. The disease affects the lymph tissue, particularly the Bursa of Fabricius (BF) (Sharma *et al.*, 2000). Chickens infected with IBDV develop immunodeficiency due to depletion of B-lymphocytes (Zhou *et al.*, 2010). The subclinical form causes major impact worldwide due to depletion of the host's immune system and is characterised by gross and microscopic lesions within the BF (Carlos Rodriguez-Lecompte *et al.*, 2005). Chickens are the only avian species known to be susceptible to clinical disease caused by the virus (Jackwood and Sommer-Wagner 2011). However, ducks, turkeys and ostriches are susceptible to infection but remain resistant to clinical disease (Sharma *et al.*, 2000). Despite the use of vaccines to control IBDV, it continues both directly and indirectly via the immunosuppressive effects of the disease, to cause large economic losses to the poultry industry worldwide, (\$1 million per year in Alabama alone) (Ivan *et al.*, 2001). The economic impact of IBDV is related to losses due to mortality, growth retardation, or rejection of carcasses, (Habib *et al.*, 2006). The indirect effects of immunosuppression brought about by this pathogen, allows other opportunistic pathogens, such as *gangrenous dermatitis*, to go unnoticed (Jackwood and Sommer-Wagner 2011).

1.3.1 Pathogenesis of IBDV

Chickens are highly susceptible to IBDV infection between weeks three to six “post hatch” *i.e.* after hatching. Experiments in which bursectomized chickens survived IBDV infection demonstrated that the BF is the main target organ for the virus (Aricibasi *et al.*, 2010). The acute phase usually lasts a week, and peak clinical signs and mortality were recorded between days 3 and 4 post-infection (Jackwood and Sommer-Wagner 2011). Commonly, IBDV has been shown to enter the animal via the gastrointestinal tract (GIT) and is then transported to other tissues by phagocytic cells, thought to be resident macrophages (Aricibasi *et al.*, 2010). The cellular receptor for IBDV has yet to be verified, but it is postulated to be the fraction crystallizable (Fc) receptor on immune cells (Elankumaran *et al.*, 1994). IBDV has been shown to infect and destroy IgM bearing B cells in active mitosis within the BF (Rodenberg *et al.*, 1994). In addition to targeting B cells, IBDV has been shown to be capable of infecting and replicating within macrophages, increasing the chance of further infection. Once infected with IBDV, the virus has been reported to cause the production of pro-inflammatory mediators and cytokines in macrophages, which peak

during the early phase of viral replication (Aricibasi *et al.*, 2010). The cytokines produced in response to IBDV infection include: interleukin (IL)-12, interferon (IFN)- γ , IL-1 β , IL6, and, in bursal cells, CXCL12 (Eldaghayes *et al.*, 2006). Within the spleen cells, IBDV induces expression of IL-1 β , IL-6, IL-18 and inducible nitric oxide synthase (iNOS) (Aricibasi *et al.*, 2010; Eldaghayes *et al.*, 2006). T cells, although not actively infected by the virus have been suggested to modulate the pathogenesis of infection by limiting viral replication in the BF during the early phase of the disease (5 days post infection). This occurs via promoting tissue damage in the bursa and delaying tissue recovery, suggested to be via the release of cytokines and their concomitant cytotoxic effects (Rautenschlein *et al.*, 2002).

Studies indicate that pathogenesis and immune responses of IBDV infection may vary depending on the age of the affected chick and the maturity of the bird's immune system (Rautenschlein *et al.*, 2007). Birds infected with IBDV at more than 2 weeks post hatch, induce T cell accumulation in the BF coinciding with the replication of the virus (Aricibasi *et al.*, 2010). These intrabursal T cells are activated and become a significant part of viral clearance but also bursal recovery (Rautenschlein *et al.*, 2007). Haase and colleagues (2007) compared IBDV pathogenesis and immune responses between 12 day old and 28 day old specific pathogen free (SPF) chickens and found that cytokine response following infection varied depending on the age difference of infected chickens. IFN- λ was up-regulated in birds inoculated at 28 days post hatch, in all tissues at 3 days and in BF and caecal tonsils at day 5, post infection. Birds inoculated at day 12 showed significant IFN- λ up regulation in BF at day 3 and in caecal tonsils at day 5, while in the spleen at 3 and 5 days post infection. This was performed in comparison with virus free mates. Further it was noted that parameters such as IBDV induced bursa lesions, accumulation of intrabursal T cells and macrophages as well as systemic stimulation did not vary between sets of infected birds. In addition, the release of nitric oxide inducing factors and virus neutralising antibodies did not vary between either set of infected birds.

The role of macrophages involved in IBDV infection has attracted the interest of researchers. It has been suggested that IBDV targets the macrophages to induce tissue lesions (Khatri *et al.*, 2005). Additionally, the mast cell and its mediators are one of

the key players involved in the inflammatory process during infection with IBDV (Jackwood and Sommer-Wagner 2011). Mast cells reside in many tissues but particularly with structures such as blood vessels and nerves, including tissues that interface the external environment (Marone *et al.*, 2002). Tryptase is the most abundant product of granules produced from mast cells. Therefore, upon degranulation vast amounts of protease is released. It is likely that tryptase plays a profound biological role in the inflammatory response (Wang *et al.*, 2008; Marone *et al.*, 2002). Wang *et al.*, (2008) studied the effect of mast cells and their mediators in chickens infected with very virulent IBDV (vvIBDV). Both mast cell population and tryptase activity was significantly increased in SPF infected chickens. Furthermore, enlarged degranulating mast cells were found to infiltrate and surround the tissue lesions suggesting a critical role for mast cells in mechanisms involved in vvIBDV infection. Data revealed that a large quantity of tryptase was present in the BF, brain and other organs of vvIBDV infected chickens whereas it was absent in the control group (Wang *et al.*, 2008). In order to understand and identify “weak links” within the viral life cycle, it has been preserved as important to understand the structure and life cycle of the virus (Campos *et al.*, 2008).

1.3.2 Viral Structure and Viral Proteins

IBDV is a bi-segmented, double stranded RNA (dsRNA) virus contained within a 60-65nm non-enveloped, icosahedral capsid. IBDV is single shelled, unlike most dsRNA viruses (Eldaghayes *et al.*, 2006). The viral genome consists of two segments, A and B. Segment A (3.2kb) contains two partial overlapping open reading frames (ORFs). The large ORF encodes a polyprotein of 110 kDa: pVP2-VP4-VP3, which when cleaved by autoproteolysis forms the viral proteins, VP2, VP4 and VP3 (Zhou *et al.*, 2010). Of note is the VP2 protein, which has been reported to be the major antigen of the virus, containing major antigenic epitopes responsible for the induction of neutralising antibodies (Heine *et al.*, 1991; Zhou *et al.*, 2010). In addition, the small ORF contains the gene VP5 (17kDa). VP5 although dispensable for viral replication *in vitro*, plays an important role in viral virulence (Deng *et al.*, 2007). VP5 has been shown to accumulate in the host plasma membrane and is considered to be involved in viral release as well as inducing apoptosis (Zierenberg *et al.*, 2004). The apoptotic process may be induced indirectly by interaction between IBDV infected cells and

non-infected cells without any viral protein being present in the uninfected cells (Rautenschlein *et al.*, 2007). This suggests that VP5 is not a prerequisite for induction of IBDV apoptosis (Rodriguez-Lecompte *et al.*, 2005).

Segment B (2.9kb) encodes the VP1 gene and the viral RNA dependent RNA polymerase (RdPd). The external surface of IBDV capsid is formed by 260 VP2 trimers, while the inner surface is formed from the self-assembly of 200 copies of the VP3 trimer (Yip *et al.*, 2007). Based on the atomic structure of IBDV viral particles, it has been suggested that VP2 forms the outermost 'protrusions' on the capsid surface (see figure 1) (Coulibaly *et al.*, 2005).

Trimeric VP2 proteins are suggested to be the responsible for receptor binding (Yip *et al.*, 2006). VP2 shares some common characteristics with other receptor binding proteins, such as the presence of antibody neutralisation escape mutations and tissue culture adaptation determinants (Yi *et al.*, 2007).

Viral proteins VP2 and VP3 are the major structural proteins of the virion, whereas VP4 is a viral encoded protease, involved in the processing of the precursor protein (Li and Vakharia 2004). VP3 is a protein on the inner leaflet of the capsid and forms a complex with VP1 (Li and Vakharia 2004). VP1 is a multifunctional protein that is responsible for viral replication and mRNA synthesis. The protein is linked covalently to the 5' ends of the genome RNA segments (Li and Vakharia 2004). VP3 has been reported to be a gene of 774bp (29kDa), corresponding to amino acids 756-1012 of the polyprotein (Segment A), remains conserved among serotype, strains and isolates of the virus (Deng *et al.*, 2007). VP3 acts as a scaffolding protein required for assembly control (Deng *et al.*, 2007).

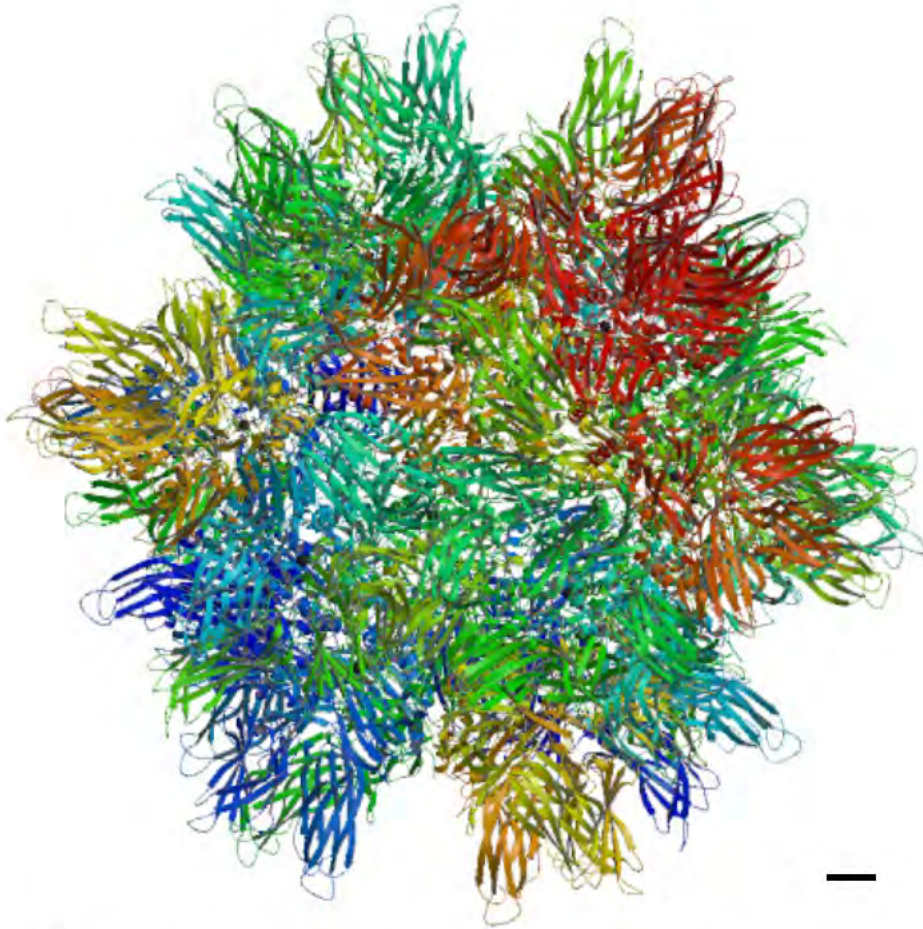


Figure 1. The supramolecular assembly of 260 VP2 capsid proteins (shown in a variety of colours) forming the icosahedral IBDV capsid. This data is derived from Protein Data Bank (PDB) reference 2GSY. Size bar represents approximately 20Å.

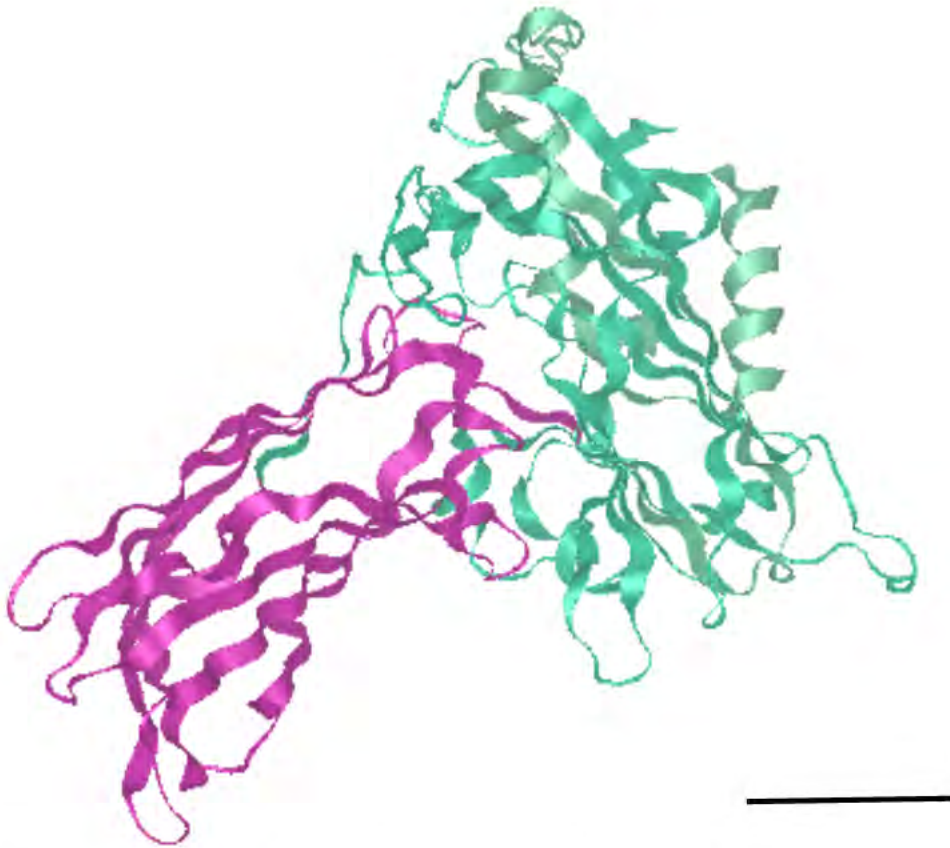


Figure 2. The structure of an isolated IBDV VP2 protein that assembles into the viral capsid shown in figure 1. The pink region describes the proposed receptor-binding region defined by the restriction enzyme sites *Acc*I -*Spe* I. This data is derived from the Protein Data Bank (PDB – 2DF7). Size bar represents approximately 20Å.

1.3.3 IBDV Serotypes

IBDV has two different serotypes, 1 and 2. Serotype 1 is pathogenic to chickens, whereas serotype 2 affects turkeys, ducks and geese (Zhou *et al.*, 2010). These viruses have restricted cell and tissue tropism, selectively infect immature B cells of BF, leading to B cell depletion and subsequent immunosuppression (Li and Vakharia 2004). Serotype 1 can be classified as classic, antigenic variant and highly virulent strains. Zierenberg *et al.*, (2004) found that B cell tropism of serotype 1 was determined by segment A. Segment B of serotype 1 could be replaced with that of serotype 2, without affecting tropism.

Classical virulent strains were first isolated in the United States in the early 1960's. Strains such as the Irwin Moulthrop (IM) strain, isolated from America (GeneBank accession number AY029166), STC, isolated from Canada (GeneBank accession number D00499) and 52/70, isolated from the UK, (GeneBank accession number D00869) enter this category (He *et al.*, 2009). These strains induce hemorrhagic inflammation and B cell depletion of BF, causing 30-60% mortality in chickens (Snyder *et al.*, 1992).

Antigenic variant strains, such as the Delaware strain, were isolated in the late 1980's from poultry farms whose flocks were vaccinated against IBDV. These viruses do not cause mortality but induce rapid bursal atrophy without triggering inflammation (Li and Vakharia 2004).

Very virulent strains (vvIBDV) emerged in several European countries and Asia in the mid 1990's, causing more than 70% mortality (Li and Vakharia 2004). The vvIBDV strains are unable to propagate in tissue cultures directly but the virus can adapt to tissue cultures and become attenuated by serial blind passages (Yi *et al.*, 2007). Infection of both chicken embryonic fibroblasts (CEF) and Vero cells were reported following tissue culture adaptation (Kwon and Kim 2004). Sequence analysis revealed that adaptation was related to the change of three amino acids on VP2, namely 253 (Glu to His), 279 (Asp to Asn) and 284 (Ala to Thr). Crystal structure analysis revealed that these three amino acids were located in the most exposed loops of projection domain of VP2, while the side chains point outwards while not participating in capsid stabilisation (Yi *et al.*, 2007; Coulibaly *et al.*, 2005). This suggests that these residues may engage directly with contact to a cellular receptor. However, to further understand the pathogenesis of IBDV, it was critical to understand the immune development of the chick.

1.3.4 Immune Development in the Chick

Gallus spp., forages for food immediately after hatching. The intake of food this soon after hatching requires the rapid development of the digestive tract to accommodate breakdown and adsorption of food. The intestinal tract therefore becomes immediately inhabited by microflora as well as the possible entry of pathogenic

bacteria (Barnes 2008). Therefore, a parallel rapid development of gut associated lymphoid tissue (GALT) is expected. However at this age the lymphocyte function in the gut develops relatively slower (Bar-Shira and Friedman 2006). GALT appears to mature in the chick toward the second week of life raising concerns for immune protection during the first week of life, however the chick at this age should remain protected via maternally derived antibodies (MDA) (Clench 1999). As in mammals, mucosal surfaces are constantly exposed to the external environment; therefore the epithelial lining and innate immune system are the first lines of defence against invading pathogens (Barnes 2008). Bar-Shira and Friedman (2006) studied the involvement of the innate immune system in defence of the chicken gut during the first week of life. Chicken IL-1 β was involved in the inflammatory response following bacterial infection or lipopolysaccharide (LPS) stimulation, induction of fever and chemokines in chickens (Clench 1999). Their data demonstrates IL1 β mRNA levels barely increase above day 0 levels in the colon and caeca, whereas a two-fold increase was seen in the duodenum at day two, post-hatching. This corresponds to the first feeding and GIT colonisation by bacteria, suggesting the chick was protected by a functionally sufficient innate immune system.

As the initial encounter with pathogens occur at the mucosal surface of the gut, it has been predicted that the oral administration of antigen would induce a local intestinal immune response (Mestecky *et al.*, 1994). However, the administration of non-replicating native antigen elicited highly variable immune responses. In mammals, 80% of all plasma cells reside in the intestinal *lamina propria* and most produce polymeric IgA (pIgA). This antibody isotype was unique for mucosal tissues and was responsible for the defence of the mucosal surfaces against pathogenic bacteria (Johansen and Bronatzaeg 2004). Lammers and colleagues (Lammers *et al.*, 2010) addressed this aspect of the chicken intestinal immune system in the absence of deliberate immunisation. Endogenous IgA in the chicken intestine was almost undetectable before 14 days of age, however, the mRNA expression levels of IgA increased rapidly from 21 days and reached maximal levels at 70 days of age. To better understand the functioning of the avian immune system and to help develop a platform technology for the development of an oral vaccine delivery system, the chicken gastrointestinal (G.I) anatomy must be understood.

1.4 Chicken G.I Anatomy

1.4.1 Proximal G.I Anatomy

Gastrointestinal anatomy in birds is different from that of mammals and has been shown to influence the pharmacodynamic and pharmacokinetic behaviour of many drugs given via the oral route. Oral therapy, vaccination and medication, accounts for over 90% of total drug administration in poultry (Vermeulen *et al.*, 2002).

Birds have no teeth; hence no grinding or sheering can occur in the buccal cavity. There is, in birds, no sharp distinction between the pharynx and the mouth. The oesophagus is divided into the cervical and thoracic regions with the cervical region being expanded to form the crop (Messenger 2010). The crop functions as a food store before passing food into the proventriculus. Crop emptying in poultry is usually completed within 3-20 hours depending on the moisture content of the food. A stable drug has been documented to pass through the crop and ventriculus, entering the duodenum within minutes following administration, (Dorrestein and van Miert 2008). The pH within the crop is an important factor for therapeutic entities given via oral administration and is maintained at about pH 6. Some investigators suggest that the presence of *Lactobacillus* in the crop can interfere with the adsorption process due to inactivation of the drug by bacteria (Vermeulen *et al.*, 2002).

The avian stomach consists of two chambers the proventriculus and ventriculus. The ventriculus, being a muscled organ rapidly disintegrates solid oral dosage forms of medication releasing their active ingredient (Enoki and Morimoto 2000). If a stable drug solution was administered the drug passes rapidly through the crop, proventriculus and ventriculus within a few minutes following administration, allowing adsorption in the duodenum (Vermeulen *et al.*, 2002). However, for the purposes of the generation of an oral vaccine, antigen adsorption and presentation was thought to occur via the ileum (Majamaa and Isolauri 1995) following the exit of the antigen over either the epithelial lining of the gut or the Payer's Patch (PP) of the ileum into the *lamina propria* (Stokes and Bailey 1996).

1.4.2 Intestinal Epithelium

Different cell types constitute the intestinal epithelium. The epithelium of villi was predominantly composed of enterocytes and goblet cells. Dispersed throughout the intestinal mucosa, lymphoid nodules called O-MALT (Organised Associated Lymphoid Tissue) individually or aggregated into PP. PPs have raised much interest due to the presence of microfold (M) cells within these structures (Rieux *et al.*, 2006). M cells deliver samples of foreign material from the lumen of the gut to the underlying organised mucosa lymphoid tissue in order to induce immune responses. M cells are specialised for antigen sampling but have been exploited as a route for pathogen entry (Brayden and O'Mahany 1998). M cells represent a potential portal for oral delivery of peptides / proteins and for mucosal vaccination since they possess a high transcytotic capacity (Neutra *et al.*, 1996). Uptake and presentation (to PP), B and T lymphocytes can lead to the generation of a mucosal immune response, in which secretory IgA (sIgA), present in the lumen, can prevent the attachment of enteric pathogens to the cell wall (Brayden and O'Mahany 1998). It is generally accepted that, at least *in vitro*, that less than 200 µm nanoparticles are taken up by M cells and delivered to the basal medium. However particles greater than 5µm are taken up by M cells, but remain entrapped in PP (Rieux *et al.*, 2006). The initial site of infection with regards to IBDV however is the BF. Knowledge of the role of the avian bursa is critical for understanding the pathogenesis and targeting of vaccination schemes.

1.4.3 The Distal G.I and The Avian Bursa of Fabricius

Distal to the ovine ileum is the large intestine and the BF. Although not integral to the G.I, the BF is located proximal to the rectal pouch at the distal end of the G.I. The primary role of the avian BF is to provide an essential microenvironment for B lymphocytes to diversify their immunoglobulin genes by gene hyperconversion (somatic hyperconversion in mammals) (Ivan *et al.*, 2001). Gene hyperconversion begins at approximately 15-17 days of incubation (DI) (pre-hatching), following the immature B cell progenitors migration into the BF. The bursal environment has been demonstrated to provide a milieu for selecting and amplifying B cells with productive Ig gene rearrangement and promoting antibody repertoire expansion (Ivan *et al.*,

2001). During the hyperconversion process, blocks of DNA sequence are transferred between pseudo-v regions to the recombined variable regions of the Ig genes. This results in the production of mature B cells that are competent to form a functional humoral immune system in the adult bird (McCormack *et al.*, 1989). The then diversified B cells leave the bursa and populate the secondary lymphoid organs around the time of hatching. However, the hyperconversion process continues until the bursa involutes at sexual maturity (Ivan *et al.*, 2001). Atrophy of the BF and depletion of B lymphocytes therefore causes severe immunosuppression for birds infected with IBDV.

1.4.4 Current Vaccination Against IBDV

Vaccination against IBDV with inactivated or attenuated live viruses is currently the only form of protection (Li *et al.*, 2006). Vaccination against infectious bursal disease virus (AviPro® IBD extreme and CEVAC® TRANSMUNE IBD) is delivered via drinking water. However, the vaccine is a live attenuated virus that is unstable within untreated water systems. Live viral vaccines should not be exposed to bright sunlight, heat, heavy metals, disinfectants and detergents, chlorine and organic matter (Vermeulen *et al.*, 2002). Hence this vaccination strategy remains very difficult to administer for the poultry farmer. Here an alternative, more stable system is proposed for the prevention of IBDV.

However, these vaccines have become less effective, due to emergence of very virulent or antigenic variant strains of the virus. Antigenic variation of IBDV and the emergence of variants have been associated with genetic changes in the VP2 gene (Mahmood *et al.*, 2007). Efforts have focused on the generation of subunit vaccines containing the IBDV polyprotein or capsid protein VP2. Chickens vaccinated with conventional IBDV vaccines are not fully protected against IBDV challenge even though antibody titre is high (Muller *et al.*, 2003). Thus there remains a large void for a novel vaccination therapy to effectively prevent IBDV both nationally and globally precluding an endemic and preventing major economic burden.

1.5 Vaccination Models

An ideal vaccine should not cause disease or negative side effects in the host whilst inducing an effective immune response that is capable of protecting against a specific pathogen (Frey 2007). Those vaccines used in the animal food production industry, should be safe to humans and the environment, offer safe administration routes (preferably oral), be stable for long durations of time, be traceable in animal populations and the environment and contain the necessary antigenic determinants to induce protective immunity (Bowerstock and Martin 1999).

1.5.1 Attenuated Viral Vaccines

A live attenuated viral vaccine is a live virus that has been engineered to lose its virulence whilst maintaining the ability to induce protective immunity (Brun *et al.*, 2008). There are many associated benefits of using a live attenuated virus over that of a killed or inactivated virus. For example, most viral proteins will be in their native conformation, presenting a broad range of epitopes to the immune system (Mahmood *et al.*, 2007). Since the translation of these viral proteins occurs in the cytosol, they are loaded onto and presented by MHC class I molecules, stimulating a cytotoxic T cell response (Levy *et al.*, 2003). Additionally, attenuated viral vaccines may be administered via the route of infection *i.e.*, orally, mimicking the infection at the site of attack (Schatter *et al.*, 2005). However, one major limitation to the use of vaccination strategies using attenuated viruses is that of safety. Attenuated viruses are potentially genetically unstable, provoking concerns regarding the reversion to virulence or differences in virulence within different hosts (McGhee *et al.*, 1992). In addition they are very expensive to develop, maintain, administer and store. Therefore modern science leads away from these vaccination strategies and towards safer alternatives. One such strategy is DNA vaccination.

1.5.2 DNA Vaccination

Previous DNA vaccination studies have demonstrated protective immune responses against IBDV. Below are some therapies that have previously been investigated for farm animals (fig 3).

1.5.2.1 DNA Vaccination via Recombinant Bacterial Vectors

Recently, live bacteria containing plasmids encoding heterologous antigen encoding genes from pathogens, have been investigated for their use as potential oral delivery vectors for DNA vaccines (Li *et al.*, 2006). Attenuated gram positive and gram-negative intracellular bacteria such as *Salmonella enterica*, have been used as carriers for efficient delivery of either DNA vaccine constructs or vaccine antigens. Live bacteria naturally possess immunostimulatory molecules such as lipopolysaccharide (LPS) that can function as an adjuvant to stimulate immune responses (Mahmood *et al.*, 2007). Additionally, live bacterial vectors are able to induce systemic immune response, including humoral, cellular and mucosal immunity against pathogenic infection (Medina and Guzman 2001). As live bacterial vectors are stable, and amenable to large-scale production, they offer potential advantages as transgenic vehicles for the delivery of immunogenic genes (Mahmood *et al.*, 2007).

Studies in chickens have shown that bacteria carrying recombinant plasmids with heterologous genes were capable of eliciting specific humoral and cellular immune responses both locally and at the systemic level (Mahmood *et al.*, 2007). Li *et al.*, (2006) constructed an attenuated *Salmonella enterica typhimurium* strain sv4089, harbouring the polyprotein gene of IBDV. This was used to test the possibility of developing live attenuated bacterial vaccination strategies, to deliver DNA vaccines against the virus. The IBDV polyprotein was expressed during both *in vitro* and *in vivo* experiments and induced IBDV-specific humoral responses affording immunoprotection against virulent IBDV after oral immunisation. However, there are concerns over the long-term safety of using these bacterial vectors.

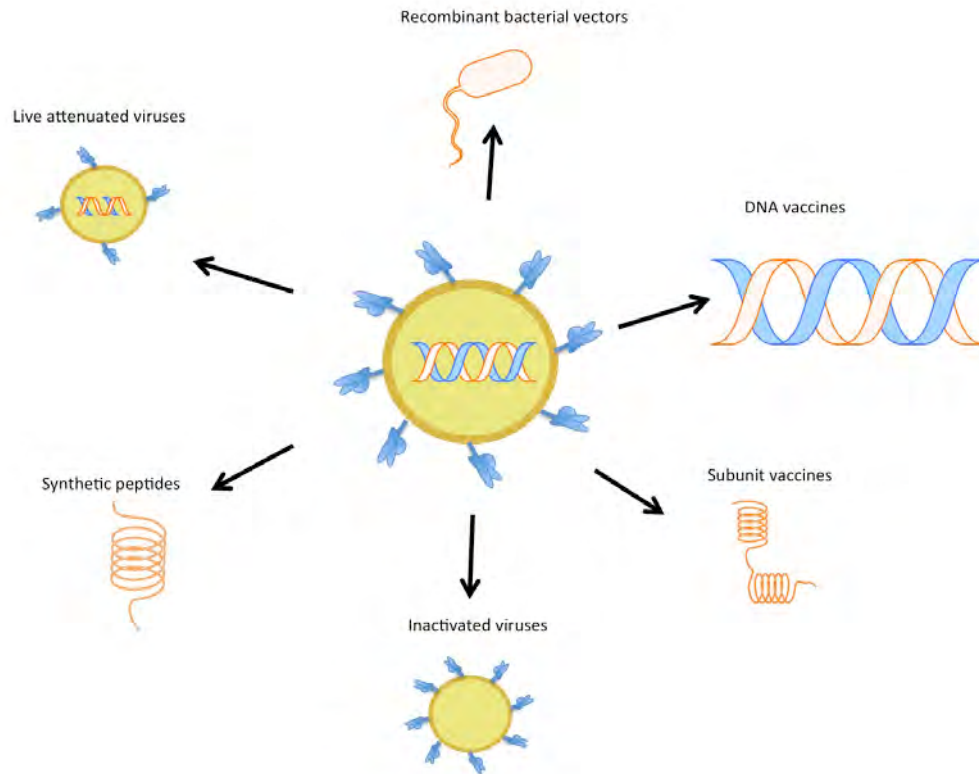


Figure 3. Proposed vaccination strategies for viral diseases, (adapted from Nikolic and Piguet 2010).

Mahmood *et al.*, (2007) studied the effects of transgenic *E.coli* DH5 α expressing the VP2 gene of vvIBDV. None of the chickens showed signs of ailment after oral vaccination at doses of $10^7 - 10^9$ colony forming units (CFU). All chickens except the control group were given a challenge of 10^5 half the egg infective dose (EID₅₀) of homologous IBDV. In the group immunised with 10^9 CFU, 95.4% of the chickens were protected at gross histopathological BF lesions, from VP2 expressing *E.coli*, and displayed no other clinical signs of disease or mortality. Chickens were protected at 10^8 CFU dosage (91%) and only 73% of chickens were protected in the 10^7 CFU treated group. However, since live vaccine strains (attenuated either by natural selection or genetic engineering) were potentially released into the environment. This raised both medical and environmental safety concerns (Frey 2007). These concerns include changes in cell, tissue and host tropism, and reversion to virulence by either incorporation of foreign genes or the acquisition of complementation genes. The

spread of undesired genes such as antibiotic resistance are also primary concerns for such vaccination strategies (Curtiss 2002).

1.5.4 *In Ovo* DNA Vaccination

In ovo vaccination at 18 DI is a relatively new method of successfully vaccinating chicken embryos. Over 80% of commercial broilers are vaccinated using this methodology in the USA, principally against Marek's disease (Gimeno 2008). In addition to promoting early immunity, *in ovo* delivery allows administration of a more uniform dose of vaccination, inducing early resistance to field challenge as oppose to manual vaccination of the neonate (Haygreen *et al.*, 2006). Automated *in ovo* delivery deposits the inoculum into the amniotic fluid, which is then imbibed by the embryo (Oshop *et al.*, 2003). Little has been published regarding the immunopathogenesis and mechanisms of immunity following *in ovo* vaccination in chicken embryos lacking a fully mature immune system (Rautenschlein and Haase 2005). It was demonstrated in 2005 by the Haase group, that IBDV pathogenesis varies significantly between *in ovo* and post hatch vaccinated birds. This was suggested to be due to the age differences of the immune system at this time (Karaca *et al.*, 1998). Substances that are inoculated *in ovo* are transported from the amnion via the mouth and trachea to the lungs and intestine which makes it comparable to the oral or conjunctival route of administration that is commonly used in post hatch birds (Rautenschlein and Haase 2005). The Haase group demonstrated that *in ovo* inoculated birds recovered faster from bursal lesions. Following depletion of functional T cells from the chickens, a significantly faster recovery rate from bursal lesions was evident, suggesting T cells have a negative effect on follicular bursal recovery (Rautenschlein *et al.*, 2002). Further indication for immature T cells with *in ovo* vaccinated birds was shown by lower IgG IBDV antibody response (Rautenschlein and Haase 2005).

Oshop *et al.*, (2003) administered a DNA vaccine encoding the genes for VP2, 3 and 4 via the *in ovo* route and observed expression in the embryonic liver and muscle. The vaccine stimulated complete protection when followed by a live viral boost. However, it is considered that a single vaccination *in ovo* may not be feasible due to the immaturity of the chicken's immune system (Haygreen *et al.*, 2006). *In vitro* experiments using the amniotic fluid display DNase activity, consistent with plasmid

degradation within 30 minutes. Hence uptake of the plasmid DNA may be incomplete and / or vary between subjects (Muir *et al.*, 2000).

Current vaccine delivery systems for IBDV are not effective and require the immunisation of birds on an individual basis. This requires the optimisation of timing in response to the decrease in maternally derived antibodies, which depends on time of hatching; an oral vaccine delivery system would be more beneficial. Live attenuated bacterial vaccines appear a more promising approach, however concerns over the release of modified bacteria into the environment and the exchange of antibiotic resistance genes, in addition to storage problems are concerns for these vectors, (Curtiss 2002).

1.6 Oral Vaccine Delivery for IBDV

It is estimated that 90% of all mammalian infections originate at mucosal interfaces. Therefore the consideration towards stimulation of mucosal immunity as well as systemic immunity is critical to produce an effective vaccine (Jertborn *et al.*, 1996). Current parental vaccination strategies fail to generate effective mucosal immunity against disease. This is critical for the immunological exclusion through IgA production or by eliminating invading pathogens at mucosal epithelial barriers (Mann *et al.*, 2009). Oral vaccine delivery would therefore offer a preferred delivery route for both veterinary and human applications due to its activation of both immunological systems (table 2).

Additionally, the oral route, prevents pain, eliminates contamination as well as lowering cost and reducing labour (Vermeulen *et al.*, 2002). However, administered bioactive drugs such as proteins are notoriously problematic in that they must persist through the hostile environment of the GIT contending with; the low pH of the stomach, high bile salt concentration, proteolytic enzymes, commensal gut bacteria and mucous secretions, whilst maintaining their antigenic nature (Mann *et al.*, 2009). Furthermore, they must persist through the intestinal lumen until a suitable site for cell adhesion and uptake can occur, thus followed by transcytosis to the *lamina propria* (Rieux *et al.*, 2006). Many studies have focused upon improving the delivery

of therapeutic moieties for oral vaccine development by their association with colloidal carriers such as polymeric nanoparticles (Brayden and O’Mahany 1998; Rieux *et al.*, 2006). Table 3 reviews a variety of mucosal delivery systems currently under investigation.

Table 2. Mucosal versus parental vaccination pros and cons.

Parameter	Mucosal vaccination	Parental vaccination
Route	Oral, nasal, rectal, vaginal, pulmonary	Intramuscular or subcutaneous
Method of administration	Self administered	Veterinary assistance required
Risk factors	Safe (dose requires monitoring)	Possible infections due to contaminated needles
Antigen dose	High	Low
Immune response	Both mucosal (IgA) and systemic (IgG)	Systemic (IgG)
Cost	Low	High due to veterinary personnel, time, labor etc.

1.6.1 Polymeric Nanoparticles

Polymeric nanoparticles are more stable in the GIT than other colloidal carriers such as liposomes (He *et al.*, 2010). Furthermore, they can protect their encapsulated drug from the harsh environments of the GIT. Among the important factors are; susceptibility to degradation by the acidic pH of the stomach, metabolism by luminal, brush border and cytosolic peptidases and poor permeability across the intestinal epithelium, due to size, charge and hydrophobicity (Brayden and O’Mahany 1998). Various characteristics of the polymeric nanoparticle may be optimised to enhance the physicochemical characteristics of the nanoparticles (*e.g.* zeta potential), drug release profiles (delayed, triggered, prolonged), and biological behaviour (targeting, bio-adhesion) of nanoparticles (Rieux *et al.*, 2006). Furthermore, the surface of the particle may be modified by the attachment of chemical entities such as poly(ethylene glycol) (PEG), poloxamers, and other bioactive molecules such as invasins and cholera toxin (He *et al.*, 2010). However, the lack of an effectively induced immune response after the oral administration of this technology has led to no successful candidate therapeutics in the market (Steffansen *et al.*, 2004) (table 3).

Table 3. Review of current strategies for mucosal vaccination.

System	Vaccine	Route of admin.	Inference	Reference
Chitosan nanoparticles and chitosan coated emulsions	Ovalbumin and cholera toxin vaccine	Nasal	NALT targeting, 0.4 μ m diameter more efficient	Nagamoto <i>et al.</i> , 2004
Chitosan nanoparticles	Diphtheria toxoid vaccine	Nasal	Promising results	Rezaei 2006
Alginate coated chitosan nanoparticle	Hepatitis B	Nasal	Humoral mucosal immunity was enhanced with alginate coated nanoparticles compared to non-coated counterparts, in mice	Borges <i>et al.</i> , 2008
PLGA nanoparticles	Hepatitis B	Oral	Promising carrier adjuvant when given orally, targeting mucosa.	Gupta <i>et al.</i> , 2007
PLGA nanoparticles	Influenza virus	Nasal	Lack of uptake by NALT and high immunogenicity	Lemoine <i>et al.</i> , 1999
PLGA microspheres	<i>Toxoplasma gondii</i> vaccine	Nasal	Study shows good potential in sheep	Stanley <i>et al.</i> , 2004
PLGA/PLA microspheres	Ricin Toxoid vaccine	Nasal	Long lasting protection	Yan <i>et al.</i> , 1996
Phosphatidylcholine, Cholesterol	Tetanus toxoid vaccine	Nasal	Adjuvant increased the IgG levels but not the sIgA levels in the nasal lavages	Tafaghodi <i>et al.</i> , 2006
Phosphatidylcholine, Phosphatidylserine, Cholesterol	<i>H. pylori</i> vaccine	Oral	The study demonstrated the fusion peptide, CtUBE retained immunogenicity and could be used as antigen	Zhao <i>et al.</i> , 2007
Phosphatidylcholine, Phosphatidylserine, Cholesterol	Inactivated Newcastle disease virus	Nasal	Antibody titers increased by 320 times	Tseng <i>et al.</i> , 2009
Archaeal polar lipids (archaeosomes)	Ovalbumin	Nasal	Shows promise as adjuvant	Patel <i>et al.</i> , 2007
Proteo-liposomes	Recombinant meningococcal opab and opaj proteins	Nasal	LPS used for adjuvant – strong effect, however when used without adjuvant showed very weak effect	de Joung <i>et al.</i> , 2004
Phosphateidylcholine	Cholera vaccine	Oral	Effective when given orally	Leelawongta won <i>et al.</i> , 2003
Span 60, cholesterol, strearylamine	Tetanus Toxoid vaccine	Oral	Humoral and cellular response elicited	Jain and Vyas 2006
Non-ionic surfactant vesicles, deoxycholic acid	Tetanus Toxoid vaccine	Oral	Increase in IgA cells in small intestine	Mann <i>et al.</i> , 2006
Virosome	Hepatitis A vaccine	Oral	Demonstrated immunogenicity and safety comparative to Epaxal	Dagen <i>et al.</i> , 2007

1.6.2 Lipid Based Oral Vaccine Delivery

The potential of numerous lipid-based technologies have been investigated for their ability to deliver vaccines. These agents include liposomes, non-ionic surfactant vesicles (NISV), NISV incorporating bile salts (bilosomes), immune stimulating complexes (ISCOMs) and cochleates (Mann *et al.*, 2009).

1.6.2.1 Bilosomes

NISVs are liposome-like structures that have extremely low toxicity and act as adjuvants. However, detergents and bile salts destabilise NISVs. To circumvent this problem, the addition of bile salts into the NISV membrane acts as a protective mechanism to stabilise the membrane (Senior 2001). Bilosomes have demonstrated the ability to protect the lipid vesicle from bile damage, initiate antigen specific antibody responses to a variety of antigenic peptide (Singh *et al.*, 2004). Mann *et al.*, (2009), found that bilosomes of 10-100nm gave a stronger T helper cell (Th1) (cellular) response relative to larger (3 μ m) diameter formulations induced a biased Th2 response as measured by comparative IgG1 and IgG2a production. However, in parenteral administration studies, large vesicles induced a Th1 response while smaller vesicles induced a Th2 response against the antigen (Brewer *et al.*, 1998). Differential Th1 / Th2 response bias following vaccination with vesicles of different size could be a cell loading issue, *e.g.* larger vesicles carry more antigen than smaller vesicles. Smaller doses of antigen preferentially up regulate Th2 responses and large doses up regulate Th1 responses. In addition Mann *et al.*, (2006) found that orally administered niosomes incorporating bile salts, induce IgA responses against bacterial protein antigens. However this remains dose dependent with a fine threshold between immune stimulation and immune tolerance. Vaccinations could therefore be enhanced by the addition of adjuvants and immunomodulators that up regulate the immune response.

1.6.2.2 Archaeosomes

Liposomes that are composed of ester-lipids are highly susceptible to degradation from bile salts and enzymes that are present within the G.I tract. To help limit the instability of these composites, archaeosomes, made from diester and / or tetraether lipids have been produced (Patel *et al.*, 2000). Archaeosomes possess unusual lipid structures, which have been shown to impart greater stability, whilst maintaining adjuvant effects and being well tolerated *in vivo* (using a murine model) (Li *et al.*, 2011). However, archaeosomes, when used as a delivery system of insulin, resulted in low release of insulin and poor biological efficacy. The negative surface charge of the archaeosomes decreased the permeability of insulin delivery to cells (Li *et al.*, 2010).

Table 4. Selected liposomal formulations for vaccine delivery that are either licensed or in clinical trials – for human use.

Name	Company	Disease	Description	Status	Reference
Epaxal ®	Crucell	Hepatitis A	Inactivated virus adsorbed to virosomes	Marketed	Bovier 2008
Inflexal ® V	Crucell	Influenza	Virosomes	Marketed	Herzog <i>et al.</i> , 2009
Vaxisome	NasVax	Influenza	Inactivated virus	Phase 2	Evan-Or <i>et al.</i> , 2011
Vaxfectin	Vical	Influenza	Plasmid DNA encoded proteins	Phase 1	Sullivan <i>et al.</i> , 2010

1.6.2.3 Virosomes

Virosomes are vaccines that contain viral components reconstituted within a unilamella vesicle. Those currently in use, or are under evaluation are predominantly derived from the influenza virus and thus being used as a vaccine for influenza (Stegann *et al.*, 2010). Virosomes are approximately 150 nm in size and composed of neuraminidase (NA), haemagglutinin (HA), phosphatidylcholine and phosphatidylethanolamine (Wilkhu *et al.*, 2011). Epaxal ® (table 4) is a licensed

virosome for Hepatitis A administered by I.M injection (Bovier, 2008). The mechanism of action of virosomes closely resembles that of the native influenza virus. HA mediates the fusion reaction between the viral envelope and the endosomal membrane allowing escape of the viral proteins into the cytosol (Gluck and Metcalfe 2003). Virosomes are capable of eliciting either a MHC class I or II response, depending on the mode of presentation of antigen to the APCs. Antigens associated with the external virosome environment will be partially proteolysed initiating an MHC class II response. Antigens that are internal to the virosome will be transported from the cytosol to the ER and displayed on MHC class I (Stegann *et al.*, 2010).

Virosomes have shown promise in chickens when targeting Newcastle disease *in vivo*. Virosomes produced using Triton X-100 rather than octylglucoside to solubilise Newcastle disease viral membrane followed by controlled detergent removal was found to be the preferred method for obtaining Newcastle disease virosomes that contained a high concentration of HA, NA and fusion protein (Homhuan *et al.*, 2004). However, it has been long established that liposomes are susceptible to bile salt dissolution and enzymatic degradation in the G.I. tract is a major barrier for oral delivery of liposome-entrapped antigen (Chen *et al.*, 1996). Encapsulated antigens are susceptible to proteolysis following premature lipid dissolution; therefore an alternative delivery strategy is required.

1.7 Adjuvants and Immunomodulators

The inclusion of adjuvants and immunomodulators can improve the quality and quantity of immune response to a given antigen (Alving 2002). Adjuvants are key to the development of effective mucosal vaccines as they can compensate for the often poorly immunogenic nature of orally and nasally administered antigens (Aguilar and Rodriguez 2007). This occurs via the induction of vaccine antigen specific humoral and / or cellular responses. Aluminium salts have been widely used vaccine adjuvants since 1926. However, since they elicit sub-optimal Th1 responses and weak cell-mediated immunity, alternatives are being evaluated (Watson *et al.*, 2012). Several bacterial enterotoxins including cholera toxin and heat labile enterotoxin (LT) of enterotoxigenic *E.coli* have previously been identified as having adjuvant activity (Quere and Girard 1999). After eliciting an antigen specific Th2 type CD4⁺ T cell

responses with high levels of IL4 and IL5 production, cholera toxin can enhance the generation of antigen specific IgG1, IgE and mucosal sIgA responses (Ohmura-Hoshino 2004). Additionally, Shiga toxin (discussed in 1.8.1) has previously been found to provide immunogenicity but not adjuvant activity when given orally to mice (Suckow *et al.*, 1994). However, more recently, Ohmura-Hoshino *et al.*, (2004) assessed a mutant form of shiga toxin 1 (Stx1) (E167Q and R170L; mStx1) and the B subunit of Stx1 (Stx1-B) as possible mucosal adjuvants for the induction of antigen specific mucosal and systemic immune responses in mice. The two distinct forms preferentially induced antigen specific Th2 type CD4⁺ T cells, which in turn generated ovalbumin specific IgG1 and IgA antibodies in the systemic and mucosal components respectively, when given nasally. Recombinant mStx1 and Stx1B supported the generation of antigen specific CD4⁺ Th2 type responses via the production of IL4, IL5, IL6 and IL10 and thereby enhanced antigen specific serum IgG1 and mucosal IgA responses. These findings suggest that these Stx1 derivatives can act as Th2 inducer type adjuvants.

Cholera toxin (CT), a virulence factor of *Vibrio cholera*, induces very strong sIgA and serum IgG antibody responses and long-term immunological memory in mammals (Muir *et al.*, 2000). The evaluation of cholera toxin as an adjuvant in chickens has had mixed success. However the identification of receptors on epithelial cells of the chicken caecum have been reported (Vervelde *et al.*, 1998). CT enhances mucosal secretory IgA (sIgA) and systemic IgG and IgA antibody responses to co-administered protein antigens in mammals. However, it is currently thought unsafe for use in human vaccination due to toxicity in its native form. Various approaches have been undertaken to eliminate the toxic effects of CT whilst maintaining its efficacy as an adjuvant (Hagiwara *et al.*, 1999). Recombinant cholera toxin B chain (CTBC) was employed as a mucosal adjuvant since the cholera toxin A chain (CTAC) subunit is responsible for toxicity (Yoshino *et al.*, 2009). The B subunit alone has been identified as the immune adjuvant agent, at least when administered intranasally or parenterally, (Broeck *et al.*, 2007) diminishing the toxic effects of the A chain. In order to establish molecules that are nontoxic but retain adjuvant effect, investigators have developed nontoxic mutants by substituting a single amino acid in the ADP-ribotransferase active centre, and double mutants by mutating the ADP-

ribosyltransferase active centre of the COOH terminal of CTAC₂ which influences movement of CT to the ER (see section 1.8.2) (Yoshino *et al.*, 2009).

1.8 The Biology of Toxin Adjuvants

Cholera toxin from *Vibrio cholerae* and shiga toxin from *Shigella dysenteriae* are related toxins and members of the AB₅ class of bacterial toxins. The A subunits have catalytic activity and are responsible for toxin related cytotoxicity. During CT intoxication, the A chain activates cAMP production eventually leading to dehydration, while Stx inactivates the cytosolic ribosomes leading to the inhibition of protein synthesis and cell death. However, the A chain requires the B subunits for efficient access to the cell. These pentameric B subunits are responsible for binding to specific glycosphingolipid cell surface receptors. B subunit trafficking is noted to be independent of the presence of the A subunit (Pina and Johannes 2005).

1.8.1 Shiga Toxin (STx)

Infections with bacteria that produce shiga toxins are responsible for widespread disease and the death. These bacteria appear to be the most common cause of hemolytic uremic syndrome (HUS). This can be characterised by thrombocytopenia, microangiopathic hemolytic anemia and renal failure. Shiga toxins are classified into different groups. Shiga toxin (Stx) produced by *Shigella dysenteriae*, being almost identical to shiga like toxin 1 (Stx1) which is produced by *E.coli*. Additionally, shiga like toxin 2 (Stx2) has a similar structure but differences in the genetic sequence give these proteins slightly different properties (Sandvig 2001). The toxicity of Stx is due to the ability of the A subunit (StxA) to block protein synthesis (Kurmanova *et al.*, 2007). The protein has *N*-glycosidase activity and removes one adenosine at position 4324 from the 5' terminus of 28s rRNA, inhibiting the binding of amino-acyl-tRNA to the 60s ribosomal subunit. This leads to the general inhibition of protein synthesis (Sandvig 2001).

Stx is composed of one A moiety, which is non-covalently associated to a pentamer of B subunits via the C terminal of the A chain (Skanland *et al.*, 2009). The B subunits are responsible for the binding to globotriaosylceramide (Gb3) receptors on the cell

surface. The interaction of shiga toxin with its receptors appears quite complex. Two of the binding sites have high affinity for the Gb3 receptors whilst the third binding site is important for the recruitment of receptors (Falguieres *et al.*, 2001). Additionally, not only the carbohydrate portion of the glycolipid molecule is important for toxin binding. The lipid tail plays an important role in toxin-receptor interaction (Sandvig 2001). The length of the fatty acids in Gb3 is important, not only for the affinity of Stx for Gb3 but also for the retrograde sorting of the toxin from endosomes to the Golgi apparatus (Spilsberg *et al.*, 2007). Cytokines (IL1 and TNF), that are produced during infection, either by LPS or induced by the Stx itself, have been shown to induce synthesis of Gb3 receptors in various cell types. Hence increasing the susceptibility to further infection (Sandvig 2001).

The A subunit was responsible for catalytic activity within the cells. However, to exert its enzymatic effect, STBC chain must be released into the cytosol, avoiding lysomotropic delivery (Kurmanova *et al.*, 2007). After binding of Stx to the receptor, the toxin is endocytosed by different endocytic pathways. The ability of the toxin to activate spleen tyrosine kinase (Syk) was an important part of the process of uptake via clathrin dependent endocytosis, (Sandvig *et al.*, 2010; Kurmanova *et al.*, 2007). It has been demonstrated that there is a concentration dependent uptake of Stx via clathrin-coated pits (Shimizu *et al.*, 2007). However, this increased uptake was not found to be dependent on the ability of the B moiety to signal but rather on the presence of the A moiety. Since the A moiety cannot enter cells alone with high efficiency, it was unknown why this should be the case. It has been hypothesised that the ability of the A chain to interact with other proteins at the plasma membrane was the likely cause or that disequilibrium of protein fusion machinery during vesicle fusion may permit small levels of cytosolic access (Sandvig *et al.*, 2010).

Once within endocytic structures, Stx requires transport to the Golgi for cytosolic translocation. It has been documented that rafts appear to be essential for Golgi transport of Stx since extraction of cholesterol inhibits this transport step, similar to previous results found for the protein ricin (Falguieres *et al.*, 2001). Additionally, p38 and protein kinase C activation by Stx has been shown to regulate the trafficking of Stx to the Golgi apparatus (Shimizu *et al.*, 2007). Skanland *et al.*, (2009) documented that p38 inhibitors and siRNA against p38 inhibit Golgi transport and protect HeLa cells from Stx.

Once in the Golgi apparatus, retrograde transport endoplasmic reticulum (ER) has been reported and there appears to be more than one mechanism involved in this process (Sandvig *et al.*, 2010). Both coat protein (COPI) dependent and independent transport routes have been demonstrated (Sandvig *et al.*, 2010). A well-studied retrograde transport system based on the KDEL receptors that traffic between the ER and trans Golgi network is utilised by other toxins such as CT.

The KDEL receptor is responsible for the ER retrieval of proteins containing a C terminal KDEL sequence (Capitani and Salles 2009). Shiga toxin doesn't contain a C terminal KDEL sequence; therefore an alternative route must be adopted, or interaction with a KDEL positive protein could be achieved to meet this end (Sandvig 2001). White *et al.*, (1999) report evidence of Stx1B transport from the trans Golgi network, to the ER by a Rab6 dependent process, that is different from the COPI dependent pathway. However this requires further investigation.

The C terminus of Shiga toxin A chain contains two cysteine residues (Cys242 and Cys261), which form a disulphide bond creating an intramolecular loop. This loop contains the sequence (Arg-Val-Ala-Arg) that is recognised and cleaved by proteases such as trypsin and furin. This gives rise to the catalytically active A1 fragment and the inactive A2 fragment, responsible for B chain binding. Furin induced cleavage occurs most efficiently at low pH (Kurmanova *et al.*, 2007). Furin independent cleavage may also occur after the toxin has passed through the Golgi apparatus. This has been studied using Brefeldin A (BFA). BFA causes the ADP-ribosylation factor (ARF)-GTPase dependant, disassembly of the Golgi apparatus and inhibits the transport of Stx B to the ER (Sandvig 2001). This prevents the catalytically active A1 fragment gaining access to the cytosol via the Sec61p translocon (Sandvig and Deurs 2002).

1.8.2 Cholera Toxin

Vibrio cholerae is a bacterial pathogen responsible for life threatening acute diarrhoea, (cholera) (Broeck *et al.*, 2007). *V. cholerae* are gram-negative bacteria belonging to the family *Vibrionaceae* prevalent in areas with poor sanitation, particularly affecting those with impaired immune systems, such as children, the

elderly and often travellers (Seas and Gotuzzo 1996). Robert Koch first suggested a causative factor protein, cholera toxin (CT) in 1884, which was demonstrated 74 years later (Finkelstein *et al.*, 1963). The genome of *V. cholerae* comprises two chromosomes, the first of which harbour all the virulence factors including CT and the toxin co-regulated pilus (TCP). TCP is utilised during *V. cholerae* colonisation within the small intestine and interacts with receptors on the epithelial lining of the intestine (Sandvig and Deurs 2002). Upon attachment, the bacterium releases the toxin, which is accompanied by the release of hemagglutinin / protease (HA / protease). This enzymatic protein nicks the cholera toxin A chain (CTAC) at Arg192, which yields two discrete CTAC₁ and CTAC₂ subunits. CTAC₁ and CTAC₂ polypeptides are held together by a disulphide bond, (Broeck *et al.*, 2007) and this proteolytic activation of cholera toxin is a requirement for the fully functional catalytically active toxin.

Cytosolic translocation of CTAC₁ leads to increased cyclic adenosine monophosphate (cAMP) levels and translocation was, similar to ST via both the Golgi and ER. Cytosolic translocation of the CTAC₁ peptide mediates cellular intoxication causing increased cAMP levels, which lead to massive electrolyte efflux into the intestinal lumen. The release of high levels of electrolytes causes a mass efflux of water, the net result being severe diarrhoea. This is paralleled by the excretion of the bacteria (Seas and Gotuzzo 1996). Affected individuals are likely to lose 10L of water per day. Consequently, there is a locally increased risk of the horizontal transmission of *V. cholerae* (Broeck *et al.*, 2007). The CTAC₁ subunit is a catalytic polypeptide displaying mono-ADP-ribosylation of the G_{sa} – subunit of a stimulatory GTP binding regulatory protein followed by stimulation of basolateral adenylate cyclase (AC) (De Haan and Hirst 2004).

CT, like STx is an oligomeric protein composed of a heterodimeric A subunit and homopentameric B subunit. The homopentameric B subunits form a ring like structure with a single binding site for the receptor monosialoganglioside (GM1) found on the apical surface of jejunal and ileum intestinal epithelial cells (Broeck *et al.*, 2007). The CTA subunit is extended above the plane of the CTBC ring consisting of two polypeptide chains as previously discussed. CTAC₂ possesses a C terminal KDEL motif

(Lys/Asp/Glu/Leu) retrieval signal which plays a role in retrograde trafficking from the Golgi to the ER.

Cellular uptake and binding of CT occurs via the GM₁ ganglioside receptor on host cell enterocytes. However these receptors are also found on peripheral nerve fibres and other eukaryotic cell types (Edwards *et al.*, 2008). GM1 is a plasma membrane embedded molecule with a ceramide lipid tail and an extracellular branched pentasaccharide chain. The terminal galactose and sialic acid residues of the pentasaccharide are required for binding to the CTB subunits (Edwards *et al.*, 2008). The binding of CTB subunits occurs both via low affinity monovalent interactions of CTBC with the carbohydrate moiety of GM₁ and high affinity interactions of pentameric CTBC polypeptides with multiple GM₁ molecules (Liljequist *et al.*, 1997).

Morphologic studies show that CT preferentially clusters into non-coated membrane invaginations, the caveolae and enters several cell types via non-clathrin coated vesicles (Chinnapen *et al.*, 2007). Further studies demonstrated the use of detergent resistant membrane fractions (DMRS) / lipid rafts during toxic CT entry (Lencer and Saslowsky 2005). Fluorescent microscopy has shown that CT enters cells via a ADP-ribosylation factor (ARF) 6 regulated pathway or even by a fourth route that is dynamin and ARF independent (Ampapathi *et al.*, 2008). Regardless of the internalisation pathway, CT ends up in both early and recycling endosomes and in caveolin containing endocytic intermediates (Lencer and Saslowsky 2005). From these intermediate carriers, CT has been shown to traffic to the Golgi (Sandvig and Deurs 2002). This trafficking step was thought to be independent of Rab7 (regulating late endosomal homo- and hetero-typic fusion (Wang *et al.*, 2011)) and Rab9 (regulating vesicular transport from the late endosome to the trans Golgi network (as monitored by the redirection of mannose-6-phosphate receptors)) GTPases (Chinnapen *et al.*, 2007; Wittmann and Rudolph 2004).

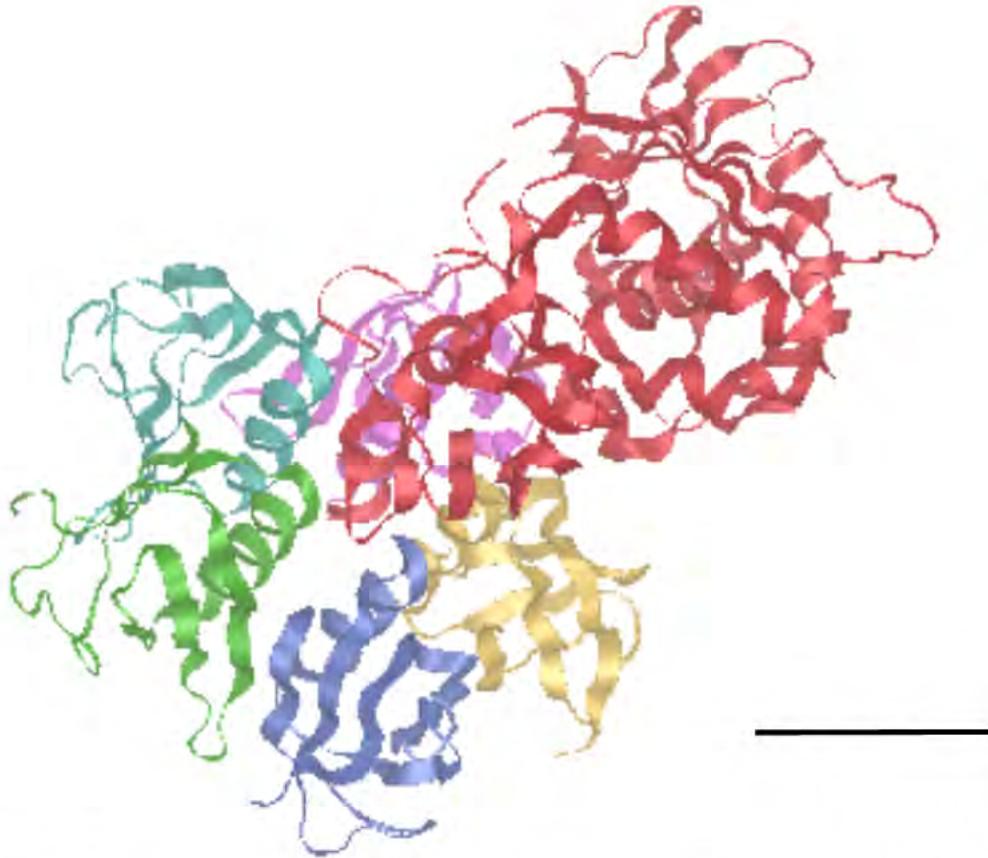


Figure 4. The structure of shiga toxin. The red region represents the catalytically active (A) chain. The green, yellow, blue, turquoise and pink regions represent five (*i.e.* pentameric) cell-binding (B) chains. This data is derived from the Protein Data Bank (1DM0). The size bar represents approximately 20 Å.

Once within the Golgi, CT was subject to ER retrieval. Since the CTAC₂ polypeptide contains a KDEL sequence, this was consistent with findings that link retrograde trafficking to the ER with COPI vesicles (Broeck *et al.*, 2007). Once within the lumen of the ER, the disassembly of CTAC₁ from CTAC₂ and CTB subunits begins (Sandvig and Deurs 2002). This process requires the cleavage of the disulphide bond linking the CTAC₁ and CTAC₂ polypeptides. This was catalysed by the ER resident protein disulphide isomerase and was assisted by Endoplasmic oxidoreductin-1-like protein (Ero1) (Broeck *et al.*, 2007). CTAC₁ is partially unfolded before utilising the ER associated degradation (ERAD) pathway to accomplish retro translocation to the cytosol (Pande *et al.*, 2007). To prevent degradation by the proteasome, the toxin has evolved to have low percentage of lysine residues. These amino acids are critical for

polyubiquitination hence degradation of misfolded or non-required proteins (Sandvig and Deurs 2002).

Once in the cytosol the CTAC₁ subunit can then interact with AC, its intracellular target. Mono-ADP-ribosylation of G_s, a component of the heterotrimeric GTP binding protein that regulates AC activity leading to constitutively active G protein with subsequent continuous activation of AC and a marked increase in the intracellular cAMP levels (Broeck *et al.*, 2007). The increased cAMP levels results in protein kinase (PKA) mediated phosphorylation of the major chloride channel in intestinal epithelial cells, the cystic fibrosis transmembrane conductance regulator (CFTR). The net increase in Cl⁻ release causes the osmotic movement of water into the intestinal lumen resulting in severe diarrhoea (Broeck *et al.*, 2007). However, the ability of CT to transcytose across polarized intestinal epithelial cells could be exploited for its potential to deliver antigens of IBDV.

1.8.2.1 Cholera Toxin Transcytosis

Transcytosis is the process by which cargo, internalised at one side of the cell can be transported (by vesicles) to the other side of the cell *i.e.* from apical to basolateral extracellular compartments (Matveer *et al.*, 2001). CT acts directly on polarized intestinal epithelial cells by binding specific glycosphingolipid receptors on the apical membrane and subsequently activating adenylate cyclase on the cytoplasmic face of the basolateral membrane (Broeck *et al.*, 2007). The mechanisms by which CT gains access to the *lamina propria* remain uncharacterised (Matveer *et al.*, 2001).

Caveolae have been thought to be involved in fluid phase uptake and transcytosis for several decades. Caveolae and lipid rafts are enhanced in the ganglioside GM₁, the endogenous receptor for CT. Multiple groups have demonstrated that caveola lipid rafts mediate CT induced signalling in human intestinal Caco-2 and T84 cells (Matveer *et al.*, 2001). Thus if cholera toxin B chain is fused in frame with an antigen to a specific animal disease, the construct should be non toxic, provide adjuvant activity and facilitate uptake by intestinal epithelial cells, facilitating the antigens

delivery to the *lamina propria* to induce a specific mucosal and systemic immune response.

Having identified a suitable set of proteins with the potential to deliver an antigen to APCs within the GALT, it was necessary to identify preformulation technologies that would be capable to delivering the attenuated toxin-VP2 antigen fusion to the ileum, such as an enteric protein delivery system.

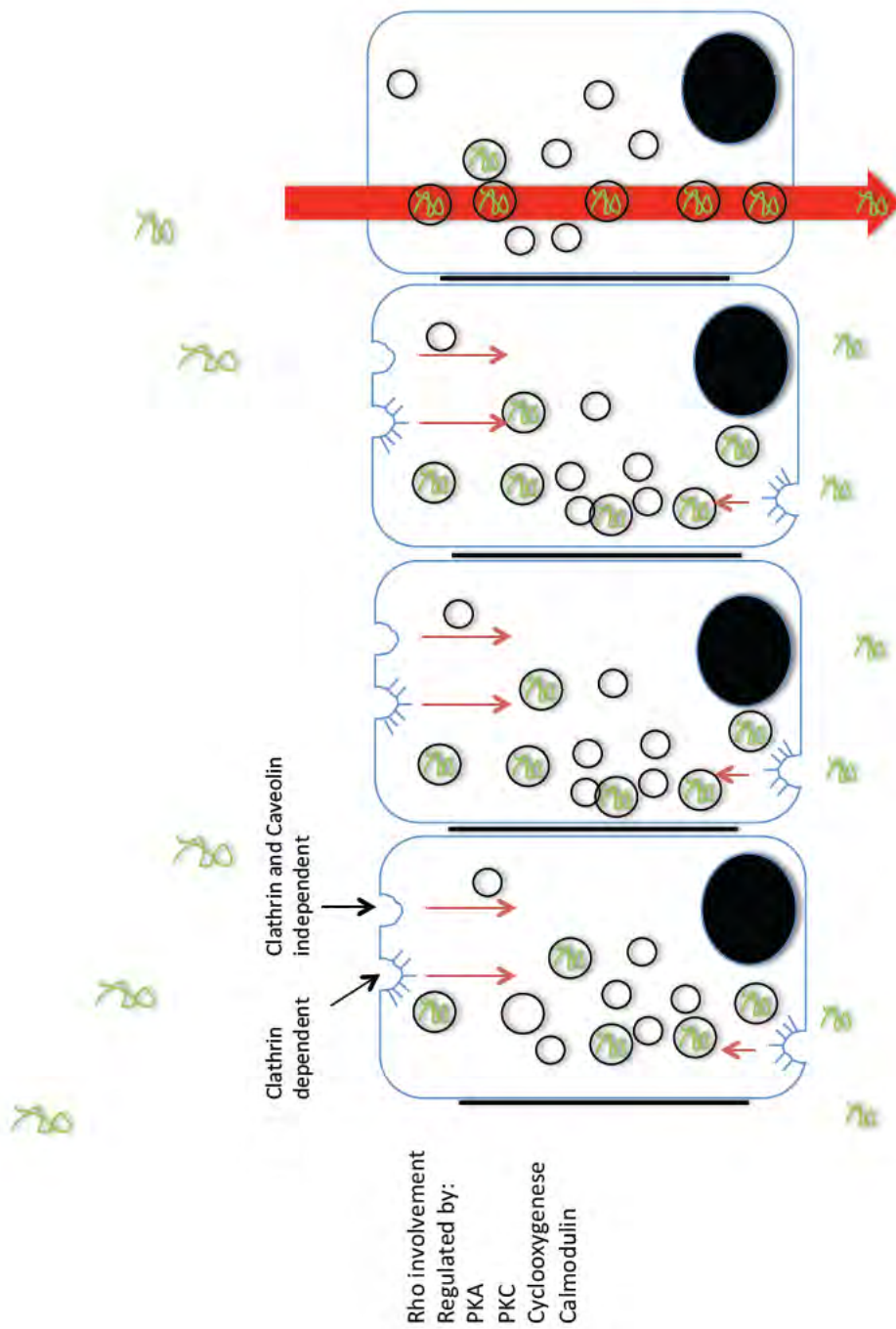


Figure 5. AB₅ toxins transcytosis across polarized epithelial cells (Adapted from Sandvig and Deurs 2005).

1.8.3 The Proposed Enteric Protein Delivery System

A nanoparticulate oral antigen delivery system was investigated herein. This system was built around a solid core of ~500nm silica. The silica, carrying a net negative charge, allowed positively charged proteins to adsorb onto its surface via electrostatic interactions (Sameti *et al.*, 2003). By decreasing the pH of an appropriate buffer, bringing the protein close to its isoelectric point, it was previously shown that proteins will adhere to the silica surface in a reversible manner (Eltohamy *et al.*, 2011), however little was known about the conformation of the protein following release. The system was then encapsulated with a variety of fatty acids. The fatty acid remained bound to the solid core drug delivery system (SCDDS) at low pH, protecting the antigen from low pH and proteases in the ventriculus, whilst releasing both the fatty acid and protein in the high pH of the small intestine. This was facilitated by the ionisation of the carboxylic acid residues (Thurikill *et al.*, 2006). Since the silica contains well-defined silanol groups at the surface, the silica nanoparticle offers many possibilities for surface modification in order to optimise the release of a protein for a particular drug delivery system (Sameti *et al.*, 2003).

The solubilisation of fatty acid to encapsulate the SCDDS has been performed by other researchers (Maheshwari *et al.*, 1992). A supercritical phase negates the need for high temperature, extreme pH or other environmental conditions, which may release and denature the immobilised protein. The subsequent release of protein load, post fatty acid dissolution has been documented (Eltohamy *et al.*, 2011). Thus it was hypothesised that the enteric protein delivery system could protect the protein through the GIT and release its “cargo” *i.e.* a recombinant antigen-toxin B chain fusion prior to toxin mediated transcytotic exit of the GIT and presentation of the antigen within the *lamina propria* via antigen presenting cells (figure 6) initiating a mucosal and systemic immune response.

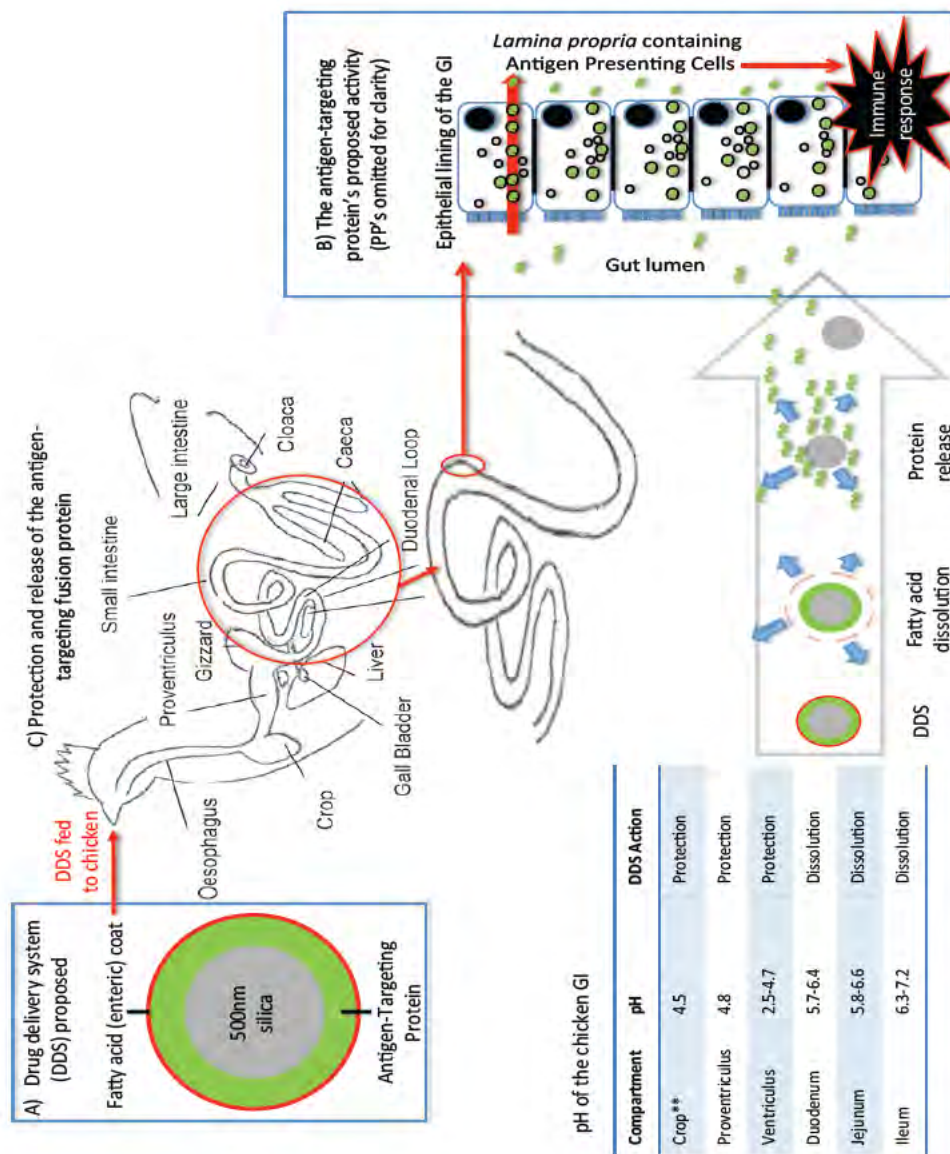


Figure 6. Proposed triggers for SCDDS activity and proposed responses necessary for the delivery of an antigen to the APCs of the *lamina propria* via an oral delivery route.

1.9 Aims of this Thesis

The aims of this thesis were: (1) To produce a model recombinant protein (GST-GFP) by: sequencing the plasmid encoding the protein, creating a map of the plasmid from the sequence data, expressing the protein, optimising protein expression and enriching the protein from bacterial lysate. (2) To characterise GST-GFP by: coomassie staining following resolution by SDS-PAGE, immunoblotting following resolution by SDS-PAGE, mass spectrometry, fluorescent spectroscopy and circular dichroism. (3) To assay protein enzymatic stability using a Protease K enzymatic assay and an *In vitro* digestion assay. (4) To characterise the SCDDS by: Scanning electron microscopy, bradford and western immunoblotting followed by densitometry for characterisation of protein on / off rates, coating of SCDDS with fatty acids by small angle neutron scattering (SANS), protection of protein cargo by *in vitro* digestion assay and incubation with protease K and conformation of released protein by CD. (4) To sub-clone toxin-antigen constructs to create recombinant genes: CTBC, VP2, STBC, CTBC GFP, VP2-CTBC, VP2-STBC and STBC GFP. (5) To analyse the toxicity of recombinant proteins using the MTT assay. (6) To analyse the transcytosis capabilities of recombinant proteins by: maintaining transepithelial electrical resistance of Caco-2 cell monolayers grown on transwell membranes, using appropriate controls such as inulin, Western immunoblotting the basal chamber for presence or absence of recombinant proteins (CTBC-VP2 and STBC-VP2).

Chapter 2: Materials and Methods

2.1 Materials

2.1.1 Equipment

The UV transilluminator, orbital shaker, micro titre plate reader and laminar flow, cell culture class II hood (Envair) was supplied by ThermoFischer, (Loughborough, UK). The sub-cell GT agarose gel electrophoresis systems, mini-PROTEAN® tetra cell, mini trans-blot, electrophoretic transfer cell and powerPac™ HC power supply were supplied by BioRad (Hemel Hempstead, UK). The French press (cell disrupter), centrifuges (Heraeus fresco 21, Sorvall® RC 6 Plus, Sorvall® Discovery M120), and the dry block heater (Talboy) were supplied by Fisher Scientific (Loughborough, UK). The matrix assisted laser desorption ionisation time of flight (MALDI-TOF) mass spectroscopy was on an Autoflex MALDI-TOF system (Bruker, Coventry, UK). The freeze dryer (Wizard 2.0 VirTis) was supplied by SP Scientific (Suffolk, UK). Circular dichroism instrument (Chirascan™) supplied by Applied PhotoPhysics, (Surrey, UK). Microscope (Nikon 90i) was supplied by Nikon (Surrey, UK). Zeta seizer (Nano Z) was supplied by Malvern (Worcestershire, UK). Transepithelial resistance measurements were recorded using Millicell ERS-2 supplied by Millipore (Darmstadt, Germany).

2.1.2 Reagents

Thiazolyl blue tetrazolium bromide (MTT reagent), isopropyl β-D-1-thiogalactopyranoside (IPTG), sodium azide, ethidium bromide (EtBr), nitrocellulose membrane (0.2µm pore size, 33cm × 3m), bovine serum albumin (BSA) were purchased from Sigma. Coomassie brilliant blue G-250, acrylamide, bis acrylamide, ammonium persulphate (APS), 2-mercaptoethanol (BME), sodium dodecyl sulphate (SDS) were purchased from BioRad (Hemel Hempstead, UK). Tris-base, ampicillin, glycerol, imidazole, NaCl, glycine, agarose were purchased from Fischer (Leicestershire, UK). Ni Sepharose (TM high performance) was supplied from GE healthcare (Buckinghamshire, UK).

2.1.2.1 Specialised Reagents

The following reagents and enzymes were purchased as molecular biology grade products from Sigma (Dorset, UK): glucose, isopropanol, tris-base, tris-Cl, chloroform, lithium chloride, EDTA (di-sodium salt), glycerol, agarose, sodium hydroxide, SDS, sodium chloride, potassium acetate, ammonium acetate, phenol: chloroform: isoamyl alcohol (25:24:1): pancreatin: porcine bile: myristic acid: stearic acid: lauric acid: palmitic acid: inulin-FITC: trichloroacetic acid: guanidinium HCl: acetone: pepsin. Silicon (IV) oxide, powder, 0.5 micron, was supplied by Alfa Aesar (Lancashire, UK).

2.1.2.2 Antibodies

Table 5. List of antibodies and suppliers.

Ab 1°	Supplier	2° WB	Supplier	2° IF	
GFP	Invitrogen (Paisley, UK)	Goat Anti-Rabbit IgG - HRP	Invitrogen (Paisley, UK)	N/A	N/A
6 histidine	Invitrogen	Goat Anti-Mouse IgG2a (γ 2a), Horseradish Peroxidase Conjugate	Invitrogen (Paisley, UK)	Alexa Fluor® 488 Goat Anti-Mouse IgG	Invitrogen (Paisley, UK)
EEA1	Invitrogen	Goat Anti-Mouse IgG2a (γ 2a), Horseradish Peroxidase Conjugate	Invitrogen (Paisley, UK)	Alexa Fluor® 488 Goat Anti-Mouse IgG	Invitrogen (Paisley, UK)
GST	Abcam (Cambridge, UK)	Goat Anti-Rabbit IgG - HRP	Invitrogen (Paisley, UK)	N/A	N/A
CTBC	Abcam (Cambridge, UK)	Goat Anti-Mouse IgG2a (γ 2a), Horseradish Peroxidase Conjugate	Invitrogen (Paisley, UK)	Alexa Fluor® 488 Goat Anti-Mouse IgG	Invitrogen (Paisley, UK)
STBC	Abcam (Cambridge, UK)	Goat Anti-Rabbit IgG - HRP	Invitrogen (Paisley, UK)	Texas Red® Goat Anti-Rabbit IgG	Invitrogen (Paisley, UK)
Actin	Abcam (Cambridge, UK)	Goat Anti-Mouse IgG2a (γ 2a), Horseradish Peroxidase Conjugate	Invitrogen (Paisley, UK)	Alexa Fluor® 488 Goat Anti-Mouse IgG	Invitrogen (Paisley, UK)
Villin	Abcam (Cambridge, UK)	Goat Anti-Rabbit IgG - HRP	Invitrogen (Paisley, UK)	Texas Red® Goat Anti-Rabbit IgG	Invitrogen (Paisley, UK)
V5	Abcam (Cambridge, UK)	Goat Anti-Rabbit IgG - HRP	Invitrogen (Paisley, UK)	Texas Red® Goat Anti-Rabbit IgG	Invitrogen (Paisley, UK)
GM130	Abcam (Cambridge, UK)	Goat Anti-Mouse IgG2a (γ 2a), Horseradish Peroxidase Conjugate	Invitrogen (Paisley, UK)	Alexa Fluor® 488 Goat Anti-Mouse IgG	Invitrogen (Paisley, UK)
TGN46	Abcam (Cambridge, UK)	Rabbit Anti-Sheep IgG - HRP	Invitrogen (Paisley, UK)	Alexa Fluor® 488 Donkey Anti-Sheep IgG	Invitrogen (Paisley, UK)

2.1.3 Organisms and Cell Lines

Chemically competent *E.coli* BL21*DE3 and *E.coli* TOP10 were supplied by Invitrogen (Paisley, UK). Vero cells were a kind gift from Professor Robert Piper at the University of Iowa, USA (ECACC MA104). Caco-2 cells (ECACC 09042001). Dimethyl sulphoxide (DMSO), [3-(4,5-Dimethylthiazol-2-yl)-2,5-diphenyltetrazolium bromide] (MTT), poly (ethyleneimine) (PEI) ($M_n \sim 60,000$) and dextran (M_r 35,000-45,000) were from the Sigma chemical company (Dorset, UK). Dulbecco's-Minimal Essential Medium (D-MEM), foetal Gibco (Paisley, UK) supplied bovine serum, Trypsin-EDTA, Penicillin-Streptomycin-Glutamine. For transcytosis studies, Caco-2 cells were grown on 24 well Transwell plates supplied by Millipore.

2.1.4 Stock Solutions

Yeast extract and Tryptone digest media (2xYT): The bacterial growth medium (2xYT) was prepared by mixing Bacto-tryptone (Fischer, Leistershire, UK) (16g) with Bacto-yeast extract (10g) and NaCl (5g) (Fischer, Leistershire, UK). This was then added to de-ionised distilled water and the final volume adjusted to 1000mL.

Tris-HCl 0.5 M (pH 6.8): was prepared by mixing 60g of tris base in 800ml of deionised water and pH of the solution was adjusted to 6.8 with 6N HCl and the final volume was made up to 1000ml with de-ionised water.

SDS-PAGE resolving gels: Different percentages of resolving gels were prepared by mixing specific volumes of 1.5M tris- buffer (pH 8.8), 10% (w/v) sodium dodecyl sulphate (SDS), de-ionised water, 10% ammonium persulphate (APS) and *N, N, N', N'*-tetramethylethylenediamine (TEMED).

SDS-PAGE stacking gel: was prepared by mixing de-ionised water (3.4ml), acrylamide/bis (0.66ml), 1.5 M tris buffer (pH 6.8) (0.83ml), sodium dodecyl sulphate (10% (w/v)) (50 μ l), ammonium persulphate (50 μ l), *N, N, N', N'*-tetramethylethylenediamine (TEMED) (10 μ l).

SDS running buffer (10x): was prepared by mixing tris base (30.2g), glycine (188g), sodium dodecyl sulphate (10g) and adjusting the volume to 1000ml with de-ionised water.

Sample buffer: was prepared by mixing 0.5M Tris-HCl (pH 6.8) (1ml), glycerol (0.8ml), sodium dodecyl sulphate (10% w/v) (1.6ml), 2-mercaptoethanol (BME) (0.4ml), bromophenol blue (1% w/v) (0.4ml), and de-ionised water (3.8ml).

SDS (10% (w/v)): was prepared by adding SDS (10g) to de-ionised water to a final volume of 100 ml.

Coomassie brilliant blue R-250 staining solution: was prepared by mixing Coomassie brilliant blue R-250 (0.25g) with methanol (40ml), de-ionised water (50ml) and glacial acetic acid (10ml).

Coomassie de-staining solution: methanol (40ml) was added to de-ionised water (50ml) and to this, glacial acetic acid (10ml) was added.

Towbin electro-blotting buffer: was prepared by adding tris-base (3g) and glycine-HCl (14.08g) to de-ionised water (800ml) and methanol (200ml). To this solution SDS (5ml 10% (w/v)) was added and the pH adjusted to 8.3. The volume was then brought to 1000ml with de-ionised water.

Western immunoblotting blocking solution: was prepared by adding non-fat dried milk (5g) to 1x PBS (100 ml final volume) containing Tween-20 (0.01% (v/v)).

Tris-acetate EDTA (TAE) (50x) buffer: was prepared by mixing tris-base (242g) with glacial acetic acid (57.1ml) and 0.5M EDTA (pH 8.0) (100ml). The volume was then adjusted to 1000ml with deionised distilled water.

Phosphate buffered saline (PBS) (10x): was prepared by added NaCl (80g), KCl (2g), Na₂HPO₄ (14.4g) and KH₂PO₄ (2.4g) to 800ml-distilled water. The pH was then adjusted to 7.4 before adjusting the volume to 1000ml with distilled water. 1 x PBS was used for experiments and autoclaved appropriately.

Blocking buffer for immunofluorescence: was prepared by adding 1% FCS (v/v) to PBS.

Mounting media: was prepared by dissolving 10mg of N-propyl gallate in 1ml PBS by heating in the microwave, taking care not to boil. Following, 100µl glycerol was added and the media was ready to use.

2.2 Methods

2.2.1 Cell Culture and Viability Techniques

Cells were maintained in an atmosphere of 5%(v/v) CO₂ at 37°C in a humidified CO₂ cell culture incubator, and these conditions were defined as standard. All manipulations were carried out aseptically in a class II tissue culture hood (Envair, Thermo, Loughborough, UK). All materials added to cell cultures were sterile, osmotically balanced and heated to 37°C. The cells were maintained in 75cm² tissue culture treated, cantered neck flasks with vented (0.2µm) tops (Sigma, Dorset, UK).

For cells grown as a monolayer, the medium was removed by aspiration and the cells washed twice with sterile phosphate buffered saline (PBS) (10ml). Cells were removed from the flask by the addition of sterile 1x trypsin, ethylenediaminetetraacetate (EDTA) (1ml). After incubation (approximately 3-5min) and gentle agitation, the monolayer was examined microscopically (x100) using an inverted microscope (90i, Nikon, Surrey, UK). Once the majority of cells were seen to be in suspension, media (9ml) containing 10% foetal calf serum (FCS) was added to neutralise the trypsin. Aliquots of the suspension were used to seed further flasks at a density dictated by the generation time (and hence split ratio) of the cell line. Residual, unused cells were autoclaved. Suspension cultures were split by removing and discarding a proportion of the culture by aspiration. The medium that was removed was then replaced with fresh media. The proportion of the cultures that was discarded was dictated by the split ratio of the cell line.

2.2.2 Cell Bank

A stock of cells were stored frozen at -80°C . First 5×10^6 cells/ml were prepared in 90% (v/v) FCS and 10% (v/v) dimethylsulphoxide (DMSO), previously sterilised by filtration (0.2 μm sterile filter (cellulose acetate supplied by Gilson, Bedfordshire, UK). Cells were disaggregated by passing them gently 3 or 4 times through a sterile 21 gauge needle, taking care not to damage the cells by generating an excess of shear force. A volume of 1-1.6ml of suspension was then transferred into a sterile cryogenic vial and this was sealed in an insulating, polystyrene box and placed at -80°C for 18h insuring a uniform drop in temperature ($\sim 1^{\circ}\text{C}/\text{min}$). Following this the vials were left at -80°C . To recover cryogenically preserved cells the vials, left with the lid one quarter turn open, were placed at 37°C inside a 30ml sterile universal bottle. This was left until the preparation was visually seen to thaw (approximately 5min). Following this the suspension was subject to centrifugation at $1\ 500 \times g$ for 10min at 22°C . The supernatant was then removed and the cells re-suspended in the appropriate cell culture media (10ml) and used to seed a 75cm^2 flask.

2.2.3 Evaluation of Cell Viability by Trypan Blue Exclusion

Trypan blue (Sigma, Dorset, UK) was supplied as a sterile 4% (w/v) solution in PBS and was first diluted 1:1 with PBS to a concentration of 2% (w/v). One volume of 2% (w/v) Trypan blue solution (in PBS) was added to a 20 μl aliquot of the cell suspension. The average number of blue (dead) and clear (viable) cells was estimated using an improved Neubauer haemocytometer. The number of cells in a known volume (0.1 x 0.1 x 0.1mm) was then recorded. The percentage of viable cells was then calculated as well as the total number of viable cells/ml (cells/ml = N° . cells in 0.1 x 0.1 x 0.1mm volume x dilution factor (from stock) $\times 10^4$). Care was taken not to overload the haemocytometer and the mean of five samples was used when estimating cell number.

2.2.4 MTT Assay to Assess Cell Viability

Caco-2, Vero and B16 adherent cells were seeded into separate, sterile, flat-bottomed 96 well, tissue culture treated plates at a density of 5×10^4 cells/well. B16 cells were, on account of their rapid generation time (Hart 1979), seeded at 1×10^4 cells/well). The culture was then left to grow for 24h in standard conditions. Prior to the end of the 24h incubation period, the materials to be assayed for toxicity (proteins) were dissolved in fresh culture medium. This was used to replace the existing media covering the cells after the designated incubation period. Typically concentrations of protein between 0-5 mg/ml were used, taking care to control for any rebuffing of the culture media. The test cultures were then incubated using standard conditions for 72h. During this time, 250mg of 3-[4,5-dimethylthiazol-2-yl]-2, 5-diphenyltetrazolium bromide (MTT) was dissolved in 50ml of PBS and filter sterilised using a 0.2 μ m filter. After the 72h incubation, 20 μ l of MTT stock was added to each well giving a final MTT concentration of 833 μ g/ml (in the media). The experiment was then left to incubate for a further 5h, again using standard conditions. After a further incubation period of 5h the culture medium was removed and 100 μ l of optical grade DMSO was added to each well. The cultures were left for 1h in DMSO and the plates were read at 550 nm using a micro titre plate reader. The results were expressed as viability (%) against polymer or protein concentration. Care was taken to control for any interaction between the assay component (other than the cells) and the MTT, especially those that might give rise to false negative results. Positive and negative controls were also performed using PEI and dextran respectively (Fischer *et al.*, 2003).

2.2.5 Preparation, Maintenance and Thawing of Frozen “Stock” Bacterial Cultures

Recombinant genes that were successfully cloned and sequenced have been entered into a laboratory database for documentation purposes. These clones have been given numbers and records are kept on expression levels, vector properties and selectable marker. Clones were stored in the -80°C freezer (Forma, Thermo, Loughborough). Similarly, cell lines have been placed in databases and numbered accordingly.

2.2.6 Growth of Transformed *E.coli*

A sterile aliquot of 2xYT media (10ml) containing ampicillin (50µg/ml) was prepared containing the transformed *E.coli*. This was cultured overnight at 37°C. Next 2xYT media was prepared, and the overnight culture added. This was left to grow at 37°C until the optical density (600nm) reaches approximately 0.6 (4h at 37°C) in a orbital shaker set at 180rpm. IPTG was added to the culture and was incubated at 37°C for a further 3 hours prior to french pressing.

2.2.6.1 Growth of *E.coli* Using Heat Shock Protocol

A sterile aliquot of 2xYT media (10ml) containing ampicillin (50µg/ml) was prepared and used as a starting culture (inoculum) for a larger 1000 mL culture or to amplify plasmids prior to their isolation. Next 2xYT media was prepared for the final plasmid culture and the starting culture (10ml) was inoculated by aseptically transferring 5ml of the overnight culture into the fresh media. This was left to incubate at 37°C until the optical density (600nm) reaches approximately 0.6 (4h at 37°C). The culture was left at 4°C overnight before heat shocking at 42°C for 2h. The bacterial culture was then chilled to 0°C rapidly and induced with IPTG. Growth was allowed to continue for 4h at 37°C, 180rpm before centrifuging the culture at 6000xG for ten minutes.

2.2.6.2 Mini-Scale Protein Production From *E.coli*

Prior to sequencing, a reasonably quick check of protein expression was performed to ascertain whether proteins could be produced from the corresponding plasmid. A sterile aliquot of 2xYT media (10ml) containing ampicillin (50µg/ml) was prepared and was used as a inoculum. Of this, 100µl was added to fresh medium containing ampicillin (50µg/ml) and left incubating for 75 minutes at 37°C, 180rpm. 1M IPTG (1.5µl) was added. The culture was left to incubate for a further 2h before a brief centrifuge at 6000xG for 2 minutes. The pellet had 180µl Laemmli buffer containing 20% BME added to re-suspend the pellet before running on SDS-PAGE gel.

2.2.7 Isolation of Plasmid DNA from *E.coli* Cultures

Isolation of plasmid DNA was performed using a Qiagen plasmid mini kit (catalogue number: 12123) (Crawley, West Sussex, UK) as per the manufacturers protocol. Briefly, 3ml of culture containing the specific plasmid was centrifuged at 6,000xG for one minute. The supernatant was removed and the pellet aspirated in P1 (re-suspension buffer). The protocol was followed and resultant plasmid eluted from the column using 30µl sterile water. Yields were analysed using the Nanodrop (2000c, Thermo, Loughborough).

2.2.8 Polymerase Chain Reaction (PCR)

Following plasmid retrieval, specific sequences were amplified using DNA, sequence specific primers. For example to check that the plasmid was the correct plasmid before undergoing further work. In a 25µl reaction, 1µl of template (1ng/µl) was placed inside a PCR tube with 0.3µl of each primer, 12.5µl green taq (Invitrogen, Paisley, UK) and 10.9µl of sterile water. The PCR tubes were then inserted into a PCR machine and put on an appropriate annealing and extension time (table 7). This depends upon the thermal midpoint of primers and length of amplified DNA. The amplified DNA was run on a gel electrophoresis for separation and analysis of size and integrity (section 2.2.8.1).

2.2.8.1 Gel Electrophoresis

Electrophoresis gels were made by the addition of 1g agarose (Sigma, Dorset, UK) to 100ml deionised water. This was heated to dissolve the agarose and 10µl of gel red added. The agarose gel was poured into a tank and allowed to set for 45 minutes. DNA was added to the wells along with DNA loading dye and DNA ladder as a control and marker in a separate well. DNA was run at 70 volts for 45 minutes but time and voltage increased or decreased depending on sample size. Gels were visualised using UV transilluminator.

2.2.8.2 Recombinant PCR

For the amplification and annealing of two recombinant genes, PCR was performed on specific plasmids with specific primers for the 5' and 3' terminus of the gene. The primers were designed so that the 3' terminal primer for joining the two genes had a flanking region of the N-terminus of the following gene. And as such, the 5' terminal primer for the following gene had a region that was complimentary to the first gene before the sequence the primer was specific to on that gene. The 5' terminal primers for the first gene were designed in the standard way, as were the 3' terminal primers from the second gene. The flanking primers were designed to be 42 nucleotides in length whereas the end primers were 21 nucleotides in length. The PCR reaction had several steps. The first reaction was to amplify gene one, with the usual 5' primer and the 3' primer that had the flanking region. The second PCR was performed to amplify the second gene using the usual 3' primer and the fusion 5' primer. Finally a third PCR reaction was performed, using the amplified product in reactions 1 and 2 as templates, and using the usual 5' and 3' primers to link the two genes together. These recombinant genes were then inserted into a pET151/D TOPO expression cassette (section 2.2.8.3).

2.2.8.3 Sub-cloning into pET151 Expression Cassette

Once suitable recombinant PCR's were obtained, they were inserted into pET151/D expression cassettes (Invitrogen, Paisley). The stoichiometric concentrations were calculated between plasmid vector and insert PCR product to ensure the correct amount of DNA was used, (molar ratio 0.5:1 PCR : TOPO). The protocol was followed; briefly, 1µl PCR product was placed inside a sterile PCR tube, with 0.5µl salt solution, 0.5µl vector, 1µl sterile water. This was incubated at room temperature for between 5 – 20 minutes (depending on the length of the insert). The sample was then placed on ice before transformation. The cloning reaction was added to 10µl *E.coli* TOP10 and left on ice for 20 minutes. Cells were then heat shocked at 42°C for 30 seconds before being put back on to ice. S.O.C (Invitrogen, Paisley, UK) (100µl) was added to the cloning reaction, and the sample put at 37°C for one hour shaking at

180rpm. The cloning reaction was spread aseptically onto agar plates containing the selectable marker and placed inside the incubator at 37°C overnight.

2.2.8.4 Evaluation of *E.coli* Clones for Plasmid Insertion

Following directional cloning, colonies were picked from a 2xYT agar plate, and placed in a PCR tube whilst also being patched on to a fresh agar plate for re-growth. Appropriate primers were used, specific for the vector and the insert, using the optimised annealing temperature. PCR was run at an extension time specific for gene size. PCR products were then run on a 1% agarose gel (w/v) containing 0.0025% gel red (v/v) for 45 minutes at 70 volts.

2.2.9 DNA Sequencing

Plasmid sequencing was performed by: DNA Sequencing and Services (University of Dundee). A concentration of 600ng of plasmid per reaction with 3.2µM per reaction was sent. Data was analysed using DNASTAR® software (2.2.9.1).

2.2.9.1 Analysis of Sequence Data

Upon the return of sequence data from DNA Sequencing and Services, University of Dundee, sequences were aligned in Seqman, (DNASTAR software, Madison, Wisconsin, USA). The software allows the alignment of homologous regions of nucleic sequence. A strategic view provides an insight into overlap of sequence data. Ensuring the depth of coverage is adequate, the alignment view was accessed. Upon satisfaction that sequence is homologous to theoretical sequence data, the sequence is put into the theoretical plasmid map and labelled as sequenced region.

2.3 Production of GST and GST-GFP proteins

E.coli MC1061 containing the pGEX 3X plasmid, that encoded GST-GFP was cultured overnight in 10ml of 2xYT (ampicillin) media. This was used as an inoculum the following morning, to induce growth within a fresh 1000ml culture of 2xYT

(ampicillin) media. *E.coli* were cultured for 3 hours before induction of protein expression with 500µl 1M IPTG. Growth was allowed to continue for a further 3 hours before centrifugation of bacteria into a pellet at 6000xG. The pellet was re-suspended in PBS and was subject to lysis using a french press (section 2.3.1).

2.3.1 Lysis of Bacteria

Re-suspended bacteria (with 200mM sodium azide and 100mM protease inhibitor tablets) were placed inside the metal cylinder and the lid and plunger put into place. The bacteria were subjected to 15,000 PSI pressure before being moved through the aperture and out of the system. The process was repeated six times before centrifugation to remove membranes and nuclear material (section 2.3.2).

2.3.2 Sedimentation of Lysed Bacteria to Remove Membrane and Chromatin

Lysed bacteria containing sodium azide (200mM), were placed inside a 40ml centrifuge tube and placed inside an SS34 rotor (Thermo, Loughborough). The samples were centrifuged at 20,000xG (4°C) for 20minutes. Following centrifugation the supernatant (containing the proteins) were purified on glutathione conjugated 4b sepharose beads (section 2.3.3).

2.3.3 Purification of Recombinant GST Containing Proteins

Glutathione conjugated 4b sepharose beads (2ml) (GE Healthcare, Bucks, UK) were placed inside a column and washed with PBS (10ml) to remove storage ethanol buffer. Bacterial supernatant (section 2.3.2) was run over the column twice by gravity flow. The column was washed again with PBS (10ml) to remove any non-specifically bound proteins before GST-GFP was eluted from the beads. For elution, 100mM reduced glutathione (pH8-9) in PBS was added and green fractions collected for dialysis (section 2.3.3.1).

2.3.3.1 Protein Dialysis

Purified protein was dialysed in dialysis (cellulose) tubing (Sigma, Dorset, UK) by placing inside an equilibrated tube and tided at either end. The tube containing the protein was placed inside 4L of PBS with a magnetic stirrer and stirred at 4°C for three hours. The PBS was changed and fresh PBS added, this was performed a total of three times. The protein was then removed from the tubing and placed inside a sterile eppendorf tube. Proteins were then characterised by SDS-PAGE (section 2.4), Bradford (section 2.3.3.2) and western immunoblot (section 2.4.2) prior to their experimental use.

2.4 Protein Characterisation by SDS-PAGE

Recombinant proteins were analysed for apparent molecular weight, degradation and purity by SDS-PAGE, Coomassie staining and western immunoblot. SDS-PAGE gels (10% acrylamide (w/v)) were cast inside 10mm glass plates. Lamellae buffer was added to the recombinant proteins before loading into the wells. Gels were typically run at 200 volts for 45 minutes but care was taken not to over run the proteins off the end of the gel. Gels were then either subject to Coomassie staining (section 2.4.1) or western immunoblot (section 2.4.2).

2.4.1 Coomassie Staining

SDS-PAGE gels were removed from the glass plates and placed into a plastic dish containing 10ml of Coomassie Brilliant Blue (0.25%). The tray was covered to prevent evaporation and placed on a rotating platform at room temperature for 4 hours. The gel was then de-stained using de-staining solution (section 2.1.4) for 3-4hours on the rotating platform. Prior to drying, the gel was placed inside PBS containing 5% glycerol (v/v) for five minutes to help reduce the likelihood of cracks. Gels were then dried between two layers of wetted cellulose acetate membranes (Sigma, Dorset, UK).

2.4.2 Western Immunoblot

Separated SDS-PAGE gels were placed inside a transfer cassette (between two sponges, Whatman paper and nitrocellulose membrane) and placed inside a transfer tank (Biorad, Herts, UK) with an ice pack to cool the buffer. Towbin buffer was added (section 2.1.4) and the gel was transferred on to the nitrocellulose membrane at 400mA for 60 minutes. Following transfer, the nitrocellulose membrane was removed from the cassette and washed with sterile PBS prior to being incubated with blocking buffer (section 2.1.4) at 37°C, rotating in an orbital shaker for 60 minutes. The blocking buffer was removed and fresh blocking buffer added (3ml) to this the appropriate dilution of primary antibody was added. The membrane was again incubated at 37°C for 1hour in the orbital shaker. The nitrocellulose membrane was then washed in PBS tween 20 (0.01% v/v) a total of three times for five minutes per wash. Following, the membrane was put back into fresh blocking buffer with the appropriate dilution of secondary antibody (table 1) for one hour at 37°C in the orbital shaker. After one hour, the membrane was removed and again washed in PBS tween 20 (0.01% v/v). The gel was then developed (section 2.4.2.1).

2.4.2.1 Developing the Western Immunoblot

The membrane that had been previously incubated with primary and secondary antibody, and washed in PBS tween 20, was covered in ECL reagents 1 and 2 (GE healthcare, Bucks, UK) and left for one minute. Following incubation, the blot was covered in cling film and placed inside an expression cassette. An X-ray film (Thermo, Loughborough, UK) was placed over the top of the blot, and the cassette closed. The cassette remained closed for the appropriate exposure time (usually between 10 seconds and 5 minutes). Following the appropriate exposure time, the X-ray film was inserted into an X-ray developer (ECOMAX supplied by PROTEC, Germany), which subsequently runs the film through an array of developing, stopping and fixing solutions image the film. The films were then scanned. In some instances the quantities of protein loaded were analysed using ImageJ software to allow the counting of pixels relative to controls that were inside the linear range (section 2.4.2.2).

2.4.2.2 Densitometry to Quantify Protein Concentration

X-ray films were scanned (section 2.4.2.1) and jpeg images saved to the computer. These images were opened in the software program ImageJ (NIH, USA) and boxes drawn around individual bands. Since a control protein sample was run, of known concentration, the pixel count was compared between the control and the other bands. This gave information into the approximate concentration in the sample band, which could be used for mass balance equations.

2.4.3 Characterisation of GST-GFP by Mass Spectroscopy

Purified GST-GFP (5mg/ml) was salt exchanged by dialysis (section 2.3.3.1) into 0.9% NaCl and given to Prof. Frank Pullen (University of Greenwich). The sample protein was kindly taken to Pfizer, (Sandwich, UK) and analysed by performing a tryptic digest prior to using an Autoflex MALDI-TOF system (Bruker, Coventry, UK). Sequences obtained were mapped back to GST and GFP regions and an absolute mass obtained.

2.4.4 Evaluation of GST-GFP Stability By Affinity Isolation

GST-GFP (500µg) (in PBS) was placed in a sterile Eppendorf tube. Glutathione conjugated 4b Sepharose Beads (GE Healthcare, Bucks, England) (200ml) was added to the tube, as per manufacturers instructions. Varying Units of protease K was added to each tube and incubated at 37°C for one hour. Following sedimentation (one min at 14,000rpm 4°C), the supernatant was measured at 492nm using a micro titre plate reader. The pellet was suspended in 1ml of PBS. 10µl of this was then added to 1ml of Laemmli buffer for analysis by SDS-PAGE and detection by western immunoblot.

2.5 Trichloroacetic Acid (TCA) Precipitation

TCA (100% v/v) of cold stock solution was added to the sample(s) of interest, to make a final concentration of 20% TCA (v/v). This was incubated at 4°C for 30mins. The sample was centrifuge at top speed for 30mins at 4°C. The supernatant was

decanted, taking care not to disrupt the pellet. Cold acetone (0.5ml) was added and the sample sheared by vortexing briefly. Following, the sample was centrifuged, at full speed for 15 minutes, 4°C. The acetone was aspirated, whilst not disrupting the pellet. The acetone washes were repeated twice. The sample was allowed to air dry. Once dry, Lamellae buffer was added and the proteins were analysed using SDS-PAGE followed by western blot immunodetection.

2.6 Transcytosis of Recombinant Proteins

To analyse whether recombinant proteins were subject to transcytosis across polarised epithelial cells, Caco-2 cells were used as a model system. Caco-2 cells (4.4×10^5) were seeded on a transwell plate and allowed to culture for 21 days. Measurements of transepithelial resistance were taken to ensure tight junction integrity. Inulin-FITC was used as a further control for tight junction integrity, and measured from the basolateral media at OD490nm periodically. Recombinant proteins (10µg/ml) were loaded onto the apical chamber and incubated for two hours, followed by a three-hour incubation. Apical and basolateral media were removed and TCA precipitation performed (section 2.5) this was followed by western immunoblot to detect recombinant proteins. Cells were subject to whole cell lysate and western immunoblot to determine the distribution of protein.

2.6.1 Analysis of Protein Trafficking in Mammalian Cells by Immunofluorescence

Cells were seeded on sterile coverslips at 1×10^5 cells / well and grown overnight. The following day, recombinant proteins (10µg) were incubated for 1 hour before washing and incubating for a further 3 hours (Caco-2 or Vero). The media used for the pulse was serum and antibiotic free and contained 200mM leupeptin as a protease inhibitor. Following the pulse, the medium was changed and complete medium added. The cells were maintained in a sterile environment at 37°C during this time frame. Following the three-hour incubation, the cells were washed three times with PBS and fixed using 2% v/v formaldehyde or methanol protocols for 20 minutes or 5 minutes respectively. The cells were washed three times in PBS before blocking in 1% FCS (v/v) for one hour. Cover slips were then removed from the 6 well plate and inverted

onto the corresponding primary antibody diluted in blocking buffer. A lid was placed on top of the box containing the cells to prevent evaporation and act as an humidifier. The box was placed at 4°C for one hour. After one hour, the coverslips were placed back into the 6 well tray (cells up) and washed three times with PBS. Again, the coverslips were removed and inverted onto parafilm containing the secondary antibody (20µl dotted onto the relevant location). The lid was placed back on and the box returned to the fridge for one hour. Following, the coverslips were removed, placed back into the 6 well tray and washed three times in PBS. The coverslips were then ready for mounting.

2.6.2 Mounting of Coverslips

Glass slides had 20µl of mounting media (Dyer *et al.*, 2013) placed onto them, and the coverslips were removed from the 6 well tray and inverted onto the glass slide. The glass slide was inverted and dabbed off on blue roll to remove any excess media. The sides of the coverslip were coated in nail polish to seal the air interface. Once the slides were labelled accordingly, the cells were imaged using 90i inverted microscope (Nikon, Surrey, UK).

2.7 Protein Adsorption onto Silica Beads

Purified, recombinant protein (GST-GFP) (10mg) was incubated with silica beads (Alfa Aesar, Lancashire, UK) (1g) in sodium acetate buffer (pH5.6) on a rotating rack at 4°C overnight. The protein-adsorbed silica was centrifuged at 6,000xG for 2 minutes. Supernatant was removed and two washes with sodium acetate buffer performed (to remove any non-bound protein). Non-bound protein was analysed by BCA assay and adsorption plots derived.

2.7.1 Fatty Acid Coating of Protein Absorbed Silica Beads

Protein absorbed silica beads (section 2.7) were immersed in 5ml pentane containing 50mg fatty acid. Pentane was allowed to evaporate by sonication at 23.55 Watts/cm²

for 30 minutes or until pentane had completely evaporated. Fatty acid coated particles were then freeze dried (section 2.7.2).

2.7.2 Freeze Drying of Fatty Acid Coated, Protein Absorbed Silica Beads

Fatty acid coated, protein absorbed silica, was freeze-dried using VirTis Wizard 2.0 freeze dryer. Thermal cycles were set as per table 2.

Table 6. Thermal cycles for freeze drying of fatty acid coated protein absorbed silica.

Step	Temperature (°C)	Time (minutes)
Thermal	+ 5	30
	- 15	30
	- 45	120
	- 20	120
	- 45	120
Drying step 1	- 20	420
	- 20	420
	- 20	120
	- 20	120
Drying step 2	+ 5	30
	- 5	30
	- 45	120
	- 20	120
	- 45	120

2.7.3 Release of GST-GFP from Fatty Acid Coated Silica Beads

Freeze dried, fatty acid coated, protein absorbed silica, was incubated in PBS at a variety of pH ranges, 37°C for three hours. The sample was centrifuged at 6,000xG for two minutes. Supernatant collected and analysed for release studies, via western immunoblot and BCA assay. Protein that remained absorbed to silica beads was analysed via western immunoblot, and mass balance performed again by western immunoblot. Protein was quantified using densitometry (section 2.7.3.1).

2.8 *In Vitro* Digestion Assay

Fatty acid coated, protein absorbed silica beads were subject to an *in vitro* digestion assay (Glahn *et al.*, 1998) where the fatty acid coated, protein adsorbed silica was placed in HCl buffer (pH2) (0.1Mol/L) with pepsin (40µg/ml) (Sigma, Dorset, UK). After an hour, NaHCO₃ (0.1Mol/L) was used to neutralize the pH (pH7.4) and porcine bile (12µg/ml) and pancreatin (2µg/ml) was added simulating lumen of the ilium. Protein that remained absorbed to silica beads was analysed by SDS-PAGE.

2.9 Circular Dichroism of Released Protein from Drug Delivery System

Released protein was inserted into a 0.1mm quartz cuvette (approximate concentration of 0.2mg/ml) and analysed at wavelengths between 190nm to 260nm, bandwidth 1nm, 20°C in PBS. Blank (PBS) was subtracted from the data and plots obtained using Prism software (GraphPad, California, USA).

Chapter 3: Characterisation of GST-GFP

In this chapter, two questions are addressed in order to further evaluate the possibility of a solid core protein adsorbed sub-micron sized fatty acid coated oral vaccine delivery system. First, can a model protein GST-GFP be produced and characterised? Further, can this recombinant protein be used as a model antigen for oral vaccine delivery?

3.1 GST-GFP

The oral vaccine delivery system described in chapter one (section 1.8.3) required the characterisation of, and interaction(s) between, a defined protein and the aforementioned silica particles. This was in order to define: protein loading on to beads, stability, on and off rates and protection from proteases. Consequently a model protein, Glutathione *S*-transferase fused in frame to green fluorescent protein (GST-GFP) was used on account of its availability, ease of production, purification and characterisation.

3.1.1 Glutathione *S*-transferase (GST)

Glutathione *S*-transferase is a multifunctional dimeric enzyme (~25kDa) that mediates the detoxification of endogenous (metabolites) and exogenous substrates (drugs, pesticides, and other pollutants). This is achieved via the covalent conjugation of reduced glutathione (GSH) to a substrate, a reaction catalysed by GST. GSH conjugation serves to convert reactive lipophilic molecules into water-soluble, non-reactive conjugate, that can be easily excreted (Singh *et al.*, 2000; Landi 2000). In mammals, three major families of GST have been identified. This delineation is based on varying subunit structures, isoelectric points, substrate conversion kinetics and immunological properties (Kim *et al.*, 2010). GST proteins are expressed at high levels in the mammalian liver constituting up to 4% of the total soluble proteins (Landi 2000). The GST family of genes is represented in all eukaryotes and appears to act to protect cells from chemical toxicants and stress (Singh *et al.*, 2000). Acquired alterations in GST activity due to enzyme induction and inhibition may also determine

the capacity to metabolise exogenous and endogenous carcinogens, thereby influencing diseases such as colon cancer (Baker *et al.*, 2002).

The use of GST as part of a model protein system was useful as GST has an affinity to glutathione-conjugated sepharose beads, facilitating an ease of protein enrichment (Scheich *et al.*, 2003). Additionally this mechanism can be employed for affinity isolation of fusion proteins (GST-GFP). The GST used herein was derived from the species *Schistosoma japonicum* and is available commercially as part of the GST-fusion system (GE healthcare, Bucks UK).

3.1.2 *Green Fluorescent Protein (GFP)*

Green fluorescent protein from the jellyfish *Aequorea victoria* has been one of the most widely used transgenic proteins in biological and medical research. GFP and other variants have been extensively used as markers for gene expression, analysis of protein : protein interactions, protein localisation and biosensors (Holder *et al.*, 2009). The ability of GFP to form a chromophore via an auto-catalysed reaction is the principle reason for the protein's utility. The chromophore is a *p*-hydroxybenzylideneimidazolidine moiety formed from residues Ser65, Tyr66 and Gly67. The maturation of the chromophore begins when the GFP folds into a nearly native conformation. A peptide backbone cyclisation begins by nucleophilic attack on Gly67's amide nitrogen on the Ser65 carbonyl carbon. The following oxidation and dehydration reactions generate an imidazolinane ring, which is conjugated to the side chain of Try66 (Lizuka *et al.*, 2011).

The folding of GFP is slow and oxidation of the chromophore is the limiting step in florescent maturation. The refolding of mature GFP is not fully reversible and it is prone to aggregation. Therefore, variants of GFP have been developed with better folding and florescent properties (Andrews *et al.*, 2007). These include cycle 3 GFP (F99S, M153T, V163A) (Holder *et al.*, 2009) and GFP mut 2 (S65A V68L S72A) (Lizuka *et al.*, 2011). The folding improvements in cycle 3 GFP have been attributed to the protein avoiding aggregation. More recently a super folder GFP (sfGFP) was developed to further minimise aggregation via enhance folding. The gene encodes the mutations found in cycle 3 GFP mutations, the enhanced GFP mutations (F64L and

S65T) and six other mutations (S30R Y39N N105T Y145F I171V and A260V). This variant was found to exhibit 100% fluorescent recovery after refolding from a urea denaturation (Andrews *et al.*, 2007).

GFP is remarkably inert; fusions to GFP are often functional despite the 237 amino acid addition to either the C or N terminal of another protein or protein domain. In addition, the resistance GFP offers to photo bleaching has advanced microscopy studies allowing long time-lapse microscopy studies (White 1999). Therefore, these advantages are useful for a model antigen delivery system.

3.2 Materials and Methods

3.2.1 Materials

The GST-GFP plasmid was a kind gift from Professor Robert Piper, University of Iowa, Iowa, USA (GenBank JN232535.1).

3.2.2 Methods

3.2.2.1 Analysis of clonal colony growth

Plasmid DNA (GST-GFP) was isolated using Qiagen miniprep kit (see chapter 2.2.6) and transformed into commercially competent *E.coli* BL21*DE3. The resulting product was streaked onto 2xYT (ampicillin) agar plates and cultured in a incubator overnight (16hrs). The following morning individual colonies were isolated and re-cultured in 2xYT (ampicillin) liquid media overnight. The following morning plasmids were isolated and PCR performed on the subsequent colonies.

3.2.2.2 Optimisation of bacterial growth to increase protein yield

E.coli incorporating the GST-GFP plasmid (1000ml) were grown for defined times prior to and following IPTG induction. At varying time intervals a small volume was

taken (2.5ml) and put inside a cuvette for analysis of turbidity via optical density 600nm (Vinderola *et al.*, 2002).

3.2.2.3 Calibration curve of GST-GFP to accurately quantify protein concentration

Increasing (known) concentrations of GST-GFP protein were analysed in a spectrophotometer at lambda max (484nm) and plotted to form a calibration curve. This was used to compare protein concentration against densitometry, BCA and Bradford assays.

3.2.2.4 Adsorption spectra of GST-GFP

The absorbance of GST-GFP was recorded from 190nm to 260nm wavelength and plotted to establish the maximum point of absorbance (designated lambda max). This was compared to published spectra (Pollok and Heim 1999).

3.2.2.5 Emission spectra of GST-GFP

As per adsorption spectra but in this instance the emission reading was analysed using a flourimeter.

3.2.2.6 Analysis of secondary structure by circular dichroism

GST-GFP protein was analysed in different buffers at constant ionic strength (0.2M). A 0.1mm quartz cuvette was used to obtain final plots. Wavelength range 190nm to 260nm, bandwidth 1nm and 2 seconds per time point. Protein concentration used was 0.3mg/ml (100µl final volume).

3.2.2.7 Protein stability analysis via GST purification

GST-GFP was incubated with 100µU protease K for one hour at 37°C. To assess conformational status of the protein, GST-GFP was re-purified using glutathione-conjugated sepharose 4b beads. The supernatant was taken and read

spectrophotometrically at a wavelength of 492nm. This was the degraded protein (not adsorbed), and the beads had 100µl of Laemmli plus BME added. The sample was separated on a SDS-PAGE gel and analysed using western immunoblot.

3.3 Results

3.3.1 Production of GST-GFP

The model protein GST-GFP was kindly provided as stated by Professor Robert Piper, University of Iowa, Iowa, USA. This plasmid was sequenced using the primers listed in table 7. The sequence describes the open reading frame (ORF) coding for GST-GFP protein within the multiple cloning site (MCS) of the pGEX 3X vector. The GST-GFP ORF is 1623bp, which would produce a protein with a predicted molecular weight (*in silico*) of 60.5kDa (figure 7).

The plasmid also encoded an ampicillin resistance selectable marker. Protein expression (GST-GFP) was regulated by the *Lac* operon, consequently isopropyl-beta-D-thiogalactopyranoside (IPTG) was used to induce high levels of protein expression in *E.coli* harbouring this plasmid. IPTG was used as a molecular “mimic” of allolactose, a lactose metabolite that triggers transcription of the *Lac* operon and thus the encoded gene; GST-GFP, located immediately down-stream of the *lac* promoter.

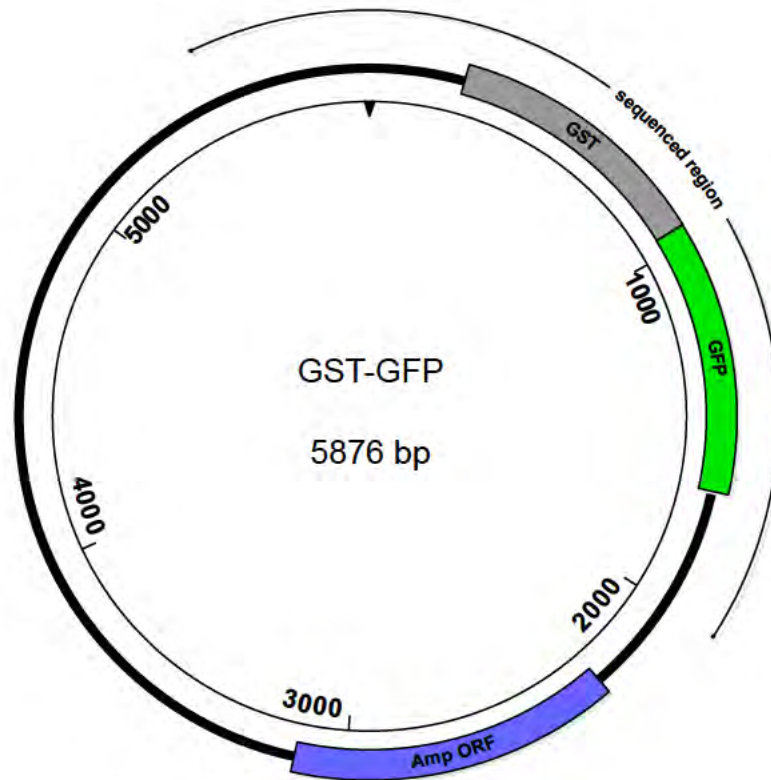


Figure 7. Graphic depiction of the plasmid encoding GST-GFP. This plasmid was derived from the pGEX 3X vector. The gene responsible for bacterial ampicillin resistance gene labeled in blue.

Table 7. List of primers used for PCR amplification, and sequencing.

Primer	Sequence	Orientation	Plasmid
27	GATAAGTACTTGAAATCCAGCAAG	5'	pGEX screening
33	ACGCGCCCTGACGGGCTTGTCTGC	3'	GST
114	GCCAGCAAAGGAGAAGAAGCTT	5'	GFP
115	AGGAAGGCACGGGGGAGGGGC	3'	GFP
116	TCCCCTATACTAGGTTATTGG	5'	GST
117	GTCACGATGCGGCCGCTCGAG	3'	GST
130	CACCATGATCAAACCTGAAATTCGGT	5'	Cloning CTBC into pET151
131	TTAATTTGCCATAGAGATAGC	3'	CTBC
149	CTGGATCCTCAGTGATGGTGATGGTGATGAT GACCGGTACGTTTACAGAGCTAGTAGAATT	3'	STBC
162	ATGAGTATTC AACATTTCCGT	5'	Amp
161	AGCTCCGGTTCCCAACGATCA	3'	Amp
163	TTCTTCTCCTTTGCTGGCCATATTTGCCATAG AGATAGCTGC	3'	CTBC GFP
164	CACCGTCTACACCATAACTCCCGCA	3'	VP2
165	GGTGCCCTCCGCCCCGTCACAATGAAAAAAA CATTATTAATA	5'	VP2-STBC
166	GGTGCCCTCCGCCCCGTCACAATGGCCAGCAA AGGAGAAGAA	5'	VP2-GFP
167	TATTAATAATGTTTTTTTCATTGTACGGGG CGGAGGGCACC	3'	VP2-STBC
168	TTCAGCGAAGTTATTTTTTCGTATCGCCAGCA AAGGAGAAGAA	5'	STBC GFP
169	TTCTTCTCCTTTGCTGGCCATACGAAAAATA ACTTCGCTGAA	3'	STBC GFP
170	ACCGAATTTTCAGTTTGATCATTGTGACGGGG CGGAGGGCACC	3'	VP2-CTBC
171	AGCCAGCCAGACGCAGACGCG	5'	CTBC sequencing primer
172	CATGGTGCCTCCGCCCCGTCACA	3'	VP2-STOP
173	GGTGCCCTCCGCCCCGTCACAATGATCAAACCT GAAATTCGGT	5'	VP2-CTBC
174	TCTTCTCCTTTGCTGGCCATTGTGACGGGGCG GAGGGCACC	3'	VP2-GFP
175	CATACTCTTCCTTTTCAATA	3'	CTBC sequencing
176	GCAGCTATCTCTATGGCAAATATGGCCAGCA AAGGAGAAGAA	5'	CTBC GFP

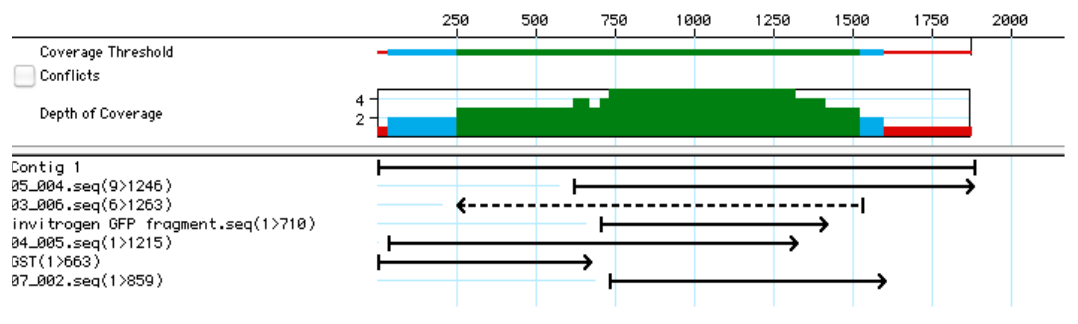


Figure 8. Contiguous, strategic view of sequence data showing depth of coverage over GST-GFP ORF.

The protein GST-GFP was produced in *E.coli* MC1061 bacteria and purified using glutathione *S*-transferase beads, to which the GST portion of the recombinant protein specifically adhered. After washing the column with PBS to remove any non-specifically bound protein, the GST-GFP protein was eluted from the column using 100mM GSH in PBS (0.5ml fractions). Initial attempts to separate proteins by SDS-PAGE revealed that two bands were evident; residual conformation of the protein was considered (figure 9).

The second protein-band unexpectedly ran between 52kDa and 42kDa. The predicted protein weight from sequenced plasmid data is 60.5kDa. A new protocol for protein production was instigated to compare whether heat shocking the bacterial culture could induce a correctly folded nature of the protein. Figure 8 demonstrates that this was not the case and the protein appeared as dual bands both before and after heat-shocking the cultures (protocol described in section 2.2.5.1). This was initially considered a possible fault in protein folding during translation, although the GFP protein remained fluorescent. Therefore, a further three plasmid clones provided by Robert Piper were analysed and compared and contrasted for their ability to produce single bands at predicted molecular weight. Plasmid numbers 208 and 209 (referring to different GST-GFP clones (section 2.2.5) produced little GST-GFP using the same protein production conditions. Plasmid 211 however yielded similar quantities of GST-GFP, (fig 10), however the same problem of double banding remained. Therefore, although “clone 211” plasmid produced high yields of protein, the 210 plasmid was deemed most useful for these studies.

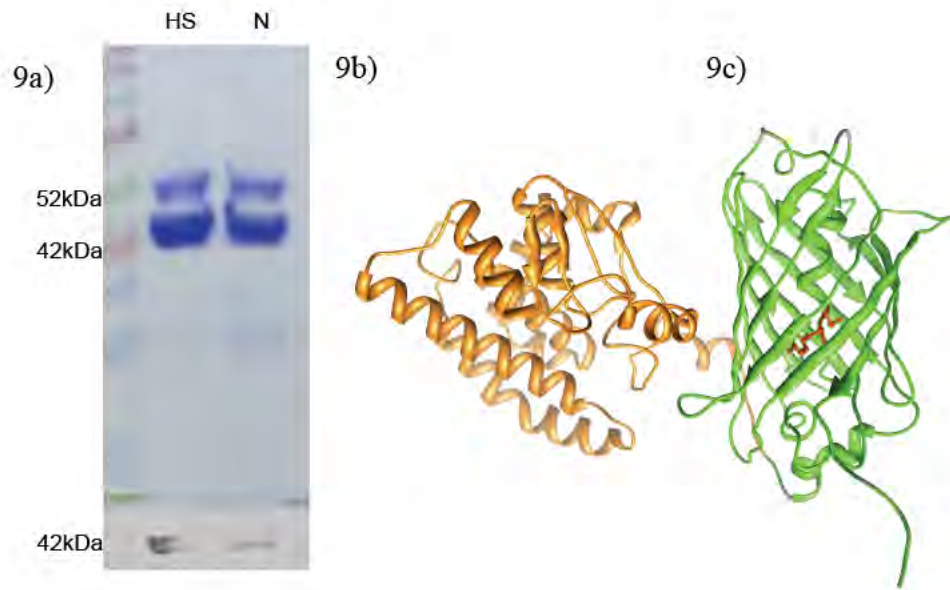


Figure 9a. Coomassie stained SDS-PAGE gel showing protein production of heat shocked (HS) and normal (N) induced *E.coli* MC1061 cultures grown for four hours pre- and post- IPTG induction. Here, 2 μ g of protein was loaded per lane. Double bands remain evident following both protocols.

Figure 9b. Here, 2ng of GST-GFP was added per well, either after the bacteria producing it had been heat shocked (HS) or not (N). GST-GFP was recognised by a α -GFP specific primary antibody used at a 1:5000 dilution. A single band was seen, however this is presumably due to protein concentration.

Figure 9c. Theoretical representation of GST-GFP produced *in silico* by I-TASSER (Zhang 2008).

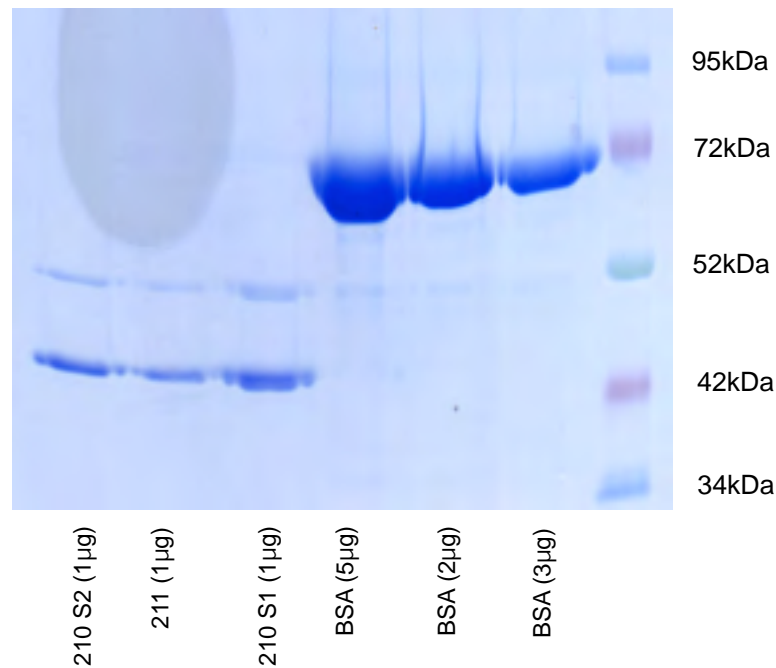


Figure 10. Comparison of protein production from plasmid 211 and 210. 1µg loaded of each protein, (S1 and S2 refer to two different batches of 210). The double banding remained in all proteins, from each plasmid.

Since double bands remained, it appeared feasible that the bacterial culture could be encoded with more than one plasmid. In attempts to confirm or dismiss this hypothesis, the transformation of chemically competent *E.coli* TOP10 cells, with the 210 plasmid was performed. The transformed bacterial cells were plated on a 2xYT (50 µg / ml ampicillin) agar plate and left to culture overnight at 37°C. Individual (clonal) colonies, containing a single plasmid, were grown as separate 50ml cultures. PCR from the plasmid obtained from the individual colonies could then be performed using primers 116 and 33 (table 7), which are specific to the GST region of the plasmid. Single bands therefore indicate a single plasmid in the bacterial colony. Figure 11 demonstrates that all the colonies tested were indeed clonal and contained the pGEX 3x plasmid.

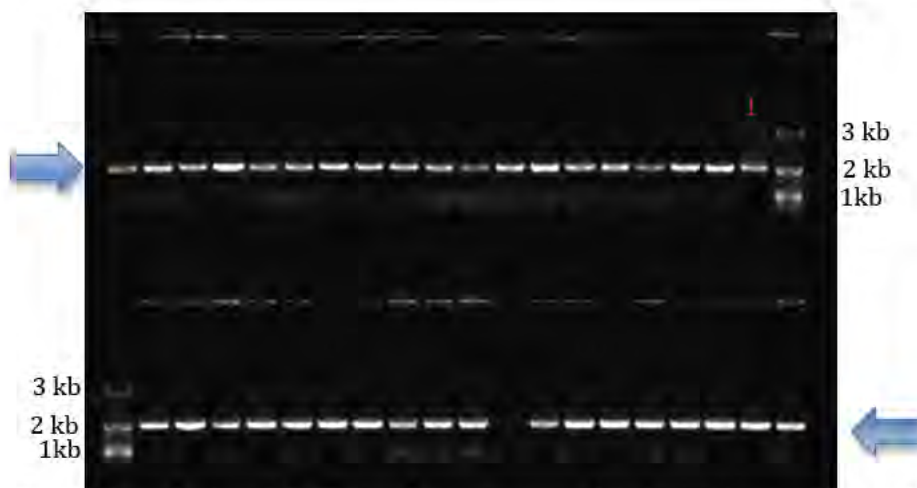


Figure 11. Gel analysis of PCR products generated using primers 116 and 33 (see table 7). Bands labeled with the blue arrow indicate clonal colonies transformed with pGST-GFP. Predicted Mw: 1.7kbp, observed ~ 2kb. Lane 1 represents a positive control for the experiment.

However, when mini-induction experiments (see section 2.2.5.2) were performed (using clonal populations of *E.coli*), two bands remained evident after western blotting and immunodetection, again at 52kDa and 42kDa. The negative control for the antibody was the protein ladder lane since the antibody for GFP was not specific for these proteins. The positive control for the antibody against GFP was previously made protein that has been found to be immunoreactive against this antibody. In spite of attempts to rationalise the double banding of GST-GFP, the problem remained. Therefore, if the protein double banding pattern was due to a conformational arrangement, this could potentially be solved by the use of 6M guanidine hydrochloride to facilitate the unfolding (and partial linearisation) of the protein. Laemmli buffer was produced, containing 6M guanidine hydrochloride and 20% (w/v) SDS. Since the presence of a high salt concentration in the Laemmli buffer caused heat distortion, the voltage at which the gel was ran and time frame for the run were altered. Figure 12 shows the comparison between running the protein with normal Laemmli compared to using Laemmli with 6M guanidine. The heat produced during the process of SDS-PAGE gel separation with 6M guanidine hydrochloride, causes distortion of the gel. Therefore it was concluded that if guanidine was required, normal Laemmli samples must be run separately in a different gel and voltage required decreasing to 110V over approximately 6 hours. However, the use of

guanidine removed the residual conformation and protein, evident at the higher molecular weight of 52kDa.

The data presented in figure 14, demonstrated further that the protein can be produced, at high concentrations (approximately 9mg/ml), purified to apparent homogeneity, and was immunoreactive for both GST-specific and GFP-specific, primary antibodies.

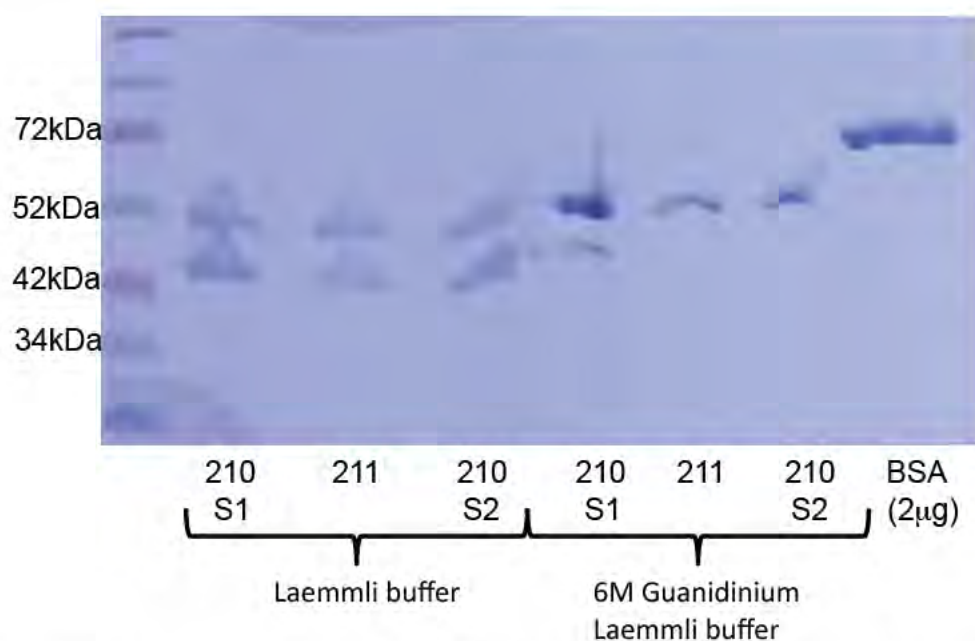


Figure 12. Coomassie stained SDS-PAGE gel. Protein was obtained from either 210 or 211 plasmid. The first three lanes were run using Laemmli buffer. Lanes 4 to 6 inclusive were run with 6M guanidine hydrochloride (Laemmli). The heat dissipated by running the protein in 6M guanidine distorted the running of the gel, hence the bands were uneven. The protein run in guanidine appeared as single entities due to the linearisation of the residual conformation in the protein structure. S1 and S2 refer to two batches of 210 being run for comparison. BSA used as a positive control for SDS-PAGE gel and Coomassie staining.



Figure 13. An immunoblot of a mini-induced GST-GFP protein (2ml), immunoreactive for 1:5000 α -GFP. *E.coli* was taken to clonal via streaking onto a 2xYT (plus ampicillin) plate and culturing overnight in a 37°C incubator. Individual colonies were taken and grown in 2xYT liquid media before inducing with IPTG. Lane 1 represents protein that has not been subjected to this procedure, thereby acting as a positive control. Lane 11 represents the negative control for α -GFP antibody. Double banding remains in all lanes, with exception of lane 11 as expected.

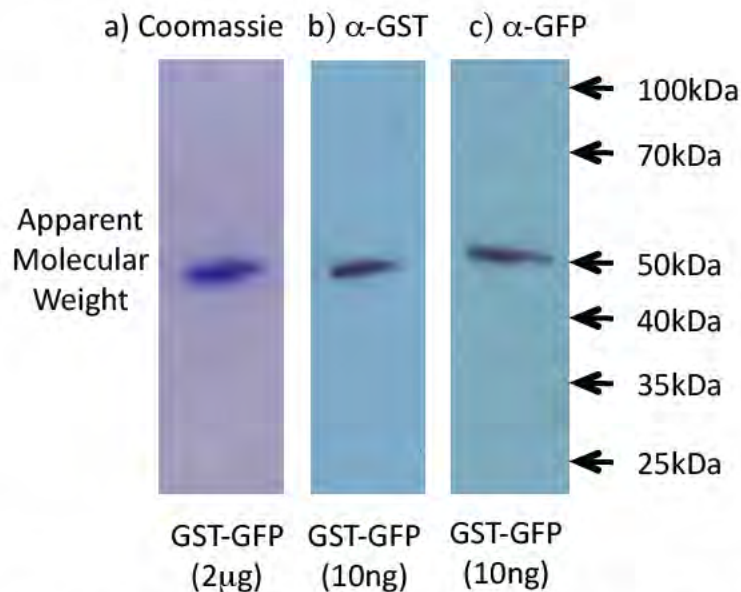


Figure 14. GST-GFP resolved on an SDS-PAGE gel run with 6M guanidine hydrochloride (Laemmli). A) showed that GST-GFP protein was purified to homogeneity and ran as a single band (with guanidine). B) GST-GFP was immunoreactive for 1: 3000 α GST at a concentration of 10ng. C) GST-GFP was immunoreactive against α GFP 1:5000 at a concentration of 10ng. Apparent Mw was ~ 50kDa. Expected Mw 60.5kDa.

3.3.2 Optimisation of *E.coli* Growth Conditions

Optimisation of bacterial culture conditions was performed to enhance the yield from each batch of culture. By recording the turbidity of the media at an optical density of 600nm, the optimal pre-IPTG condition was determined. The data in figure 15 shows that under the documented culture conditions, exponential phase of bacterial growth stops at around 110 minutes (1hr 40 minutes). This was performed using different clonal populations of GST-GFP in *E.coli* TOP10. Similar analysis was performed post-IPTG addition (figure 17). The stationary phase begins at approximately 300 minutes (5 hours), however the exponential phase decreases earlier at around 130 minutes (2hrs 15minutes). Therefore, the optimal post IPTG growth time should cease at around 2 hours for optimal bacterial expression. Exceeding the logarithmic stage of growth leads to the stationary phase, hence bacteria cease to divide further and metabolic products build up with a decrease in available nutrients. This leads to the death phase whereby the bacterial culture rapidly decreases in number. Therefore there is an undesired effect in allowing bacteria to culture over the optimal time.

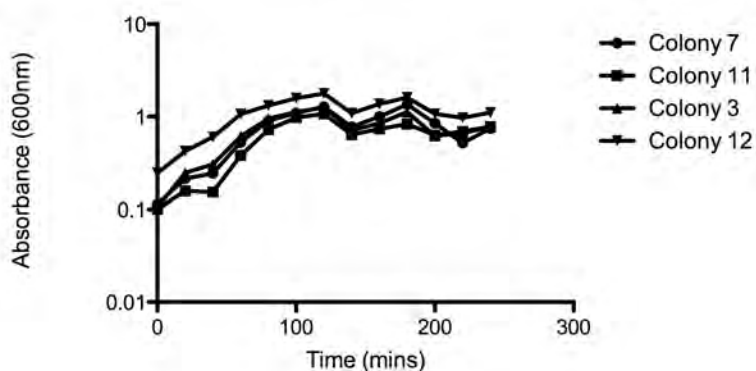


Figure 15. Optimisation of bacterial growth time pre-IPTG induction in *E.coli* TOP10 bacteria containing the clonal 210 plasmid. OD_{600nm} measurements taken to observe turbidity.

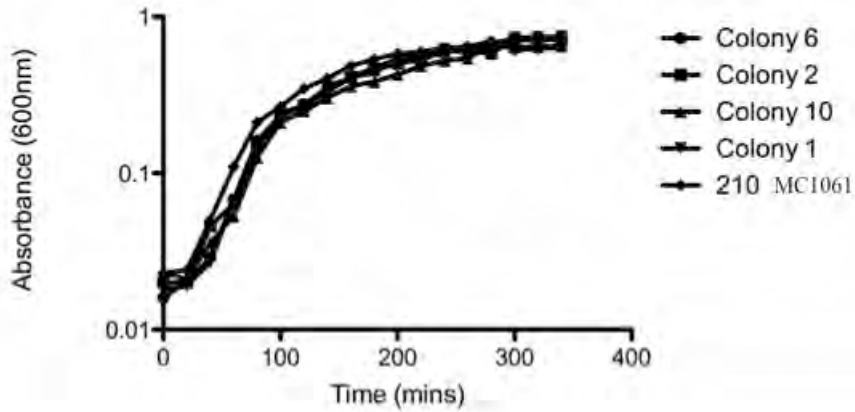


Figure 16. Analysis between growth of *E.coli* TOP10 bacteria and MC1061's both containing a clonal copy of 210 pre-IPTG induction. At 200 minutes the culture had reached saturation point in both cell types, hence it is concluded that IPTG induction should take place at this time.

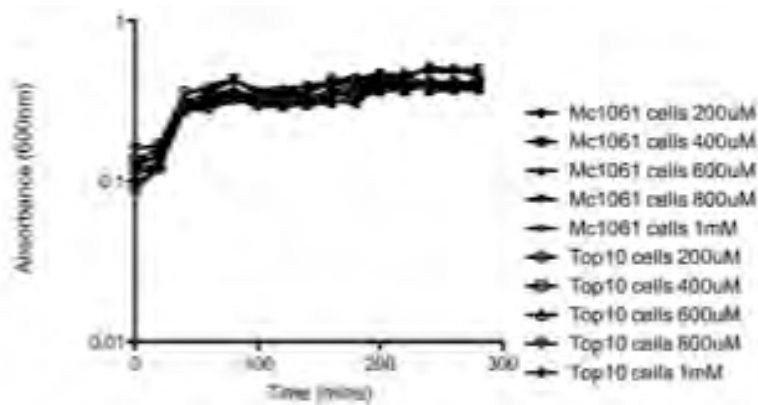


Figure 17. Analysis of bacterial turbidity (growth) at 600nm post-IPTG induction for protein expression. Start time at 200 minutes (figure 16). *E.coli* MC1061 and *E.coli* TOP10 bacteria were used with a clonal population of 210 plasmid. The IPTG concentration was analysed in both cell types. It was observed that both bacterial types and IPTG concentration have minimal aptitude on this experiment as bacterial number stabilises within 50 minutes post induction.

A similar experiment was repeated using *E.coli* MC1061 bacterial cells versus *E.coli* TOP10. There appeared to be little difference between the two bacterial strains, with the stationary phase commencing at 120 minutes (2hours) post-IPTG induction (figure 17). In addition, the concentration of IPTG appears not to significantly alter the rate of bacterial growth. It is hypothesised that there would be an affect on the concentration of protein obtained from each sample.

To help ascertain the protein concentration, a calibration curve was constructed using known concentrations of GST-GFP, which was related to absorbance at the lambda max (484nm) (figure 18). This relationship was plotted and a regression describing this relationship attained by increasing the concentration from 0µg, in increments of 100ng up to the pure concentration of the batch in question (8.24µg).

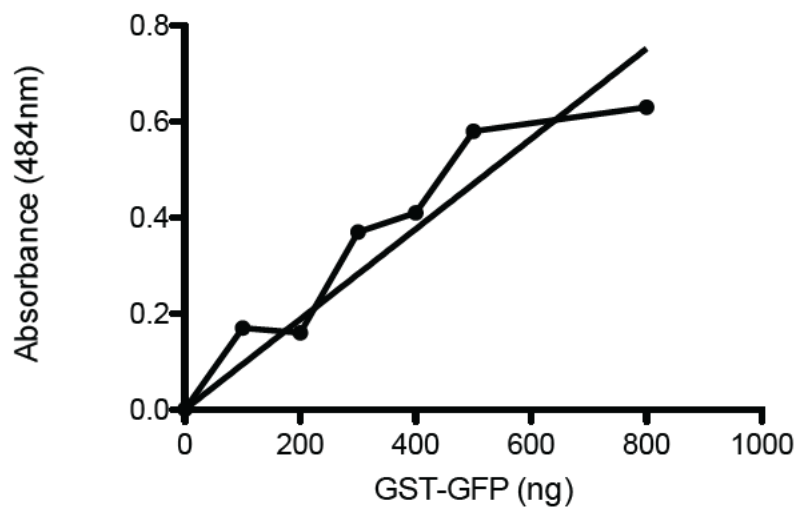


Figure 18. Calibration curve of GST-GFP protein at known concentration. Readings were taken using OD_{484nm}.

3.3.3 GST-GFP Characterisation

In silico, GST-GFP had a predicted molecular weight of 60.5kDa, based on the presence of encoded amino acids. However, upon analysis by SDS-PAGE, the apparent molecular weight of GST-GFP was ~52kDa. To help understand the discrepancy between these sizes, matrix assisted laser desorption ionisation – time of flight mass spectroscopy (MALDI-TOF MS) was performed.

Since the model antigen GST-GFP was used to investigate the first proof of concept of the SCDDS, it was necessary to understand what the secondary structure of GST-GFP looked like before and after release from the delivery system. This could then be analysed for any significant differences, which would demonstrate whether the protein was protected by the fatty acid layer.

3.3.3.1 Mass Spectroscopy

GST-GFP protein was salt exchanged into NaCl solution at 0.9% (w/v) and given to Professor Francis Pullen (University of Greenwich). The sample was then subject to MALDI-TOF MS, with and without trypsin digestion. The mass of the protein via this analytical method was deconvoluted and determined to be 53600.22 Daltons (figure 19 and 20). The predicted molecular weight of the protein *in silico* was 60.5kDa, 8kDa away from the observed (52kDa).

Upon analysis of the tryptic digest sequence of GST-GFP; sections of protein were identified using the original amino acid sequence. Upon analysing this data, it was apparent that there was a region at the carboxyl terminus of the protein, which cannot be detected after mass spectroscopic analysis (figure 20).

Furthermore, truncations of the protein *in silico* were undertaken (table 8). Eventually, by omitting the N terminal methionine, (which is not uncommon due to post translational modification), and removing 43 amino acids from the C terminal of the protein, a predicted mass of 53600.22 Daltons was obtained. When comparing this weight to that obtained by mass spectroscopy, there was 0.22 of a Dalton difference. Therefore it was possible that the C terminal was cleaved post-translationally. When

this region of the protein was identified via GenBank, the sequence appears to be that of a syntaxin protein from *Plasmodium vivax* (a malarial protozoa). Since this plasmid was obtained from Prof Robert Piper, who was interested in this species of protozoa, he was contacted and it was confirmed that this region was intended to generate polyclonal antibodies.

The insight gained into GST-GFP following analysis via mass spectroscopy yielded a final sequenced plasmid map of GST-GFP, with the mature protein labelled, (figure 21).

The zeta potential was analysed via titration and found to be at pH 4.7. This was evidently somewhat different from the predicted pI of 6.602 that was obtained via DNASTAR® software. This difference appears to be due to the *in silico* analysis of amino acids present in the protein structure, but discounting any thought for the conformation and interaction involved in the protein folding itself.

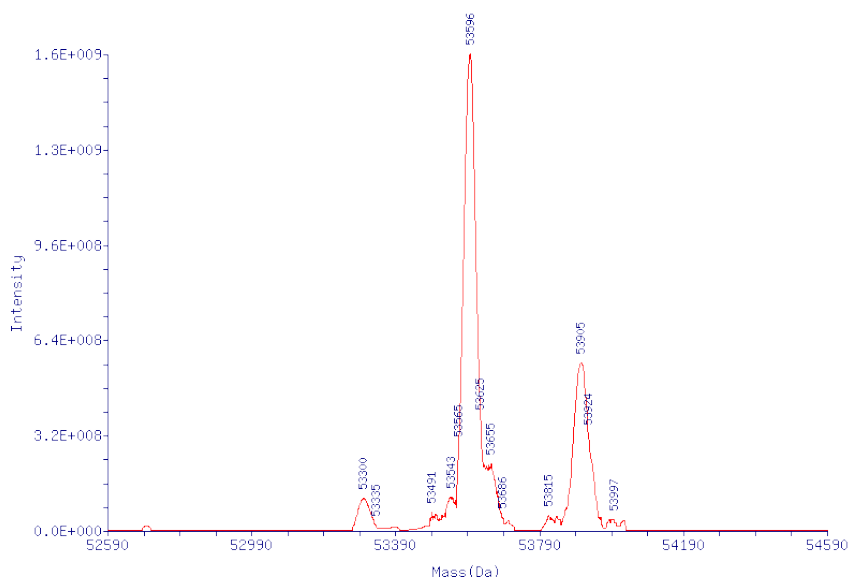


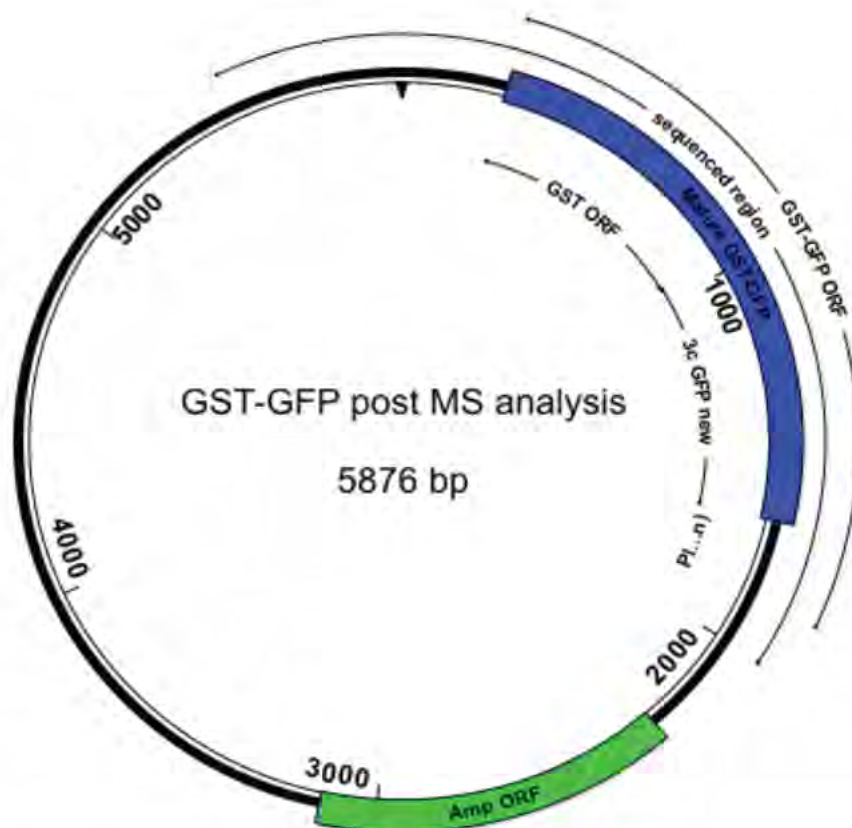
Figure 19. Deconvolved MALDI-TOF of GST-GFP. Mw observed at 53600.22 Daltons. The predicted Mw was 60.5kDa.

MSPILGYWKIKGLVQPTRLLEYLEEKYEEHLYERDEGDKWRNKK
 FELGLEFPNLPYYIDGDVKLTSMAIRYIADKHNMLGGCPKERA EI
 SMLEGAVLDIRYGVSR IAYSKDFETLKVDFLSKLPEMLKMFEDRLC
 HKTYLNGDHVTHPDFMLYDALDVVLYMDPMCLDAFPKLVCFKKR
 IEAIPQIDKYLKSSKYIAWPLQG WQATFGGGDHPPKSDLIEGRGIPG
 NSSMASKGEELFTGVVPILVELDGDVNGHKFSVSGEGEGDATYGKL
 TLKFICTTGKLPVPWPTLVTTFSYGVQCFSRYPDHMKRHDFKSA
 MPEGYVQERTISFKDDGNYKTRAEVKFEGDTLVNRIELK GIDFKED
 GNILGHKLEYNYN SHNVYITADKQKNGIKANFKIRHNIEDGSVQLA
 DHYQQNTPIGDGPVLLPDNHYLSTQSALSKDPNEKRDMVLLFV
 TAAGITHGMDELYKSGSGPVLAVPSSDPLVQCGGIALKGN SADIQHS
 GGRSSLEGPFKPADQPR LCLLVASHLLFAPPPCLP
 Green - GST sequence
 Red - GST sequence coverage
 Blue - GFP sequence
 Pink - GFP sequence coverage
 SDLIEGRGIPGNSS = GST sequence blasted!
 SGSGPVLAVPSSDPLVQCGGIALKGN SADIQHSGGRSSLEGPFKPAD
 QPRLCLLVASHLLFAPPPCLP = *Plasmodium vivax* (syntaxin)

Figure 20. Analysis of protein sequence obtained from trypsin digests. Both GST and GFP sequences were identified. The C terminal (black writing) appears to be absent from the protein structure. Upon blast search for this region it was apparent that this is a syntaxin protein from *Plasmodium vivax*. However, the C terminal was cleaved during or after protein production the function of GST-GFP was unaltered.

Table 8. Truncations of GST-GFP, omitting various amino acids to achieve the mass observed via trypsin digest and MALDI-TOF.

NT-Truncation	Mass (Daltons)	pI
M + 11	5354425	6.285
M + 10	5338107	6.285
M + 5	5288155	6.472
M + 2	52539.11	6.377
M + 1	52410.98	6.377
M	52323.90	6.377
M - 1	52192.70	6.377
M - 2	52121.62	6.377
CT-Truncation		
Δ 472	5373142	6.062
Δ 471	53603.25	5.968
Δ 470	53440.08	5.968
N terminus Methionine and C terminal truncation Δ 472	53600.22	6.062
Target Mass	53600	



Predicted MW of Mature Protein	Actual MW via MS	pI predicted	Zeta potential
53600.22	53600	6.062	4.07

Figure 21. Revised plasmid map of construct 210 incorporating data from mass spectroscopy. The mature region of protein, shown in blue, was cleaved at the C terminus in comparison with the original ORF shown as a line in the inner circle of the plasmid. The predicted Mw of the mature protein and observed, along with pI, PCS and zeta potential were also determined.

3.3.3.2 Characterisation of GST-GFP by Spectroscopy

Since the lambda max for this particular recombinant GFP is unknown it was simple to use the published wavelength of 490nm for eGFP. However, since this is a recombinant protein with a N terminal GST protein fused in frame, the excitation and emission spectra may differ from that of previously published for GFP alone. Figure 21, shows the lambda max for the excitation and emission spectra of GST-GFP to be

484nm, thus this was used for all further experiments. For the emission spectra, figure 22 showed the lambda max to be 490nm with a small shoulder at 498nm. This is comparable with published eGFP excitation and emission spectra (Pollock and Heim 1999).

3.3.3.3 Characterisation of GST-GFP by Circular Dichroism Spectroscopy

GST-GFP was used as a model protein antigen to assist in the characterisation of the model oral vaccine delivery system *i.e.* the binding, release and protection studies. An analytical tool utilised to study the folding of the protein was circular dichroism. The data in figure 26 shows the native structure of GST-GFP and GST alone. Both GST and GST-GFP were assessed in the presence of different buffers at a range of pH. The circular dichroism spectra has been characterised following addition to each buffer, (figures 23 to 27). In addition a denatured spectra of GST ad GST-GFP was analysed via the addition of 6M guanidine hydrochloride so that if a denatured spectra were to arise following release from the silica beads, there would be understanding as to what to expect in such circumstances (figures 28 and 29).

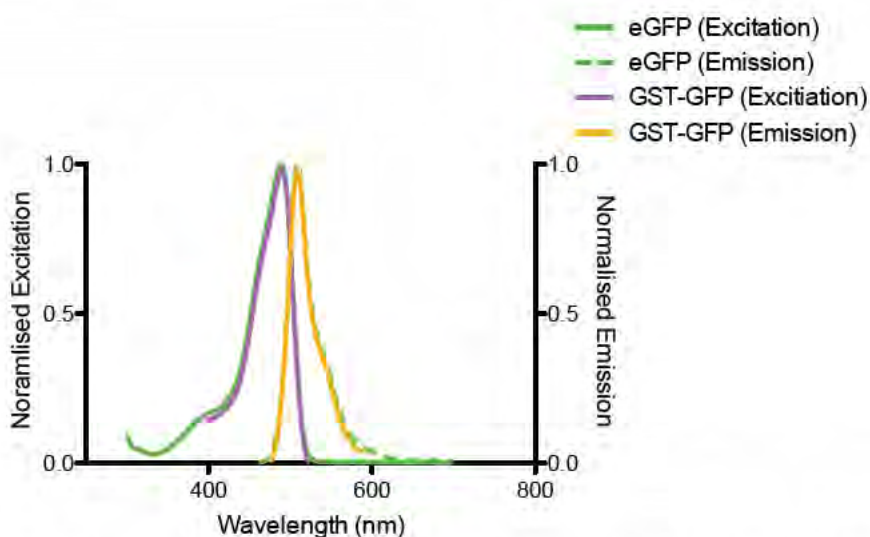


Figure 22. Excitation and emission spectra comparison between eGFP and GST-GFP over a range of wavelengths to obtain lambda max for the florescent protein. Lambda max was documented at 484nm.

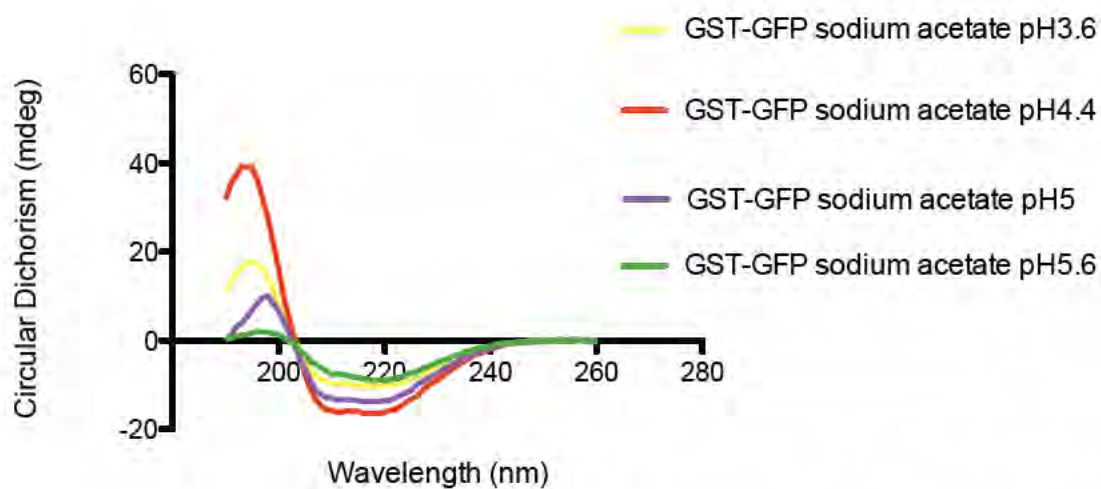


Figure 23. CD spectra of GST-GFP in sodium acetate buffer. Ionic strength 0.2M. Range of pH values.

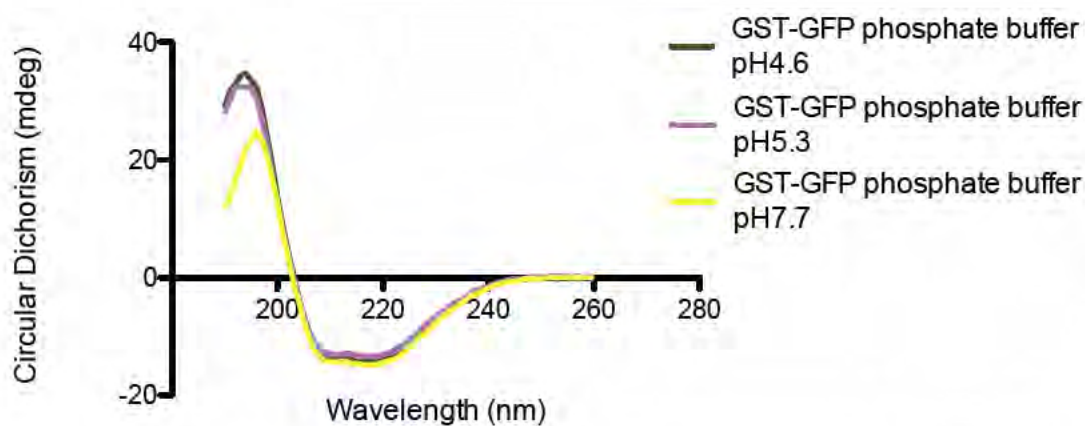


Figure 24. CD spectra of GST-GFP in phosphate buffer. Ionic strength 0.2M. Range of pH values.

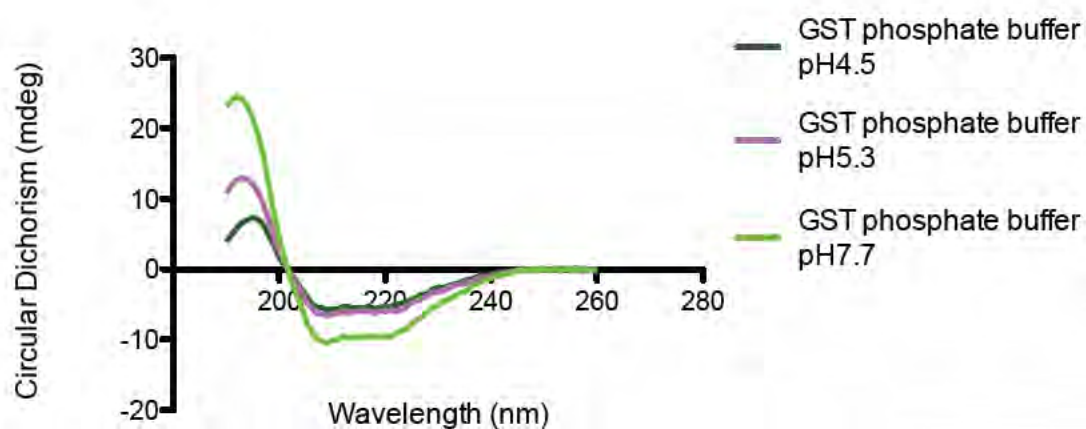


Figure 25. CD spectra of GST in phosphate buffer. Ionic strength 0.2M. Range of pH values tested.

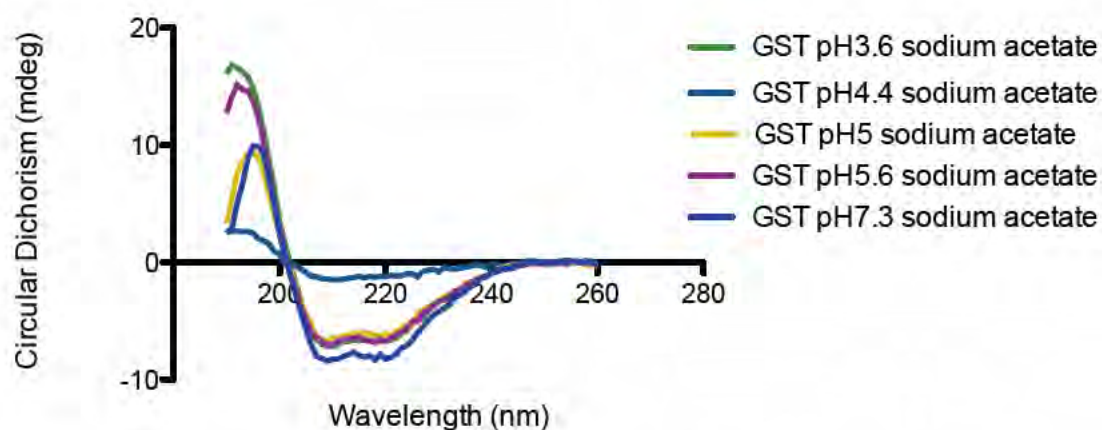


Figure 26. GST CD spectra in sodium acetate buffer. Ionic strength 0.2M. A range of pH values tested.

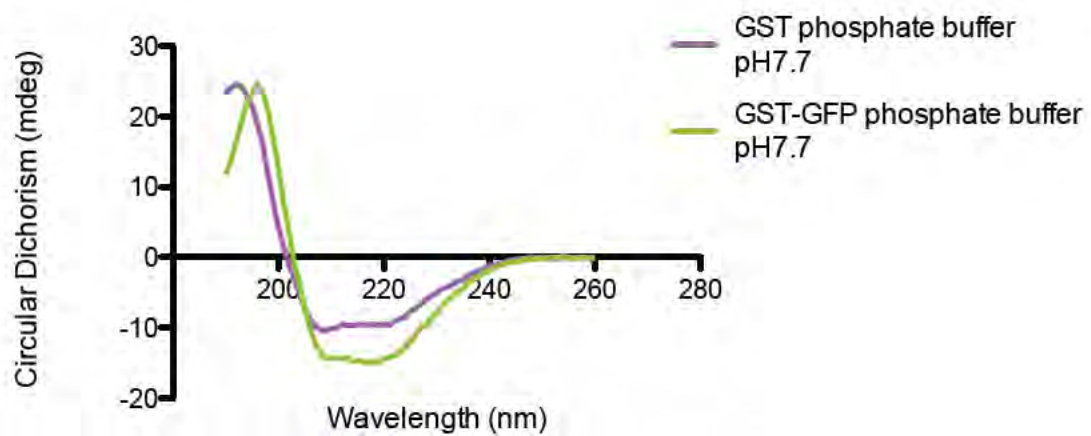


Figure 27. CD spectra of GST and GST-GFP in phosphate buffer. Ionic strength 0.2M, pH7.7.

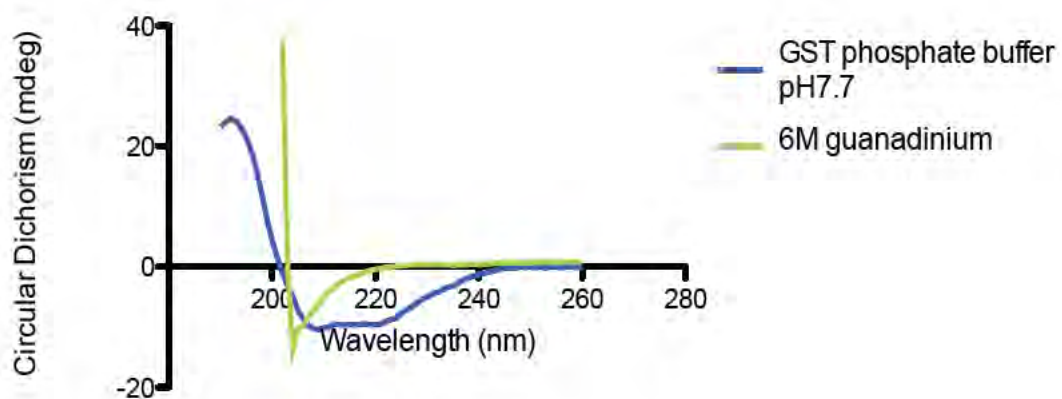


Figure 28. CD spectra of native versus denatured GST.

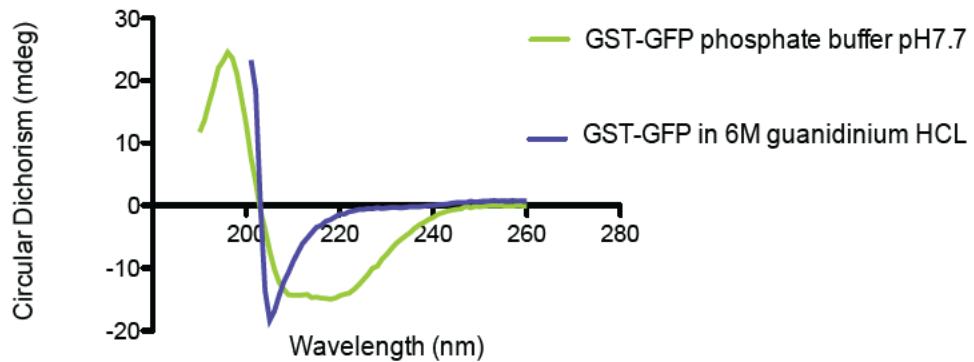


Figure 29. CD spectra of native versus denatured GST-GFP.

3.3.4 Assay of GST-GFP Enzymatic Stability Against Protease Degradation

GST-GFP stability was assessed both in the presence of defined proteases and without the addition of exogenous proteases in order to provide a base line to compare subsequent stability experiments. Once adhered to the silica beads it was hypothesised that the conformational stability would prevent protein degradation from proteases and heat. It was hypothesised that if the protein could not move once adhered to a solid support, it would be protected against proteolytic degradation (Puu *et al.*, 2000). Before testing the hypothesis that GST-GFP will be stabilised on silica beads, it was necessary to establish the stability of the protein in phosphate buffered saline (PBS), with and without the addition of proteases. Using the fluorescent spectrometer set to an excitation of 484nm, emission readings were taken every five minutes for the first half hour then every 30 minutes for 7hr 30minutes. Figure 31, shows that the emission spectra did not decrease over this time frame at 37°C. GST-GFP is detectable by GFP specific antibodies with out a decrease in apparent molecular weight after 37 hours (lane 14) at 37°C. Input can be seen (fig 31). However, the concentration appears to increase as the time frame increases. This was most likely due to evaporation of the solvent (water) from the cuvette. Parafilm remained over the top of the cuvette to prevent this eventuality but unfortunately was not completely effective.

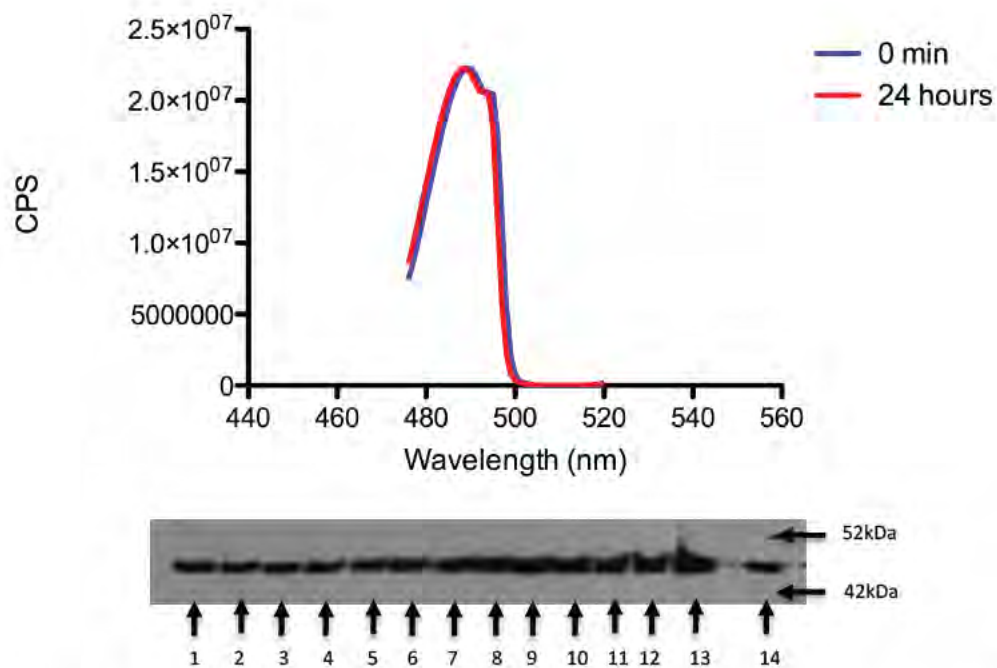


Figure 30. Analysis of GST-GFP protein by western blot followed by immunodetection, 20ng ran per well. Samples taken at 30-minute intervals from cuvette during emission profile. No degradation was seen in any of the samples taken.

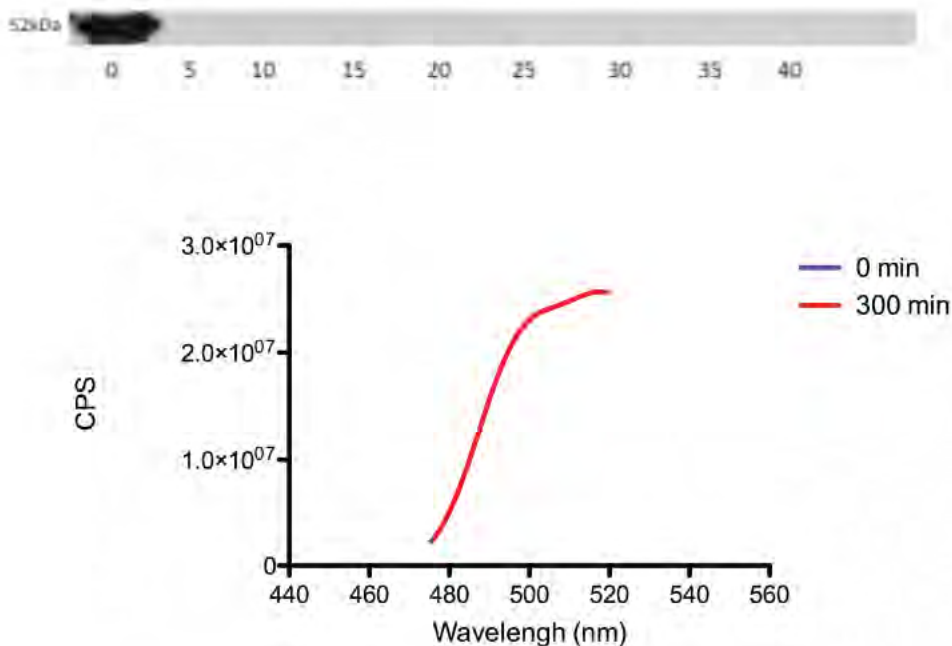


Figure 31. Emission profile of GST-GFP post addition of Protease K (10U). The emission profile appeared not to decrease over the course of 300 minutes at 37°C. The control at time zero is directly behind the red curve and hence no change in spectra seen over this time frame. Since 1 unit should degrade 1mM tyrosine per minute and 10 units were added it would be expected that this protein should be degraded within this time. The western blot followed by immunodetection were unsuccessful due to protein not being present, or degraded beyond recognition of the antibody. Therefore it was concluded that although the protein structure was being degraded, the fluorescence remains due to the three-arginine residues in the chromophore. Therefore, the fluorescent spectrometer was not used for future experiments.

Since the protein remained stable at 37°C over 24 hours, the protein was incubated with Protease K. By understanding the kinetics of protein degradation of GST-GFP, the stability could be assessed when the protein was adhered to silica beads. The predominant site of cleavage is the peptide bond adjacent to the carboxyl group of aliphatic and aromatic amino acids with blocked α amino groups. The unit definition for protease K was: one unit will hydrolyze urea-denatured hemoglobin to produce colour equivalent to 1mmole (181g) of tyrosine per minute at pH 7.5 at 37°C. The experiment was repeated in the fluorescent spectrometer at 37°C. An excess (10U of protease (according to the unit definition)) was added to 500 μ g of protein. However,

there remains no change in the emission spectra of GST-GFP over the time frame of 5 hours. This experiment was repeated several times (n=5). However, the fluorescent emission remained even after the protein was no longer recognised by anti-GFP antibodies. It was concluded, that despite the β barrel of GFP, being degraded by protease (figure 31 panel a), the chromophore at the centre of what was the β barrel, remained fluorescent, emitting light at 490nm after excitation.

Since fluorescent spectroscopy could not be used to reliably analyse the integrity of the GST-GFP in the presence of proteases, a new method utilising the GST portion of the protein was developed. This method required the incubation of GST-GFP with Protease K for 60 min on a shaking platform, in the presence of glutathione conjugated beads (section 2.3.3). After 60min, the reaction was subject to sedimentation (10,000 x g for 2 min at 4°C) and supernatant removed for analysis in a UV spectrophotometer (figure 33) (section 2.2.8). The centrifuged beads then had Laemmli buffer added and were subject to western blotting and immunological detection (figure 33). Figures 32 to 34 show that after the addition of 100 μ U of protease K into 500 μ g of GST-GFP, the absorbance of the supernatant (after the removal of material with intact GST domains) was not depleted. This indicated that the protein was degraded since GST was not binding to the beads. The data in figure 32 supports this hypothesis, since the western blots analysis of GST-GFP, using a GFP specific primary antibody, showed that the molecular weight of the GST-GFP remained stable until the protease concentration was increased to 100 μ U. Increasing concentrations of protease K further shows that the protein was completely undetectable by the antibody.

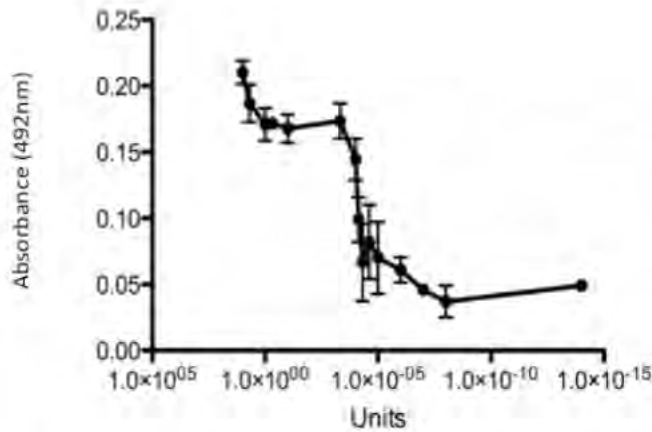


Figure 32. Decrease of absorbance of GFP following GST isolation on beads (n=16). Absorbance decreases in accordance with protein degradation due to lack of affinity of GST to beads. At 100 μ U a sharp decrease in absorbance is visualised in relation to protein degradation.

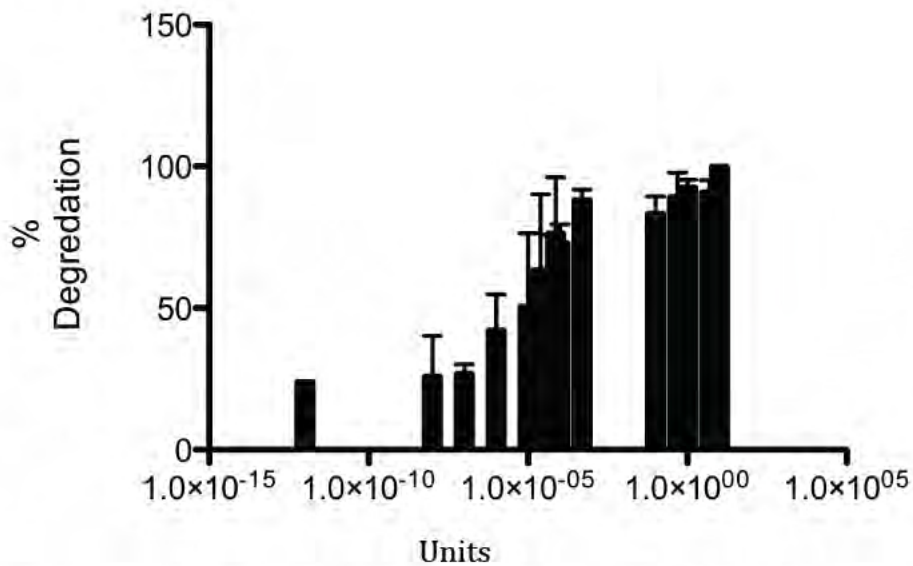


Figure 33. Percentage degradation of GST-GFP following addition of varying units of protease K (n=16). A sharp decrease in stability is evident at >100 μ U of protease. Data corresponds to figures 20 and 22 in that GST binding to beads was inhibited at these concentrations and hence absorbance from GFP increases at concentrations above this value.

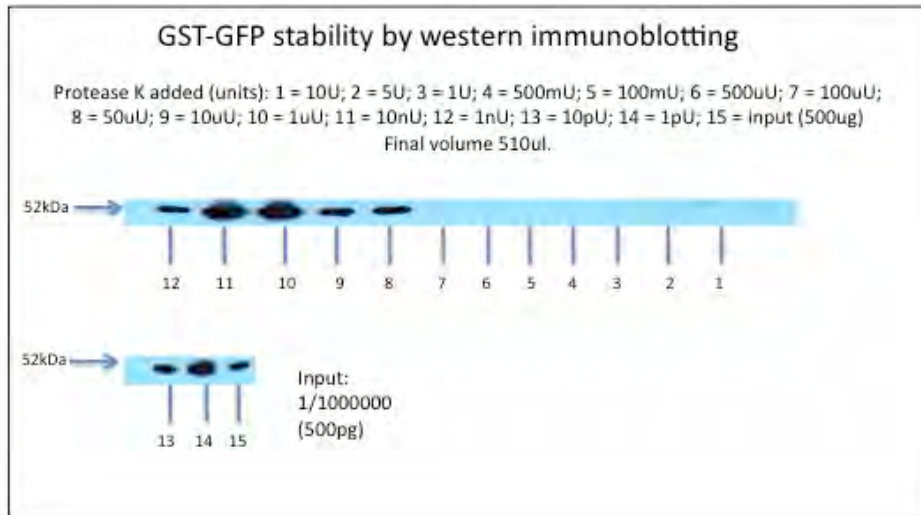


Figure 34. Stability of GST-GFP over 1 hour at various concentrations of protease K (n=16). It was evident that at protease concentrations of $> 100\mu\text{U}$, 500 μg of protein, as per input (15) protein was degraded beyond recognition of αGFP . Data supports figures 20 and 21.

3.3.5 *In Vitro* Toxicity of GST-GFP Measured Using a Cell Culture Model

The toxicity of GST-GFP was analysed by a MTT (3-(4,5-Dimethylthiazol-2-yl)-2,5-diphenyltetrazolium bromide) assay, in three cell lines; Vero (African green monkey kidney epithelial cells), Caco-2 (heterogeneous human epithelial colorectal adenocarcinoma cells) and B16 (mouse malignant melanoma) cells. Since this protein would be tested *in vitro*, it was essential to have information on the toxicity of the protein. The data in figure 34 shows that in all of the three cell lines tested, the protein was non-toxic relative to positive and negative controls, poly(ethyleneimine) (PEI) and dextran respectively, over 72 hours.

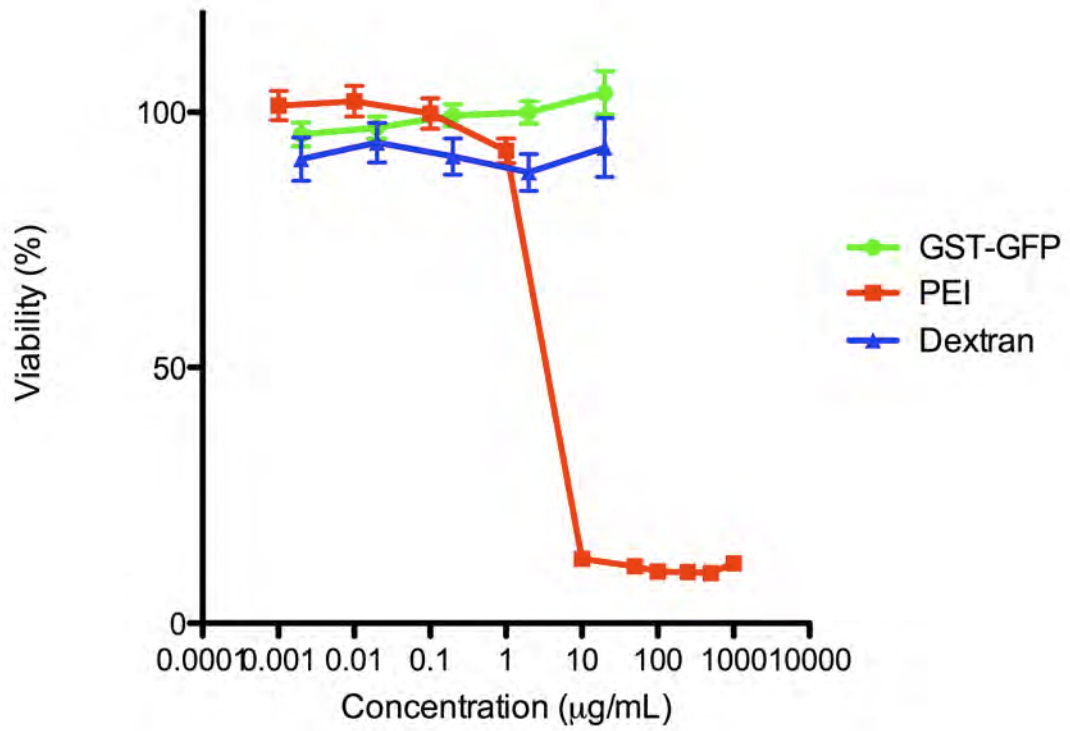


Figure 35. Toxicity of GST-GFP to Vero the cell line (n=8). Polyethylenimine (PEI) was used as a negative control for cell viability, dextran was a positive control for cell viability. GST-GFP was found to be non-toxic.

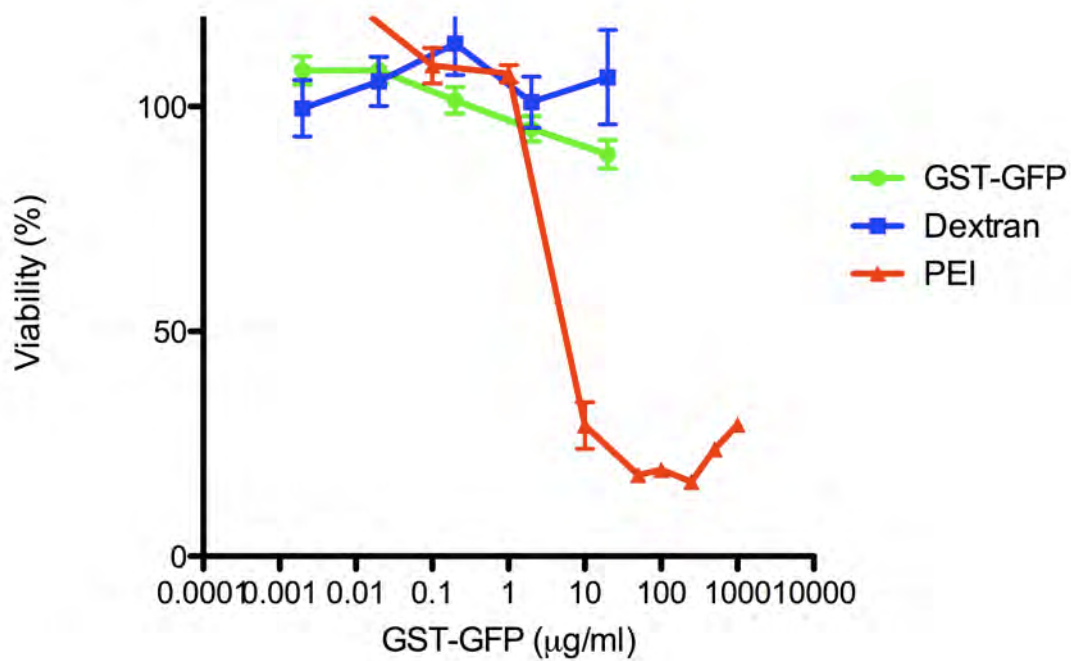


Figure 36. Toxicity of GST-GFP to the B16 the cell line (n=8). Polyethylenimine (PEI) was used as a negative control for cell viability, dextran was a positive control for cell viability. GST-GFP was found to be non-toxic.

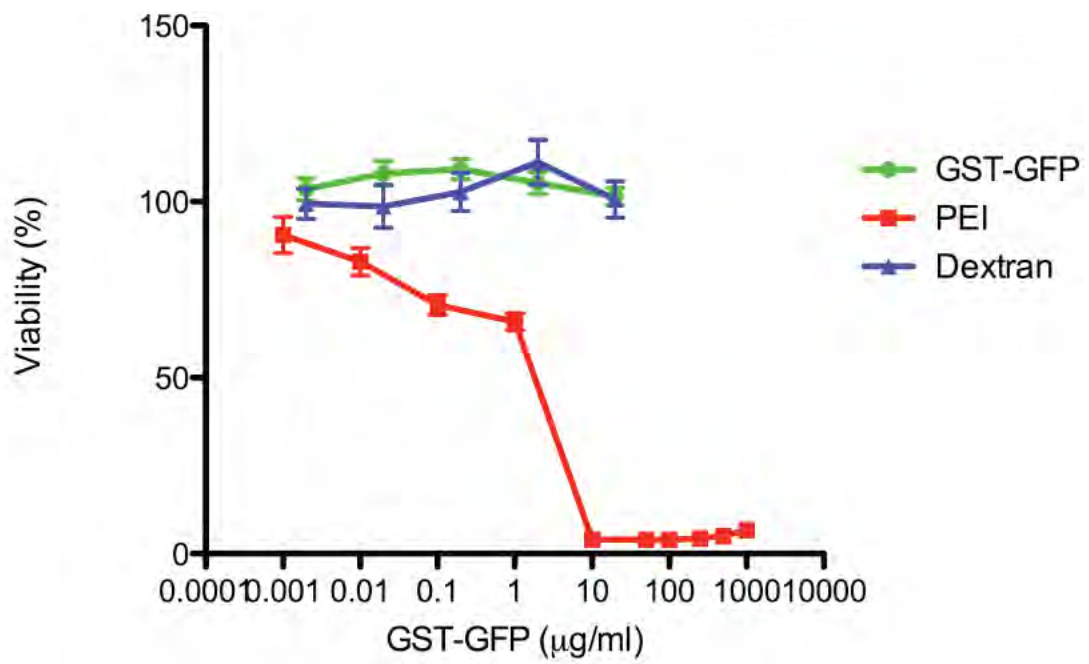


Figure 37. Toxicity of GST-GFP to the Caco-2 cell line (n=8). Polyethylenimine (PEI) was used as a negative control for cell viability, dextran was a positive control for cell viability. GST-GFP was found to be non-toxic.

3.4 Discussion

3.4.1 Production of a Model Protein (GST-GFP)

A plasmid encoding GST-GFP (kindly provided by Robert Piper, University of Iowa, Iowa) (Urbanowski *et al.*, 1999) was sequenced using the primers described in table 4 (GenBank JN232535.1). Following sequence analysis, the plasmid vector was found to be pGEX 3X and of the open reading frames (ORFs) within the plasmid, one was found within the multiple cloning site, containing the nucleotide sequence encoding a GST (Smith and Johnson 1988) upstream of nucleotide sequence encoding a 3cGFP domain (Butera *et al.*, 2005). Sequencing data revealed that GST-GFP expression was regulated by a modified version of the LacZ operon, which could be induced using the galactose analogue IPTG. Bacterial lysis was achieved using a french press pressure cell to avoid the possibility of GST-GFP detergent interaction, which could result in GST-GFP conformational relaxation (Otzen 2002). Conformational relaxation may also give rise to artefacts when examining protein conformation by CD as described later in this section.

Expressed protein GST-GFP was assayed using SDS-PAGE. Coomassie detection was used to characterise the apparent molecular weight of the enriched GST-GFP protein eluted from reduced glutathione (GSH) conjugated sepharose (Frangioni and Neel 1993). SDS is an ionic detergent that binds to the vast majority of proteins at a constant ratio of 1.4g SDS / g protein. However, a few proteins such as tubulin do not bind at this ratio, which affects the rate of migration in SDS PAGE electrophoresis, (Webb *et al.*, 1977). Other factors influencing protein migration in SDS PAGE gels include incorrect polyacrylamide percentage (increased or decreased resistance to migration), excess salt concentration, and protein modifications such as glycosylation or phosphorylation, and residual secondary and tertiary structure (Schagger and Jagow 1987).

In apparent contradiction to the predictions made from the sequencing efforts (*i.e.* GST-GFP having a predicted molecular weight of 60.5 kDa), after SDS PAGE, the affinity-isolated protein was distributed between two bands measuring approximately 45kDa and 52kDa (see table 9). The reason for this discrepancy could have been due

to premature transcriptional termination during bacterial protein expression (Sorensen and Martensen 2005). Consequently a comparison between protein production protocols was undertaken utilising the phenomena of “heat shock”. Heat shock genes are a subset of a larger group of genes, coding for molecular chaperones *i.e.* proteins that are involved in “house-keeping” functions within the bacterial (as well as mammalian) cell (Sorensen *et al.*, 2003). These molecular chaperone proteins are involved in regulating protein folding and unfolding, and degradation of misfolded or aggregated proteins, after heat shocking to 42-45°C for a short duration of 30 seconds (Sonna *et al.*, 2002). Therefore, correct protein folding of GST-GFP could be improved using this protocol. After following the “heat shock” protocol, two bands were detected at the same apparent molecular weight as before (figure 9) indicating that premature transcriptional termination was not likely to account for the distribution of GST-GFP molecular weight as resolved by SDS-PAGE.

As there were four different clones encoding GST-GFP readily available, it was deemed necessary to analyse each of the plasmids for their ability to produce GST-GFP. The analysis of other plasmids was used to assess whether all plasmids produced equal yields of protein and whether the protein made would produce one or two bands at predicted molecular weight. Plasmid numbers 208 and 209 resulted in yields of protein at approximately 0.1mg/ml as oppose to 8mg/ml obtained from clone 210. The molecular weight of GST-GFP produced by these plasmids was equal to the 210 plasmid of between 42kDa and 52kDa, with two apparent bands. Therefore, these clones were not subject to further analysis. Clone 211 produced GST-GFP with an equivalent yield to clone 210 (8mg/ml), however, upon further analysis *i.e.* SDS-PAGE followed by Coomassie staining, two bands were documented as before (similar to clone 210) (figure 9).

Table 9. Apparent versus observed molecular weights of GST-GFP.

Experimental Protocol	Mass (kDa)	Evidence
DNA Sequencing	60.5	Figure 20
MALDI-TOF MS	53.6	Figure 18
SDS-PAGE and Coomassie / immunodetection	52 and 45	Figure 9, 11, 13

It was possible that the bacteria “stock” culture, containing clone 210 (the GST-GFP plasmid) could also contain a second plasmid (Smith *et al.*, 1993). Isolating the

plasmids contained within the “stock” culture and re-transforming them into fresh clonal *E.coli* could control for the phenomena of plasmid contamination (Fiedler and Wirth 1988). This would result in clonal populations of bacteria (*i.e.* a colony derived from one transformed bacterium) containing only one type of plasmid (Smith *et al.*, 1993). Plasmids contained within a clonal populations of bacteria were isolated and assayed using PCR in order to detect variations within the size of the GST-GFP ORF. This assay utilised primers specific to the extreme 3’ and 5’ ends of the ORF encoding for GST-GFP identified within the clone 210 sequencing data. The molecular weights of the PCR products generated using the clonal bacterial colonies as a PCR template were all identical, indicating that there was only one species of plasmid prevalent within the “stock” culture of clone 210 (Figure 11).

Lysates generated from solubilising IPTG-induced 1 mL clonal bacterial cultures (containing the re-transformed 210 plasmid), were also subjected to immunological analysis using a primary antibody specific for GFP (figure 13). The results of this experiment also demonstrated that the dual banding of immunoreactive proteins previously documented was not due to a second aberrant plasmid being present within the bacterial “stock” culture. This result corroborates the PCR assay previously described.

Consequently, it was concluded that the double banding observed was due to either: post-translational modification of the protein (Mann and Jensen 2003) or residual secondary structure within a proportion of the isolated protein (See *et al.*, 1985).

The hypothesis that residual secondary structure was responsible for the two apparent molecular weights of GST-GFP was tested using Laemmli buffer containing 6M guanidine hydrochloride (figure 12). The uneven resolution of the protein documented was probably due to thermal distortion produced when running samples at such a high salt concentration (See *et al.*, 1985). The proteins run under conditions of high salt appear to have resolved into a band of one apparent molecular weight (figure 12) measuring 52 kDa. As the resolved band was of the higher of the two molecular weights observed, it was possible that residual secondary conformation was causing the observed phenomena. However this data did not exclude the possibility that the

higher salt concentrations was more effective at arresting protease mediated post-translational modification (Rigaut *et al.*, 1999).

In order to test the hypothesis that post-translational modification was responsible for the distribution of protein molecular weight after resolution with SDS-PAGE, a more accurate assessment of the proteins mass was required (Jurinke *et al.*, 2004). To this end the mass of the protein was attained using MALDI TOF mass spectrometry (MS) (Doman and Aebersold 2006). Following the deconvolution of data describing the mass of the whole protein, a lower than predicted mass was observed (figure 19 and 20 and table 8). The mass obtained from MS roughly corresponded to the higher molecular weight band resolved by SDS PAGE (Table 4). As there was some discrepancy between the MS data (53 kDa), the mass data from SDS-PAGE (52kDa) and the predicted mass of the protein derived from the plasmid sequence (60.5kDa), a tryptic digest followed by MALDI TOF MS was performed (Hale *et al.*, 2000). The mass of the oligopeptides produced by trypsin digestion corresponded to the mass of groups of amino acid (Keller *et al.*, 2002), which were identified within the predicted amino acid sequence of the protein (Hale *et al.*, 2000). Following the iterative mapping of trypsin fragments to the predicted primary structure of the protein (based upon DNA sequence), most of the predicted amino acids contained within the predicted primary structure were identified (figure 19). This allowed a revision of the predicted data generated from DNA sequencing efforts, given the absence of presence of N- and C terminal amino acids.

Cleavage of an N terminal methionine from a protein is a common occurrence (Giglione *et al.*, 2004). In bacteria approximately 40% of proteins retain an N terminal methionine, cleaved by the enzyme methionyl-amino peptidase (MAP) (Hirel *et al.*, 1989). Further, the cleavage of amino acids upstream of amino acid 472, (which corresponded to the beginning of the protozoan syntaxin sequence) gave a predicted mass that matched the observed mass generated by MS analysis. The observed mass of the protein, relative to the revised prediction, (*i.e.* with the absence of the aforementioned amino acids), was corroborated by the examining the mass of the trypsin generated peptide fragments relative to GST-GFP primary structure. Table 8 reports an accord between the predicted and empirically observed data describing not only the mass but also the amino acid sequence of GST-GFP. However this doesn't

account for the discrepancy in mass observed during protein resolution by SDS-PAGE. This discrepancy may be due to the limited accuracy of protein resolution by SDS-PAGE, which is known to be, at best approximate (Webb *et al.*, 1977). This is due to shortcomings such as residual protein conformation and is underlined by the denotation “apparent molecular weight” which is applied to the standards used to calibrate SDS PAGE resolution (See *et al.*, 1985).

The hypothesis that post-translational cleavage of the N terminal Met and C terminal syntaxin sequence could be further tested by examining the immunoreactivity of the protein relative to an antibody specific to plasmodium syntaxin. Given the expense and obvious problems associated with raising an antibody to a labile protein (Konthura *et al.*, 2005) and the relative benefit of this activity to the project as a whole, this line of enquiry was not pursued.

From the MS and SDS-PAGE, immunoblotting and sequencing data it was possible to measure the mass of GST-GFP and relate this to the proteins amino acid sequence. This was viewed as critical to understanding the data generated when examining; the ratio of protein : silica interactions (section 3.3.3) and protein stability (section 3.3.4). Protein : silica ratio, and protein stability were viewed as essential to characterise the usefulness of the proposed drug delivery system.

Having begun to characterise the protein and ascertained the sequence of the material that was being used to characterise the drug delivery system, it was thought prudent to investigate the optimal bacterial culture condition, relative to protein yield. Figure 14 documents the growth of the bacterial cultures and at 110 minutes the bacteria enter the stationary growth phase (Zwieteing *et al.*, 1990). *E.coli* remain one of the most attractive systems for high yields of recombinant protein production due to the ability for rapid growth at high density, on inexpensive substrates, the well-characterised genetics and the availability of an increasingly large number of cloning vectors, (Baneyx 1999). The strain or genetic background for recombinant protein expression is of high importance. Strains used for expression should be deficient in the most harmful proteases, maintain the expression plasmid stably and confer the genetic elements relevant to the expression system (Sorensen and Martensen 2005). Such strains include *E.coli* BL21 and MC1061 chemically competent bacteria.

Therefore, it was important that induction with IPTG should be performed before the start of the stationary phase (at approximately 40 minutes (before the end of the exponential peak)). The start of the stationary phase was mediated by the lack of available nutrients, or build up of metabolic by products that restrict the number of cells that can be supported, (Yates *et al.*, 2007).

The data in figure 17, shows the empiric determination of the optimal post-induction growth time for clone 210. In this instance bacterial growth enters the stationary phase at 2 hours post induction. Hence continuing past this stage was suboptimal for protein production since culture nutrients were utilised and metabolic waste products increased. (Yates *et al.*, 2007).

The data in figure 16 shows the comparison post IPTG conditions comparing *E.coli* TOP10 and MC1061 bacteria encoding the plasmid. There appears to be no significant difference between cell types. This is not unexpected, since MC1061 bacterial cells are the parent cells of TOP10, (Casadaban and Cohen 1980).

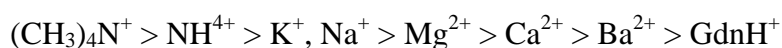
3.4.2 Characterisation of GST-GFP

In order to understand whether a protein would still be biologically active following its adsorption to and release from a silica surface, further characterisation of GST-GFP secondary and tertiary structure was undertaken in relation to the pH and ionic strength of the proteins environment. Thus, if the process of loading and release onto silica beads affected the protein in any way, changes in protein conformation would be evident.

Initially the adsorption and emission profiles for GST-GFP were obtained and were documented in figure 22. They were comparable with previously published spectra (Voityuk *et al.*, 2001). Next the spectra of GST and GST-GFP were obtained using circular dichroism (CD). This was done in order to measure the degree of protein folding before and after adsorption to the silica surface. The data in figure 27 shows the CD spectra of GST versus GST-GFP at physiological pH and ionic strength (0.2M). Conditions were then altered to assess what impact this had on the folding of the protein. Changes in buffer (to influence the interactions between ions and

proteins) and pH were altered in addition to the spectra of GST-GFP and GST in 6M guanidine hydrochloride (to denature the protein), thus comparisons could be made. It was evident that in the presence of 6M guanidine hydrochloride, both proteins, GST and GST-GFP, do not yield a CD spectra since secondary structure was eliminated (Pajot 1975).

The data in figures 23 and 24 show the change in CD spectra of GST-GFP in two different buffers, phosphate buffer and sodium acetate, at a range of pH values and at a constant ionic strength of 0.2M. There appears to be a less significant change in protein folding in phosphate buffer at every pH when compared to protein in sodium acetate buffer. Differences in CD spectra of both proteins, GST and GST-GFP in phosphate or sodium acetate buffers is most likely due to the ions presence within the buffer as dictated by the Hofmeister series (Panayiotou and Freitag 2005). Salts may stabilise, destabilise or have no effect on protein stability depending on the type and concentration of salt, nature of ionic interactions and the charged residues in the protein (Wang 1999). The effect of salts at high concentration correlates with the Hofmeister lyotropic series:



The Hofmeister series shows that anions and cations to the left of the series deliver the greatest stabilising effect. By increasing ionic strength these salts may enhance hydrophobic interactions and reduce solubility of hydrophobic groups in proteins (Timasheff 1993). In addition, water accumulation is enhanced surrounding the protein. The combination of these effects results in more compact and stable proteins (Wang 1999).

The CD spectra of GST was also documented at the same pH and buffering conditions as GST-GFP, in order to assess the change in CD spectra mediated by the GST portion of GST-GFP (figures 25 and 26). Adsorption at 240nm (and below), was principally due to the peptide bonds. The different types of regular secondary structure found in proteins, gives rise to characteristic CD spectra in the far UV range,

(Visser *et al.*, 2002). A number of algorithms exist which utilise data from the far UV CD spectra to provide an estimate of secondary structure composition of proteins (Kelly *et al.*, 2005) (figure 38). Therefore, data generated in correlation with GST and GST-GFP can be used to estimate the percentage of secondary structure difference between the two proteins.

Similarly to GST-GFP, the buffer appeared to have an effect on the extent in change of folding of GST. Finally, a native versus denatured protein CD spectra was obtained for both GST and GST-GFP. Proteins were denatured in 6M guanidine hydrochloride (Pajot 1976) (figures 28 and 29). The purpose of obtaining CD spectra in varying conditions will enable analysis of protein conformation and function following the release from silica beads (Chapter 2 section 2.2.5).

3.4.3 Assay of Protein Stability and Toxicity

It was predicted that a protein immobilised upon a silica beads would be resistant to protease degradation, however the extent of resistance would likely be proportional to the extent of the protein's immobilisation (Puu *et al.*, 2000). Consequently, the stability of GST-GFP after exposure to a protease was documented.

Initially GST-GFP was incubated at 37°C over 450 minutes without any additional protease and fluorescent spectroscopic analysis was performed in parallel with western blot followed by immunodetection using α -GFP. Figure 30 shows that fluorescent emission did not decrease over the duration of the experiment and protein integrity was confirmed using western blot followed by immunodetection blot analysis and a primary antibody specific for GFP. To characterise the stability profile of the protein after exposure to protease K, the experiment was repeated with the addition of protease K (Ebeling *et al.*, 1974). Although the fluorescent spectra of GFP appeared unaltered, the protein was no longer immunoreactive when probed with an antibody specific for GFP relative to a control (figure 31).

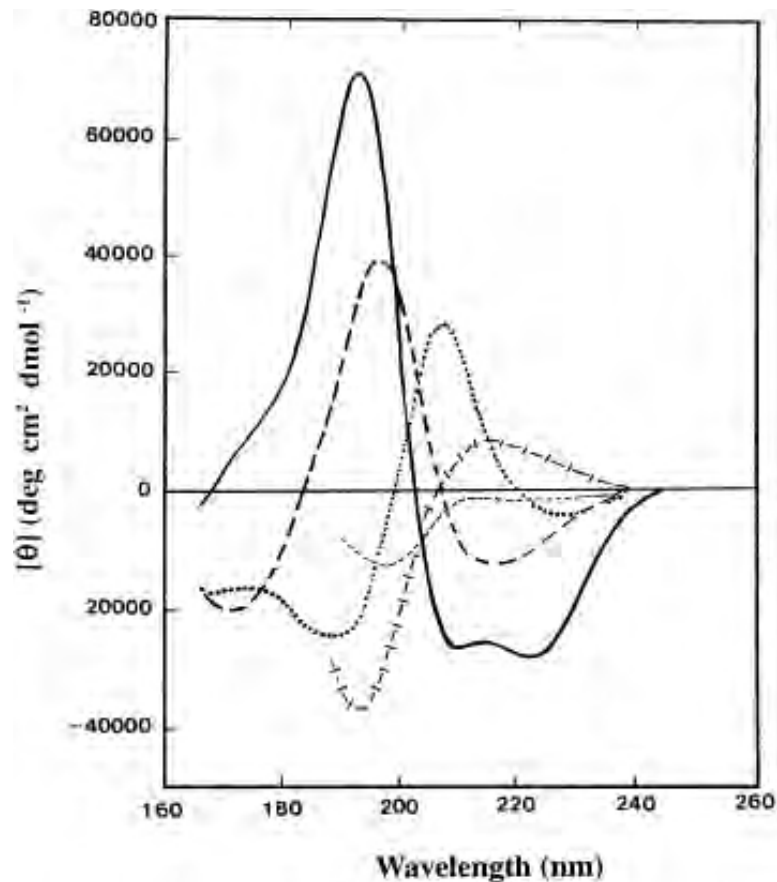


Figure 38. Far UV circular dichroism spectra associated with various types of secondary structure (Kelly *et al.*, 2005). Solid line – α helix; long dashed line – β sheet; cross dashed line – extended β helix; dotted line – type I β turn; short dashed line – irregular.

This indicated that the GFP chromophore emitted fluorescent light after the remainder of the protein was degraded. Hence GFP fluorescence did not provide clear evidence into the conformation or integrity of the protein. This observation is corroborated in the literature describing GFP (Chiang *et al.*, 2001). As the integrity of GST-GFP could not be reliably assayed using GFP fluorescence an alternative, cheap, quick and reliable method of assaying protein integrity was developed.

As GST has an affinity for glutathione conjugated sepharose beads (GE healthcare), (glutathione being the ligand for GST), it was hypothesised that this phenomena may be used to recover active GST protein, post-digestion (protocol in section 2.2.9). Since protease K would not have any interaction with glutathione (Viljanen *et al.*, 2008), GST-GFP was purified from the protease reaction.

By incubating the protein with glutathione beads in the presence of various concentrations of protease K, at 37°C over 1 hour, then sedimenting briefly for one minute, both the pellet and supernatant could be analysed via spectrophotometry, and by immunoblotting to determine the molecular weight of any immunoreactive protein either associated with glutathione-conjugated sepharose beads (*i.e.* in the pellet) or not (in the supernatant). The data (figures 32 to 34) clearly shows that in the presence of 100µU of protease K, over 1 hour, the protein was degraded as indicated by increased fluorescence in the supernatant fraction and loss of protein detected within the pellet. This data was of significance as it provided a negative control for subsequent protein stability experiments.

Since GST-GFP was to be used in cell lines for future analysis of intracellular trafficking in relation to toxin-antigen fusion proteins, the toxicity of GST-GFP was analysed. Analysis occurred in three cell lines; Caco-2 (colon epithelial tumour cell line), Vero, from African green monkey (kidney epithelial cells) and B16 (mouse melanoma cell lines) (Cosentino *et al.*, 2010; Mendonca *et al.*, 2002; Wong and Minchin 1996). These cell lines were chosen due to the nature of the oral vaccine delivery system testing in intestinal monolayers (Caco-2). Toxicity of the protein to the cells would limit the use of GST-GFP in this model. B16 and Vero cell lines were chosen as comparisons for toxicity. The protein was found to be non-toxic in all three-cell lines, relative to positive and negative controls (PEI and dextran respectively) (figure 34). PEI was known to be highly toxic and was consequently a good positive control for toxicity with IC₅₀ 17µg/ml and 30µg/ml after 24 and 6-hour incubation periods with HEX293 cells (Aravindan *et al.*, 2009). Dextran however is a polymer of glucose moieties and was therefore non-toxic to cells. IC₅₀ cannot be obtained for dextran up to 5 mg/ml (Richardson *et al.*, 1999).

3.5 Conclusion

Glutathione S-transferase fused in frame to green fluorescent protein (GST-GFP) was an ideal model antigen to characterise the proposed SCDDS due to the nature of the fusion protein, (not being too dissimilar from the candidate recombinant proteins discussed herein). The model antigen (GST-GFP) can be produced in large quantities

for a recombinant protein (~8mg/ml) and has excitation and emission spectra profiles that correspond with previously published spectra. Protein production has been optimised by analysis of bacterial growth curves and appropriate induction times obtained. Since SDS-PAGE appeared to be inaccurately resolving the protein, with an apparent molecular weight some 7kDa from *in silico* predicted molecular weight, MALDI-TOF MS was performed on the sample. Mass spectroscopy revealed a C terminal truncation and N terminal methionine removal as post-translational modifications. This aberration did not affect the model protein, since the gift providers (Prof. Piper) had an interest in *Plasmodium vivex* from where this truncation was derived. Since GST-GFP was to be used as a model antigen to characterise the SCDDS, the native structure of the protein was evaluated by CD. Both individual recombinant proteins *i.e.* GST and GFP were analysed and comparisons made to GST-GFP fusion protein. To help understand how the CD data may change upon denaturation, CD measurements were recorded in the presence of 6M guHCl. This data can now be compared to CD data from released GST-GFP from SCDDS (Chapter 2 section 2.2.5). The recombinant protein GST-GFP, was non toxic to Vero, Caco-2 and B16 cells, and will therefore be used as a negative control for toxicity in future transcytosis experiments (section 6.2).

Chapter 4: Characterisation of a Solid Core Drug Delivery System

In this chapter, four questions were addressed: 1) Could GST-GFP be immobilised (adsorbed) onto a silica solid core? 2) Could the protein-adsorbed silica be coated in fatty acid? 3) Would this enteric coat protect GST-GFP from low pH and proteases? 4) Finally it was asked if the model protein could be released from the fatty acid and protein coated silica and if the processing associated with the immobilisation and release of the proteins altered the protein's secondary conformation?

4.1 Introduction

The gold standard for vaccine administration has been documented to be via the oral route (Jones 2000). This method has provided a myriad of benefits to both the animal farming and health care industries. Previous strategies have not been successful due to limited antigen protection (Lubben *et al.*, 2002). The use of live viral vaccines, though occasionally efficacious, has led to concern over reversion to virulence or tissue damage due to viral propagation. Alternative strategies have included the use of synthetic formulations to effect antigen delivery such as; antigen entrapment within poly(lactide-co-glycolide) chitosan or alginate, micro- or nano-particulates (Singh and O'Hagan 1998). These systems aim to improve parameters; extend residence time, reduce gastric and intestinal degradation, enhance adsorption and reduce the amount of antigen required to induce significant immune response (Singh and O'Hagan 1998). However, these systems are structurally unstable "soft" materials, often prone to hydrolysis in the G.I tract. This often leads to premature release of protein or drug leading to degradation before reaching the effector site (Wang *et al.*, 2012). None of these systems proposed thus far have been able to overcome all of the associated challenges of oral vaccine delivery. Non-degradable nanoparticles such as gold and silica have also been used to immobilise antigens intended for oral vaccination (Minato *et al.*, 2003). These systems may protect protein drugs following encapsulation with polymers or fatty acids (Rigby *et al.*, 2008). Of these enteric coats, short chain fatty acids were investigated as an alternative to PLGA, since release was triggered in a similar pH responsive manner, which can be controlled over time by functionalization of the silica surface. In addition, it was thought that the presence of

additional fatty acids in the intestinal lumen might promote uptake of hydrophilic molecules (Hackett *et al.*, 2012).

Whilst each enteric coat (described above), has both advantages and limitations, here silica has been investigated as a core onto which proteins may interact via electrostatic interactions (Tang *et al.*, 2011). Silica was considered a lead SCDDS due to its overall net negative charge and excellent stability, enabling the loading of positively charged protein drugs with high efficiency. Being abundantly distributed in nature and having good biocompatibility, the FDA have approved silica as Generally Recognised as Safe (GRAS) and widely used in food additives and cosmetics (Wen *et al.*, 2012; Tang *et al.*, 2012). The active release of drug from silica nanoparticles can be generated either by pH, chemical, enzymatic response or external stimuli, all of which can be optimised and functionalized easily by surface modification of the silica surface (Arruebo 2012).

The silanol groups on the silica surface can be functionalized by grafting organic silanes ((RO₃)SiR') by optimizing drug surface interactions, usually by linking drug via ionic or ester bonds (Hoffmann *et al.*, 2006). Ionic interactions may also be formed when amino groups are linked to carboxylic acid functionalized silica, which may be used to deliver protein antigens. The release of antigen from lipid vectors involves two mechanisms; the first dependent on concentration diffusion related to surface area, and the second on degradation of carrier matrix (Kong *et al.*, 2012). The effect of particle size, lipid digestibility and drug adsorption are often controversial topics with contrasting effects of size (Vallet-Regi *et al.*, 2007).

The physical chemistry of nanoparticles either with adsorbed protein or without, is complex. Particle size and density has been documented to ultimately control diffusion through mucosal interfaces (Florence and Hussain 2001). Particle size influences the uptake through M cells as well as diffusion through the 218µm +/- 81.07µm mucosal layer (Fyderek *et al.*, 2009). Silica beads of ~500nm (manufacturers specifications), were chosen due to the size limitation of transcytosis, therefore removing any presumed toxicity issues that may arise. The silica was

hypothesed to be excreted following the release of the protein antigen, and not taken up into the body.

4.1.1 Aims of this Chapter

The aims of this chapter were to establish if:

- 1) the silica particles could be used to immobilize a model protein as a function of pH;
- 2) the protein immobilised upon the silica could be coated with fatty acid;
- 3) the aforementioned coating by fatty acid afforded protection against proteases (*i.e.* similar to the stomach);
- 4) altering the pH (to a value similar to that of the intestine) could be used to trigger the dissolution of the fatty acid and the release of the protein from the surface of the silica particles;
- 5) the secondary structure of the protein was conserved after release from the silica.

Table 10. Fatty acids tested and the corresponding properties.

Fatty acid	Melting temperature	Chain Length
Lauric acid	43.2°C	12:0
Myristic acid	54.4°C	14:0
Palmitic acid	62.9°C	16:0
Stearic acid	69.6°C	18:0

4.2 – Materials and Methods

4.2.1 Materials

In addition to the materials listed in chapter 2, the following methodologies were used:

Equipment see 2.1.1

4.2.2 Methods

In addition to the methods listed in chapter 2, the following methodologies were used:

4.2.2.1 Analysis of Silica Beads Using SEM

Approximately 1mg of silica beads were placed onto a sample stub (Hitachi SU8030) and the excess beads removed by passing a current of air over the stub. The stub was mounted and placed inside the SEM (Hitachi SU8030). Once the microscope was adjusted for focus and stigmatism, images were collected using the top upper detector (Hitachi SU8030), analysing backscattered and secondary backscattered electrons. The working distance was approximately 2.3mm with a voltage of 0.7kV.

4.2.2.2 GST-GFP Immobilisation Upon Silica Particles

GST-GFP (10mg) was dialysed into sodium acetate buffer pH5.6 and placed inside a 15ml test tube containing 100mg silica (IV) oxide powder (Alfa Aesar 7631-86-9) overnight, rotating at 4°C.

4.2.2.3 Characterisation of Protein Immobilised Upon Silica Particles

For the protein adsorption studies, the silica was collected by centrifugation (6000rpm for two minutes). The supernatant was collected and analysed via BCA assay to quantitate adsorption to silica beads.

4.2.2.3.1 Quantitation of Protein Mass Using the BCA Assay

BCA reagent was mixed at a ratio of 50:1 with $\text{CuSO}_4 \cdot 5\text{H}_2\text{O}$ and this was then incubated with sample for 30 minutes at 37°C prior to assaying their optical density at a wavelength of 562nm. Absolute protein quantities and protein concentration were calculated using a standard curve where known amounts of GST-GFP had previously been analysed via this assay and data plotted.

4.2.2.3.2 Quantitation of Protein Mass Using Densitometry

Protein absorbed silica was centrifuged (section 4.2.2.3) and Lamellae buffer added. The resulting solution was analysed by SDS-PAGE followed by western immunoblot. A control of known quantity (10ng) of purified GST-GFP was used. The resulting X-ray film image was scanned and analysed using ImageJ software. The control band was counted for pixels using the software, and compared to the unknown bands to obtain a concentration. Care was taken to ensure the bands were not overloaded.

4.2.2.3.3 Production of Deuterated GST-GFP

The model antigen (GST-GFP) in *E.coli* MC1061 was cultured in 2xYT media, containing ampicillin. However, the media was produced with 70% D_2O : 30% H_2O thus incorporating enough D_2O to allow contrast matching experiments in the neutron beam.

4.2.2.4 Characterisation of Silica Particles and Protein Immobilised on Silica Particles Using Small Angle Neutron Scattering

Samples were prepared with adsorbed GST-GFP that had been produced in the usual manner (section 4.2.2.2) or by the same method but using deuterated protein (section 4.2.2.3.3) and then placed in 2mm Hellma cells which were mounted in a rotating rack to obviate the slow sedimentation of the silica particles under the effect of gravity. Three sample detector distances (1.1m, 8m and 39m), with appropriate collimation, were employed, using incident neutrons with wavelength 8\AA . Data were put onto an absolute scale by reference to the scattering from 1mm of water, and

normalized to a common baseline. The data were ultimately fitted to a multi-shell model.

4.2.2.5 Fatty Acid Coating of GST-GFP Immobilised on Silica Particles

Fatty acids (10mg) (table 10) were solubilised in 2ml pentane (Chapter 4 section 4.2.2.4). To this, 50mg of protein-absorbed silica was added which had been previously prepared as in section 4.2.3.2. The pentane was evaporated by either sonication at 60kHz or by stirring on a magnetic plate stirrer in a fume hood. The SCDDS was then freeze-dried (Chapter 2 section 2.7.2).

4.2.3 Assessing the Degree of Protein Protection Afforded by Fatty Acid Coating Using an *In vitro* Digestion Assay at Low pH

Fatty acid coated, protein adsorbed silica was placed in HCl (0.1M) with pepsin (40µg/ml) (p6887, Sigma, Dorset, UK) (Glahn *et al.*, 1998). After an hour, NaHCO₃ (0.1M) was used to neutralise the pH (pH7.4) and porcine bile (12µg/ml) (B8611, Sigma, Dorset, UK) and pancreatin (2µg/ml) (P3292, Sigma, Dorset, UK) was added simulating lumen of the duodenum. After incubation in the simulated stomach assay (4 hours, 37°C) 8.6mg (86%) of protein was found to be intact after 4 hours at 37°C relative to either free protein (10mg degraded), or protein adsorbed to silica without a fatty acid coating (10mg degraded) (figure 4b).

4.2.4 GST-GFP Release From Fatty Acid Coated Silica Beads

The protein-absorbed silica was incubated at varying times in buffers with defined pH. Following incubation, the silica was sedimented by centrifugation at 6000 x g for two minutes before collecting the supernatant and analysing via BCA assay (section 2.7) for protein released, ensuring the concentrations were within the linear range of the assay.

4.2.5 Analysis of Released GST-GFP Secondary Structure by CD

GST-GFP (0.3mg/ml) was placed inside a 0.1mm quartz cuvette and into the sample holder. The sample was placed inside the instrument (Chirascan™, Applied Photophysics), and analysed between 190-260nm, at 2 seconds per time point, 1nm bandwidth, 20°C for three repeats. The data was plotted in molar ellipticity to account for slight variations in concentration between released and control protein.

4.3 Results

Silica was chosen as a core onto which a model antigen (GST-GFP) was absorbed and encapsulated in a range of fatty acids. First, the silica was characterised to assess the size, charge and surface characteristics. This was performed by dynamic light scattering (DLS), measuring zeta potential (Malvern zeta sizer) and by small angle neutron scattering (SANS) (table 11). The silica beads were shown to be approximately $600\text{nm} \pm 29$ (table 11), a size that would not facilitate transcytotic translocation of the intact SCDDS over the epithelial lining of the gut.

The size of silica beads were further characterised using field emission gun scanning emission microscopy (FEG-SEM) to assess surface structure and size before and after protein adsorption and fatty acid coating (figure 39). The FEG-SEM data corresponds to zeta sizing measurements with a size of $477\text{nm} \pm 81\text{nm}$ ($n = 20$).

Model antigen GST-GFP, was absorbed to silica beads by manipulating the charge of the protein with low pH buffers. Sodium acetate buffer, pH 5.6 was used to absorb the protein to the silica beads, which was left rotating at 4°C overnight (section 2.7). The beads were centrifuged and washed three times before quantifying the percentage of absorbed protein. Approximately 75% of GST-GFP ($500\mu\text{g}$) adsorbed onto the silica bead (50mg) by decreasing pH to 5.6 in sodium acetate buffer (figure 40) as analysed by BCA assay (section 2.7). Thus a 1:100 ratio of protein : silica was required for optimal protein loading.

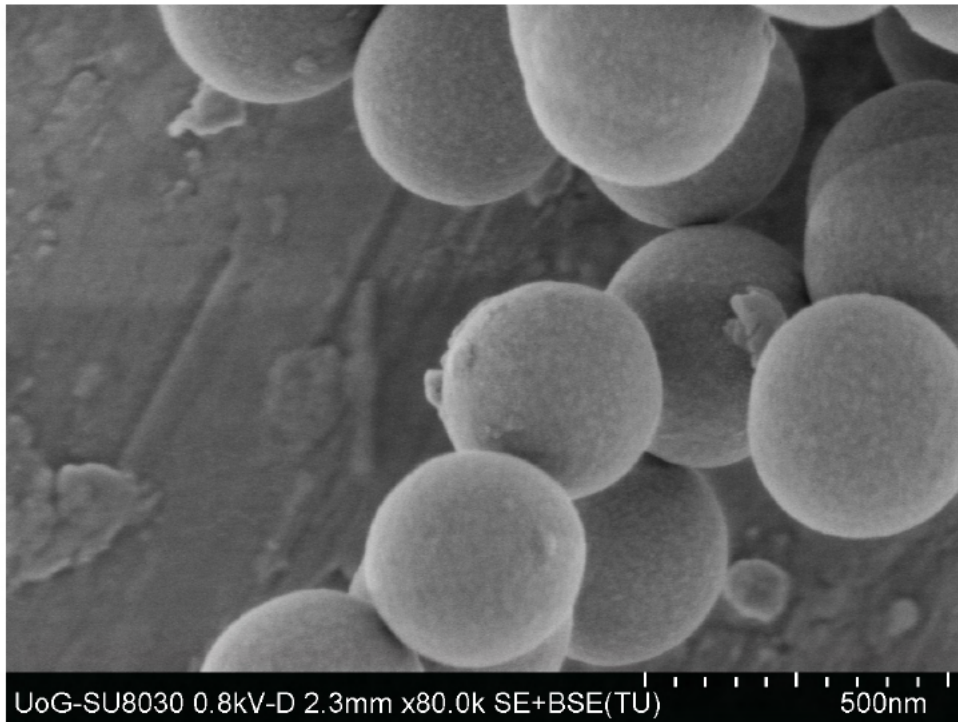


Figure 39. FEG-SEM image. Representative of the population of silica beads used herein.

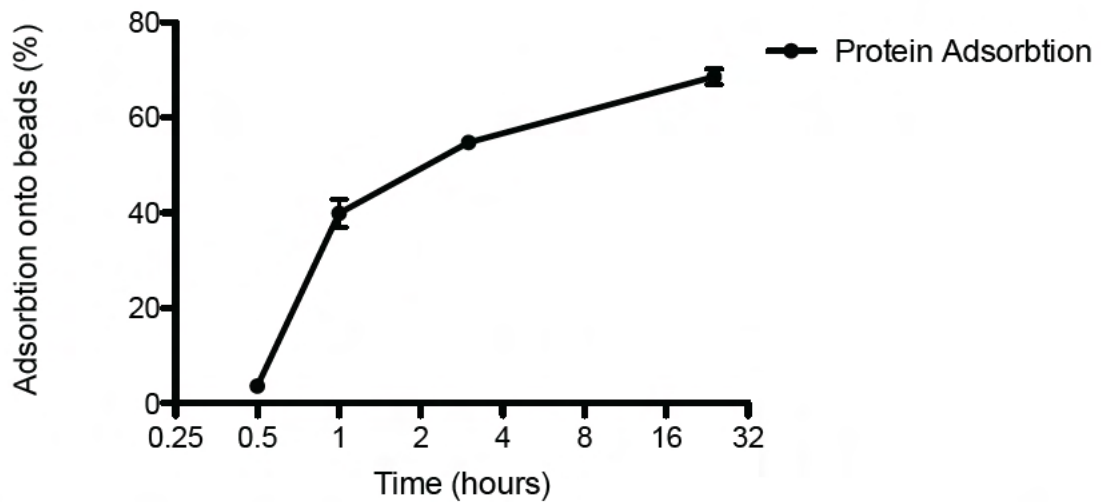


Figure 40. Protein adsorption (10 μ g) to silica beads (100 μ g) measured by BCA assay (n= 8).

The protein-adsorbed silica was characterised by small angle neutron scattering (SANS) (figure 42) using the continuous neutron source at ILL. This technique enables the visualisation of colloids, proteins, polymers *etc.* on the molecular scale. SANS was used to characterise the thickness of the protein layer using a series of contrast-matched samples (figure 41). To this end, the model protein GST-GFP was produced in both deuterated and hydrogenated forms. This was performed by culturing *E.coli* MC1061 containing the GST-GFP plasmid in 2xYT media with 70% D₂O. The model antigen was then purified and characterised in exactly the same manner described in Chapter 3 (section 3.3.1), and adsorbed to the silica beads overnight.

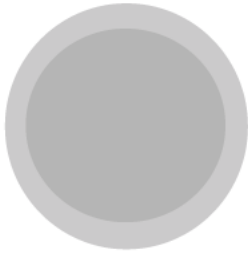
The SANS data showed that the protein coated silica particles; appear discrete, (*i.e.* not aggregating); with a radius of $3300 \pm 10 \text{ \AA}$ ($330 \pm 1 \text{ nm}$); and corona of adsorbed protein some $120\text{-}160 \text{ \AA}$ ($12\text{-}16\text{nm}$) thick. The absolute intensities are entirely consistent with these dimensions and the known composition of the system, suggesting water content within the protein layer of some 30-40% (w/v). The thickness of the protein layer was slightly greater (1.5-2x) than the theoretical GST-GFP size (8.4nm) (calculated using I-TASSER, Roy *et al.*, 2010) consistent with polymer adsorption theories (Fleer *et al.*, 1993). These values are in agreement with the light scattering data (table 11), which shows an increase in particle size of $10 \pm 3.2\text{nm}$ upon protein adsorption.

Table 11. Analysis of SCDDS, size and charge.

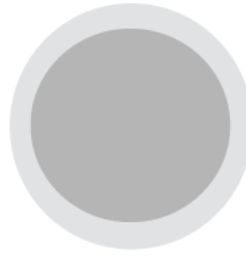
	ζ Pot ^e (mV)	Size (nm)	SANS (nm)
GST-GFP	-16.7	12	N/A
Silica	-43.3	623	600
Silica + Protein	-41.5	631	720
Silica + Protein +MA	-17	679	N/A

Solvent – D2O

1) h-(GST-GFP) 'Drop'
particle



2) d-(GST-GFP) This is controlling
for the CORE.



Solvent – D20:H2O

3) h-(GST-GFP) Silica
invisible, protein scatters –
SHELL



4) d-(GST-GFP) For completeness
of investigation



Figure 41. Cartoon depicting the series of contrast matching techniques used to visualise protein corona.

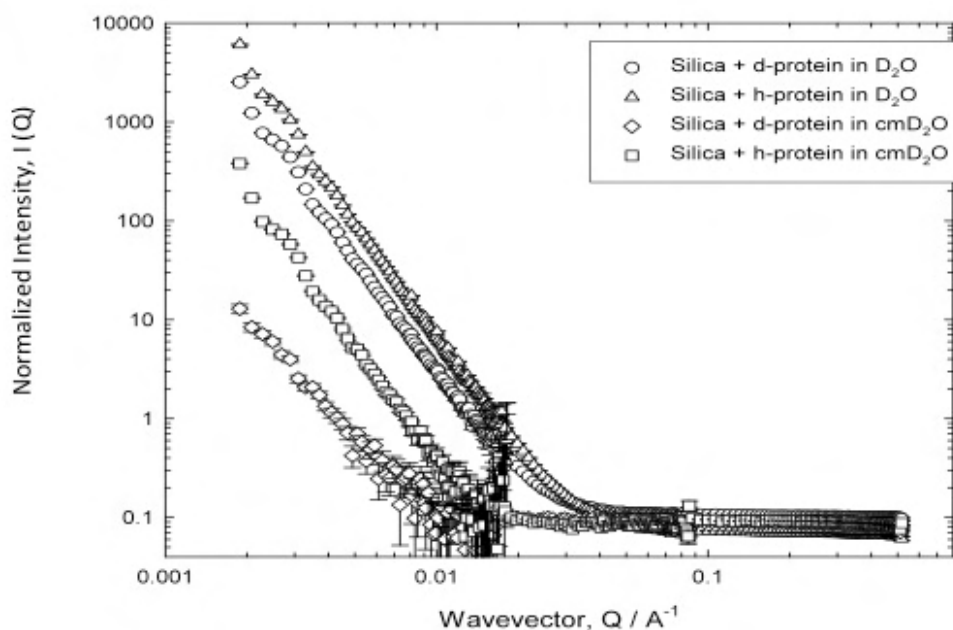


Figure 42. SANS data obtained by series of contrast matching techniques. Data normalized to buffer baseline.

However, in order to ensure the protein was protected from the low pH of the stomach and from a myriad of proteases that are present within the G.I tract, a protective coating must be completely covering the protein layer. Four fatty acids have been used to coat the surface of the protein silica complex, namely lauric, myristic, palmitic and stearic acid. Previously supercritical CO₂ had been used to solubilise lipids (Kong *et al.*, 2012) and subsequently coat material intended for drug delivery. Supercritical CO₂ fatty acid coating did not work well in this instance, producing aggregates of particles. Consequently pentane was used to solubilise fatty acids and coat the protein-adsorbed silica, a novel undertaking. Each fatty acid was assessed for the ability to protect GST-GFP from protease K, previously analysed for the ability to degrade this protein (Chapter 3 section 3.3.4). The data in figure 43 demonstrated that all fatty acids were capable of protecting GST-GFP from 500µU protease k comparative to control of GST-GFP alone and GST-GFP adsorbed to silica beads. However, myristic acid showed the best protection (100% protection, detected by Western immunoblot and using densitometry (section 2.4.2.2)) and thus was chosen to be the lead fatty acid to continue experiments with from this point forwards.

Additionally, a stimulated gastric digestion assay was undertaken to analyse whether myristic acid was capable of protecting GST-GFP from low pH with the presence of pepsin. The pH was increased after one hour (section 2.8) and bile and pancreatin was added to simulate the small intestine. Protein was analysed by western immunoblot to assess whether any degradation had occurred.

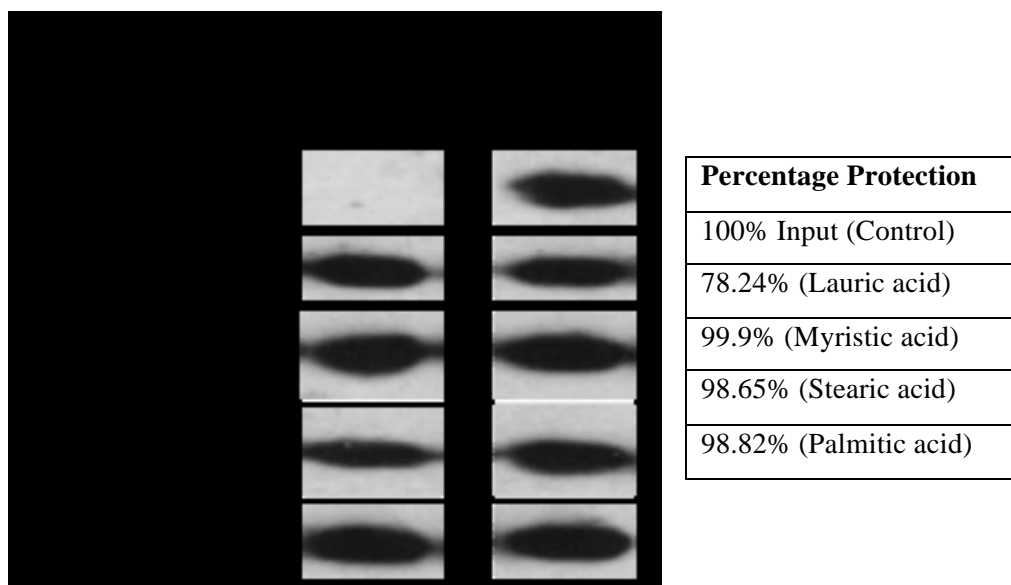


Figure 43. Protein absorbed silica particles were coated with four different fatty acids, (myristic, lauric, steric and palmitic) and assessed for their ability to protect GST-GFP from protease K. All four fatty acids could protect GST-GFP comparative to a control of uncoated GST-GFP absorbed particles (in the + panel). The negative controls are fatty acid coated GST-GFP absorbed beads that have not been incubated with protease K. Myristic acid was chosen as a lead candidate for its ease of use.

In addition, two protocols were investigated to analyse which one offered greater protection to the model antigen. The first protocol involved pentane evaporation via sonication, whilst the second involved stirring the SCDDS allowing the pentane to evaporate. The system whereby the pentane was evaporated by sonication produced fine particles whereas the stirring method produced particles that appeared to aggregate. The products obtained from these protocols, were subject to the *in vitro* digestion assay (Glahn *et al.*, 1998) (figure 45). The method employing sonication protected GST-GFP from degradation during this process, whereas the stirring

protocol did not. The sonication method was then used from this point forward for further investigations.

To optimise the system, different weights of myristic acid was used to assess the coating of the surface of the silica bead with adsorbed protein. GST-GFP adsorbed silica, coated with myristic acid ($10^{-2}\mu\text{M}$) was protected from heating at 42°C , however when the weight of myristic acid was below this point, protection was lost. This corresponded to Pockel's point. Agnes Pockel (in 1891) discovered that the surface area that was needed for a binding group was 20\AA . The surface area of the silica core was calculated to predict the amount of fatty acid required to form a monolayer on the silica surface. This was calculated to be $10^{-2}\mu\text{M}$. The data in figure 44 suggests that when this monolayer is lost, the protein is degraded.

The enteric coat protected GST-GFP from proteases and heat, however the question remained whether the protein was released in an active configuration. To help understand this notion, the circular dichroism spectra of GST-GFP before adsorption, after release, and after fatty acid coating and release was analysed (figure 48) and in each instance showed (via CDNN, AppliedPhotophysics, Surrey, UK) the structure of the protein remains constant. This demonstrates, for the first time, that protein can be protected, and released by this system without disrupting the secondary structure of the protein.

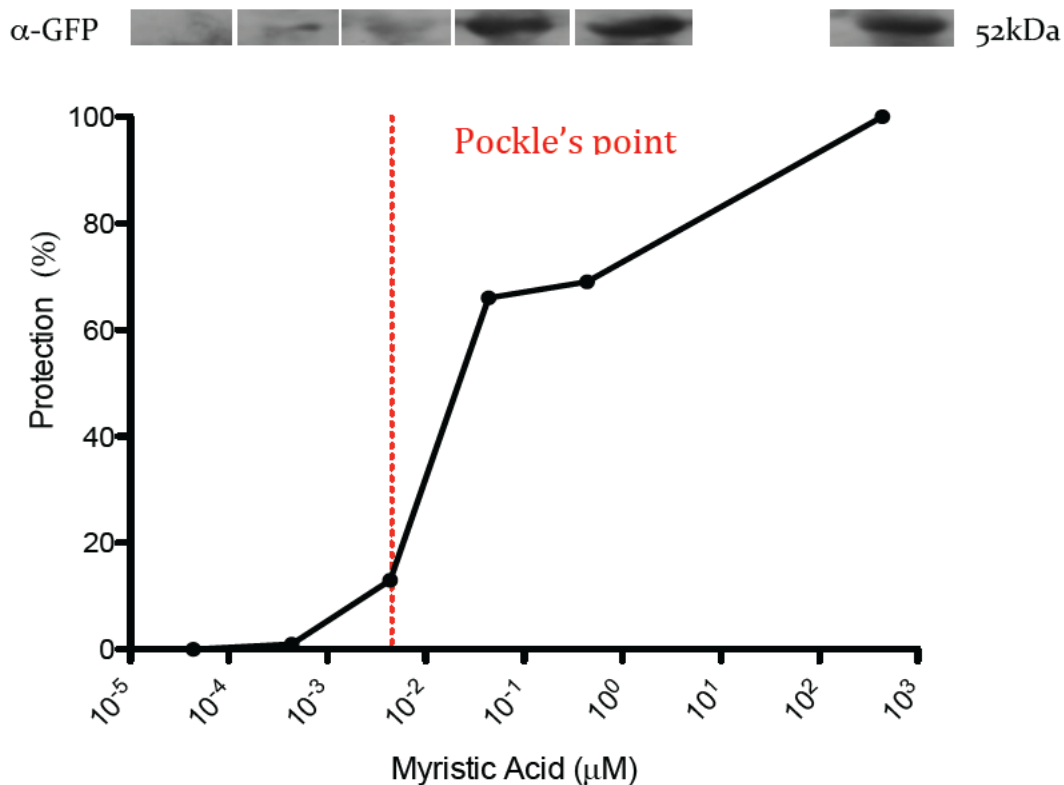


Figure 44. Dilutions of fatty acid to analyse how much myristic acid was required to protect GST-GFP from 42°C heat over two weeks.

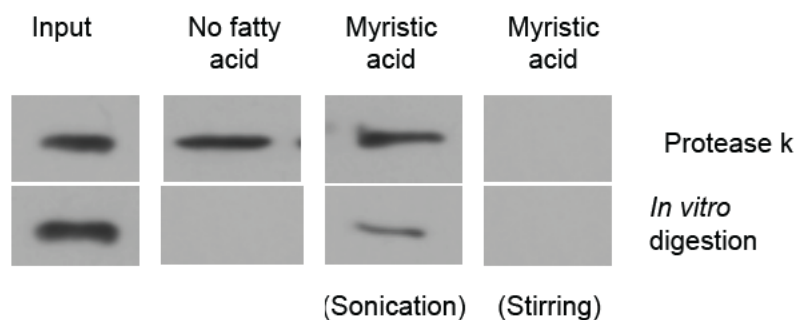


Figure 45. Protection of GST-GFP following myristic acid coating. Two protocols were used to assess the ability to protect GST-GFP. The first was sonication of the SCDDS to remove the pentane, the second was gentle stirring allowing the pentane to evaporate over time. Protection shown against protease K and *in vitro* digestion.

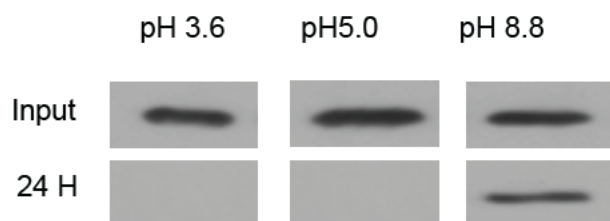


Figure 46. GST-GFP release from fatty acid coated silica beads was analysed in response to increase in pH. No release was seen from the SCDDS until the pH reached 8.8.

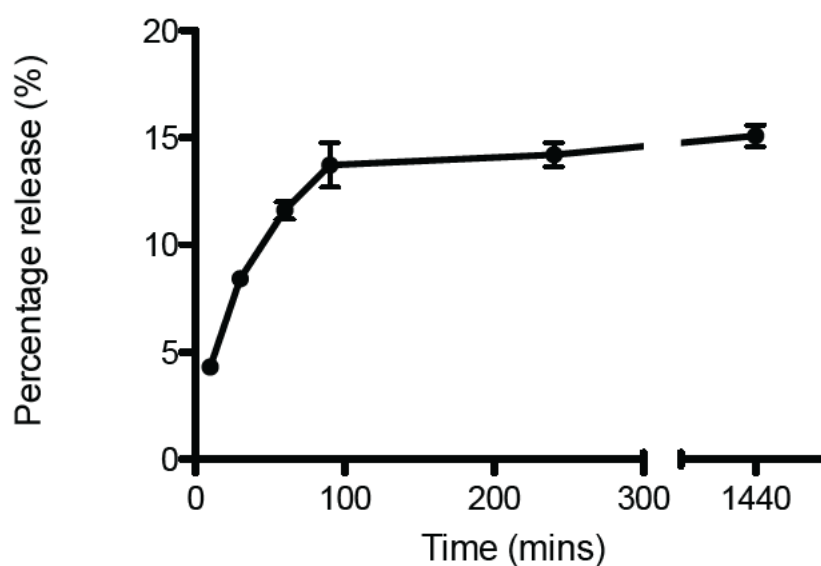
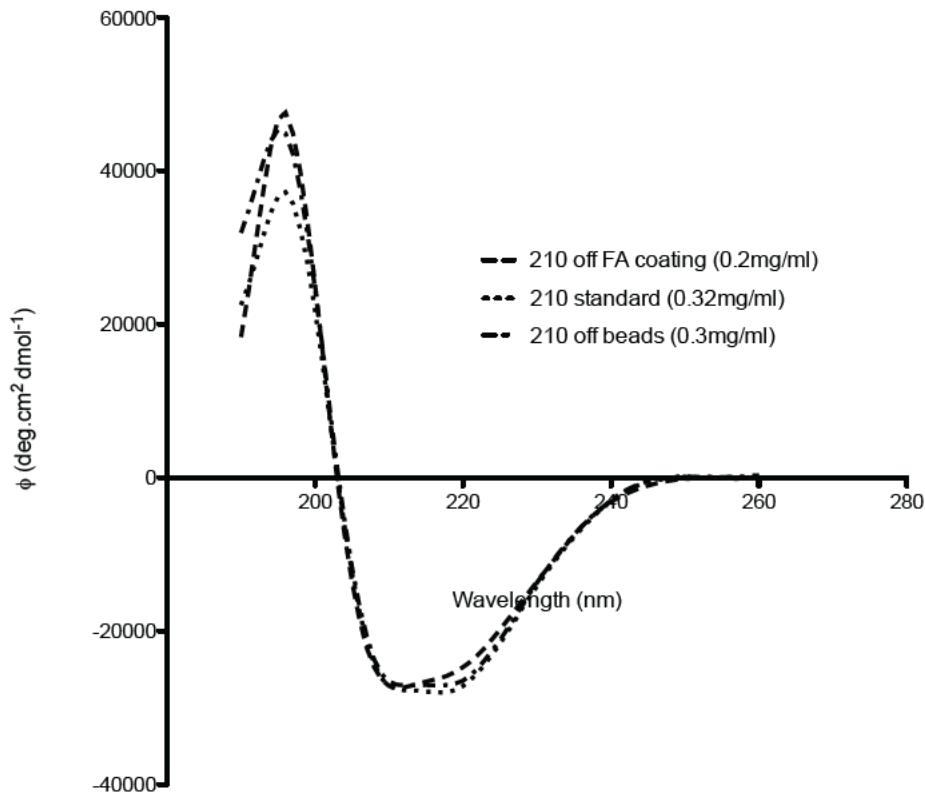


Figure 47. Protein release from silica beads, quantified using BCA assay (n=8). The released protein was purified from the supernatant using glutathione sepharose beads. This demonstrates there is no significant change in tertiary structure of the protein.

CD spectra of GST-GFP post release from silica NP (NP-FA) and myristic acid coated NP (NP+FA)



Molar Ellipticity	GST-GFP	Released protein - FA	Released protein + FA
α -Helix	16.9%	16.9%	16.9%
β -sheet	20.8%	20.8%	20.8%
Random Coil	43.3%	43.3%	43.3%

Figure 48. Circular dichroism of released GST-GFP from silica beads before and after fatty acid coating.

GST-GFP was released from the SCDDS by changing the buffer conditions, increasing the pH to 8.8, simulating the alkaline environment within the small intestine (Jain and Vyas 2006). A variety of pH ranges were initially investigated, but GST-GFP was found to dissociate at pH8.8. With increasing pH, above pH8.8 GST-GFP continues to be released, but since this range was far surpassing the physiological parameters, only the lower ranges were valid (figure 46). At pH8.8 GST-GFP was detected in the supernatant (~1/10th input) comparative to pH3.6 and pH5.0.

Since release was less than optimal, at ~15%, investigations into ionic strength and volume of buffer were initiated. Solutions ranging from 0M ionic strength (*i.e.* water) to an ionic strength of 2M, of NaCl was used to evaluate the effect of salt. In contrast to the literature, it appeared that GST-GFP was released at a higher rate, in lower ionic strength solutions to those of higher ionic strength (figure 49). The reasons for this are not understood, but suggested to be related to the Hofmeister series. The Hofmeister series suggests that cations such as sodium are responsible for decreasing the solubility of hydrophobicity. Hence, the more insoluble the myristic acid, the less likely it will dissociate from the silica bead allowing protein release. Since the ionic concentration of the small intestine is high (0.14M) (Liu *et al.*, 2009), this will need further investigation at a later date.






	Protein Release as a Function of Ionic Strength (ng)				
Control (10ng)	0	0.00125	0.0125	0.125	0.25
					

Figure 49. Protein release as a function of ionic strength.







Input	1/1600	1/1600	1/1600	1/1600	1/1600	+ve control
Volume	0.5ml	1.0ml	3.0ml	5.0ml	10.0ml	10ng
						

Figure 50. Protein release from silica beads as a function of volume.

In addition, the volume of buffer to the weight of fatty acid coated, protein absorbed silica was investigated to establish the presumed effect of drinking. prior to oral administration of vaccine and whether this would facilitate enhanced release. To this end, 100mg of fatty acid coated, protein absorbed silica was analysed for release in 0.0125M NaCl solutions at varying volumes, from 500µl to 10ml (figure 50). GST-GFP was not detected using western immunoblot, until 3ml of solution was used. Thereafter, GST-GFP increased in release rate over the time frame of 3hours comparative to 10ng GST-GFP positive control.

4.4 Discussion

The characterisation of model protein has been carried out using multiple analytical techniques such as circular dichroism (CD) (section 3.3.3.3), mass spectroscopy (MS) (section 3.3.3.2), and western blot (WB) prior to analysing the released protein, see Chapter 3 section 3.3.3. This was performed to 'characterise what we have in the pot' before and after release from the SCDDS.

The silica was characterised for signs of porosity and size under field emission gun scanning electron microscopy (FEG-SEM) (figure 39). The size of the silica beads was 477±153nm (n=20). This was further analysed using Malvern zeta sizer, which described the silica beads to be approximately 600nm ± 23. The discrepancy was thought to be due to calibration of the FEG-SEM, since SANS experiments correlated with the DLS data (table 11). However, due to temporal constraints this hypothesis was never tested. The model protein GST-GFP adsorbed to the silica surface via presumably electrostatic interactions by changing the pH of the buffer. Since GST-GFP has a measured pI of 4.6, the sodium acetate buffer pH was decreased to pH5.6 to yield enough positively charged residues to enable adsorption. Protein adsorption was characterised by BCA assay. Binding efficiency of GST-GFP was calculated to be 1:100 ratio of protein to silica and hence every experiment thereafter had 10mg of GST-GFP: 1g silica beads. However, this may vary with increased amounts of silica since the binding area would increase with available surface area. Since GST-GFP could adsorb to the surface of the silica beads, there was a requirement to understand the physical chemistry of these nanoparticles. To perform this task, dynamic light

scattering was performed. Zeta potential and zeta size measurements were analysed to investigate whether there was any significant size or charge increase. The size of the particles increased 8.4nm when GST-GFP was absorbed to the silica beads. This was suggestive that there was a single protein layer. However, to further characterise the system, the use of SANS was employed. This technique uses neutrons to analyse the molecular structure of the complex (Niemann *et al.*, 2008). The data generated enabled the determination of the thickness of the protein corona, some 120Å in diameter. From this, it was possible to calculate the hydrated content of the protein corona. The theoretical calculated size of GST-GFP from I-TASSER analysis was 8.4nm, therefore it was concluded that there was a 40% (w/v) water content present in the corona.

To demonstrate proof of concept, the SCDDS must be able to protect the protein from low pH of the stomach, and from proteases that are present within the G.I tract. To establish this concept, the SCDDS was coated in a variety of fatty acids. Four fatty acids were investigated, myristic, palmitic, stearic and lauric acid, all with varying properties and chain length. Since these fatty acids have high melting temperatures (table 10) there are obvious limitations in how to coat the SCDDS with these lipids. Previously groups have used supercritical CO₂ to solubilise the lipids (Illum *et al.*, 2012). Unique to this work, an alternative method of solubilising the fatty acids in a non-polar solvent of pentane was used. It has been previously shown that group three organic solvents such as pentane do not either stabilize or destabilise proteins (Asakura *et al.*, 1977; Graber *et al.*, 2007) although the reasons for this was not completely understood, but was most likely due to the hydrophobic sites within the protein primary structure (Wishnia and Pinder 1966). Pentane was therefore used as a solvent to solubilise a variety of fatty acids listed in table 10. The pentane was evaporated using two techniques, one, which allowed the evaporation of pentane while stirring the solution, and the other whereby the delivery system, was sonicated gently, allowing the pentane to evaporate. Both these systems were analysed using the *in vitro* digestion assay (Glahn *et al.*, 1998).

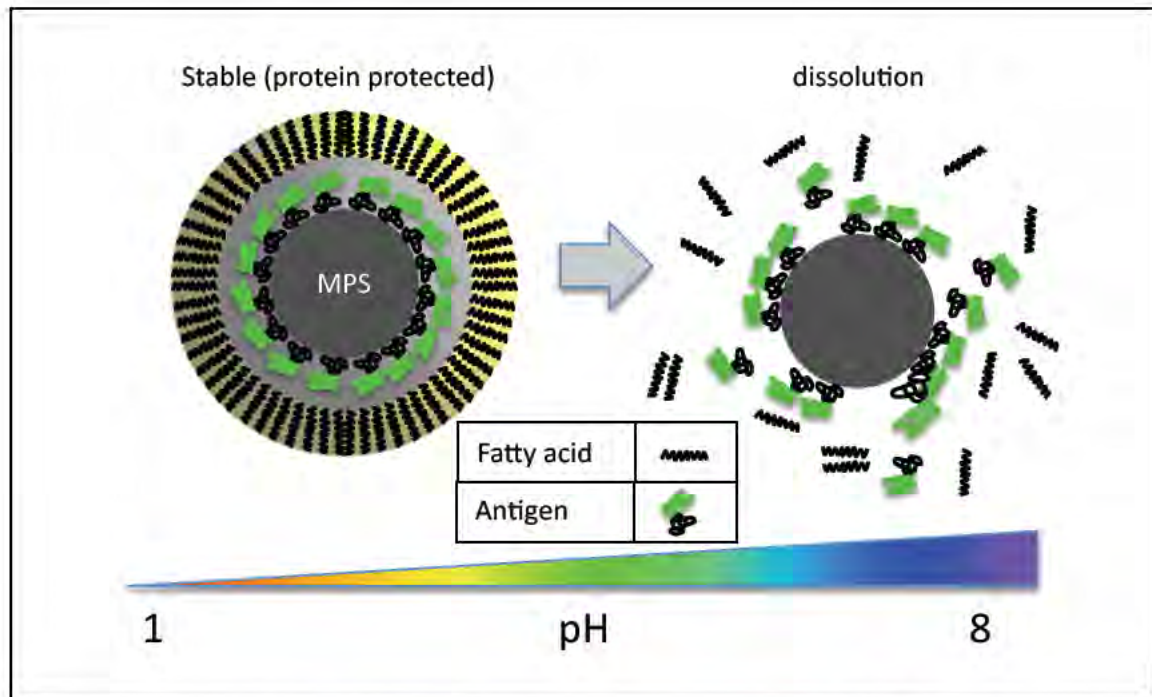


Figure 51. Schematic of SCDDS showing silica core, adsorbed model protein and fatty acid corona.

The *in vitro* digestion assay was used to simulate the environment of the stomach and the intestine, demonstrating protection of GST-GFP. The SCDDS was placed in HCl at pH2 with the addition of pepsin to simulate a stomach environment. After an hour, the pH was increased by the addition of NaHCO_3 and bile was added. The increased pH prevents the action of pepsin but simulates a small intestine environment. The data in figure 45 shows that two protocols were used for coating of beads with fatty acid as described above. The sonication protocol along with *in vitro* digestion assay protected the protein from low pH, pepsin and bile salts whereas the stirring protocol did not.

The antigen that will be delivered to initiate an immune response must be protected from the stomach but also be released in the small intestine to be effective. It was therefore necessary to test this hypothesis with the use of varying pH buffers (figure 46). Protein remained adsorbed to the beads at pH 3.6 and pH5.0, but was found in the supernatant at pH8.8 (figure 46). Thus, the protein appears to remain attached and protected at low pH while released at high pH (consistent with the small intestine).

Since protection had been demonstrated, questions pertaining to the silica surface area arose. The silica bead surface area has small pores on the surface. These pores may

possibly allow the protein to fit into these pores allowing more protein to bind. The surface area of the silica available for protein binding was calculated. This could then be used in relation to fatty acid binding. Since the minimum area for binding of a fatty acid head group was approximately 20 Å (Pockels 1891) it begs the question about the surface coating of fatty acid over the SCDDS surface. If there is too much fatty acid, was the coating greater than one layer thick? Was the coating irregular? Therefore, based on the calculation of surface area, dilutions of fatty acid were undertaken until a point where protection was no longer evident (figure 44). At 10^{-2} μM of fatty acid coating 50mg of silica previously coated with protein, the signal from western blot and immuno-detection slowly disappeared. At a concentration of 10^{-3} μM, the protein was degraded at 42°C over 24 hours comparative to a control. Thus, despite a large amount of fatty acid relative to surface area, the protein remains protected regardless of coating. If the monolayer integrity was incomplete due to too little fatty acid, the protein was degraded. Hence it was most likely that the FA coat was not a monolayer but was complete if not multi-layered.

The model protein, GST-GFP was released by increasing pH to a point where the protein became neutral or slightly negatively charged at pH 8.8 and was detected in the supernatant using western immunoblot with an anti-GFP antibody. Protein was shown to release over 90 minutes before reaching a plateau. Fifteen percent of the adsorbed protein was released whilst the remainder appears to show a favourable environment with the silica particle (fig 47). This may be optimised by altering surface charge of the silica by functionalization (Hoffmann *et al.*, 2006). However, the protein that was released must be in a conformationally active configuration to demonstrate protection by SCDDS. To this end, the secondary structure was determined by CD to compare and contrast the protein spectra of GST-GFP before and after adsorption to the silica particle. CD spectra of released protein, following GST immobilisation using glutathione beads shows the protein remains unchanged using CDNN software (Applied PhotoPhysics, Surrey). Therefore it was concluded that the adsorption and release to the surface of silica does not alter the structure of the model protein.

Since protein release was low ~15% over 90 minutes, salt concentration was analysed. The ionic strength in the G.I tract has been shown to change depending on food intake type and amount, (Gupta *et al.*, 2002) therefore it was critical to understand how the SCDDS may release protein in low or high ionic strength environments. The data in figure 49 shows in varying ionic strengths of NaCl, protein release from silica beads changes. Interestingly, GST-GFP releases from SCDDS at lower ionic strength and decreases as ionic strength increases. These results correlated to the literature whereby protein was shown to release at lower ionic strengths (Steri *et al.*, 2013). Since the silica surface can be functionalized to optimise protein loading and release, these parameters may be optimised in the future for a variety of proteins and altered based on pI of protein used (Kharlamova *et al.*, 2010).

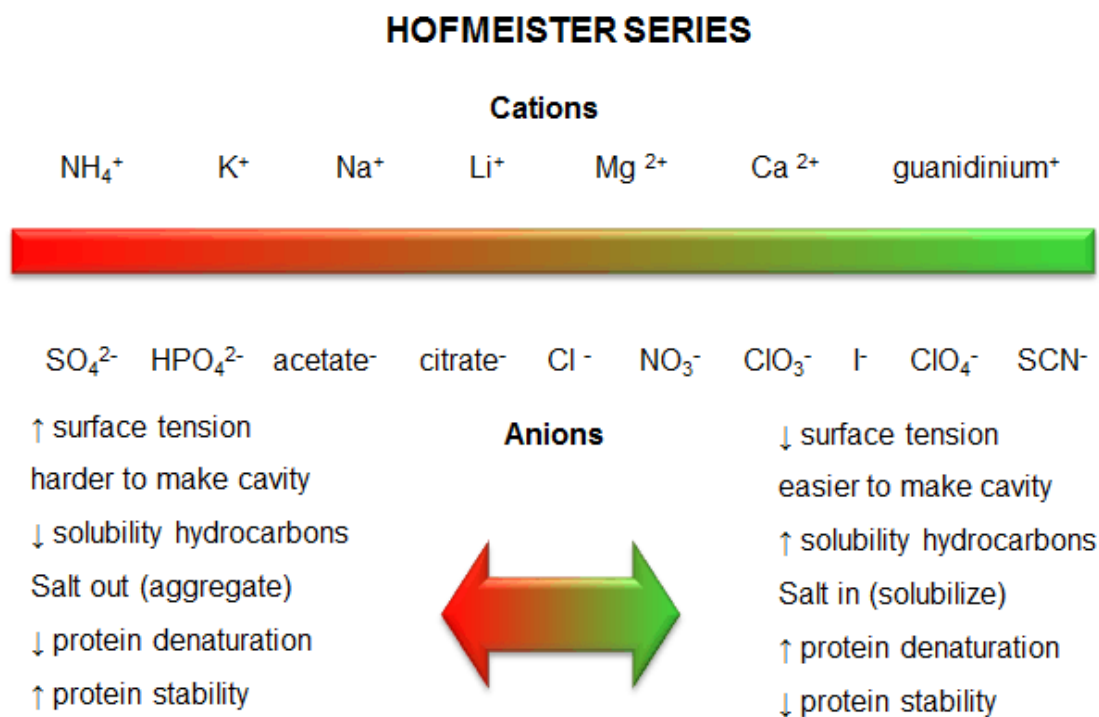


Figure 52. The Hofmeister series: the effect of salts.

4.5 Conclusion

Silica particles of ~500nm diameter, can adsorb a model protein (GST-GFP), and be coated in a variety of fatty acids. These fatty acids can be solubilised in pentane and sonication used to evaporate the solvent. Following the coating, the protein was protected from protease k, pepsin, low pH and heat (42°C). The surface coating of the fatty acid was likely not to be in a mono-layered form but complete as opposed to partial covering. Protein release was increased by low ionic strength solutions in a high volume. However the silica beads may be functionalized for greater release profiles (Hoffmann *et al.*, 2006). The released protein had identical (secondary structure, by CD) to protein before adsorption on to silica beads, hence it was concluded that this process does not destroy GST-GFP. This SCDDS system may be used instead of cold storage of vaccines or protein drugs, and was critical for moving the platform technology of oral vaccination forward. The SCDDS may be optimised for a myriad of protein antigens in a simplistic manner with regard to charge and loading.

Chapter 5: Cloning and Expression of Recombinant Proteins to Facilitate Transcytosis Across a Polarised Caco-2 Cell Monolayer

This chapter set out to answer the following questions: Could recombinant PCR be performed to fuse in frame trafficking proteins such as cholera toxin to an antigen from IBDV (VP2)? Could these recombinant proteins be expressed? Were these proteins fully folded in a conformationally functional form? And finally, could these proteins mediate transcytosis across monolayers of polarised Caco-2 cells?

5.1 Introduction

Chapter 4 showed that a model antigen (GST-GFP) was successfully adsorbed to silica beads. This protein-absorbed silica was coated in myristic acid, which ultimately protected GST-GFP from degradation by proteases. When the protein was released, the secondary structure was almost identical to that of the pre-processed protein when assayed by CD. In view of this it was deemed necessary to move towards the use of an antigen with application to veterinary or medical needs, as well as a protein that could facilitate the movement of the antigen out of the lumen of the GI. Consequently, the sub-cloning, expression and trafficking of the identified proteins were analysed. Cholera (Lencer *et al.*, 1995) and Shiga toxin B chains (Malyukova *et al.*, 2009), have both been reported to be able to facilitate the transcytotic exit of material out of the lumen of the intestine, and into the *lamina propria*. It was therefore hypothesised that these proteins, when fused in frame to the antigen (VP2) would remain capable of this feat.

5.1.1 Toxins and Membrane Trafficking

Cholera and Shiga toxin B chains have been reported to be responsible for cellular binding and intracellular trafficking of the protein toxin (Lencer *et al.*, 1995; Malyukova *et al.*, 2009). Cholera toxin (CT) has been documented to be restricted from transepithelial diffusion in relation to size. Lencer *et al.*, (1995) found that in order to activate the basolateral associated cAMP over-activation, CT is transported via an intracellular (transcytotic) pathway to the *lamina propria* beneath. The same is

believed to be true of shiga toxin (Malyukova *et al.*, 2009). If these proteins were responsible for independent transcytosis, it was considered possible that if fused in frame to an antigen (VP2), that they would be able to deliver the antigen to the *lamina propria*. Additionally, these two toxins act as adjuvants, stimulating the immune response and enhancing the effect of the vaccine (Ohmura *et al.*, 2005).

Structurally, these two proteins are very similar as seen in figure 53. They both have a catalytically active A chain, and “base” consisting of a pentameric assembly of B chain molecules (Merritt and Hol 1995). For this study, the B chain sequences were identified from GenBank, and sub-cloned into pET151 plasmid vector for expression in *E.coli* BL21*DE3 and analysis. For sub-cloning, the insert required the inclusion of a 5' CACC nucleotide sequence for directional ligation *i.e.* to help prevent the gene being inserted in the incorrect direction into the plasmid vector. All genes were analysed for insertion into the pET151 vector using PCR and analysed for size and type of plasmid. They were then sent for sequencing to the University of Dundee (DNA Sequencing and Services) and the returned sequences were aligned and analysed using DNASTAR software.

Cholera

Shiga

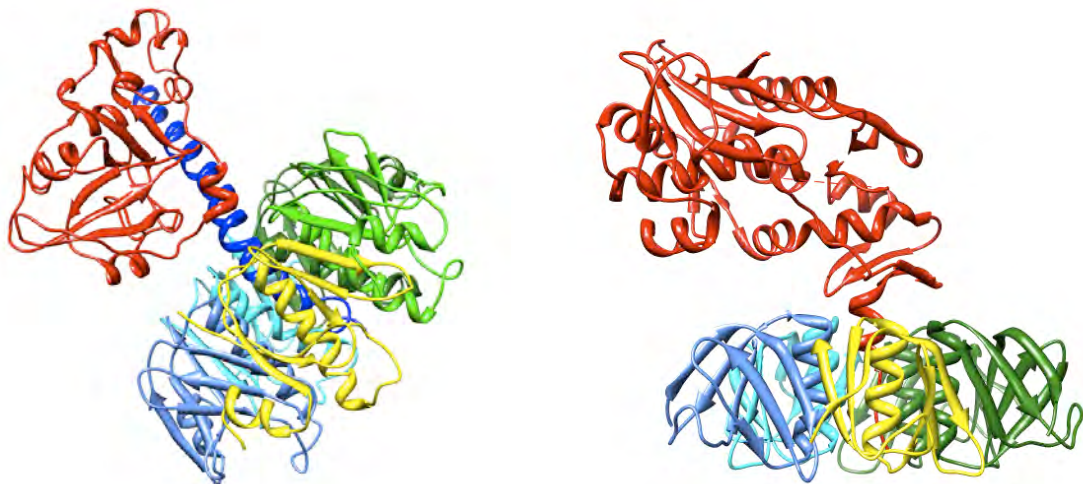


Figure 53. Cholera and Shiga toxin, sequences obtained from protein data bank (1XTC) and (IR4Q) respectively. The A chain at uppermost region of protein (red). Blue helical region – the portion of the protein, cleaved upon entry to endoplasmic reticulum. The B subunits, in different colors, are representing each individual chain of the pentameric structure.

Table 12. Genes required for cloning, and their specific uses.

Plasmid Name	Gene	Purpose	Reference
pCTBC	CTBC	Control for the effects of CTBC toxicity and transport across epithelial monolayers	Sandvig and Deurs (2002)
pSTBC	STBC	Control for the effects of STBC toxicity and transport across epithelial monolayers as well as antigenicity	Sandvig and Deurs (2002)
pV2a	<i>Acce</i> I - <i>Spe</i> I fragment of IBDV VP2	Control of the effects of both the antigen and trafficking domain of fusion proteins	Azad <i>et al.</i> , (1994)
pV2b	<i>Sma</i> I- <i>Xho</i> I fragment of IBDV VP2	Control of the effects of both the antigen and trafficking domain of fusion proteins	Azad <i>et al.</i> , (1994)
pGFP	GFP	Control for CD spectra, toxicity, negative controls for cellular trafficking	Dietz and Bahr (2004)
pGEX	GST	Control for CD spectra, toxicity, negative controls for cellular trafficking	Aatsinki and Rajaniemi (2005)
pVP2-GFP	VP2-GFP	Control for toxicity and cellular trafficking	Dietz and Bahr (2004) and Azad <i>et al.</i> , (1994)
pCTBC VP2a	VP2-CTBC	Trafficking of antigen across polarised cellular monolayers	Azad <i>et al.</i> , (1994) and Sandvig and Deurs (2002)
pSTBC VP2	VP2-STBC	Trafficking of antigen across polarised cellular monolayers	Azad <i>et al.</i> , (1994) and Sandvig and Deurs (2002)

The proteins identified, *i.e.* STBC and CTBC and the antigen (VP2), were fused in frame by using recombinant PCR. Primers were designed to perform this task. The forward primer for (gene 1) was derived from gene sequence for the 5' end of the proposed ORF, with a CACC added at the far 5' end for directionality. The second (reverse) primer was in the reverse complementary orientation to the 3' end of to gene 1 (at the 5' end of the proposed ORF), whilst also containing, additional downstream (3') sequence corresponding to the reverse complementary 12 nucleotide bases specific for the 5' end of the second gene (whilst ensure the removal of any stop codons). The second PCR reaction required primers designed to either the 5' end of the second protein, coded for by the 3' end of the ORF, fused downstream to 12 nucleotides complimentary to the 3' end of the first gene (again omitting any stop codons). The far 3' primer required for the second PCR reaction was in the reverse compliment orientation to the far 3' end of the desired (second) ORF, ensuring there was a stop codon added, denoting the end of the proposed, recombinant ORF (figure 54).

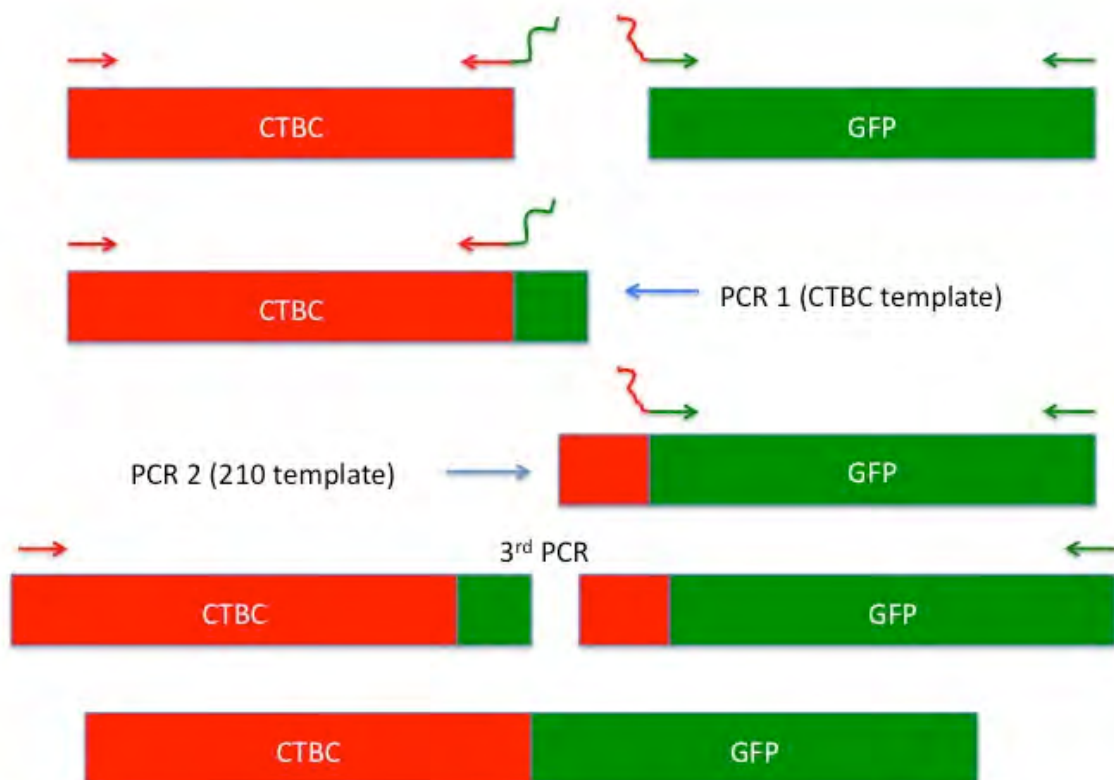


Figure 54. Cartoon displaying the process of recombinant PCR, using CTBC-GFP as an example.

5.1.2 Understanding the Mechanisms of Transcytosis

Transcytosis is a modified form of endocytic membrane transport utilised during the movement of macromolecular cargo from one face of the cell to the other *i.e.* from apical to basolateral. This process utilises a membrane bound carrier and allows the tight junctions responsible for maintaining cell-cell contact to remain closed (Ellis and Luzio 1995). It is a strategy that has evolved to selectively move material between two different environments. In polarized epithelial cells, movement of material can occur in either direction *i.e.* apical to basolateral or basolateral to apical (Tuma and Hubbard 2003).

In relation to an immune response, “antigen sampling” is the first step in the role of the mucosal immune response and entails the apical to basolateral delivery of soluble and particulate antigens to the underlying MALT (Cardone *et al.*, 1994). M cells principally carry out this transcytotic event. Later in the immune response polymeric IgA, secreted by activated plasma cells will be transcytosed from the basolateral to apical environment to help bind and remove the associated pathogen (Tuma and Hubbard 2003). Therefore, it was considered that if an *in vitro* model for transcytosis could be used, analysis of the recombinant protein’s ability to across into the *lamina propria* could be investigated. As the Caco-2 model has been very well characterised (Hilgers *et al.*, 1990) and widely adopted by industry (Yamashita *et al.*, 2000), despite the species differences associated with different veterinary models, it was considered useful in this instance.

Table 13. Examples of molecules capable of transcytosis.

Adult intestine	Cell type	Cargo	Direction	Receptor / carrier	Comments	Reference
	M cells in Peyers patch	Antigen, pathogens	A-B	Phagocytic and clathrin mediated	Thick glycolax thought to permit entry. Exit presumed to be from prelysosomal to exocytosis.	Tuma and Hubbard 2003
	Absorptive enterocytes	dIgA, newly synthesized apical plasma membrane proteins	B-A	pIgA receptor, unknown		Ellis and Luzio 1995
	Absorptive enterocytes in terminal ileum	Vit B12	A-B	Clathrin coated vesicles		Cardone <i>et al.</i> , 1994

To analyse whether these recombinant proteins were capable of transcytosis across the intestinal epithelium, Caco-2 cells were used as an *in vitro* assay (Shah and Shen 2000). Caco-2 cells are heterogeneous human epithelial colorectal adenocarcinoma cells that can differentiate under specific conditions, becoming polarised and resemble enterocytes of the small intestine (Sambury *et al.*, 2005). Upon differentiation, Caco-2 cells display microvilli on the apical side and have the presence of tight junctions between adjacent cells (Shah and Shen 2000). They also display small intestinal hydrolase enzyme activities such as sucrase-isomaltase (Artursson *et al.*, 2001). Caco-2 cells are often used in the pharmaceutical industry to model the small intestine and the presumed traffic of drugs across the intestinal epithelium (Artursson 1990). To

ensure the cells are differentiated and to control for the diffusion of drug molecules between cells whereby tight junctions have not formed, the cells must be grown on a transwell insert (Sambury *et al.*, 2005) as confluent monolayers (figure 57). Transepithelial resistance (TER) was used as a marker of intact confluent monolayers in addition to inulin-FITC. TER has been used extensively as a control for tight junction integrity by measuring the electrical resistance between the apical and basolateral chambers. An increase in resistance can be observed when the monolayer is complete and a TER curve was plotted to ensure, for these cells, under these conditions, that the tight junctions are fully formed (Yamashita *et al.*, 2000). In addition to TER, inulin was used as a control for tight junction integrity. Tight junctions serve as the rate-limiting barrier to passive movement of hydrophilic solutes across intestinal epithelia (Turner *et al.*, 1997). Hence inulin being a polymer of fructose has been widely used as a control for tight junction integrity.

5.1.3 Characterisation of Tight Junctions

Tight junctions are one mode of cell-cell adhesion in both endothelial and epithelial cellular sheets (Furse *et al.*, 1993). Tight junctions act as primary barriers to the diffusion of solutes through the intracellular space, therefore creating a boundary between the apical and basolateral compartments (Tsukita *et al.*, 2001). Differentiated monolayers of Caco-2 cells express tight junction proteins, regulating the paracellular movement of molecules (Furse *et al.*, 1993). Tight junctions are held together by transmembrane proteins occludin and claudin (Tsukita *et al.*, 2001) (figure 55). These transmembrane proteins interact with zona occludin 1 (ZO-1) pulling the two opposing cells into tight proximity (figure 55). To help characterise whether the Caco-2 cell model was differentiated, these tight junction proteins were utilised. Caco-2 cells were grown on glass slides for a series of time frames. The Caco-2 cell monolayer was aldehyde fixed at these time points and immuno-labelled for ZO-1 and occludin, the hypothesis being that undifferentiated monolayers would not display these tight junction proteins, whilst differentiated monolayers would (Furse *et al.*, 1993). This experiment helped to further characterise the cell line and understand the exact time required for Caco-2 cell differentiation.

5.1.4 Intracellular Markers for Endocytosis and Transcytosis

How do membrane bound vesicles deliver their cargo to the correct target domain? This is a complex question that is still only partly understood. Members of three protein families are central players in vesicle targeting and fusion:

- i) Soluble N – ethylmaleimide sensitive protein (SNAREs) which are a group of cytoplasmically orientated integral membrane proteins that are present on vesicles (v-SNARE) or target membrane (t-SNARE).
- ii) The Syntaxin-binding protein 1 (Sec1) / mammalian uncoordinated (Munc1) proteins
- iii) Small molecular weight GTP binding proteins – rabs.

The formation of the SNARE complex produces a scaffold for the sequential recruitment of two proteins; NSF and Synaptosomal-associated protein 25 (α -SNAP) (soluble NSF attachment protein) (Bennett 1995). The protein, NSF has been documented to be an ATPase whose catalytic activity leads to the disruption of the cis-SNARE complex. This event has been considered to lead to membrane fusion (Bennett 1995).

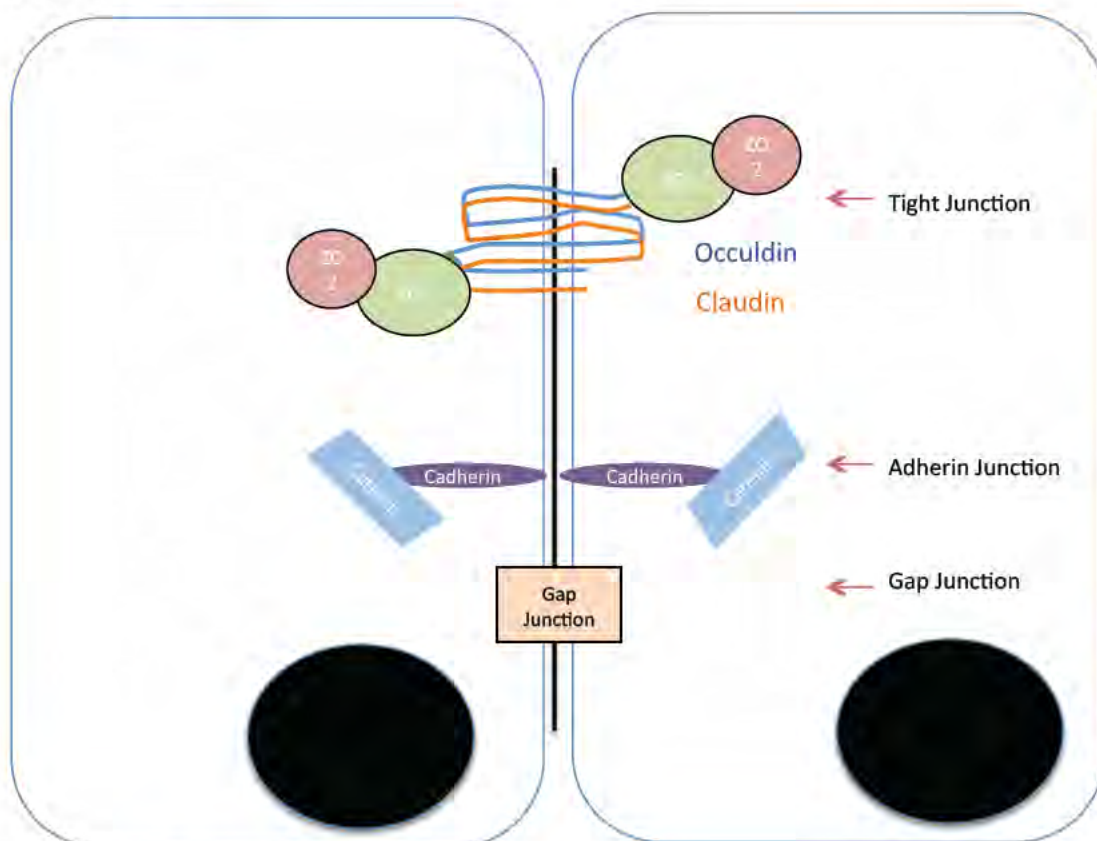


Figure 55. Regulation of paracellular transport.

To ensure fidelity of membrane trafficking, the formation of SNARE complexes has to be tightly regulated. One of the regulatory factors is known to be the rab proteins. Rab proteins are transport vesicle associated, low molecular weight GTP-binding proteins that regulate multiple trafficking pathways (Bennett 1995). The rab proteins are physically associated with each organelle as well as the associated transport vesicle (figure 56). Rabs act as molecular switches regulating the formation, transport, tethering and fusion of transport vesicles (Hutagalung and Novick 2011). The Rab proteins activate the tethering proteins that pull together two vesicles (the target vesicle and the acceptor vesicle), into close proximity. This allows the v-SNARE and the t-SNARE to interact leading to the fusion of the membranes and mixing of intra-vesicle material (Manford *et al.*, 2012).

To analyse the trafficking of the recombinant proteins, it was necessary to utilise a variety of intracellular markers. To this end, markers associated with definitive trafficking pathways were used. To analyse whether the proteins were within an early endosome, antibodies raised against the tethering protein early endosome associated protein 1 (EEA1) were used. Similarly, antibodies against lysosome associated membrane protein 2 (LAMP2), Golgi marker 130 (GM130) were used to label the lysosome and Golgi respectively (Mosossen *et al.*, 2008).

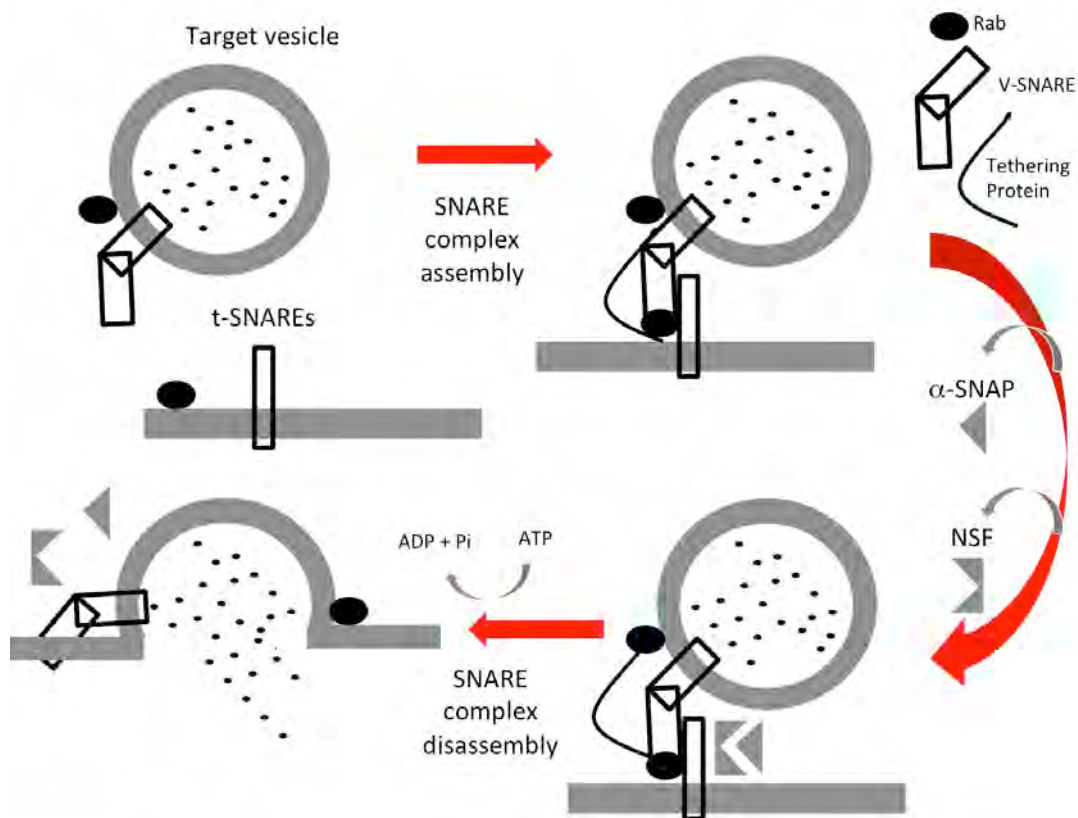


Figure 56. Cartoon representing SNARE assembly and disassembly that is required for the maintenance of vesicle fusion.

5.1.5 Analysing Cell Toxicity

There are a variety of methods used to assess cellular toxicity that work using different mechanisms. The trypan blue assay for example, measures cell toxicity by the accumulation of blue dye in dead cells. The cells that are blue are no longer able to pump the dye out and hence are no longer viable (Strober 2001). In contrast, a MTT assay (3-(4,5-dimethylthiazol-z-yl)-2,5-diphenyltetrazolium bromide) is a colorimetric assay for measuring the activity of cellular enzymes that reduce the tetrazolium dye, MTT and into an insoluble formazon salt, which turns purple when solubilised in DMSO (van Meerloo *et al.*, 2011). This can be read in a micro titre plate reader at A540nm. For analysing the toxicity of the recombinant proteins, and analysing Caco-2 cell growth, these assays were both employed.

5.1.6 *In vitro* Cell Models

Caco-2 cells are the most commonly used *in vitro* cellular system for measuring transcytosis, since they differentiate furthest along the crypt-to-villus axis and are the easiest to transfect (Ellis and Luzio 1995). Differentiation takes approximately 20 days *in vitro*. However, differentiated Caco-2 cells lack the thick glycocalyx expressed by mature enterocytes *in vivo*, (Tuma and Hubbard 2003) which must be kept in mind when designing experiments. Other cell lines have been used as cellular model of transcytosis such as HT29 (human colorectal adenocarcinoma) and T84 (human colon carcinoma) cell lines. Both these cell types lack differentiation into a fully mature state, are harder to transfect and do not form as tight, tight junctions. Therefore, in this instance, Caco-2 cells were chosen as a model cellular system of transcytosis.

Caco-2 cells, are a widely used model for transcytosis experiments, however for comparisons of cell toxicity induced by recombinant proteins, and protein trafficking, Vero cells are useful. Vero cells are isolated from the kidney of the African Green Monkey (Nahapetiion *et al.*, 1986). They have a doubling time of 24hours and have a small z-plane, which makes imaging less challenging for trafficking studies. Therefore, Vero cells were used in this study to image the trafficking of recombinant proteins and to analyse any associated toxicity.

Aims of the work described in this chapter:

- i) To clone and sequence recombinant proteins discussed in section 2.2.8
- ii) To evaluate whether these recombinant proteins could be produced
- iii) To characterise the recombinant proteins by SDS-PAGE and western immunoblot
- iv) To culture and characterise Caco-2 cells
- v) To analyse whether the recombinant proteins could transcytose across monolayers of Caco-2 cells

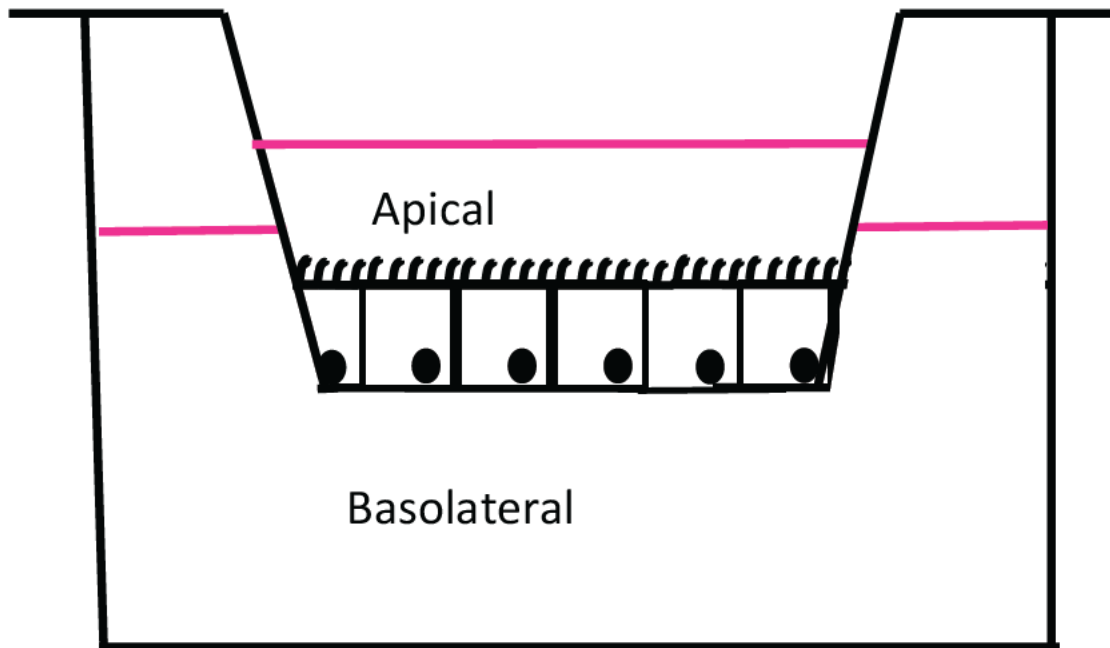


Figure 57. Schematic representation of Caco-2 cells grown on transwell filter.

5.2 Materials and Methods

Recombinant gene sub-cloning: 2.2.8.3

Protein expression: 2.3

5.2.1 Primer design for recombinant PCR

Primers were designed to be complementary for the first twelve nucleic acids of the 5' region of the gene with an additional CACC sequence for sub-cloning into pET151 plasmid vector. The 3' region was designed to be complementary to the final twelve nucleic acids ensuring a stop codon was inserted. For recombinant PCR, primers were designed, at the junctions, to be complementary for the final twelve nucleic acids of gene 1, ensuring the stop codon was removed. The next twelve nucleic acids were complementary for gene 2. When the two amplified genes were used as templates and the far 5' and 3' primers used, the two genes were produced in frame. This was sub-cloned into pET151 plasmid vector.

5.2.2 Polymerase chain reaction (PCR) for amplifying regions of gene interest

Sterile PCR tubes were used and into them placed; 1µl template (500pg), 0.3µl primer one (25pM), 0.3µl primer two (25pM), 12.5µl polymerase mix and 11.9µl sterile water. PCR tubes were then inserted into thermocycler (MJ mini, Biorad, Hertfordshire). Depending on the predicted length of the gene section to be amplified, the extension time was altered *i.e.* for an 1kb amplification, there was an extension time of 1 minute. The annealing temperature was altered depending on the thermal midpoint (T_m) of the primers. The amplified DNA was then analysed using gel electrophoresis.

5.2.3 Gel electrophoresis to analyse amplified gene products

A 1% agarose gel was prepared by solubilising 1g agarose in 100ml water by gentle heating. To this, 10µl gel red was added and poured into a gel tank. Combs were inserted into the gel and allowed to solidify at room temperature. Following solidification, the gel was immersed in TAE buffer inside the gel tank, and amplified PCR product added to wells alongside a DNA ladder. Typically gels were run for 50 minutes at 70 volts.

5.2.4 Sub-cloning in pET151 plasmid vectors

For sub-cloning a kit from Invitrogen was purchased (pET151/D TOPO). Amplified DNA was diluted to reach a molar ratio of 1:1 (vector : insert ratio). The product (1µl) was placed inside a sterile PCR tube along with 0.5µl vector. To this, 0.5µl salt solution and 1µl sterile water was added. The solution was left at room temperature for ten minutes before adding to 25µl *E.coli* TOP10 and leaving on ice for twenty minutes. The cells were heat shocked for precisely 30 seconds at 42°C before returning to the ice. Super optimal broth with catalytic repressor (S.O.C.,) media (100µl) was added and the tube was placed inside a rotating 37°C incubator for one hour. The product was spread over a 2xYT plate containing ampicillin and left overnight at 37°C. The following morning, colonies were identified and a small amount of each colony, placed inside a PCR tube, and subsequently onto a small

patch of fresh agar plate for re-culture. The selected colonies were analysed for gene insert and plasmid identity using plasmid and gene specific primers. These products were analysed by gel electrophoresis, and products at predicted molecular weight were sent for sequencing.

5.2.5 Sequencing of sub-cloned constructs

Plasmids were purified from bacteria by using a commercially available Qiagen mini prep kit. Plasmids were sent for sequencing to DNA Sequencing and Services – University of Dundee at concentrations of 600ng plasmid per reaction in a volume of 30µl per reaction. A reaction is classed as one template per primer combination. Primers were sent at a concentration of 3.2pM/µl with no less than 10µl per tube due to potential evaporation.

5.2.6 Sequencing analysis using DNASTar

Contiguous sequences were returned by DNA Sequencing and Services, and aligned using the module SeqMan software from DNASTar (Madison, Wisconsin, USA). It was ensured that the sequences were in the correct orientation, and that there was adequate coverage over the entire gene and junctions. The theoretical gene sequence and regions upstream and downstream of the gene (plasmid region) was also covered. The consensus sequence was analysed for mutations and frame. The gene was translated using DNASTar module - Editseq and then BLAST searched using GenBank to ensure the gene was identifiable to other clones. Once there was certainty regarding these aspects, the sequenced data was inserted into the plasmid map.

5.2.7 Plasmid transformation into *E.coli* for protein expression

Purified plasmids were analysed for concentration using the Nanodrop 2000, and 10ng plasmid placed in a tube containing 25µl *E.coli* BL21*DE3 (Invitrogen, Paisley, UK) and placed on ice. This was left for thirty minutes before heat shocking at 42°C for precisely 30 seconds. The reaction was placed on back on ice. Room temperature (S.O.C.,) media (100µl) was added and the tube placed inside a 37°C incubator for

one hour. During this time, 10ml 2xYT media containing ampicillin was placed inside a sterile polypropylene centrifuge tube and placed inside the incubator to reach temperature (37°C). The reaction was then added to the fresh warmed media inside the falcon tube and left at 37°C overnight to culture.

5.2.8 Protein production

The overnight (16hr) transformed *E.coli* BL21*DE3 cells were added to a 1 litre fresh culture of 2xYT the following morning and cultured for three hours before induction of protein production with 200µM IPTG. The cells were cultured for a further three hours before sedimentation by centrifugation. Centrifugation at 6000 x G was performed to pellet the cells prior to re-suspension in 2ml PBS. Protease inhibitor was added at 1:10 ratio of protease : cell suspension, and the re-suspended cells were lysed using a french press pressure cell, (Thermo, Herts, UK) at 15,000 PSI for five repeats. Sodium azide (4ml of 0.1M) was added to the lysed cells and the volume brought up to 40ml with PBS. This was sedimented by centrifugation at 18,000 x G for thirty minutes. The supernatant was poured over an equilibrated Talon bead bed (2ml) and allowed to flow through at 4°C by gravity flow. The column was washed with three-bed volumes 10mM imidazole in PBS before elution into 500µl aliquots with 100mM imidazole. A quick analysis of protein fractions in PBS was performed by Bradford assay, and most concentrated fractions pooled for dialysis. Dialysis was performed by placing the purified protein into dialysis tubing (Sigma, Dorset, UK), and placing inside a bottle containing 4L of 1 x PBS. This was put a 4°C for 4 hours stirring before being changed and repeated three times. The protein was recovered and stored at -80°C until required.

Caco-2 cell sub-culturing – refer to section 2.2.1

Caco-2 cell freezing and thawing – refer to section 2.2.5

5.2.9 Caco-2 growth curves by MTT assay

Caco-2 cells were seeded at 1×10^4 cells/ml in a 96 well plate and cultured over a total of 27 days. At intervals over this time frame, an MTT assay was performed on one row of the plate (n=8). The absorbance readings were taken and plotted to obtain the growth curve.

5.2.9.1 Caco-2 viability by trypan blue assay

Caco-2 cells were seeded at 1×10^4 cells/ml in a 96 well plate and cultured over a total of 27 days. At intervals over this time frame, a trypan blue assay was performed on one row of the plate (n=8). Trypan blue stock solution (0.4%) was prepared in PBS. Trypan blue stock (0.1ml) was added to 1ml cells. A haemocytometer was loaded with the solution and examined under low magnification (10x). The total number of cells was counted, along with the number of blue cells. The viable cell count (%) was calculated and viable cells plotted to obtain the cell viability over the duration of the growth curve experiment.

$$\text{Viable cells (\%)} = [1 - (\text{no. blue} / \text{total no. cells})] \times 100$$

5.2.9.2 Characterisation of TER

Caco-2 cells were seeded at 1×10^5 cells / well in a transwell 24 well plate (Millipore, Billerica, MA). Complete media was added to the basolateral chamber (24ml) and a total of 400 μ l complete media added to the apical chamber. Cells were cultured for 30 days and TER measurements recorded over this time frame. The TER measurements were plotted and optimal TER obtained.

5.2.9.3 Characterisation of Caco-2 cell differentiation by analysing increased villin production

Caco-2 cells were cultured in six well plates and seeded at 1×10^5 cells / well. Media was changed every two days. On days 3, 7, 13 and 21 cells were lysed (n=4) using

Lamellae buffer with BME. Glass beads were added to the lysed cells and vortexed for two minutes to help shear the DNA and reduce viscosity. The samples were loaded into an SDS-PAGE gel and separated at 200 volts for 45 minutes. The proteins were transferred to a nitrocellulose membrane at 400mA for one hour before being subject to western immunodetection. The membrane was cut in half at approximately 50kDa and the high molecular weight section incubated with α -Villin, the low molecular weight section incubated with α -actin as a loading control (table 5). The x-ray film was developed and results analysed.

5.2.9.4 Analysis of tight junction integrity by inulin diffusion

Caco-2 cells were seeded at 1×10^5 cells / well in a transwell 24 well plate. The cells were cultured for 21 days or until TER reached stable levels of 380 Ohms. Inulin-FITC (200 μ M) was added to the apical chamber and samples collected from the basolateral chamber over 24hours. The samples were measured using a micro titre plate reader set at A540nm and plotted as percentage viability.

5.2.9.5 Analysis of recombinant protein trafficking by immunofluorescence microscopy

Caco-2 cells were seeded at 1×10^5 cells / well and cultured for 19 and 21 days. Cells were fixed using aldehyde or methanol (for LAMP staining). Aldehyde fixation – cells were left in 2% (w/v) paraformaldehyde for 20 minutes. Methanol fixation – cold methanol (stored at -20°C) was placed over the cells, which were then placed inside the -20°C for five minutes. The methanol was removed and the cells gently washed three times in PBS. Both fixing protocols then followed the same protocol: Cells were blocked for one hour in 1% (v/v) FBS blocking solution in PBS. Following, a wet paper towel was placed inside a plastic box and parafilm placed on top. Dilutions of the appropriate primary antibodies were made and 20 μ l of each antibody was spotted onto the parafilm. The glass coverslips were removed from six-well plate and inverted on to the appropriate spotted antibodies. The lid was placed on top of the box and left in the dark at 4°C for one-hour or overnight. Following, the coverslips were placed back into the six well plate, (ensuring turned into the correct

orientation) and washed three times in PBS. Fresh parafilm was placed inside the box, and the secondary antibodies were diluted accordingly and spotted onto the film. The coverslips were again inverted and placed on to the corresponding antibodies. The lid was placed on the box and placed inside a 4°C fridge for one hour. Following, the coverslips were removed and placed back inside the six well plate. All coverslips were washed three times in PBS and then mounted onto glass slides for imaging.

5.2.9.6 Mounting cover slips onto microscope slides for cell imaging

Mounting media (20µl) was added to a glass slide and coverslip inverted and placed on top (cells down). Excess media was carefully removed by blotting on paper towel, and nail varnish used to seal the edges of the slide. Once dry, the slides were imaged (section 2.6.2).

Vero cell culture – refer to section 2.2.1

5.2.9.7 Investigation of recombinant protein trafficking in Vero cells

Vero cells were seeded at 1×10^5 cells / well, and cultured overnight in complete media. The following morning, the media was changed, and serum free media used. Recombinant proteins were added (10µg/ml) and left at 37°C in the incubator for one hour. Following, the media was removed and the cells were washed three times in PBS. Fresh complete media was added to the wells, and the plate was placed back inside the incubator for three hours. The cells were then fixed, immuno-stained (section 2.6.1) and imaged (section 2.6.2).

5.2.9.8 Analysis of recombinant proteins ability to transcytose across monolayers of Caco-2 cells

Caco-2 cells were culture on transwell membranes in a 24 well plate until confluence and differentiation was determined as previously described. Recombinant proteins were added to the apical chambers (10µl/ml) with serum free media and left at 37°C in a cell culture incubator for one hour. Following, the media (in the apical chamber)

was removed and replaced with fresh complete (warmed) media (section 2.2.1). The plate was placed back inside the 37°C, 5% CO₂ incubator for three hours. At the end of the experiment, the apical and basolateral media was removed and stored separately. The cells were lysed using Lamellae buffer. The media was subject to TCA precipitated to concentrate the proteins (section 2.5), and Lamellae buffer was added to the pellet. The fractions were analysed by western immunoblot, and identified using specific antibodies against the specific proteins *e.g.* CTBC recognised by α -CTBC and STBC recognised by α -STBC at predicted molecular weight. During these experiments, TER and inulin measurements were recorded as previously described.

5.3 Results

5.3.1 Analysis of Shiga Toxin Clones from the Database

Since GST-GFP as a model antigen was fully characterised, attentions turned towards the cloning and sequencing of toxin-antigen genes. In parallel to the experiments characterising GST-GFP described in chapter 3.3.1, efforts to clone plasmids capable of expressing both relevant antigens and antigen-toxin B chain fusion proteins in *E.coli* were undertaken.

Three plasmids encoding STBC were provided by Mark Stamnes, (University of Iowa, Iowa, USA). As the sequence of these constructs were not known (in the Richardson laboratory), these plasmids were sequenced. Clone numbers 230, 231 and 232 refer to database entries for each of these constructs (Chapter 5 section 5.1.2). Upon sequencing the ORFs and vector junctions (figures 58 to 60), it was found that 230 and 231 contained a gene for STBC, which was in a pGEM plasmid vector. These constructs lacked six-histidine epitope tag for protein purification and, consequently were not used further. However, plasmid number 232, derived from a pET11a plasmid vector contained a six-histidine epitope tag on the C terminus of the protein (figure 60). The protein was produced and purified using Talon resin and was immuno-reactive to antibodies raised against six-histidine at the predicted molecular weight of 17kDa (Sandvig and Deurs 2002).

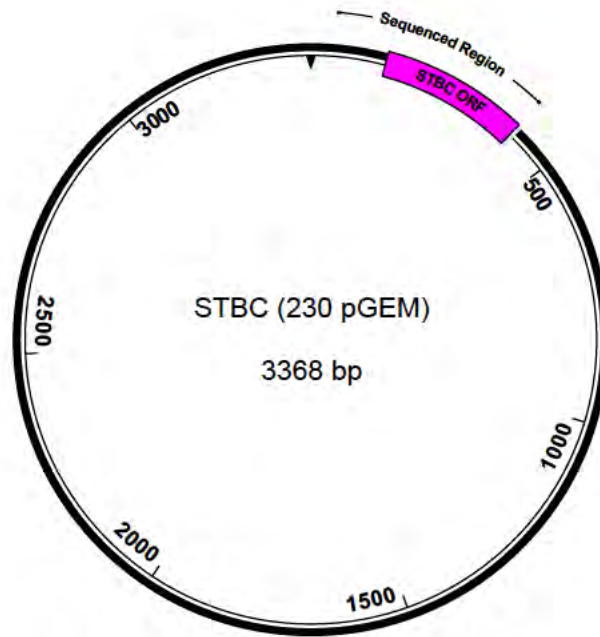


Figure 58. Sequenced plasmid map of 230 in pGEM vector.

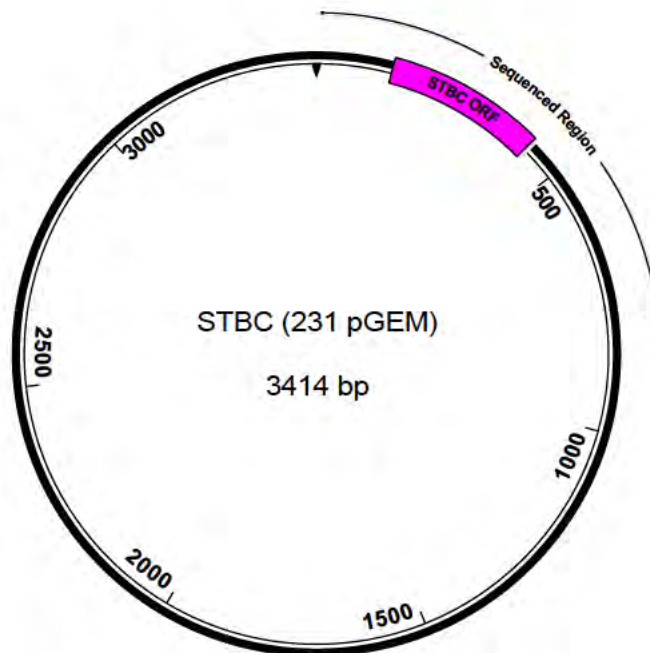


Figure 59. Sequenced plasmid map of 231 STBC ORF is in pGEM vector. Therefore it is not expressible in the current form.

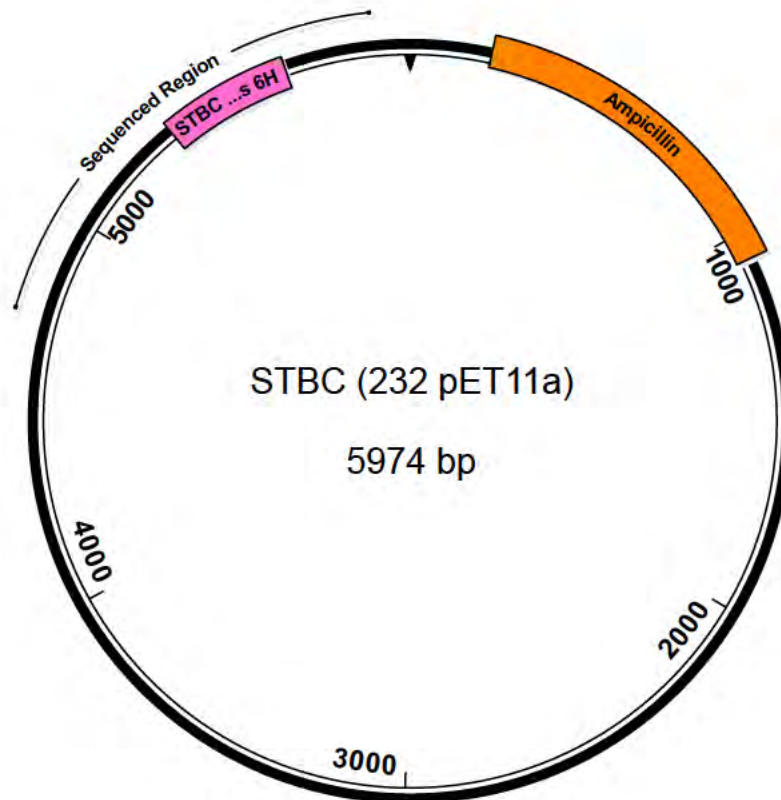


Figure 60. Sequenced plasmid map of STBC within vector pET11a. The region was sequenced with a range of primers, seen in table 7.

The appropriate STBC plasmid (232) was used to amplify the STBC gene with the forward primer designed to add CACC to the N terminus for sub-cloning into pET151 and the reverse primer designed without a stop codon, but including complementary sequence to GFP (some 12 nucleotides in length). Similarly, GFP was amplified from the 210 plasmid encoding GST-GFP, previously described in chapter three. Primers were designed with a forward primer encoding 12 nucleotides that were complementary to STBC and 12 nucleotides complementary to GFP. The reverse primer was complementary to GFP with a stop codon (TAA) to end the gene transcript. The final PCR used both for the forward and reverse primers to anneal the two genes in frame. This product consequently, was sub-cloned into pET151 as STBC GFP (figure 61). The plasmid was fully sequenced using multiple primers, sequencing backwards and forwards across the construct, ensuring junctions were well covered. The contiguous sequences were aligned using DNASTar software, and mapped back

into the plasmid map, ensuring the ORF was correct. The protein sequence was searched via BLAST to ensure the gene was exactly what was expected.

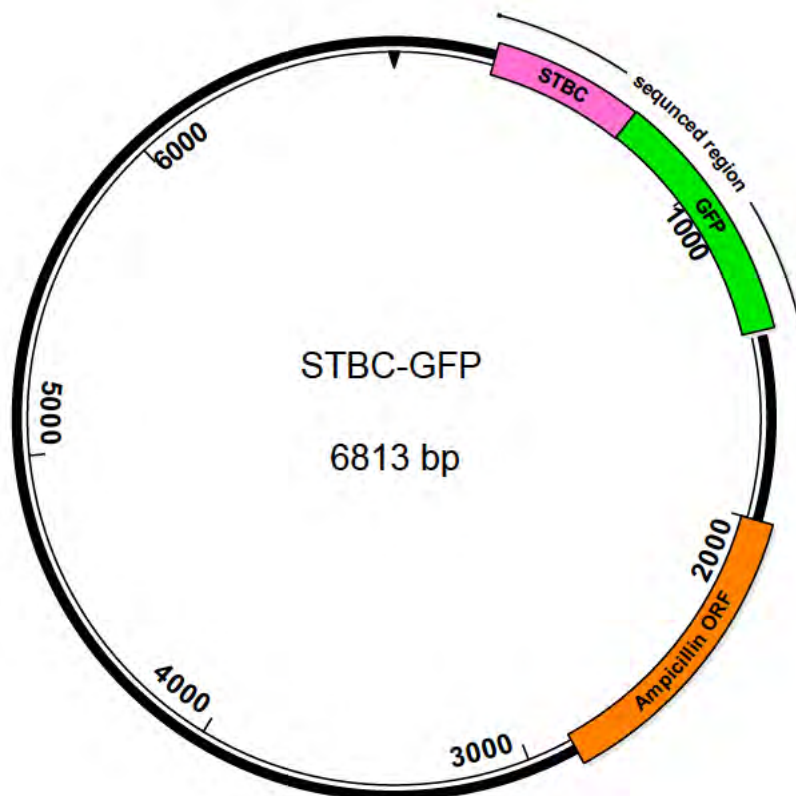


Figure 61. Sequenced plasmid map of STBC fused in frame with GFP.

5.3.2 Cholera Toxin

The B chain of cholera toxin was then sub-cloned from a pUC57 plasmid (produced by Bio Basic Inc (BBI), Ontario, Canada), into a pET151 plasmid vector. Colonies were screened for the gene using a vector forward and gene specific reverse primers (table 7). The colonies that were positive for orientation and the presence of the gene, were sent for sequencing at DNA Sequencing and Services - a spin off company at the University of Dundee. The plasmid was fully sequenced using primers in table 7, ensuring a large portion of vector region was covered. A mini induction experiment was performed and analysed for detection of the protein after SDS-PAGE. The gel was subject to transfer onto a nitrocellulose membrane and incubated with antibodies for 6 hisidine. The western blot followed by immunodetection showed an

immunoreactive band at the predicted molecular weight for CTBC at 17kDa (figure 39).

Following the successful cloning of CTBC, subsequent cloning of CTBC fused in frame to GFP was performed. CTBC was cloned N terminal to GFP. The purpose of this clone is to watch the trafficking of CTBC in live or fixed cells. Since GFP remains fluorescent inside cells, the distribution and location of CTBC could be tracked (see Chapter 1 section 1.8.1). Since GFP is fully cloned, fused in frame to GST (210), and CTBC is fully cloned and sequenced, the two genes could be amplified by PCR and fused to each other. The mid-ORF primers were designed so that half would be anti-complimentary to homologous regions of either GFP or CTBC and the other half, the tail region, would be anti-complimentary to homologous regions of the opposite gene (figure 54). The first PCR utilised template specific for the primers, *i.e.* GST-GFP plasmid or CTBC plasmid. The second PCR used the opposite primers and template and the third PCR combined these two amplified products and use the 5' and 3' primers to amplify the entire gene sequence. After this stage, the amplified product could then be cloned into the pET151 vector.

As with previous cloning attempts, after CTBC GFP cloning, colonies were picked and analysed for their gene insert using gene specific and vector specific primers, (table 7) (protocol in section 2.2.8.3). Care was taken to ensure the annealing temperature used in the reaction was correct so that unspecific binding did not occur which could potentially lead to false positives (figure 63). Once certain of the colonies with gene insert that were correctly orientated, plasmids were sent for sequencing. Upon analysis of sequence data, a plasmid map of CTBC GFP was made, (figure 65) (see protocol in Chapter 2 section 2.2.9.1).

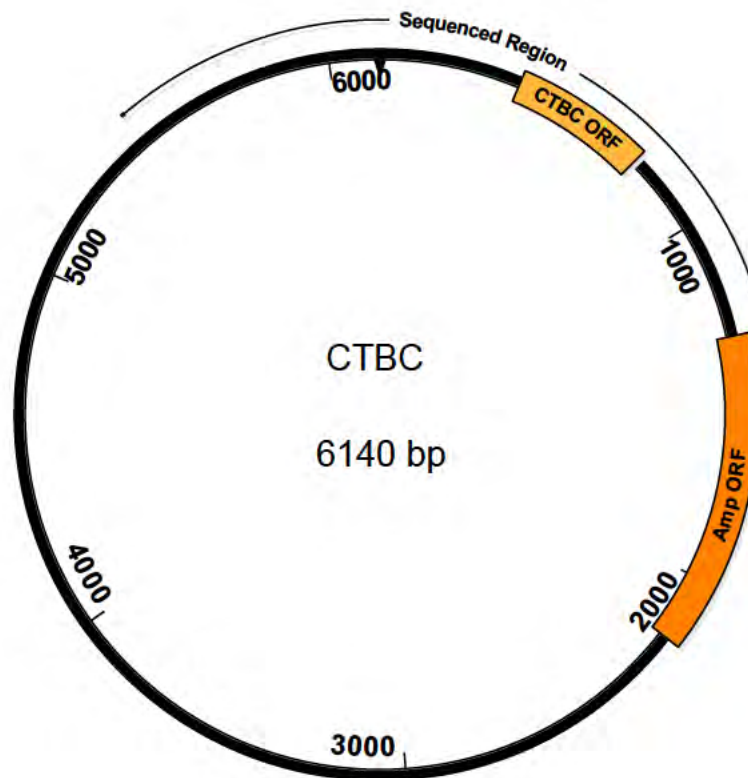


Figure 62. Sequenced plasmid map of CTBC within pET151 vector. The gene was sequenced with a range of primers, seen in table 7.

5.3.3 VP2 Antigen

The VP2 gene from IBDV is a large gene with many corresponding GenBank accession numbers. This is due to strain and the nature of antigenic drift as well as genetically engineered mutations and deletions. To ensure the correct gene was ordered from BioBasicInc (BBI), a theoretical plasmid map was made (figure 66). The sequence used was obtained from an expired USA patent (5,350.575) by Azad *et al.*, (1994) that had generated antibodies against the VP2 protein (represented by a green arrow in figure 66). From there, VP2 fragments identified in the patent (US5,350.575) were sub-cloned into the *E.coli* expression cassette pET151 for antibody generation. The regions identified for sub cloning were on an *Acc*e I-*Spe* I fragment (restriction enzyme sites) and a *Sca* I to *Xho* I fragment. To ascertain whether the sequence is homologous to other published vvIBDV sequences, an

overlay was performed. Since there was homology between these sequences, a phylogenetic tree was generated (figure 67). The phylogenetic tree demonstrates there is good sequence homology between vvIBDV (Gomes *et al.*, 2005) and the strain taken from the patent – the Australian field isolate 002-73. Lastly, to further analyse the sequence chosen, a megalign (DNASTar) analysis was performed to overlay the consensus sequences from many isolates. Although base pair substitutions are evident, there remain fewer alterations between vvIBDV and the sequence chosen. Therefore, the whole Australian field isolate 002-73 sequence was ordered for Bio Basic Inc and efforts will be made to sub-clone firstly the two regions of interest.

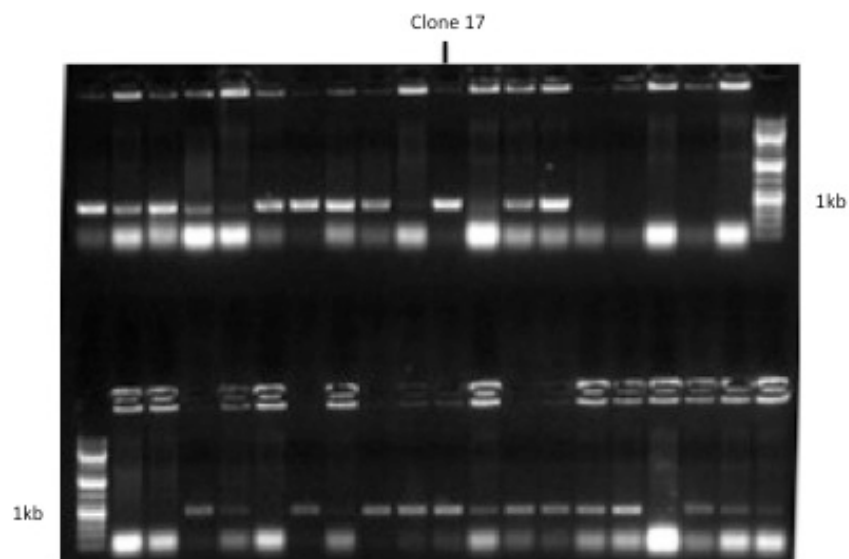


Figure 63. Analysis of bacterial colonies taken from 2xYT plate (plus amp) following TOPO cloning into pET151 vector. Primers used were 130 and T7 reverse (table 7). Predicted Mw 718bp from DNASTar software. Observed ~ 1kb. Since these colonies appeared to be around the predicted Mw, six were sent for sequencing.

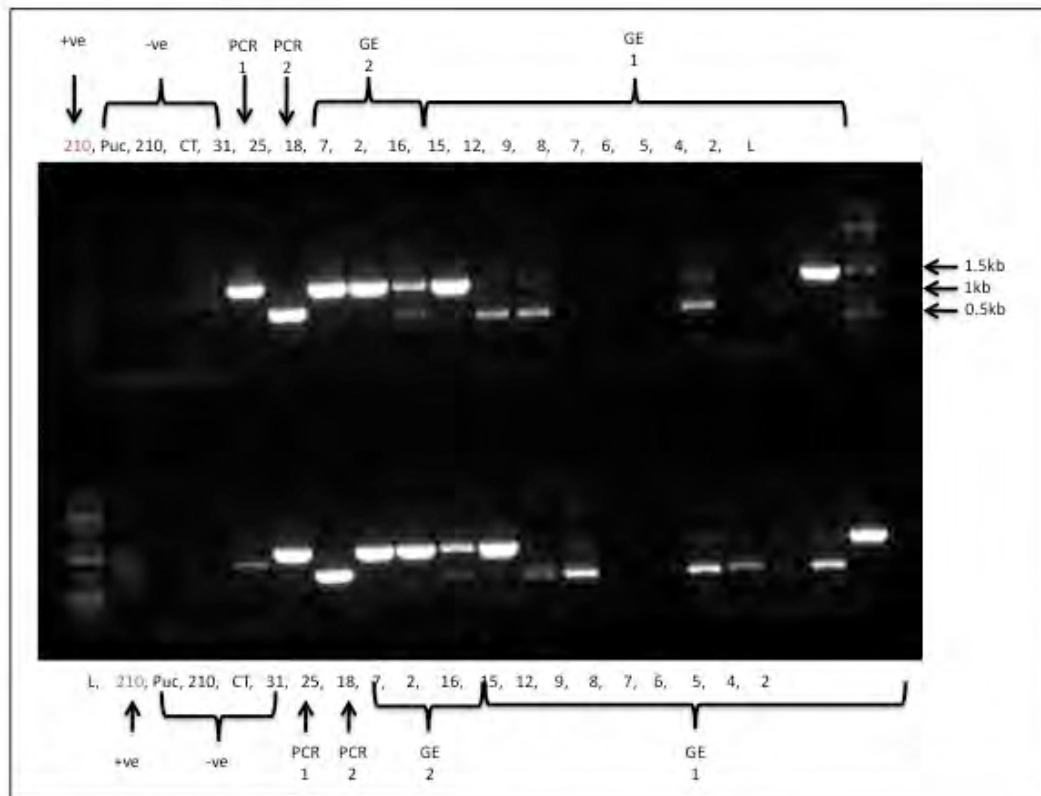


Figure 64. 1% (w/v) agarose gel. The gel was run for 45 minutes at 70 volts. Primers used were V5f and 115r. Predicted molecular weight ~ 1349bp. The positive control for 210 (GST GFP) plasmid used primers 116f and 115r. Predicted molecular weight ~ 1620bp. 2, 16, (GE1), 7, 18, (GE2), 31(PCR 1) appear to be positive and controls behaving in predicted manner.

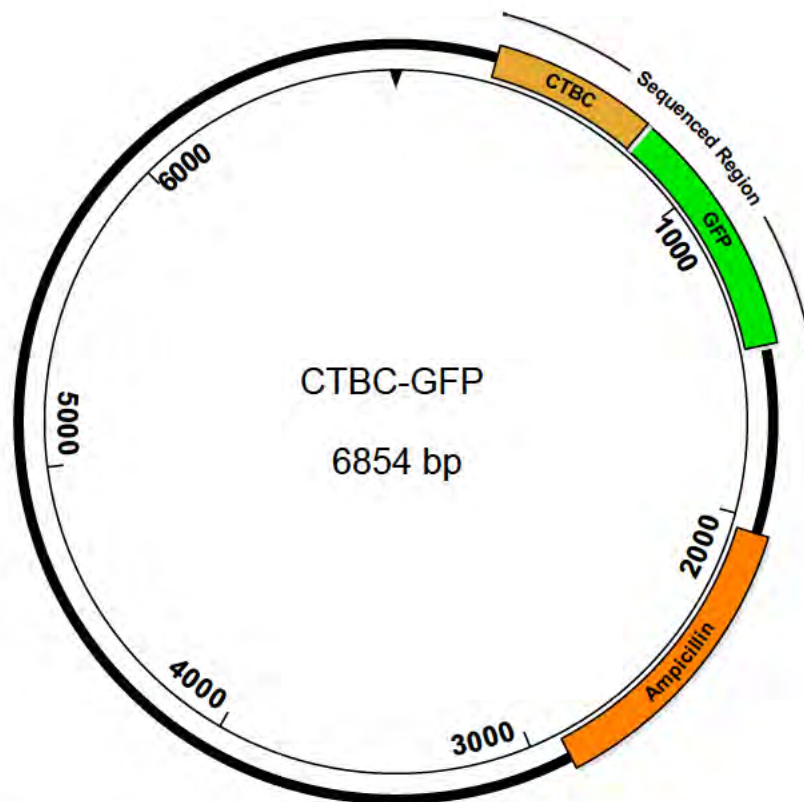


Figure 65. Sequenced plasmid map of CTBC fused in frame to GFP on the C terminal.

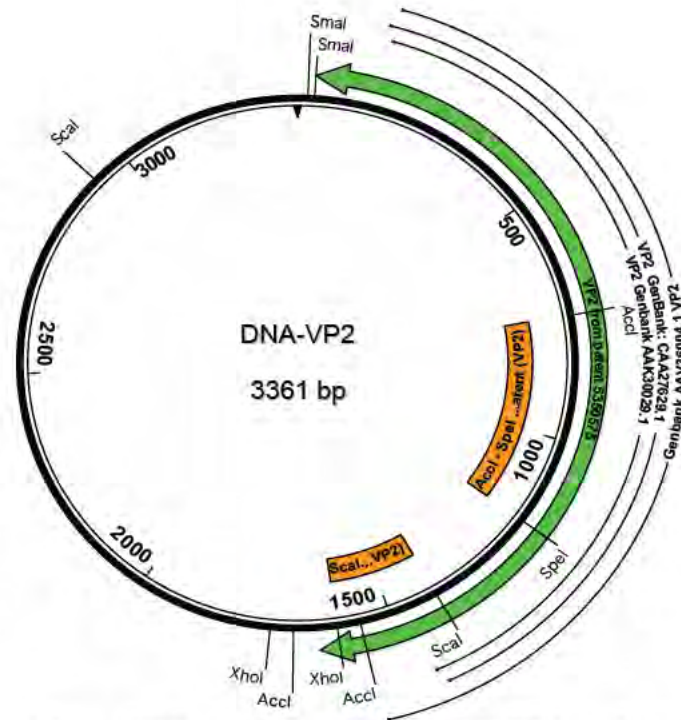


Figure 66. Map of large ORF (from Segment A of IBDV), polyprotein of 110 kDa: pVP2-VP4-VP3. Data obtained from US patent 5,350.575. This was aligned with multiple VP2 gene sequences from GenBank. However, patent data shows that the area of VP2 required for antibody specificity is that of the orange region within the inner plasmid. Restriction enzyme sites are labeled for obtainment of the patented region of interest.

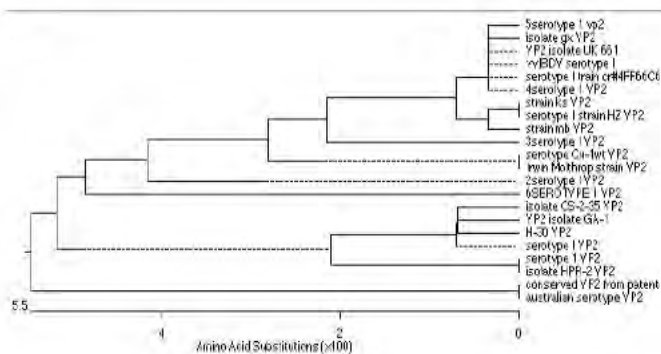


Figure 67. Phylogenetic tree of various VP2 sequences found from GenBank. vvIBDV, serotype 1 was required for this thesis hence the less antigenicity and most constant regions of homology were required. This figure showed that the consensus used was most consistent with that of vvIBDV from serotype 1.

VP2 (*Acc*e I-*Spe* I) was amplified out of the BBI plasmid, using primers designed as previously described (table 7). The amplified product was sub-cloned into pET151/D TOPO vector, analysed for insertion before sending for sequencing to DNA Sequencing and Services using multiple primers to cover the entire gene and the junctions. The protein was expressed at predicted molecular weight of 15.4kDa (section 2.3).

Similarly, VP2 fragment *Sma* I-*Xho* I was amplified using specific primers (table 7) and sub-cloned in the usual manner into pET151 vector. The successfully cloned plasmids were fully sequenced and aligned in DNASTAR prior to being BLAST searched to ensure the gene fragment was correct. The protein was expressed at predicted molecular weight of 11kDa (table 14).

To deliver the antigen (VP2) a trafficking component was required to facilitate exit from the G.I tract into the *lamina propria*. To fulfil this requirement, VP2 was fused in frame by recombinant PCR to both trafficking proteins, CTBC and STBC.

VP2 and CTBC were amplified using primers designed (table 7) and annealed using recombinant PCR. Colonies were again screened for the presence of the insert and sent for sequencing. Successful colonies were stored in the -80°C freezer and entered into the database. The protein was expressed and purified and western immunoblot demonstrated the protein was at the apparent molecular weight as predicted (table 14).

Cloning efforts were also employed against VP2-STBC, which was fused in frame using recombinant PCR previously described. The amplified gene product was diluted to ensure the correct stoichiometric ratios were met (1:1) and sub-cloned in pET151 vector. Colonies were screened and selected for sequencing, and once again sent to DNA Sequencing and Services. Once successful, plasmid maps were designed and the protein was expressed using *E.coli* BL21*DE3 (table 14).

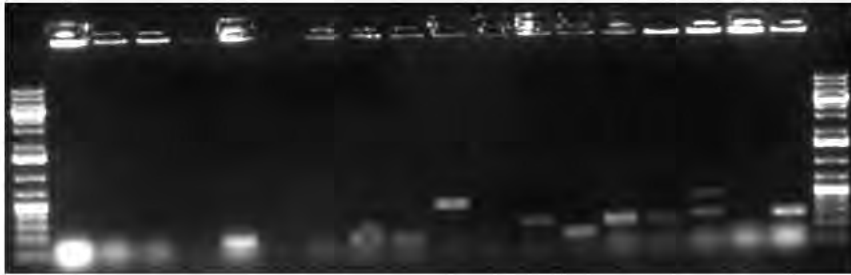


Figure 70. Successful colony number 10, with present insert VP2 (*Acc*e I - *Spe* I). Sent for sequencing to DNA Sequencing and Services.

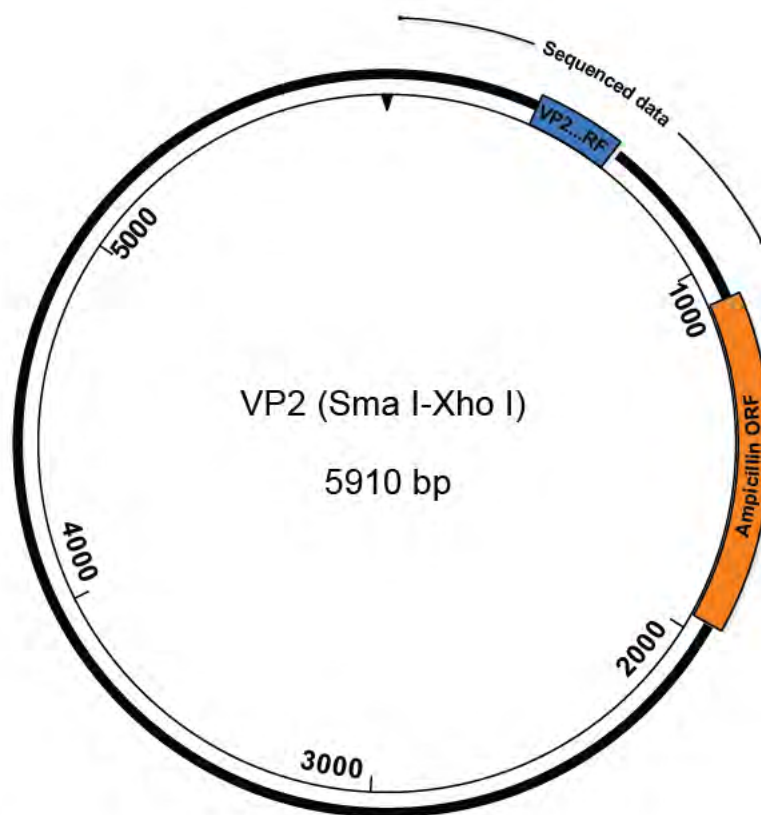


Figure 71. Sequenced plasmid map of VP2 (*Sma* I-*Xho* I fragment).

VP2 was also fused in frame with GFP for use as a control for trafficking. Primers were designed in a similar fashion, however the GFP reverse primer was designed to remove the syntaxin portion of the 210 (GST-GFP encoding plasmid) gene. Colonies were analysed for gene insertion using PCR and sequenced.

A further clone of GFP was also produced, omitting the syntaxin region that was present in the 210 plasmid. This gene was required as a trafficking control for transcytosis, and was produced with six-histidine, V5 epitope tags. The gene was amplified, from the 210 plasmid, using a CACC ligation forward primer, and reverse primer designed to be specific for the end of the GFP sequence with the addition of a TAA stop codon. As with other cloning attempts, colonies were analysed via PCR, and those deemed to have the presence of the insert in the correct plasmid were sent for sequencing. Ultimately, a plasmid map with the sequenced data was produced. The protein GFP was then expressed after being transformed into *E.coli* BL21*DE3 cells (table 14).

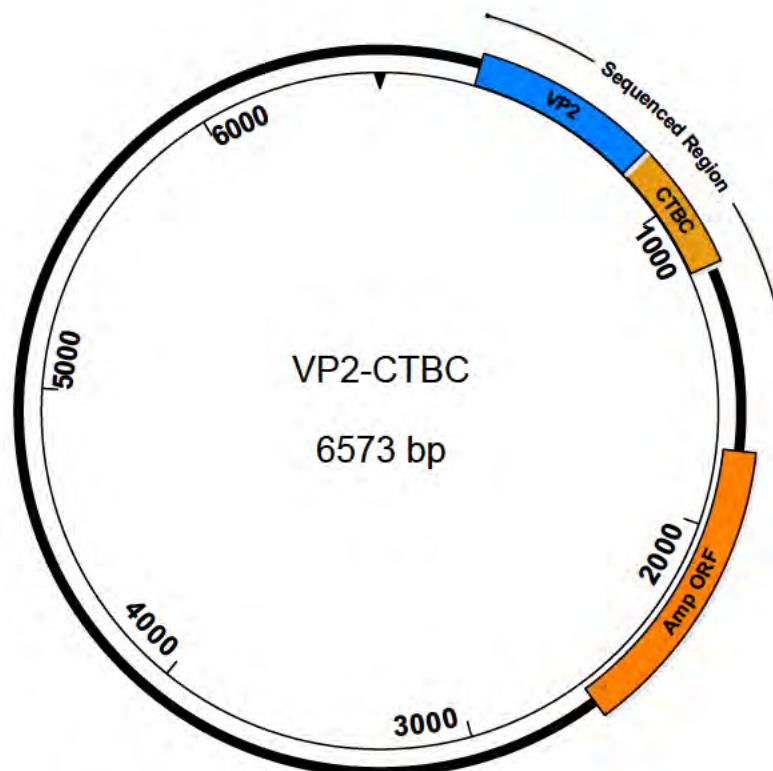


Figure 72. VP2 antigen fused in frame to CTBC.

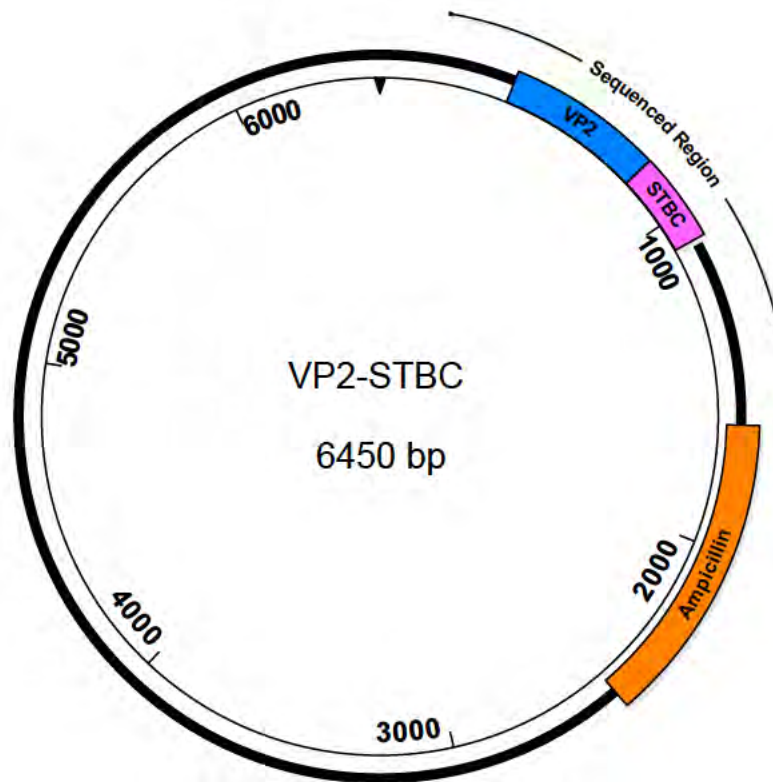


Figure 73. VP2 (*Acc* I - *Spe* I fragment) fused in frame to CTBC.

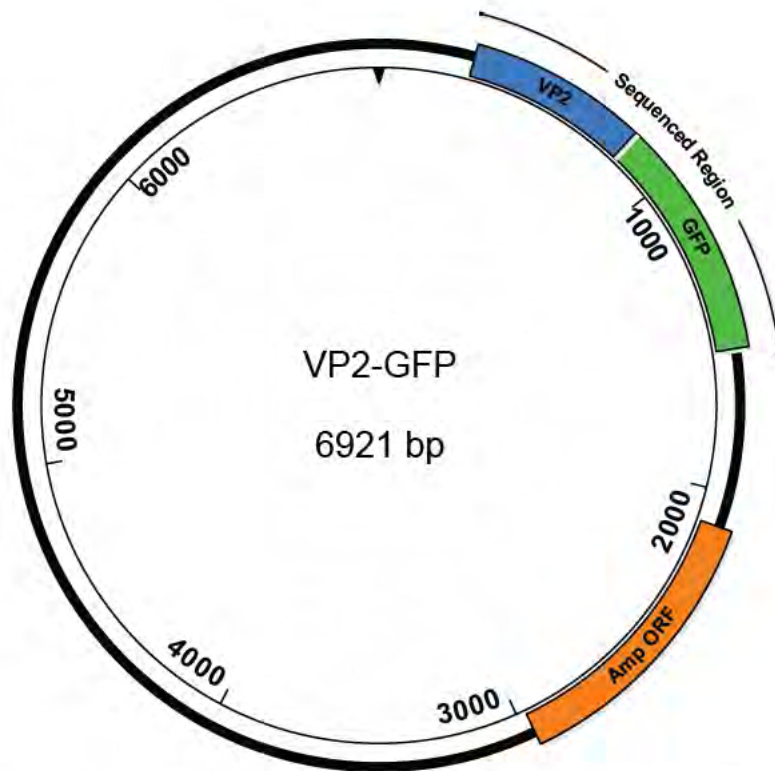


Figure 74. VP2 (*Acce I to Spe I* fragment) antigen fused in frame to GFP.

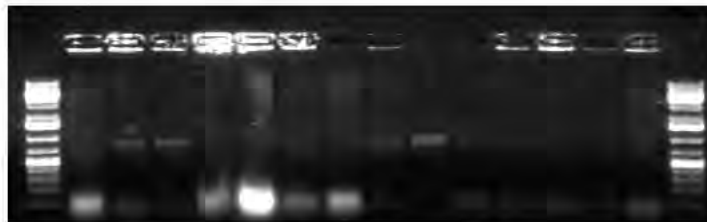


Figure 75. Successful colony encoding the GFP sequence. Plasmid 2 was sent for sequencing.

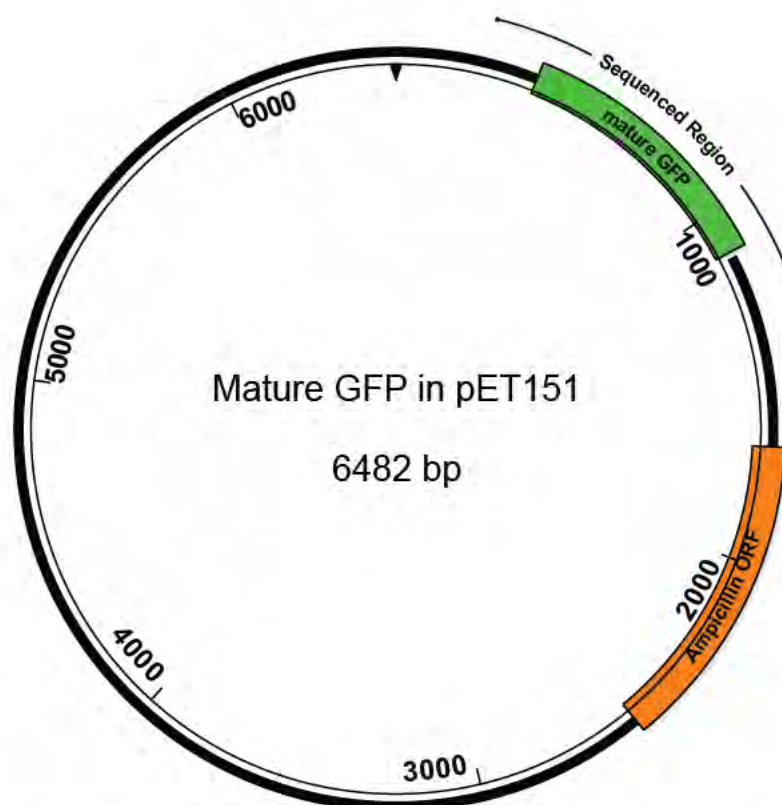


Figure 76. GFP (minus syntaxin encoding sequence) cloned into pET151 plasmid vector and sequenced.

Table 14. Recombinant proteins, their purpose and protein expression.

Recombinant Gene	Cartoon	Purpose	Protein blot
STBC		Trafficking control	11kDa
CTBC		Trafficking control	18.2kDa
STBC-GFP		Trafficking control	42kDa
CTBC-GFP		Trafficking control	44kDa
GFP		Negative control for trafficking	30.7kDa
STBC-VP2		Antigen delivery	28.1kDa
CTBC-VP2		Antigen delivery	32.8kDa
VP2		Antigen delivery control	15kDa

5.3.4 Recombinant Protein Expression and Characterisation

Following the successful cloning of the recombinant genes, there was a requirement to understand whether these proteins could be expressed, at what levels and were they subject to encapsulation by inclusion bodies? Each plasmid was isolated from the bacterial cells using a Qiagen mini prep kit and a concentration of DNA obtained using the Nanodrop 2000 (Thermo Scientific, Loughborough UK). All of the genes that were cloned into pET151 (Invitrogen; Paisley, UK) plasmid vectors required transformation into *E.coli* BL21*DE3 cells for protein expression (section 5.2). Each plasmid that had been transformed into *E.coli* BL21*DE3 cells was cultured for three hours in 2xYT media containing ampicillin, before being induced for protein expression with IPTG. The cells were then cultured for a further three hours before being sedimented to a pellet. The pellet was lysed using a French press releasing the cells proteins. The recombinant proteins were all purified using Talon beads that have an affinity for the six-histidine epitope tag. Quantification of the proteins was performed using Bradford and BCA assays (section 2.4.2.2) prior to analysis by SDS-PAGE and western immunoblot. All purified proteins produced bands using antibodies raised against six-histidine at predicted molecular weight (table 14).

It was then important to understand whether these recombinant proteins would be toxic to cells. Since these proteins were hypothesised to be able to traffic and antigen (VP2) to the *lamina propria*, there was a keen concern over their toxicity. A MTT assay was performed as previously described (section 2.2.4). The recombinant proteins, STBC / CTBC / VP2 were all shown to be non toxic to Vero cells up to 1mg/ml (figure 77) comparative to a negative control for toxicity, dextran and a positive control for toxicity, PEI. The same was found to be true in Caco-2 cells up to 1mg/ml when seeded at 1×10^5 cells / well (figure 78).

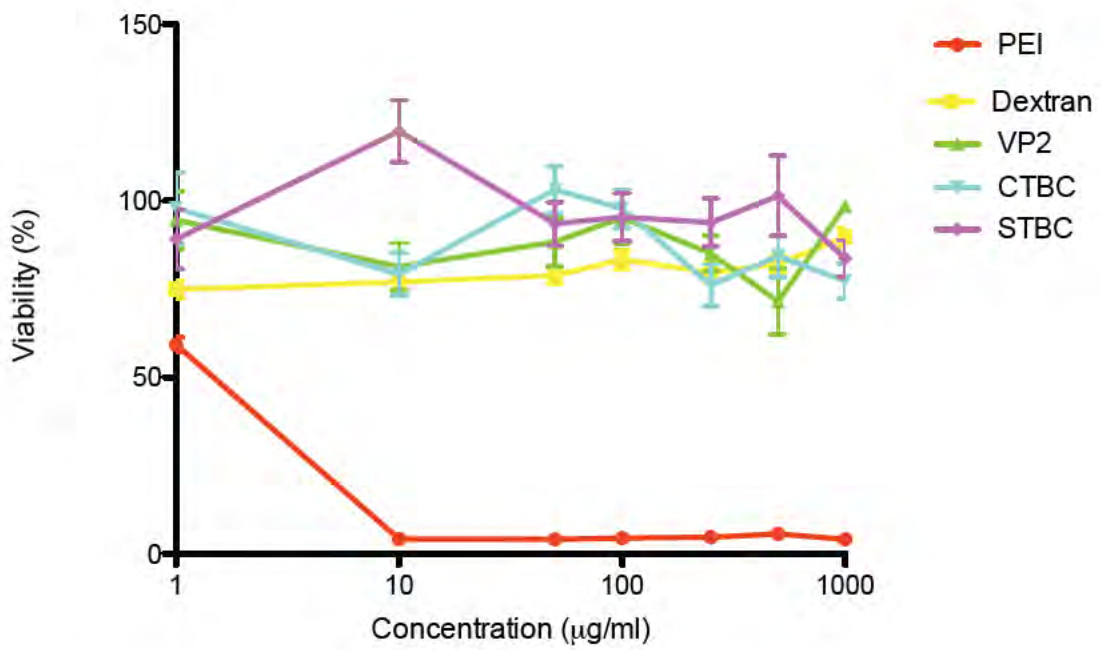


Figure 77. Toxicity of recombinant protein to Vero cells, using MTT assay (n=16).

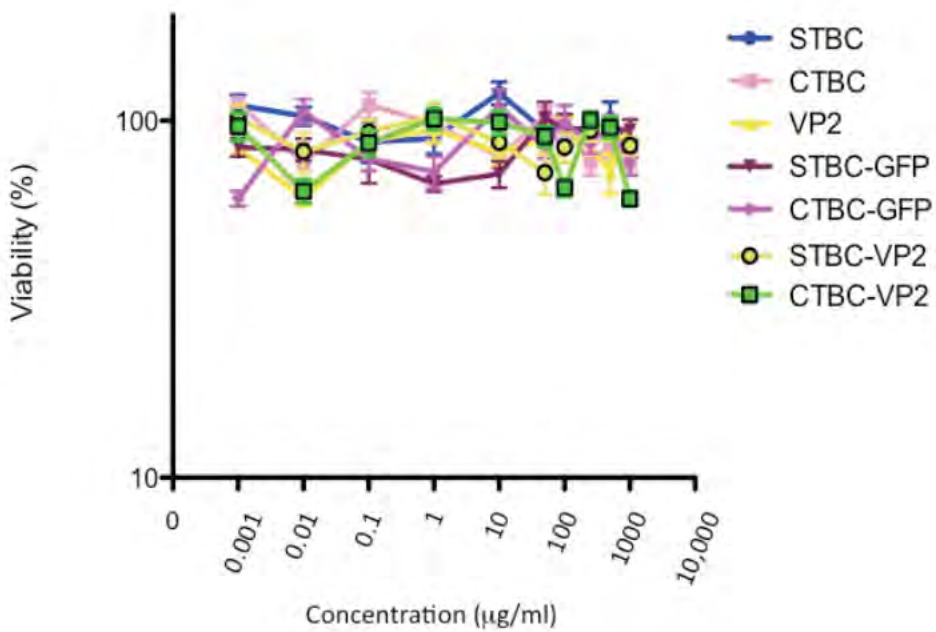


Figure 78. Toxicity of recombinant proteins to Caco-2 cells (n=16).

5.3.5 Characterisation of Caco-2 Cells

Caco-2 cells were firstly analysed for their growth rate. Cell seeding has been documented to be crucial for differentiation (Tuma and Hubbard 2003), and documented in the literature to have a doubling time of 3 days (Chantret *et al.*, 1994). However, since Caco-2 cells are known to differ between laboratories, the doubling time for the cells used in these experiments was checked. Caco-2 cells were seeded at 1.2×10^5 cells per ml (9×10^3 cells per well) in a 96 well plate. The data in figure 79 shows that the Caco-2 cells used have a doubling time of approximately six days. However, there is a sharp drop in absorbance at day 20 post-seeding. The reason for this was considered to be due to a decrease in metabolic activity upon differentiation. However, to test this hypothesis a trypan blue assay was performed to test for Caco-2 cell viability (figure 80). These cells have 100% cell viability over 25 days, and therefore it was concluded that the decrease in absorbance seen in figure 79 was due to a decrease in metabolic activity upon cell differentiation.

Differentiation of Caco-2 cells was also analysed by the increased presence of Villin. Villin is an actin binding protein associated with the actin core bundle of the brush border, and thus used as a marker of differentiation (Bretscher and Weber 1979). Cells were grown over 21 days in a six well plate and lysed using Lamellae and BME on days 5, 7, 10, 13 and 21. The lysed cells were loaded into an SDS-PAGE gel and subject to western immunoblot. The nitrocellulose membrane was cut in half at approximately 65kDa to allow for the use of two antibodies. The first antibody was specific for actin, as a loading control, and the second antibody - specific for villin. Thus there was certainty that the increase in villin was not due to uneven loading of the wells. As expected from the literature, a significant increase in villin was seen by day 21 as a marker of Caco-2 cell differentiation.

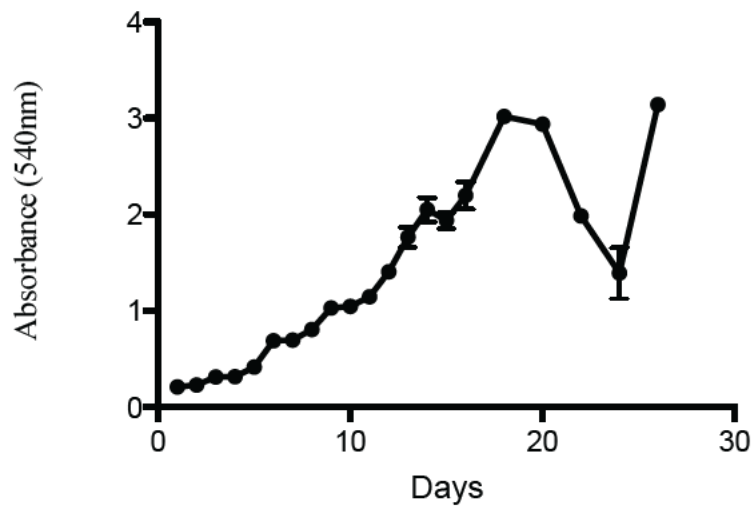


Figure 79. Growth curve of Caco-2 cells using MTT assay (n=8).

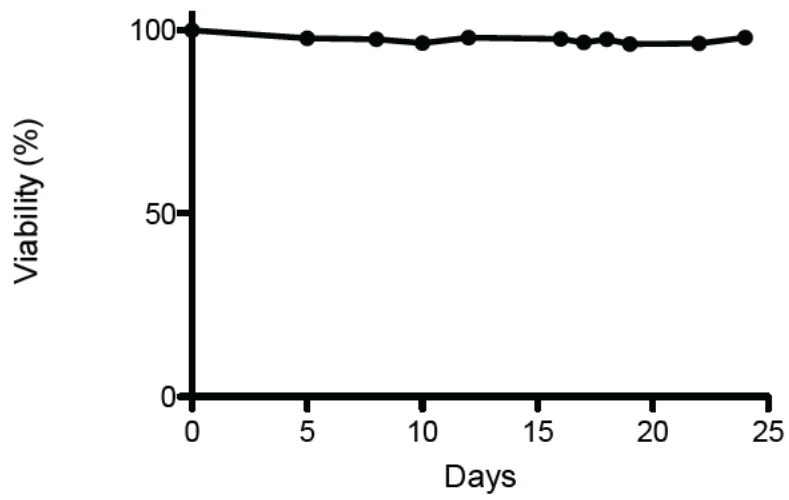


Figure 80. Caco-2 cell viability using trypan blue assay (n=8).

In addition, these Caco-2 cells were characterised for the length of time required to obtain a plateau in TER. This would confirm the monolayer was complete and tight junctions were formed. As this varies between laboratories, this needed to be confirmed using these cells, with this TER instrument. It was shown that over 30 days, the Caco-2 cells hit a plateau in TER at day 19 and remained stable for the duration of the experiment (up to day 30). TER readings peaked at approximately 380 Ohms. Therefore, for transcytosis experiments, it was concluded that these cells required a TER of 380 Ohms prior to beginning experiments, and that this should be the resistance on the completion of the experiment.

To characterise the confluence and differentiation of the Caco-2 monolayer, immunofluorescent microscopy was used. The Nikon 90i microscope was used to visualise the cells and a variety of markers. Caco-2 cells were analysed for tight junction integrity before and after differentiation. For the confluent, non-differentiated experiment, cells were seeded at 1×10^5 cells / ml and grown on sterile glass slides for 17 days prior to fixing. Antibodies against Golgi marker (GM130) and occludin and zona occludin-1 (ZO1) was used. Figure 82 shows images taken using these markers and since these cells are not differentiated, the signal and location of occludin and ZO1 is sparse. Occludin is associated with vesicles as opposed to the membrane and ZO1 can be seen to be beginning to localise around the membranes of opposing cells.

A similar experiment was performed, again seeding Caco-2 cells at 1×10^5 cells / ml, but allowing growth over 23 days. DAPI was again used to label the nucleus to help visualise the cells due to the large z-axis. Since these cells were differentiated, ZO1 can be seen along the cell membranes of adjacent cells, linking the tight junctions. Occludin, although could be optimised further, can be seen in vesicles along these membranes.

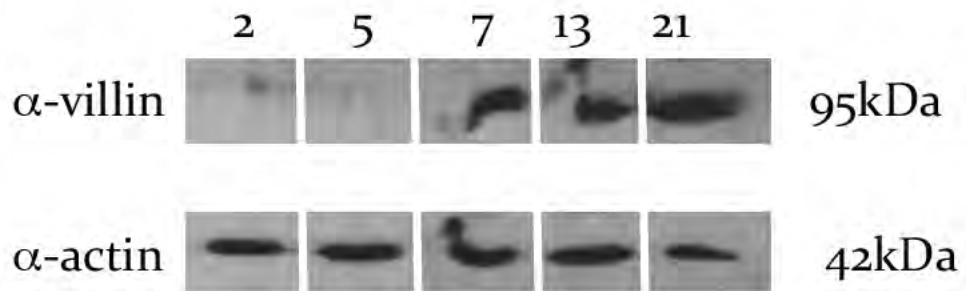
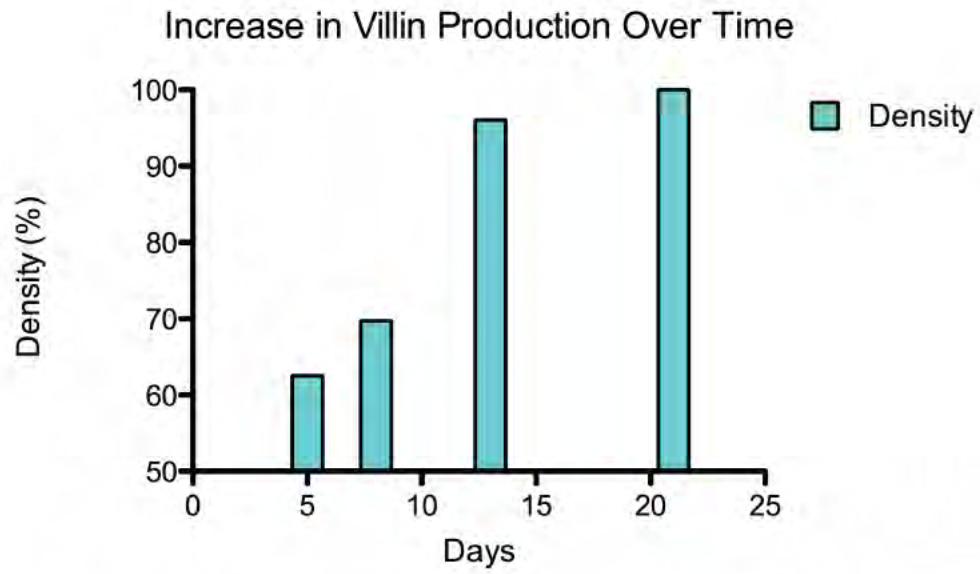


Figure 81. Increase in villin production over 21 days, with a loading control of α -actin (n=6).

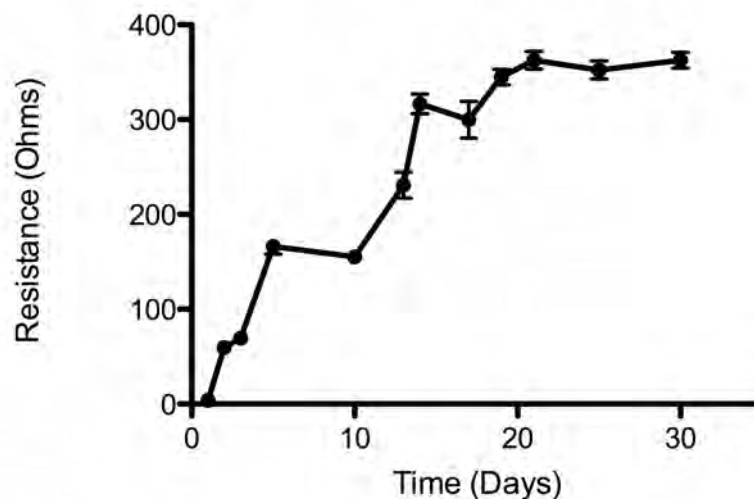
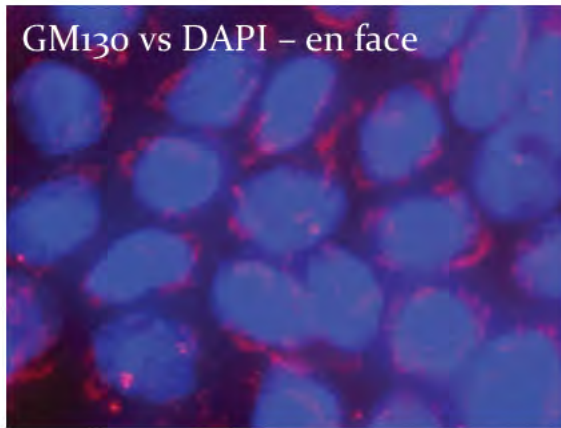


Figure 82. TER increased over time (30 days) in Caco-2 cells (n=16).

The recombinant proteins discussed in detail in section 5.1.1, were then analysed for any effects to the Caco-2 cell monolayer that may jeopardise the transcytosis experiments. These experiments used the control for paracellular transport, inulin and TER. Inulin was controlling for any gaps in tight junctions that may allow the molecule to slip between the adjacent cells, whilst TER was measuring the resistance. Since toxicity studies had been performed, and there were no apparent toxic effects to Vero cells up to 1mg/ml, 10µg / well of the recombinant protein was added to the apical chamber of the transwell 24 well plate. Inulin-FITC was measured in the basolateral chamber at intervals over 24 hours by reading the absorbance at 494nm. In parallel, TER readings were taken over this time frame to ensure there was not any associated toxicity causing the tight junctions to open. Figures 85 to 87 show that TER measurements in all instances remained stable at approximately 380 Ohms, consistent with the characterisation data. Inulin was not detected in the basolateral chamber during the experiments. Therefore it was concluded that these recombinant proteins do not affect the integrity of the tight junctions.



20 μ m

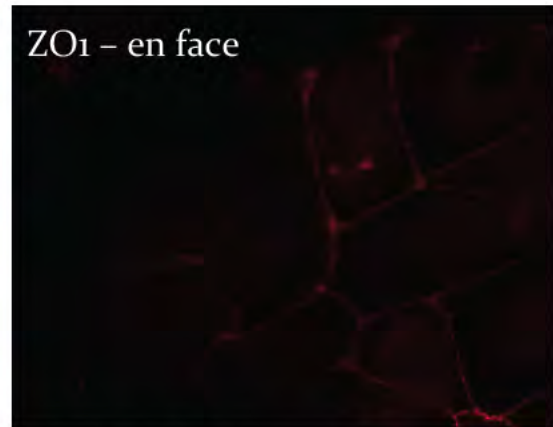
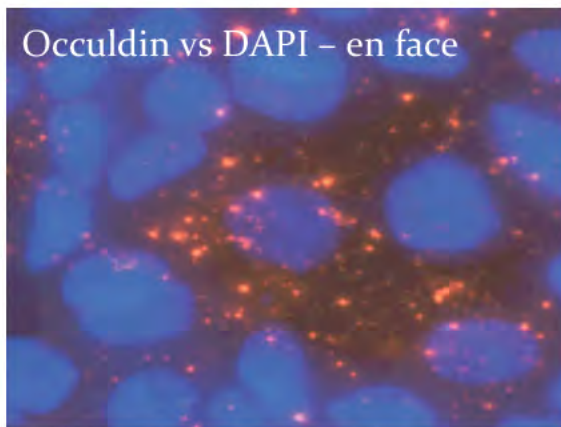
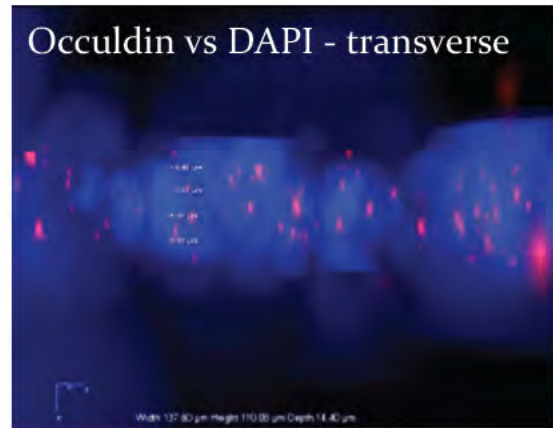


Figure 83. Confluent, non-differentiated Caco-2 cells. DAPI staining the cellular nucleus in all images. GM130 antibody used to label the Golgi. Occludin antibody labeling the tight junctions between adjacent cells. A transverse image used to demonstrate the location of occludin.

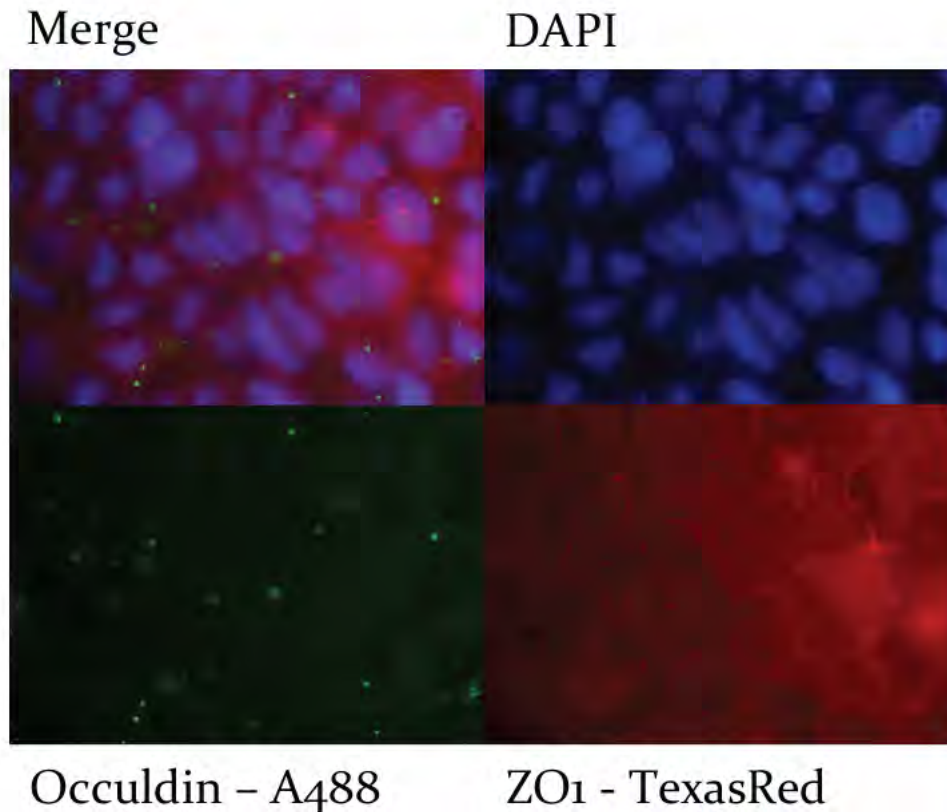


Figure 84. Confluent differentiated Caco-2 cells. DAPI used to help visualize the cells due to large Z-axis. ZO1-TexasRed showed tight junctions between cells, occuldin localized to these regions.

5.3.6 Characterisation of Cellular Trafficking in Vero Cells

Since it was not known whether the recombinant proteins would be capable of transcytosis across a confluent, differentiated Caco-2 cell monolayer, the location of the recombinant proteins was analysed in Vero cells by immunofluorescent microscopy. Vero cells were used instead of Caco-2 cells, as there were fewer issues with the z plane and time of growth. Vero cells were seeded at 1×10^5 cells / well and the following day subject to “pulse and chase” experiment with the recombinant proteins. Cells were then subject to aldehyde fixation (methanol in the case of LAMP2) and antibody incubation.

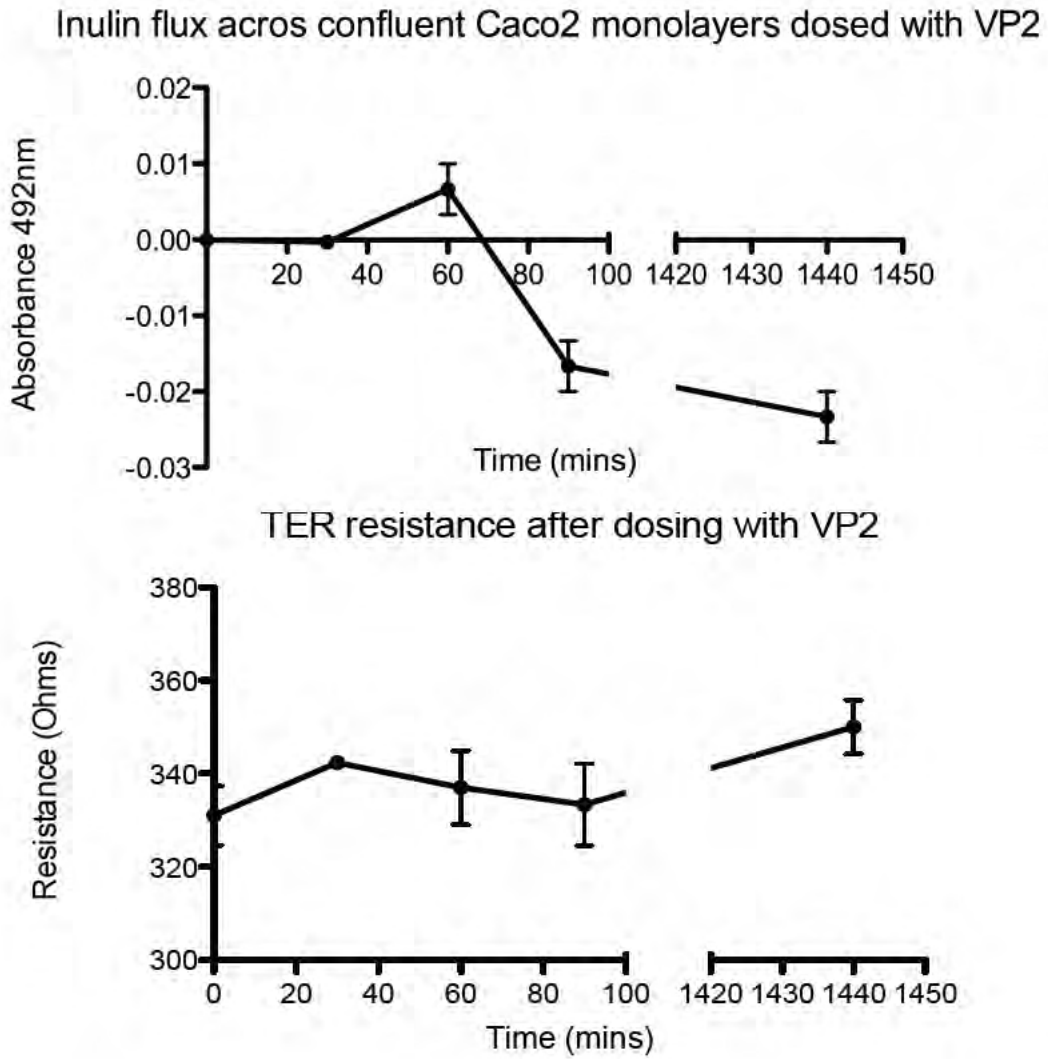
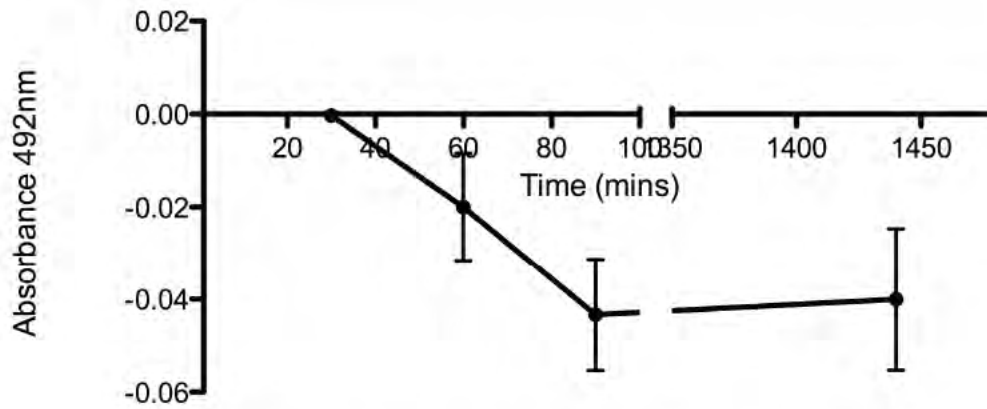


Figure 85. Characterisation of tight junction affects in the presence of VP2 (10 μ g/well) (n=8).

Inulin flux across confluent Caco2 monolayers dosed with STBC



TER resistance of Caco2 cells with STBC

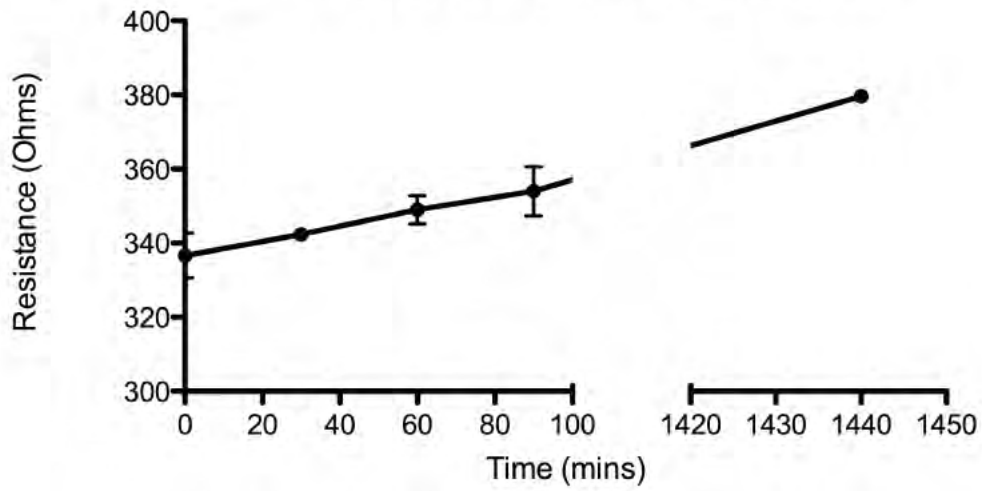
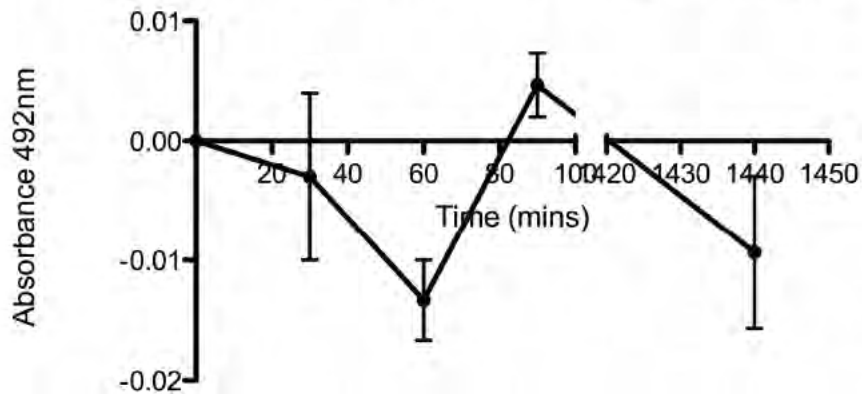


Figure 86. Inulin flux and TER of Caco-2 cells over 24 hours with the presence of 10 μ g/well purified and dialyzed STBC (n=8).

Inulin flux across confluent Caco2 monolayers dosed with CTBC



TER resistance after dosing with CTBC

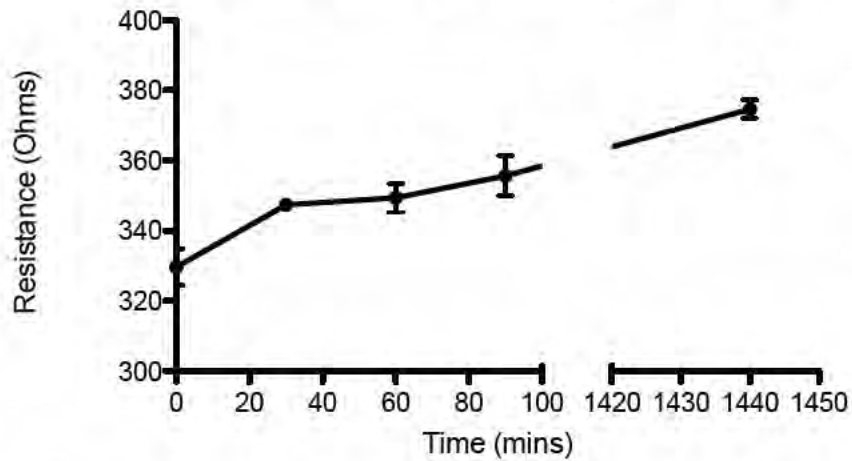


Figure 87. Inulin flux and TER measurements over 24 hours with the presence of 10mg/well purified and dialyzed CTBC (n=8).

CTBC was added to the cells at a concentration of 10 μ g/well since this concentration was known not to be toxic (figure 77 and 78). Leupeptin, (20 μ M) a broad-spectrum protease inhibitor was also added to the cells to prevent any degradation of protein inside the lysosome. Cells were labelled with either LAMP or EEA1 antibodies with the recombinant protein (CTBC) labelled with Texas Red. Figure 88 shows that CTBC does not co-localise with the lysosome (LAMP), is out of the early endosome (EEA1), four hours post experiment, as expected and appears to have a hazy like appearance either indicating membrane bound or cytosolic signal.

Similar experiments were performed with 10µg/well CTBC VP2. Again, leupeptin was used to prevent lysosomal degradation and the same types of antibody were used. CTBC VP2 appears to avoid lysosomal degradation by not localising with the lysosome and has passed through the early endosome in the four-hour time frame. Interestingly, CTBC VP2 appears to localise to the external nuclear environment, and it was thought this could be Golgi associated. Sandvig (2002) reported that 5-10% cholera toxin was capable of reaching cytosolic targets, however due to temporal constraints this hypothesis was not tested.

The data in figure 90 shows the localisation of VP2 antigen. It appears that VP2 enters Vero cells, perhaps by fluid phase endocytosis. VP2 does not appear to co-localise with the lysosome or the early endosome at four hours post dose. However due to temporal constraints, the direct location of VP2 was not fully characterised.

Similar results were found with purified STBC when dosed at the same concentration (10µg/well) with leupeptin and using the same time frames (figure 91). STBC, however appeared to co-localise more with LAMP than CTBC or CTBC VP2. There appeared, as expected, no co-localisation with the early endosome four hours post dose (figure 91).

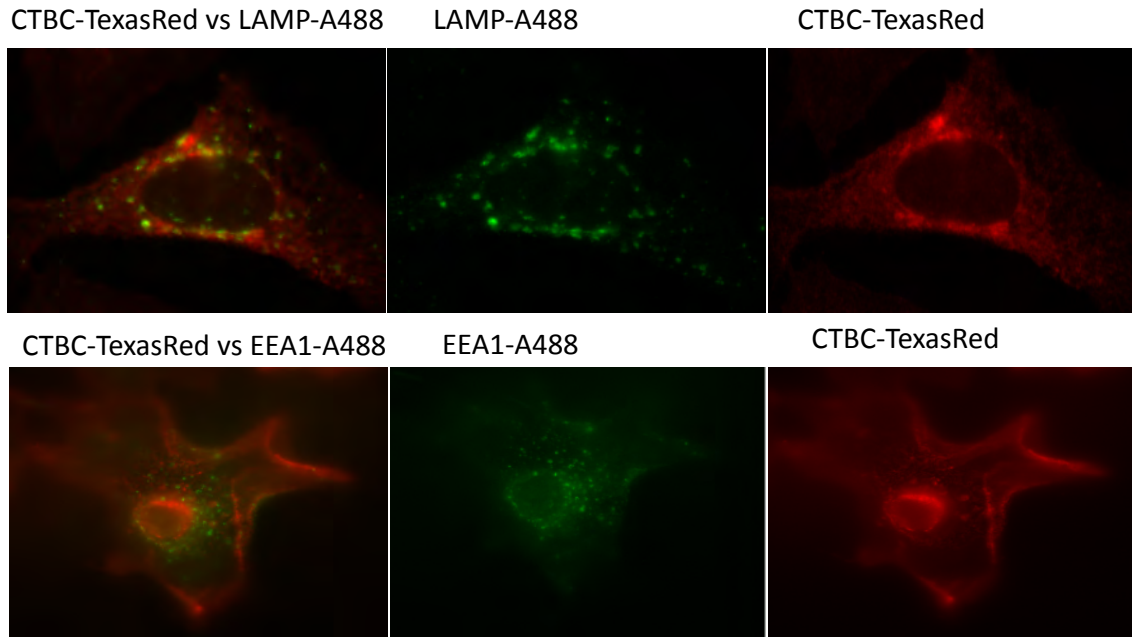


Figure 88. CTBC pulsed into Vero cells for one hour followed by a three-hour chase. Cells were fixed using either aldehyde (bottom) or methanol (top) and labeled with appropriate antibodies for immunofluorescent microscopy.

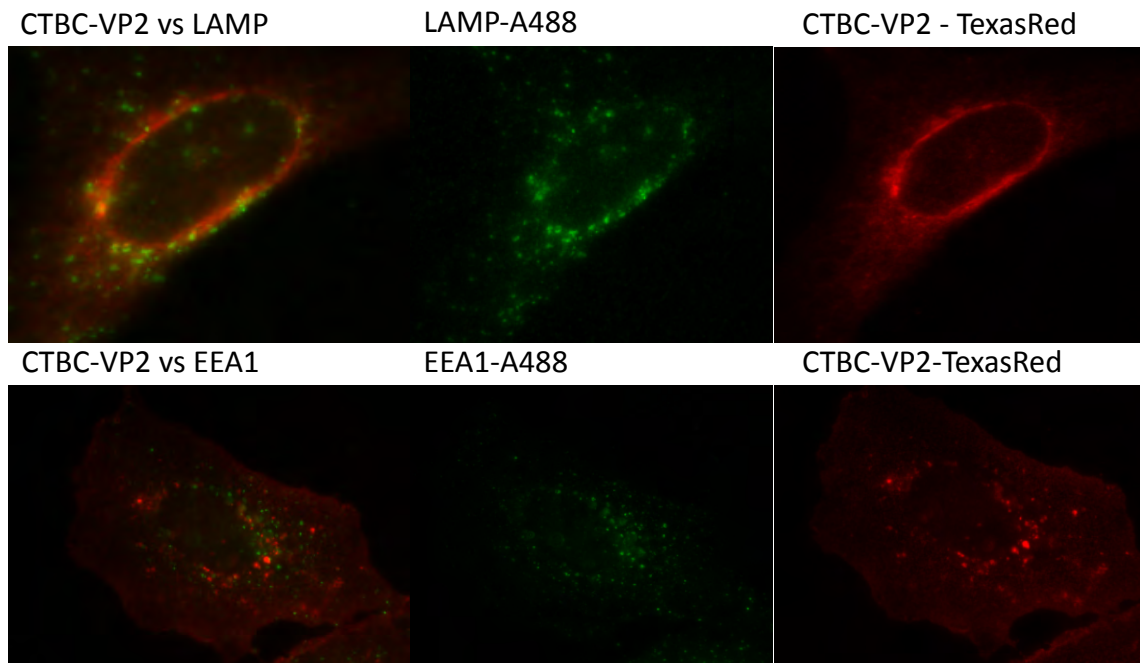


Figure 89. CTBC VP2 chased into cells for one hour, pulsed for three hours prior to cell fixing and labeling with antibodies. Images taken using Nikon 90i microscope, in different channels for each fluorophore.



Figure 90. VP2 chased into cells for one hour, pulsed for three hours prior to cell fixing and labeling with antibodies. Images taken using Nikon 90i microscope, in different channels for each fluorophore.

5.3.7 Analysis of Recombinant Proteins Ability to Traffic Across Monolayers of Polarised Caco-2 Cells

As the recombinant proteins trafficked to a location within the Vero cells that was not completely understood, and appeared to escape lysosomal degradation, transcytosis experiments were initiated in Caco-2 cells. Caco-2 cells were grown for 21 days with a seeding density of 1×10^6 cells/ml. Before beginning the experiments, the TER was measured to ensure the resistance was optimal (380 Ohms). All experiments used 10 μ g/well of the recombinant protein in question, 20 μ M leupeptin and pulsed for one hour followed by three-hour chase. Following this protocol, cells were lysed to assess for any intracellular presence of recombinant protein. Inulin was analysed for in the basolateral chamber as discussed previously (section 5.1.1) and apical and basolateral chambers were subject to TCA precipitation and analysed for the presence of protein in question by western immunoblot with the appropriate antibodies.

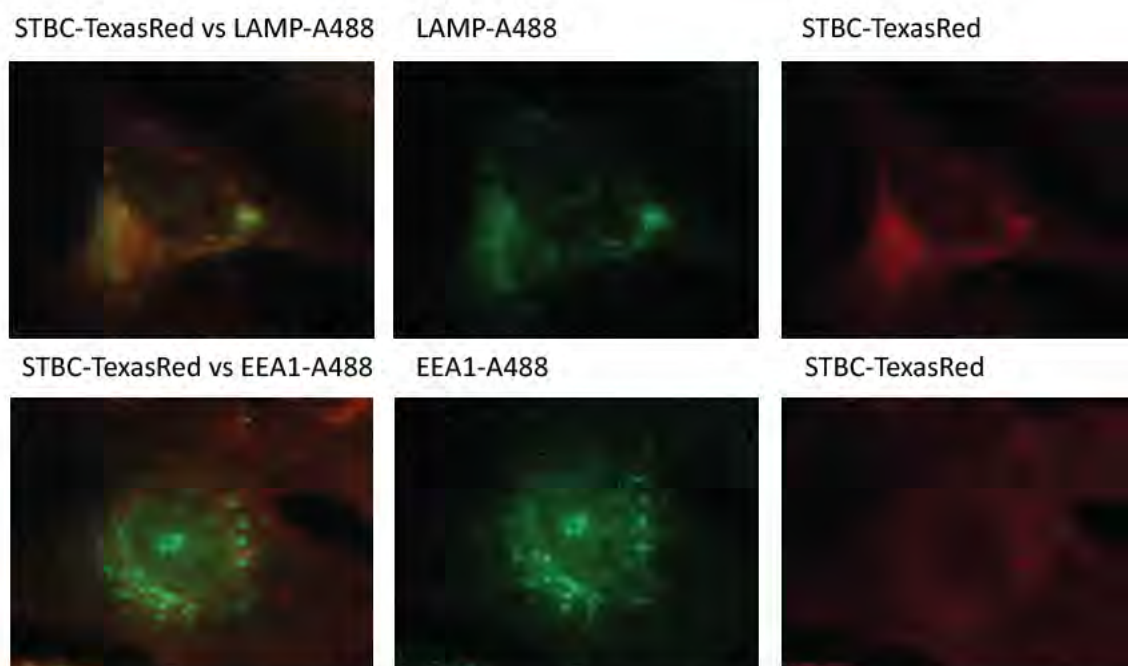

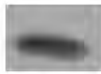

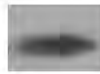
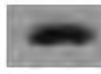









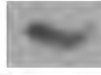

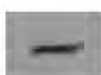

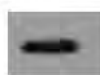



Figure 91. STBC chased into cells for one hour, pulsed for three hours prior to cell fixing and labeling with antibodies. Images taken using Nikon 90i microscope, in different channels for each fluorophore.

The data in table 15 showed that both recombinant proteins CTBC and CTBC VP2 appear to translocate across polarised Caco-2 monolayers. Following TCA precipitation, these proteins can be detected using a 6 histidine antibody specific for CTBC VP2 and α -CTBC antibody against CTBC. The presence of both these proteins can also be detected in the cell lysate. However, for the recombinant proteins STBC, STBC VP2 and VP2, no protein is detected following TCA precipitation in the basolateral chamber, however low levels are detected in the apical chamber which suggests the proteins are not taken up completely, but there is also the presence of the proteins inside the cells. Therefore there must be some uptake of these proteins by Caco-2 cells however no protein traffics through the cells and uptake must be sub-optimal. During these experiments it was crucial that inulin did not pass through into the basolateral chamber and that TER remained constant (figures 92 and 93), these controls were in place to ensure that the proteins were not passing directly between cells.

Table 15. Analysis of transcytosis by the recombinant, purified proteins (n=23).

	CTBC	CTBC-VP2	STBC	STBC-VP2	VP2
Input					
Basolateral					
Apical					
Cell Lysate					

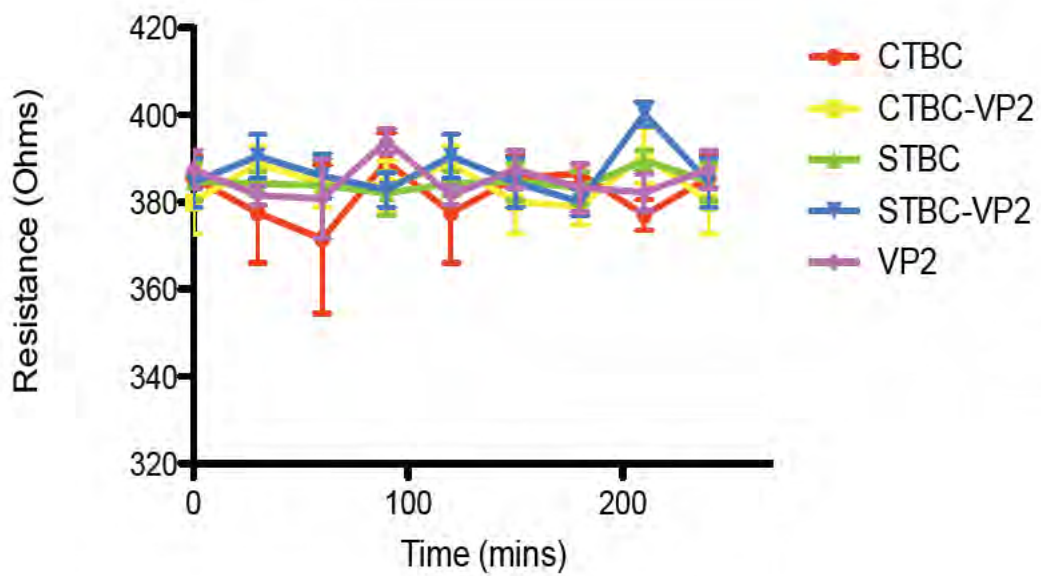


Figure 92. TER measurements over 240 minutes, during transcytosis experiments (n=23).

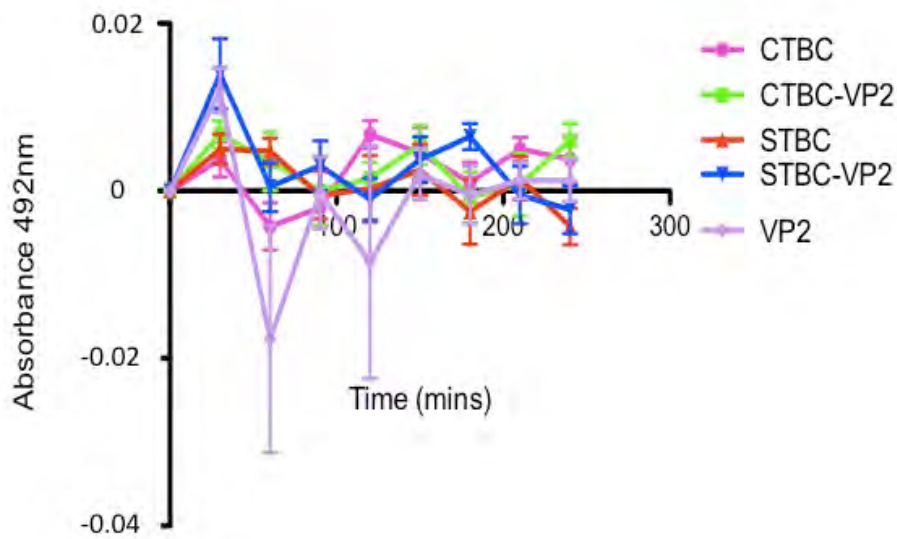


Figure 93. Inulin measurements over 240 minutes, during transcytosis experiments (n=23).

5.4 Discussion

The SCDDS had demonstrated first proof of concept in the ability to adsorb and protect a model antigen (GST-GFP) from degradation by proteases and unfolding due to low pH. The model antigen was released with increased pH, with no significant changes to the secondary conformation of the protein via CD. It was therefore necessary to clone the recombinant proteins that were hypothesised to cross the intestinal epithelium to deliver the antigen to immune cells therein. There were three plasmids encoding STBC, with unknown sequence, in unknown plasmid, kindly donated by Professor Mark Starnes, (University of Iowa, Iowa, USA). However, to ensure the sequence of STBC was correct and in an expressible vector, sequencing of the plasmids was performed. Primers were designed to anneal to variable regions within STBC, to sequence back and fourth across the gene and junctions of the plasmid (table 7). Two of the clones, designated 230, 231 (in the Richardson laboratory database), were found to be in a pGEM plasmid, and hence not suitable for protein expression (Swick *et al.*, 1992) (figures 58 to 60). Therefore these plasmids were no longer used. However, plasmid number 232, was found to be in an *E.coli* expression cassette pET11. In addition within the ORF was a sequence that encoded a

C terminal six-histidine epitope for protein purification (Schmitt *et al.*, 1993) (figure 60). The gene sequence was in frame, and was BLAST searched to ensure the gene encoded the correct protein.

The sequence for CTBC was located by searching multiple sequences on GenBank. A well-cited sequence encoding CTBC (GenBank accession number: AAD51360) was chosen. Bio Basic Inc (BBI) cloned this sequence into a pUC19-cloning vector (plasmid) that laced a bacterial promoter. A theoretical (*in silico*) plasmid map of the gene inserted into pET151 plasmid was created, and used to help design primers for the amplification and sub-cloning into pET151. The pUC19 plasmid containing CTBC sequence was purified from bacterial lysate using a commercially available, Qiagen plasmid mini-prep kit. Primers were used to amplify the CTBC sequence, with the 5' primer including a CACC overhang to assist with directionality when sub-cloning. The amplified product was subject to insertion into the pET151 plasmid vector using optimised conditions (section 2.2.8.3) (figure 62). Colonies were analysed the following day for plasmid and gene insert (figure 64), and sent for sequencing accordingly. Contiguous sequences were aligned and compared with known sequence of gene and plasmid to ensure there were no mutations affecting the protein sequence. Protein sequence was checked using BLAST algorithm.

A similar method was employed for the VP2 gene. However, since VP2 was known to be highly mutagenic, being a capsid protein from a virus, a highly conserved region of the gene had to be located (figure 66) (Yamaguchi *et al.*, 1996). An expired patent was found (US patent 5,350.575), describing a highly conserved region of VP2, thought to be responsible for cellular binding. Two regions within the VP2 gene were thought to be highly conserved. One between restriction enzyme site *Acc*e I-*Spe* I, and the other between *Xho* I-*Smo* I. Multiple VP2 sequences were aligned in a phylogenetic tree (figure 67) and compared to the conserved region in the patent. The gene sequence closest to the patent sequence was therefore chosen as a lead candidate for cloning and analysis. The sequence was codon optimised for expression in *E.coli* and ordered from BBI. A theoretical plasmid map was designed using DNASTar, in the pET151 plasmid vector. As with CTBC, this map was used to help design primers for amplification and sequencing. The plasmid was purified from the bacterial lysate, amplified and inserted into pET151/D TOPO as previously described. Colonies were

analysed for insertion and sequenced. The contiguous sequences were aligned and a sequenced plasmid map generated (figure 69).

Since all three genes has been cloned into expressible plasmids, and sequenced, primers were designed to fuse in frame (with no stop codon) the two corresponding genes (table 12). Primers were designed to link the two genes as described in section 5.1. The three PCR reactions were performed and once satisfactory amplified sequences were achieved (via gel electrophoresis), these products were sub-cloned into pET151 as previously described. The colonies were analysed for the desired insert and sequenced by DNA Sequencing and Services (University of Dundee, UK). Sequenced plasmid maps were then generated (figures 61, 65 to 66, 69, 71 to 76).

All of the sub-cloned genes were inserted into the pET151 plasmid and stored inside *E.coli* TOP10 in the -80°C freezer. These bacteria are used for plasmid propagation, not protein expression. Hence, the plasmids required the transformation into BL21*DE3 bacteria (section 5.2). Following transformation the bacteria was cultured for 3 hours before inducing protein expression with IPTG, and then cultured for a further 3 hours. Bacteria were lysed and the protein purified using Talon resin (Schmitt *et al.*, 1993), since all proteins contained a six-histidine epitope tag. The purified proteins were dialysed to remove any residual imidazole that was used for elution purposes. Following dialysis, the proteins were quantified and characterised by SDS-PAGE followed by western immunoblot. All of the proteins described, produced bands on an X-ray film, at predicted molecular weight using antibodies raised against six-histidine (table 5). The toxicity of the recombinant proteins was also analysed in both Vero and Caco-2 cells (van Meerloo *et al.*, 2011). Since these proteins were going to be used to analyse transcytosis capabilities across Caco-2 cells, it was necessary to assess any toxic effects. All recombinant proteins were not toxic to either Vero or Caco-2 cells up to a concentration of 1mg/ml (figures 77 and 78). Since these proteins are non-toxic, thoughts turned towards whether they would be suitable to deliver the antigen VP2.

In vitro cell models have some advantages over *in vivo* systems in that there is less variation than one may encounter with animal models. In addition, *in vitro* systems allow control over parameters such as temperature. Although not physiological, the

ability to alter these parameters provides a greater insight into the mechanisms of transcytosis (Cardone *et al.*, 1994). However, these advantages are often offset by the lack of *in vivo* physiological context.

A good *in vitro* cell model should be able to recapitate the *in vivo* system in the types, amounts and kinetics of cargo transported across the cellular barrier (Cardone *et al.*, 1994). When cells are grown on filters with media above and below the cellular level, a three-dimensional arrangement simulates *in vivo* conditions (Tuma and Hubbard 2003). A confluent monolayer must be obtained by seeding the correct density of cells, avoiding confluence being achieved at different times across the filter. This can cause profound effects regarding cellular differentiation (Ellis and Luzio 1995).

Therefore, Caco-2 cells were characterised for a number of traits. The first was to characterise the growth of these cells. Since Caco-2 cells are known to differ between laboratories (Shah and Shen 2000), the growth of these particular cells was analysed. The data in figure 78 show that by MTT assay, these Caco-2 cells have a doubling time of six days. However there appears to be a sudden drop in viability at day 22 before suddenly increasing. This was thought to be due to a decrease in metabolic activity upon differentiation. To test this hypothesis, a trypan blue assay was undertaken to assess for cell viability (van Meerloo *et al.*, 2011). Figure 80 shows that the cells are 100% viable over this time, hence the decrease in absorbance during the MTT assay was considered a drop in metabolic activity upon differentiation.

To further characterise the Caco-2 cells, markers of cellular differentiation were analysed. Caco-2 cells were cultured in a sterile six well plate, and lysed using Lamellae buffer on different days. The proteins in the cell lysate were separated by SDS-PAGE and transferred on to a nitrocellulose membrane. Following, the membrane was cut in half, at approximately 50kDa. The membranes were then treated with two different antibodies following blocking. The high molecular weight section was incubated with α -villin and the low molecular weight section, incubated with α -actin. Actin antibody was used as a loading control to ensure that there was even loading across the experimental time frame. Villin antibody, detects the increase in villin as the cells differentiate. Villin is a brush boarder protein and thus associated

with Caco-2 cell differentiation (Deschenes *et al.*, 2001). The data in figure 81 shows that villin was not detected on day 3, but increased from day 7 to day 21. This data corresponded to published literature on Caco-2 differentiation (Shah and Shen 2000).

The transcytosis experiments required that the Caco-2 monolayer remained intact, with no compromise to tight junction integrity (Deschenes *et al.*, 2001). To ensure this was occurring, TER was measured. TER measures the electrical resistance over the cell monolayer, if the cell monolayer was intact, the higher then resistance. Any gaps in the cell monolayer, would result in decreased resistance and therefore the experimental data would be invalid. To characterise the typical resistance of an intact monolayer, TER was measured from day zero to day thirty. Figure 82 shows that TER begins to plateau at day twenty and stabilises at approximately 380 Ohms until the end of the experiment at day thirty. Therefore, during transcytosis experiments it was known that the resistance for these cells, using this instrument, should remain stable at approximately 380 Ohms.

Tight junctions between Caco-2 cells contain a variety of proteins as discussed in section 5.1. Antibodies raised against tight junction proteins; ZO1 and occludin, were used to label fixed Caco-2 cells and characterise the tight junctions between cells. This was performed in both non-differentiated, confluent Caco-2 cells, and confluent, differentiated Caco-2 cells. The data in figure 83 shows that non-differentiated cells display some ZO-1 staining which can be seen faintly between the junctions of adjacent cells (Zahraoui *et al.*, 1994). Occludin can be seen in vesicular components lining these junctions. DAPI was used to stain the nucleus, which in these cells in particular, helps to visualise the cells when imaging. The confluent, differentiated Caco-2 cells displayed a greater amount of ZO-1 and occludin staining, lining the cell boundaries as expected of differentiated Caco-2 cells (Zahraoui *et al.*, 1994).

Inulin flux and TER had previously been characterised in these Caco-2 cells (section 5.1). However, it was important that TER readings and any inulin flux were kept constant during transcytosis experiments. Therefore, the TER and inulin absorbance readings were recorded over 24 hours in the presence of a non-toxic concentration of STBC / CTBC / VP2 (10µg/well). Figures 85 to 87 show that with these three

proteins, the TER remains reasonably constant, and inulin is not detected in the basolateral chamber over this time frame. Therefore it was concluded that these proteins would not have any significant effect on the tight junctions during transcytosis experiments.

Since the recombinant proteins were considered to be ideal candidates for transcytosis across the Caco-2 cell monolayer, the trafficking of these proteins was analysed first in Vero cells (Elliott and O'Hare 1997). Vero cells were used, as the growth time is much faster than Caco-2 cells as they gave a good idea of cellular location. Vero cells were cultured on sterile cover slips at 1×10^6 cells / well overnight. The following day the media was changed to serum and antibiotic free and $10\mu\text{g}/\text{well}$ of recombinant protein added to individual wells with $20\mu\text{M}$ leupeptin. Cells were left for one hour in the incubator at 37°C before the media was changed, including 10% FBS (v/v) and antibiotics. Cells were incubated for a further three hours prior to fixation. All of the experiments used antibodies directed against LAMP2, a lysosomal marker and EEA1, an early endosome associated tethering protein. Figure 88 shows Vero cells treated with CTBC. There appeared to be no co-localisation between LAMP2 and EEA1 at the time frames tested. However, there was a hazy appearance on the surface of the cell indicating the possible presence of surface bound material (Gross *et al.*, 2003). Similar results were found for CTBC VP2, with no co-localisation with LAMP or EEA1 (figure 89). VP2 was also investigated via this mechanism. Again, there appeared no co-localisation between EEA1 and LAMP but a hazy appearance indicating either the presence of surface bound protein or cytosolic protein (figure 90). However due to temporal constraints this hypothesis was not tested. STBC displayed similar results to CTBC in that there appeared to be a region of surface bound protein but no co-localisation between LAMP and EEA1 (figure 91). Interestingly, CTBC and CTBC VP2 appear to localise to the exterior of the nucleus, suggesting an interaction with the Golgi. However this hypothesis again was not tested due to temporal constraints.

The recombinant proteins were then analysed for their ability to cross Caco-2 monolayers. Caco-2 cells were cultured on Transwell membranes for 21 days as previously described (section 5.2) (Shah and Shen 2000). Prior to experiments the

TER was recorded to ensure there was adequate resistance, indicating that the tight junctions were complete. The media was changed to serum and antibiotic free, 200µM leupeptin (Sigma, Dorset, UK) and the protein of choice was added. TER measurements and inulin flux were recorded at 30 min intervals for the duration of the experiment. The basolateral and apical chambers had the media removed at the end of the experiment (four hours) and was subject to TCA precipitation. TCA precipitation was used as a method to concentrate any proteins present in these chambers, whilst the cells were lysed with lamellae buffer. Each component was separated on a SDS-PAGE gel and subject to western immunoblot. Each protein was probed using either a CTBC or STBC antibody or six-histidine antibody for VP2 alone. The data in table 15 shows that CTBC and CTBC VP2 was detected in the basolateral chamber (1/10th input) at predicted molecular weight. STBC, STBC VP2 and VP2 were detected in small amounts (1/10th input) in the apical chamber and the remainder in the whole cell lysate, indicating that the Caco-2 cells took some, but not all of these proteins up. None of these proteins were detected in the basolateral chamber. Some (90%) CTBC and CTBC VP2 were found inside the Caco-2 cell lysate, perhaps subject to degradation of cytosolic trafficking. Figures 92 and 93 show that TER remained stable during these experiments and inulin was not detected in the basolateral chamber.

This chapter set out the importance of a trafficking partner to be able to deliver an antigen (VP2) to the *lamina propria*. Recombinant PCR was used to fuse in frame a variety of potential VP2 fusions to trafficking partners (CTBC / STBC). These recombinant genes were sequenced and expressed following transformation into *E.coli* BL21*DE3. These proteins were found to be non-toxic to both Vero and Caco-2 cells and did not affect tight junctions. Caco-2 cells were characterised for growth and found to have a doubling time of six days. TER was found to stabilise at 380 Ohms when fully differentiated and confluent. Tight junctions were characterised by immunofluorescent microscopy using antibodies raised against ZO-1 and occludin (Zahraoui *et al.*, 1994). Differentiated cells were found to have higher levels of expression of these proteins, localised to the membrane. In addition, villin production increased over 21 days with a loading control of actin used to ensure even loading of cell lysate. Finally, transcytosis experiments were performed with the recombinant

proteins. CTBC and CTBC VP2 were both detected in the basolateral chambers whilst STBC / STBC VP2 and VP2 were not. All proteins were detected inside the cellular lysate indicating cellular delivery. Therefore, it was concluded that CTBC and CTBC fused in frame to VP2 are capable of delivering the antigen (in this case VP2) to the *lamina propria* of cells (*in vitro*).

Chapter 6: General Discussion

The aim of this work was to design a system capable of effecting immunisation by delivering a protein antigen to the *lamina propria* after its oral administration (Hoffmann *et al.*, 2006). Given the impact of diseases such as IBDV upon global food security, a formulation suitable for administration to livestock was paramount to this design (Tseng *et al.*, 2009) (Chapter 1).

Having identified an IBDV protein previously used to inoculate livestock (VP2), and hyper-conserved sequences within the VP2 gene (being responsible to receptor binding (Yip *et al.*, 2007) (figure 67)), the hyper-conserved VP2 region was sub-cloned into a bacterial expression cassette. However, given the difference in yield between the VP2 containing fusion proteins sub-cloned during this work and a model recombinant protein (GST-GFP), initial questions fundamental to the formulation of this protein delivery system were addressed with the latter rather than the former (Chapter 3 section 3.1).

The data that established that proteins could be both adsorbed onto, and released from a silica core, posed a variety of questions about the mechanisms responsible for the protein accessing the *lamina propria* (Chapter 4 section 4.3). Possible uptake mechanisms were thought to be dependant upon several factors, including the overall size of the delivery system, the biology of the carrier protein fused in frame with the antigen and the release rate of the protein from the silica (Tang *et al.*, 2011) (Chapter 4 section 4.3). Given that the mechanistic studies required to address the questions posed above would require *in vivo* or *ex vivo* experimentation (such as an everted gut-sack model (Carreno-Gomez *et al.*, 1999)), and the preliminary nature of this study, a strategic decision was made to ask more fundamental questions addressing feasibility *in vitro*. However it needs to be emphasised that the proposed *in vivo* studies are of equal importance to the *in vitro* studies undertaken herein and should be addressed in the immediate future, having now shown proof of concept *in vitro*.

Each of these issues deserves attention and they are addressed below. Particle size, shape and charge are accepted to dictate how a particle interacts with a cell. Size will

directly determine if a particle can subject to fluid-phase pinocytic capture (Richardson and Duncan, 2013). Particles larger than 200 nm, whilst being subject to phagocytic clearance by the reticuloendothelial system are generally too big to be subject to pinocytic uptake (Richardson and Duncan, 2013). Consequently particles larger than 200nm will need to release their cargo (protein) prior to translocation over the epithelial lining of the gut. Translocation of the fat depleted delivery system still carrying a substantial quantity of the carrier fused to the antigen may have enhanced antigenic properties by virtue of being colloidal in nature (Patel *et al.*, 2007). This then impacts upon the required release rate of the protein, or even the desire to adhere the antigen to the silica in preference to the carrier protein, which could be mobile within a coroner surrounding the solid core. This carrier protein mobility could facilitate its interaction with a cognate cellular receptor (Pina and Johannes 2005). The choice of carrier protein may also dictate efficacy as currently it is unknown whether passage over the epithelial lining of the gut versus translocation in the M cells of the Peyer's patch will provide a more robust immune response (Artursson 1990). The benefits of Peyer's patch versus non-Peyer's patch presentation to the immune system have yet to be fully investigated, however in theory it would be relatively easy to investigate this hypothesis experimentally. This could be achieved by comparing the effect attributed to a recombinant invasin protein (thought to be responsible for Peyer's patch uptake) fused to VP2 and incorporated into the system characterised herein, with the STBC and CTBC –VP2 fusions characterised herein (Chapter 5) (Brun *et al.*, 2008). Ultimately not only could serum antibody titres against VP2 be compared but also the distribution of the silica along the GI.

Further characterisation of these proposed systems would have been undertaken using the methodologies developed herein such as SANS (Chapter 4 section 4.3). Indeed had time allowed the SANS studies could have been extended to investigate not only the protein corona on the surface of the silica, but also the fatty acid coat. These experiments would have been easier if the size of the silica were reduced to 50µm as there may have been fewer opportunities for a second reflection of the neutrons (section 4.2.2.4). The use of a smaller silica bead would also alter the binding and release profile of the antigen since the surface area would increase. This technology is

vastly preferable to zeta sizing as the resolution is higher and sedimentation can easily be stopped using a rotating rack (as previously described, Chapter 4 section 4.2.2.4).

Having performed the mechanistic studies outlined above the optimisation of protein loading and release could then be addressed. As protein adsorption is driven by electrostatic interactions, it is not unreasonable to hypothesise that the surface functionalization of the silica could be used to either enhance protein binding, enabling a higher loading via a more ordered assembly within the protein corona, or alter the release profile such that it is no longer within the physiological range (Hoffmann *et al.*, 2006).

Beyond the physicochemical characterisation and manipulations previously discussed, there remains the discovery that the secondary conformation of the STBC and CTBC containing fusion proteins was conserved after their release. What is not known is the effect of tertiary conformation upon the propensity of these constructs to translocate across epithelial barriers (Whitmore and Wallace 2008). As both STBC and CTBC form pentamers in the wild and the formation of these pentamers is necessary for the association of the C terminal domain of the A-chain, it is possible that multimerisation impacts upon the unusual trafficking of these proteins (Sandvig *et al.*, 2010). It is also not known how the recombination of either the C and N terminal ends of these proteins affects multimerisation and indirectly trafficking or trafficking directly (Sandvig 2005).

Finally, had time permitted, the last *in vitro* experiment to perform would provide the last milestone prior to conducting the proposed *in vivo* investigations. This experiment would require CTBC VP2 to be absorbed to the silica beads and fatty acid coated, this SCDDS would be placed onto Caco-2 cells and the pH increased slightly. CTBC VP2 would be analysed to investigate whether the protein was capable of release from the beads and then transcytosis across the Caco-2 cells thereafter.

Further applications of this system may be in the clinical arena as it is possible that should the data generated from inoculating livestock show efficacy, the translation of this technology into the clinic should be relatively simple. Applications may include vaccination against protein agents of bioterrorism, such as anthrax (using PA83

protein, the principle component in BioThrax vaccine) (Brown *et al.*, 2010) fused in frame to the carrier protein (*i.e.* CTBC) or even attenuated ricin (*i.e.* using the attenuated ricin A chain associated with the RiVax vaccine (Olsnes 2004). Equivalently, this technology could be used to prevent communicable diseases, such as TB from invading the reticuloendothelial system by immunising people against the TB antigen (Ag85a, Ag85b, Ag85c) prior to exposure (Jain *et al.*, 2008).

In conclusion, a solid silica nanoparticle can be utilised to immobilise protein via electrostatic interactions (Chapter 4). This arrangement can then be coated with a fatty acid enteric coat affording protection against proteolytic degradation (Chapter 4). The protein release profile from the solid core, whilst sub-optimal, demonstrates utility as a drug delivery system (Chapter 4). Additionally, it has been shown that recombinant CTBC and CTBC VP2 fusion proteins can translocate across a model epithelial barrier, making them future candidates for incorporation into a drug delivery system similar to that characterised herein (Chapter 5). This body of work demonstrates potential application as an oral vaccine delivery system warranting further research and development.

Chapter 7: References

- Aatsinkia, J.T and Rajaniemib, H.J. (2005) 'An alternative use of basic pGEX vectors for producing both N- and C terminal fusion proteins for production and affinity purification of antibodies.' *Protein Expression and Purification*. **40** (2): 287-291.
- Aguilar, J.C and Rodriguez, E.G. (2007) 'Vaccine adjuvants revisited.' *Vaccine*. **25** (19): 3752-3762.
- Alving, C.R. (2002) 'Design and selection of vaccine adjuvants: animal models and human trials.' *Vaccine*. **20** (3): 56-64.
- Ampapathi, R.S., Creath, A.L., Lou, D., Craft, J.W., Blanke, S.R and Legge, G.B. (2008) 'Order-Disorder-Order Transitions mediate the Activation of Cholera Toxin.' *Journal of Molecular Biology*. **377** (3): 748-760.
- Andrews, B.T., Schoenfish, A.R., Ray, M., Waldo, G and Jennings, P.A. (2007) 'The Rough Energy landscape of Superfolder GFP is Linked to the Chromophore.' *Journal of Molecular Biology*. **373** (2): 476-490.
- Aravindana, L., Bicknella, K.A., Brooksb, G., Khutoryanskiya, V.V and Williamsa, A.C. (2009) 'Effect of acyl chain length on transfection efficiency and toxicity of polyethylenimine.' *International Journal of Pharmaceutics*. **378** (1-2): 201-210.
- Aricibasi, M., Jung, A., Heller, E.D and Rautenschlein, S. (2010) 'Differences in genetic background influence the induction of innate and acquired immune responses in chickens depending on the virulence of the infecting infectious bursal disease virus (IBDV) strain.' *Veterinary Immunology and Immunopathology*. **135** (1-2): 79-92.
- Arinaminpathy, N., McLean, A.R and Godfray, H.C.J. (2009) 'Future UK land use policy and the risk of infectious disease in humans, livestock, and wild animals.' *Land Use Policy*. **26**: s124-s133.
- Artursson, P. (1990) 'Epithelial transport of drugs in cell culture: A model for studying the passive diffusion of drugs over intestinal absorptive (Caco-2) cells.' *Journal of Pharmaceutical Science*. **79**: 476-482.
- Artursson, P., Palm, K and Luthman, K. (2001) 'Caco-2 monolayers in experimental and theoretical predictions of drug transport.' *Advanced Drug Delivery Reviews*. **46**: 27-43.
- Arruebo, M. (2012) 'Drug delivery from structured porous inorganic materials.' *WIREs Nanomedicine Nanobiotechnology*. **4**: 16-30.
- Asakura, T., Adachi, K and Schwartz, E. (1977) 'Stabilizing Effect of Various Organic Solvents on Protein.' *The Journal of Biological Chemistry*. **253** (18): 6423-6425.
- Baker, H.J., Alpert, L.C., Compton, C.C., Maslen, A and Kirby, G.M. (2002) 'Loss of glutathione S-transferase (GST) m phenotype in colorectal adenocarcinomas from patients with a GSTM1 positive genotype.' *Cancer Letters*. **177** (1): 65-74.
- Baneyx, F. (1999) 'Recombinant protein expression in Escherichia coli.' *Current Opinion in Biotechnology*. **10** (5): 411-421.
- Barnes, E.M. (2008) 'The Intestinal Microflora of Poultry and Game Birds During Life and After Storage.' *Journal of Applied Microbiology*. **46** (3): 407-419.

- Bar-Shira, E and Friedman, A. (2006) 'Development and adaptation of innate immunity in the gastrointestinal tract of the newly hatched chick.' *Developmental and Comparative Immunology*. **30** (10): 930-941.
- Bennett, M. (1995) 'SNAREs and the specificity of transport vesicle targeting.' *Current Opinion in Cell Biology*. **7**: 581-586.
- Beyer, W and Turnbull, P.C.B. (2009) 'Anthrax in animals.' *Molecular Aspects of Medicine*. **30** (6): 481-489.
- Borges, O., Cordeiro-da-Silva, A., Tavares, J., Santarém, N., de Sousa, A., Borchard, G and Junginger, H. E. (2008) 'Immune response by nasal delivery of hepatitis B surface antigen and codelivery of a CpG ODN in alginate coated chitosan nanoparticles.' *Eur. J. Pharm. Biopharm.* **69** (2): 405-416.
- Bowerstock, T.L and Martin, S. (1999) 'Vaccine delivery to animals.' *Advanced Drug Delivery Reviews*. **38** (2): 167-194.
- Bowersock, T.L., HogenEsch, H., Suckow, M., Porter, R.E., Jackson, R., Park, H and Park, K. (1996) 'Oral vaccination with alginate microsphere systems.' *Journal of Controlled Release*. **39**: 209-220.
- Bovier, P.A. (2008) 'Epaxal: a virosomal vaccine to prevent hepatitis A infection.' *Expert Review of Vaccines*. **7**: 1141-1150.
- Brayden, D.J and O'Mahany, D.J. (1998) 'Novel oral drug delivery gateways for biotechnology products: polypeptides and vaccines.' *Pharmaceutical Science and Technology Today*. **1** (7): 291-299.
- Bretscher, A and Weber, K. (1979) 'Villin: The major microfilament-associated protein of the intestinal microvillus.' *Proceeding of the National Academy of Sciences*. **76** (5): 2321-2325.
- Brewer, J., Tetley, L., Richmond, J., Liew, F.Y and Alexander, J. (1998) 'Lipid vesicle size determines the Th1 or Th2 responses to entrapped antigen.' *Journal of Immunology*. **161** (8): 4000-4007.
- Brun, A., Albina, E., Barret, T., Chapman, D.A.G., Czub, M., Dixon, L.K., Keil, G.M., Klonjowski, B., Potier, M.F., Libeau, G., Ortego, J., Richardson, J and Takamatsu, H.H. (2008) 'Antigen delivery systems for veterinary vaccine development: Viral vector based delivery systems.' *Vaccine*. **26** (51): 6508-6528.
- Broeck, D.V., Horvath, C and De Wolf, M.J.S. (2007) '*Vibrio cholerae*: cholera toxin.' *The International Journal of Biochemistry and Cell Biology*. **39** (10): 1771-1775.
- Brown, W., Ralston, A and Shaw, K. (2008) 'Positive transcription control: The glucose effect.' *Nature Education*. **1** (1).
- Butera, D., Piazza, R.M.F., Mclane, M.A., Chammas, R and Silva, A.M.M. (2005) 'Molecular engineering of an EGFP / disintegrin-based integrin marker.' *Toxicon*. **46** (2): 178-184
- Campos, D., Mendez, V and Fedotov, S. (2008) 'The effects of distributed life cycles on the dynamics of viral infections.' *Journal of Theoretical Biology*. **254** (2): 430-438.
- Capitani, M and Sallese, M. (2009) 'The KDEL receptor: New functions for an old protein.' *FEBS Letters*. **583** (23): 3863-3871.

- Carlos Rodriguez-Lecompte, J., Nino-Fong, R., Lopez, A., Markham, R.J.F and Kibenge, F.S.B. (2005) 'Infectious Bursal Disease Virus (IBDV) induces apoptosis in chicken B cells.' *Comparative Immunology, Microbiology and Infectious Disease*. **28** (4): 321-337.
- Carreno-Gómez B, Woodley JF, Florence AT. (1999) 'Studies on the uptake of tomato lectin nanoparticles in everted gut sacs.' *International Journal of Pharmaceutics*.**183**(1): 7-11.
- Cardone, M., Smith, B., Song, W., Mochly-Rosen, D and Mostov, K.E. (1994) 'Pharbol myristate acetate-mediated stimulation of transcytosis and apical recycling in MDCK cells.' *Journal of Cellular Biology*. **124**: 717-727.
- Casadaban, M.J and Cohen, S.N. (1980) ' Analysis of gene control signals by DNA fusion and cloning in Escherichia coli.' *Journal of Molecular Biology*. **138** (2):179-207.
- Caskie, P., Davis, J and Moss, J.E. (1998) 'The beginning of the end or the end of the beginning for the BSE crisis.' *Food Policy*. **23** (3-4): 231-240.
- Chamel, B. (1998) 'New emerging zoonoses: a challenge and an opportunity for the veterinary profession.' *Comparative Immunology, Microbiology and Infectious Disease*. **21** (1): 1-14.
- Chantret, I., Rodolosse, A., Barbat, A., Dussaulx, E., Brot-Laroche, E., Zweibaum, A and Rausset, M. (1994) 'Differential expression of sucrase-isomaltase in clones isolated from early and late passages of the cell line Caco-2: evidence for glucose-dependent negative regulation.' *Journal of Cell Science*. **107**: 213-225.
- Chen, H., Torchilin, V and Langer, R. (1996) 'Polymerized liposomes as potential oral vaccine carriers: stability and bioavailability.' *Journal of Controlled Release*. **42**: 263-272.
- Chiang, C.F., Okou, D.T., Griffin, T.B., Verret, C.R and Williams, M. (2001) 'Green Fluorescent Protein Rendered Susceptible to Proteolysis: Positions for Protease-Sensitive Insertions.' *Archives of Biochemistry and Biophysics*. **394** (2): 229-235.
- Clench, M.H. (1999) 'The avian cecum: Update and motility review.' *Journal of Experimental Zoology*. **283** (4-5) 441-447.
- Cohen, J.E. (2003) 'Human Population: The Next Half Century.' *Science*. **302**: 1172-1175.
- Cormack, B.P., Valdiviaa, R and Falkowa, S. (1996) 'FACS-optimised mutants of the green fluorescent protein (GFP).' *Gene*. **173** (1): 33-38.
- Cosentino, S., Gravaghia, C., Donettic, E., Donidaa, B.M., Lombardid, G., Bedonic, M., Fiorillia, A., Tettamantia, G and Ferrarettoa, A. (2010) 'Caseinphosphopeptide-induced calcium uptake in human intestinal cell lines HT-29 and Caco2is correlated to cellular differentiation.' *The Journal of Nutritional Biochemistry*. **21** (3): 247-254.
- Coulibaly, F., Chevalier, C., Gutsche, I., Pous, J., Navaza, J., Bressanelli, S., Delmos, B and Rey, F.A. (2005) 'The Birnavirus crystal structure reveals structural relationships among icosahedral viruses.' *Cell*. **120**: 761-772.
- Cripps, A.W., Kyd, J.M and Foxwell, A.R. (2001) 'Vaccines and mucosal immunization.' *Vaccine*. **19** (17-19); 2513-2515.
- Curtiss, R. (2002) 'Bacterial infectious disease control by vaccine development.' *Journal of Clinical Investigation*. **110** (8): 1061-1066.

Dagan, R., Amir, J., Livni, G., Greenberg, D., Abu-Abed, J., Guy, L., Ashkenazi, S., Froesner, G., Tewald, F and Schaetzl, H. M. (2007) 'Concomitant administration of a virosome-adjuvanted hepatitis a vaccine with routine childhood vaccines at age twelve to fifteen months: a randomized controlled trial.' *Paediatric Infectious Disease Journal*. **26** (9): 787.

de Jonge, M. I., Hamstra, H. J., Jiskoot, W., Roholl, P., Williams, N. A., Dankert, J., Alphen, L and van der Ley, P. (2004) 'Intranasal immunisation of mice with liposomes containing recombinant meningococcal OpaB and OpaJ proteins.' *Vaccine* **22** (29-30): 4021-4028.

De Haan, L and Hirst, T.R (2004) 'Cholera toxin: A paradigm for multi-functional engagement of cellular mechanisms.' *Molecular membrane Biology*. **21**: 72-92.

Del Vecchio, P., Graziano, G., Granata, V., Barone, G., Mandrich, L., Rossi, M and Manco, G. (2002) 'Denaturing action of urea and guanidine hydrochloride towards two thermophilic esterases.' *Biochemical Journal*. **367**: 857-863.

Deng, X., Gao, Y., Gao, H., Oi, X., Cheng, Y., Wang, X and Wang, X. (2007) 'Antigenic structure analysis of VP3 of infectious bursal disease virus.' *Virus Research*. **129** (1): 35-42.

Deschenes, C., Vezina, A., Beaulieu, J.F and Rivard, N. (2001) 'Role of p27(Kip1) in human intestinal cell differentiation.' *Gastroenterology*. **120** (2): 423-438.

Dietz, G and Bahr, M. 'Delivery of bioactive molecules into the cell: the Trojan horse approach.' *Molecular Cellular Neuroscience*. **27**: 85-131.

Domon, B and Aebersold, R. (2006) 'Mass Spectrometry and Protein Analysis and Protein Analysis.' *Science*. **312** (5771): 212-217.

Dorrestein, G.M and van Miert, A.S.J.P.A.M. (2008) 'Pharmacotherapeutic aspects of medication of birds.' *Journal of Veterinary Pharmacology and Therapeutics*. **11** (1): 33-44.

Dubendorf, J.W and Studier, F.W. (1991) 'Controlling basal expression in an inducible T7 expression system by blocking the target T7 promoter with lac repressor.' *Journal of Molecular Biology*. **219** (1): 45-59.

Dumon-Seignovert, L., Cariot, G and Vuillard, L. (2004) 'The toxicity of recombinant proteins in Escherichia coli: a comparison of overexpression in BL21 (DE3), C41(DE3) and C43(DE3).' *Protein Expression and Purification*. **37** (1): 203-206.

Duncan, R and Gaspar, R. (2011) 'Nanomedicine(s) under the Microscope.' *Molecular Pharmaceutics*. **8**: (6) 2101-2141.

Dyer, P.D.R., Kotha, A.K., Pettit, M.W.P and Richardson, S.C.R. (2013) 'Imaging Select Mammalian Organelles Using Fluorescent Microscopy: Application to Drug Delivery.' *Cellular and Subcellular Nanotechnology*. 195-209.

Ebeling, W., Hennrich, N., Klockow, M., Metz, H., Orth, H.D and Lang, H. (1974) 'Proteinase K from Tritirachium album Limber.' *European Journal of Biochemistry*. **47** (1): 91-97.

Edwards, K.A., Duan, F., Baeumner, A.J and March, J.C. (2008) 'Fluorescently labeled liposomes for monitoring Cholera toxin binding to epithelial cells.' *Analytical Biochemistry*. **380** (1): 59-67.

- Elankumaran, S., Kumaran, K., Chandran, N., Palaniswami, K.J and Uenugopalan, A.T. (1995) 'Agglutination of chicken lymphocytes by infectious bursal disease virus.' *Veterinary Microbiology*. **44**: 93-99.
- Eldaghayes, I., Rothwell, L., Williams, A., Withers, D., Balu, S., Davidson, F and Kaiser, P. (2006) 'Infectious Bursal Disease Virus: Strains that Differ in Virulence Differentially Modulate the Innate Immune Response to Infection in the Chicken Bursa.' *Viral Immunology*. **19** (1): 83-91.
- Elliott, G and O'Hare, P. (1997) 'Intracellular Trafficking and Protein Delivery by a Herpesvirus Structural Protein.' *Cell*. **88** (2): 223-233.
- Ellis, J.A and Luzio, J.P. (1995) 'Identification and characterisation of a novel protein (p137) which transcytoses bidirectionally in Caco-2 cells.' *Journal of Biological Chemistry*. **270**: 20717-20723.
- Elslinger, M.A., Wachter, R.M., Hanson, G.T., Kallio, K and Remington, S.J. (1999) 'Structural and Spectral Response of Green Fluorescent Protein Variants to Changes in pH.' *Biochemistry*. **38**: (17) 5296-5301.
- Eltohom, M., Shin, U.S and Kim, H.W. (2011) 'Silica nanoparticles with enlarged nanopore size for the loading and release of biological proteins.' *Materials Letters*. **65** (23-24): 3570-3573.
- Enoki, Y and Morimoto, T. (2000) 'Gizzard myoglobin contents and feeding habits in avian species.' *Comparative Biochemistry and Physiology – Part A: Molecular and Integrative Physiology*. **125** (1): 33-43.
- Even-Ora, O., Joseph, A., Itskovitz-Cooper, N., Samirac, S., Rochline, E., Eliahua, H., Goldwasser, I., Balasingam, S., Mandl, A.J., Lambkin-Williams, R., Kedarb, E and Barenholz, Y. (2011) 'A new intranasal influenza vaccine based on a novel polycationic lipid-ceramide carbamoyl-spermine (CCS). II. Studies in mice and ferrets and mechanism of adjuvanticity.' *Vaccine* **29**: 2474-2486.
- Falguieres, T., Mallard, F., Baron, C., Hanau, D., Lingwood, C., Goud, B., Smerio, J and Johannes, L. (2001) 'Targeting of Shiga Toxin B – Subunit to retrograde transport route in association with detergent-resistant membranes.' *Molecular Biology of the Cell*. **12**: 2453-2468.
- Fasanella, A., Gelante, D., Garofolo, G and Jones, M. (2010) 'Anthrax undervalued zoonosis.' *Veterinary Microbiology*. **140** (3-4): 318-331.
- Fiedler, S and Wirth, R. (1988) 'Transformation of bacteria with plasmid DNA by electroporation.' *Analytical Biochemistry*. **170** (1): 38-44.
- Finkelstein, R.A., Mukerjee, S and Rudra, B.C. (1963) 'Demonstration and quantification of antigen in Cholera stool filtrates.' *Journal of Infectious Diseases*. **113**: 99-104.
- Fischer, D., Li, Y., Ahlemeyer, B., Krieglstein, J and Kissel, T. (2003) 'In vitro cytotoxicity testing of polycations: influence of polymer structure on cell viability and hemolysis.' *Biomaterials*. **24** (7): 1121-1131.
- Florence, A.F and Hussain, N. (2001) 'Transcytosis of nanoparticle and dendrimer delivery systems: evolving vistas.' *Advanced Drug Delivery Reviews*. **50** (1): S69-S89.
- Frangioni, J.V and Neel, B.G. (1993) 'Solubilisation and Purification of Enzymatically Active Glutathione S-Transferase (pGEX) Fusion Proteins.' *Analytical Biochemistry*. **210** (1): 179-187.

Frey, J. (2007) 'Biological safety concepts of genetically modified live bacterial vaccines.' *Vaccine*. **25** (30): 5598-5605.

Furuse, M., Hirase, T., Itoh, M., Nagafuchi, A., Yonemura, S., Tsukita, S and Tsukita, S. (1993) 'Occludin: a novel integral membrane protein localizing at tight junctions.' *Journal of Cell Biology*. **123** (6): 1777-1788.

Fyderek, K., Strus, M., Kowalska-Duplaga, K., Gosiewski, T., Wedrychowicz, A., Jedynak-Wasowicz, U., Śladek, M., Pieczarkowski, S., Adamski, P., Kochan, P and Heczko, P. (2009) 'Mucosal bacterial microflora and mucus layer thickness in adolescents with inflammatory bowel disease'. *World Journal of Gastroenterology*. **15** (42): 5287-5294.

Ganapathy, K., Bufton, A., Pearson, A., Lemiere, S and Jones, R.C. (2010) 'Vaccination of commercial broiler chickens against avian metapneumovirus infection: a comparison of drinking water, spray and oculo-oral delivery methods.' *Vaccine*. **28** (23): 3944-3948.

George-Chandy, A., Eriksson, K., Lebens, M., Wardstrom, I., Schon, E and Holmgren, J. (2001) 'Cholera Toxin B Subunit as a Carrier Molecule Promotes Antigen Presentation and Increases CD40+ and CD86 Expression on Antigen-Presenting Cells.' *Infection and Immunity*. **69** (9): 5716-5725.

Giglione, C., Boularot, A and Meinnel, T. (2004) 'Protein N terminal methionine excision.' *Cellular and Molecular Life Sciences*. **61** (12): 1455-1474.

Gimeno, I.M. (2008) 'Marek's disease vaccines: A solution for today but a worry for tomorrow?' *Vaccine*. **26** (3): C31-C41.

Ginzberg, A., Cohen, M., Sod-Moriah, U., Shany, S., Rosenshtrauch, A and Arad, S. (2011) 'Chickens fed with biomass of the red microalga *Porphyridium* sp. have reduced blood cholesterol level and modified fatty acid composition in egg yolk.' *Journal of Applied Phycology*. **12** (3-5): 325-330.

Glahn, R.P., Lee, O.A., Yeung, A., Goldman, M.R and Miller, D.D. (1998) 'Caco-2 cell ferritin formation predicts nonradiolabeled food iron availability in an in vitro digestion Caco-2 cell culture model.' *Journal of Nutrition*. **128** (9): 1555-1561.

Gluck, R and Metcalfe, I.C. (2003) 'Novel approaches in the development of immunopotentiating reconstituted influenza virosomes as efficient antigen carrier systems.' *Vaccine* **21** (7-8): 611-615.

Goldberg, A (2003) 'Protein degradation and protection against misfolded or damaged proteins.' *Nature*. **426**: 895-899.

Gomes, A.D., Abreu, J.T., Redondo, R.A.F., Martins, N., Resende, J.S and Resende, M. (2005) 'Genotyping of Infectious Bursal Disease Virus Strains by Restriction Fragment Length Polymorphism Analysis of the VP1, VP2 and VP3 Genes.' *Avian Diseases*. **49**: 500-506.

Gross, C., Koelch, W., Demaio, A., Arispe, N and Multhoff, G. (2003) 'Cell surface-bound heat shock protein 70 (Hsp70) mediates perforin-independent apoptosis by specific binding and uptake of granzyme B.' *Journal of Biological Chemistry*. **278**: 41173-41181.

Gupta, P. N., Khatri, K., Goyal, A. K., Mishra, N and Vyas, S. P. (2007) 'M-cell targeted biodegradable PLGA nanoparticles for oral immunization against hepatitis B.' *J. Drug Target.* **15** (10): 701-713.

Gupta, P, Vermani, K and Garg, S. (2002) 'Hydrogels from controlled release to pH-responsive drug delivery.' *Drug Delivery Today.* **7** (10): 569-579.

Guttman, J.A and Finlay, B.B. (2009) 'Tight junctions as targets of infectious agents.' *Biochimica et Biophysica Acta – Biomembranes.* **1788** (4): 832-841.

Brown,

Graber, M., Irague, R., Rosenfield, E., Lamare, S., Franson, L and Hult, K. (2007) 'Solvent as a competitive inhibitor for candida antarctica lipase B.' *Biochimica et Biophysica Acta.* **1774**; 1032-1037.

Habib, M., Hussain, I., Irshad, H., Yang, Z., Shuai, J and Chen, N. (2006) 'Immunogenicity of formaldehyde and binary ethylenimine inactivated infectious bursal disease virus in broiler chicks.' *Journal of Zhejiang University Science.* **7** (8): 660-664.

Hale, J.E., Buter, J.P., Knierman, M.D and Becker, G.W. (2000) 'Increased Sensitivity of Tryptic Peptide Detection by MALDI-TOF Mass Spectrometry Is Achieved by Conversion of Lyseine to Homoarginine.' *Analytical Biochemistry.* **287** (1): 110-117.

Hardwicke, J., Ferguson, E.L., Moseley, R., Stephens, P., Thomas, D.W and Duncan, R. (2008) 'Dextrin-rhEGF conjugates as bioresponsive nanomedicines foe wound repair.' *Journal of Controlled Release.* **130**: 275-283.

Hart, I.R. (1979) 'The selection and characterization of an invasive variant of the B16 melanoma.' *American Journal of Pathology.* **97** (3): 587-600.

Hayiwara, Y., Komase, K., Chen, Z., Matsuo, K., Suzuki, Y., Aizawa, C., Kurata, T and Tamura, S. (1999) 'Mutants of Cholera toxin as an effective, safe adjuvant for nasal influenza vaccine.' *Vaccine.* **17** (22): 2918-2926.

Haygreen, E.A., Kaiser, P., Burgess, S.C and Davidson, T.F. (2006) 'In ovo DNA immunisation followed by a recombinant fowlpox boost is fully protective to challenge with virulent IBDV.' *Vaccine.* **24** (23): 4951-4961.

He, C., Hu, Y., Yin, L., Tang, C and Yin, C. (2010) 'Effects of particle size and surface charge on cellular uptake and biodistribution of polymeric nanoparticles.' *Biomaterials.* **31** (13): 3657-3666.

He, C.Q., Ma, L.Y., Wang, D., Li, G.R and Ding, N.Z. (2009) 'Homologous recombination is apparent in Infectious Bursal Disease Virus.' *Virology.* **384** (1): 51-58.

Hearnden, V., Sankar, V., Hull, K., Juras, D.V., Greenberg, M., Kerr, A.R., Lockhart, P.B., Patton, L.L., Porter, S and Thornhill, M.H. (2012) 'New developments and opportunities in oral mucosal drug delivery for local and systemic disease.' *Advanced Drug Delivery Reviews.* **64** (1); 16-28.

Heffernan, C., Nielsen, L., Thomson, K and Gunn, G. (2008) 'An exploration of the drivers to bio-security collective action among a sample of UK cattle and sheep farmers.' *Preventive Veterinary Medicine.* **87** (3-4): 358-378.

Heine, H.G., Haritou, M., Failla, P., Fahey, K and Azad, A. (1991) 'Sequence Analysis and Expression of the Host Protective Immunogen VP2 of a Variant Strain of Infectious Bursal Disease Virus Which Can Circumvent Vaccination With Standard Type I Strains.' *Journal of General Virology*. **72**: 1835-1843.

Herzog, C., Hartmann, K., Künzi, V., Kursteiner, O., Mischler, R., Lazarl, H and Gluck, R. (2009) 'Eleven years of Inflexal® V—a virosomal adjuvanted influenza vaccine.' *Vaccine* **27**: 4381-4387.

Hilgers, A., Conradi, R and Burton, P. (1990) 'Caco-2 cell monolayer as a model for drug transport across the intestinal mucosa.' *Pharmaceutical Research*. **7** (9): 902-910.

Hirel, P.H., Schmitter, M.J., Dessen, P., Fayat, G and Blanquet, S. (1989) 'Extent of N terminal methionine excision from Escherichia coli proteins is governed by the side-chain length of the penultimate amino acid.' *PNAS*. **86** (21): 8247-8251.

Hoffmann, F., Cornelius, M., Morell, J and Froba, M. (2006) 'Silica-Based Mesoporous OrganiC Inorganic Hybrid Materials.' *Angewante Chemie International Edition*. **45**: 3216-3251.

Holder, A.N., Ellis, A.L., Zou, J., Chen, N and Yang, J.J. (2009) 'Facilitating chromophore formation of engineered Ca²⁺⁺ binding green fluorescent proteins.' *Archives of Biochemistry and Biophysics*. **486** (1): 27-34.

Homhuana, A., Prakongpana, S., Poomvisesb, P., Maasc, R.A., Crommelind, D.J.A., Kerstene, G.F.A and Jiskoot, W. (2004) 'Virosome and ISCOM vaccines against Newcastle disease: preparation, characterization and immunogenicity.' *European Journal of Pharmaceutical Sciences*. **22** (5): 459-468.

Hutagalung, A and Novick, P. (2011) 'Role of Rab GTPases in Membrane Traffic and Cell Physiology.' *Physiological Reviews*. **91** (1): 119-149.

Iizuka, R., Yamagishi-Shirasoki, M and Funatsu, T. (2011) 'Kinetic study of de novo chromophore maturation of fluorescent proteins.' *Analytical Biochemistry*. **414** (2): 173-178.

Ivan, J., Nagy, N., Magyar, A., Kaaskovics, I and Meszaros, J. (2001) 'Functional restoration of the bursa of fabricius following in ovo infectious bursal disease vaccination.' *Veterinary Immunology and Immunopathology*. **79** (3-4): 235-248.

Jackwood, D.J and Sommer-Wagner, S.E. (2011) 'Amino acids contributing to antigenic drift in the Infectious Bursal Disease Birnavirus (IBDV).' *Virology*. **409** (1): 33-37.

Jain, S and Vyas, S. P. (2006) 'Mannosylated niosomes as adjuvant-carrier system for oral mucosal immunization.' *Journal of Liposome Research*. **16** (4): 331-345.

Jain R, Dey B, Dhar N, Rao V, Singh R, et al. (2008) Enhanced and Enduring Protection against Tuberculosis by Recombinant BCG-Ag85C and Its Association with Modulation of Cytokine Profile in Lung. *PLoS ONE* **3** (12): e3869.

Jenkins, H.E., Wodroffe, R and Donnelly, C. (2008) 'The effects of annual widespread badger culls on cattle tuberculosis following the cessation of culling.' *International Journal of Infectious Diseases*. **12** (5): 457-465.

Jertborn, M., Svennerholm, A.M and Holmgren, J. (1996) 'Intestinal and systemic immune responses in humans after oral immunisation with a bivalent B subunit 01/0139 whole cell cholera vaccine.' *Vaccine*. **14** (15): 1459-1465.

Johansen, F and Bronotzaeg, P. (2004) 'Transcriptional regulation of the mucosal IgA system.' *Trends in Immunology*. **25**: 150-157.

Jones, R. (2000) 'Oral vaccine delivery.' *Journal of Controlled Release*. **65** (1-2): 49-54.

Jurinke, C., Oeth, P and Boom, D. (2006) 'MALDI-TOF Mass Spectrometry.' **26** (2): 147-163.

Karaca, K., Sharma, J.M., Winslow, B.J., Junker, D.E., Reddy, S., Cochran, M and McMillen, J. (1998) 'Recombinant fowlpox viruses coexpressing chicken type I IFN and Newcastle disease virus HN and F genes: Influence of IFN on protective efficacy and humoral responses of chickens following in ovo or post hatch administration of recombinant viruses.' *Vaccine*. **16** (16): 1496-1503.

Keller, A., Nesvizhskii, A.I., Kolker, E and Aebersold, R. (2002) 'Empirical Statistical Model to Estimate the Accuracy of Peptide Identification Made by MS/MS and database Search.' *Analytical Chemistry*. **74** (20): 5383-5392.

Kelly, S.M., Jess, T.J and Price, N.C. (2005) 'How to study proteins by circular dichroism.' *Biochimica et Biophysica Acta (BBA) - Proteins & Proteomics*. **1751** (2): 119-139.

Kesik, M., Saczynska, K., Szewczyk, B and Plucienniczak, A. (2004) 'Inclusion bodies from recombinant bacteria as a novel system for delivery of vaccine antigen by the oral route.' *Immunology Letters*. **91** (2-3): 197-204.

Kharlamova, A., Prentice, B., Huang, T and McLuckey, S. (2010) 'Electrospray Droplet Exposure to Gaseous Acids for the Manipulation of Protein Charge State Distributions.' *Analytical Chemistry*. **82** (17): 7422-7429.

Khatri, M., Palmquist, J.M., Cha, R.M and Sharma, J.M. (2008) 'Infection and activation of bursal macrophages by virulent infectious bursal disease virus.' *Virus Research*. **113**: 44-50.

Kim, J.H., Dahms, H.U., Rhee, J.S., Lee, Y.M., Lee, J., Han, K.N and Lee, J.S. (2010) 'Expression profiles of seven glutathione S-transferase (GST) genes in cadmium-exposed river pufferfish (*Takifugu obscurus*).' *Comparative Biochemistry and Physiology Part C: Toxicology and Pharmacology*. **151** (1): 99-106.

Kobayashi, S and Konishi, Y. (2008) 'Transepithelial transport of flavanone in intestinal Caco-2 cell monolayers.' *Biochemical and Biophysical Research Communications*. **368** (1): 23-29.

Kong, S.D., Sartor, M., Hu, C.M., Zhang, W., Zhang, L., Jin, S. (2012) 'Magnetic field activated lipid-polymer hybrid nanoparticles for stimuli-responsive drug release.' *Acta Biomaterialia*. In Press.

Konthura, Z., Hustb, M and Dübelb, S. (2005) 'Beyond the Identification of Transcribed Sequences: Functional, Expression and Evolutionary Analysis.' *Gene*. **364**: 19-29.

Kurmanova, A., Llorente, A., Poleskaya, A., Garred, O., Olsnes, S., Kozlov, J and Sandvig, K. (2007) 'Structural requirements for furin induced cleavage and activation of Shiga toxin.' *Biochemical and Biophysical Research Communications*. **357** (1): 144-149.

Kwon, H.M and Kim S.J. (2004) 'Sequence analysis of the variable VP2 gene of infectious bursal disease virus passaged in Vero cells.' *Virus Genes*. **28**: 285-291.

Kyle, D. (2006) 'Delivery of disease control in aquaculture and agriculture using microbes containing bioactive proteins.' Patent Applications Publication. US2006/0263820A1.

Lammers, A., Wieland, W.H., Kruijt, L., Jansma, A., Straetemans, T., Schats, A., Hartog, G and Parmentier, H.K. (2010) 'Successive immunoglobulin and cytokine expression in the small intestine of juvenile chicken.' *Developmental and Comparative Immunology*. **34** (12): 1254-1262.

Landi, S. (2000) 'Mammalian class theta GST and differential susceptibility to carcinogens: a review.' *Mutation research / Reviews in Mutation Research*. **463** (3): 247-283.

Leelawongtawon, R., Somroop, S., Chaisri, U., Tongtawe, P., Chongsanguan, M., Kalambaheti, T., Tapchaisri, P., Pichyangkul, S., Sakolvaree, Y and Kurazono, H. (2003) 'CpG DNA, liposome and refined antigen oral cholera vaccine.' *Asian Pacific Journal Allergy Immunology*. **21** (4): 231.

Lemoine, D.; Deschuyteneer, M.; Hogge, F.; Pr at, V. (1999) 'Intranasal immunization against influenza virus using polymeric particles.' *J. Biomaterial Sci. Polym. Ed.* **10** (8): 805-825.

Lencer, W.I., Moe, S., Rufo, P.A and Madara, J.L. (1995) 'Transcytosis of Cholera toxin subunits across model human intestinal epithelia.' *Proceedings of the National Academy of Sciences of the United States of America*. **92**: 10094-10098.

Levy, A.M., Davidson, I., Burgess, S.C and Heller, E.D. (2003) 'Major histocompatibility complex class I is downregulated in Marek's disease virus infected chicken embryo fibroblasts and corrected by chicken interferon.' *Comparative Immunology, Microbiology and Infectious Diseases*. **26** (3): 189-198.

Lencer, W., Moe, S., Rufo, P and Madara, J. (1995) 'Transcytosis of cholera toxin subunits across model human intestinal epithelia.' *Proceedings of National Academy of Sciences*. **92**: 10094-10098.

Lencer, W and Saslowsky, D. (2005) 'Raft trafficking of AB₅ subunit bacterial toxins.' *Biochimica et Biophysica Acta (BBA) – Molecular Cell Research*. **1746** (3): 314-321.

Li, F., Lizio, R., Meier, C., Petereit, H.U., Blakey, P and Basit, A. (2009) 'A novel concept in enteric coating: A double-coated system providing rapid drug release in the proximal small intestine.' *Journal of Controlled Release*. **133** (2): 119-124.

Li, L., Fang, W., Li, J., Fang, L., Huang, Y and Yu, L. (2006) 'Oral DNA vaccination with the polyprotein gene of infectious bursal disease virus (IBDV) delivered by attenuated Salmonella elicits protective immune responses in chickens.' *Vaccine* **24** (33-34) 5919-5927.

Li, Z., Chenb, J., Sunb, W and Xu, Y. (2010) 'Investigation of archaeosomes as carriers for oral delivery of peptides.' *Biochemical and Biophysical Research Communications*. **394** (2): 412-417.

Li, Z., Zhang, L., Sun, W., Ding, Q., Hou, Y and Xu, Y. (2011) 'Archaeosomes with encapsulated antigens for oral vaccine delivery.' *Vaccine*. **29** (32): 5260-5266.

Liljequist, S., Stahl, S., Andreoni, C., Binz, H., Uhlen, M and Murby, M. (1997) 'Fusions to the Cholera toxin B subunit influence on pentamerization and GM1 binding.' *Journal of Immunological Methods*. **210** (2): 125-135.

Li, M and Vakharia, V.N. (2004) 'VP1 protein of infectious bursal disease virus modulates the virulence in vivo.' *Virology*. **330** (1): 62-73.

Loving, C.L., Vincent, A.L., Pena, L and Perez, D.R. (2012) 'Heightened adaptive immune responses following vaccinations with a temperature sensitive, live attenuated influenza virus compared to adjuvanted, whole-inactivated virus in pigs.' *Vaccine*. **30** (40): 5830-5838.

Lubben, I.M., van Oudorp, F., Hengeveld, M.R., Onderwater, J.J.M., Koerten, H.K., Verhoef, J.C., Borchard, G and Junginger, H.E. (2002) 'Transport of Chitosan Microparticles for Mucosal Vaccine Delivery in a Human Intestinal M-cell Model.' *Journal of Drug Targeting*. **10** (6): 449-456.

Mahmood, M.S., Hussain, I., Siddique, M., Aktar, M and Ali, S. (2007) 'DNA vaccination with VP2 gene of very virulent infectious bursal disease virus (vvIBDV) delivered by transgenic *E.Coli* DH5a given orally confers protective immune responses in chickens.' *Vaccine*. **25** (44): 7629-7635.

Majamaa, H and Isolauri, E. (1995) 'Evaluation of the gut mucosal barrier: Evidence for increased antigen transfer in children with atopic eczema.' *Journal of Allergy and Clinical Immunology*. **97** (4): 985-990.

Malyukova, I., Murray, K., Zhu, C., Boedeker, E., Kane, A., Patterson, K., Peterson, J., Donowitz, M and Kovbasnjuk, O. (2009) 'Macropinocytosis in Shiga toxin 1 uptake by human intestinal epithelial cells and transcellular transcytosis.' *American Journal of Gastrointestinal and Liver Physiology*. **296**: 78-92.

Mann, J. F. S., Scales, H. E., Shakir, E., Alexander, J., Carter, K. C., Mullen, A. B and Ferro, V. A. (2006) 'Oral delivery of tetanus toxoid using vesicles containing bile salts (bilosomes) induces significant systemic and mucosal immunity. *Methods*. **38** (2): 90-95.

Manford, A.G., Stefan, C.J., Yuan, H.L., MacGurn, J.A and Emr, S.D. (2012) 'ER-to-Plasma Membrane Tethering Proteins Regulate Cell Signaling and ER Morphology.' *Developmental Cell*. **23** (6): 1129-1140.

Mann, J.F.S., Scales, H.E., Shakir, E., Alexander, J., Carter, K., Mullen, A and Ferro, J. (2006) 'Oral delivery of tetanus toxoid using vesicles containing bile salts (bilosomes) induces significant systemic and mucosal immunity.' *Methods*. **38** (2): 90-95.

Mann, J.F.S., Shakir, E., Carter, K.C., Mullen, A.B., Alexander, J., and Ferro, V.A. (2009) 'Lipid vesicle size of an oral influenza vaccine delivery vehicle influences the Th1 / Th2 bias in the immune response and protection against infection.' *Vaccine*. **27** (27): 3643-3649.

Mann, M & Jensen, O. (2003) 'Proteomic analysis of post-translational modifications.' *Nature Biotechnology* **21**: 255 – 261.

Marone, G., Galli, S.J and Kitamura, Y. (2002) 'Probing the roles of mast cells and basophils in natural and acquired immunity physiology and disease.' *Trends in Immunology*. **23** (9): 425-427.

Martins, S., Sarmento, B., Souto, E.B., Ferreira, D.C. (2007) 'Insulin-loaded alginate microspheres for oral delivery – Effect of polysaccharide reinforcement on physicochemical properties and release profile.' *Carbohydrate Polymers* **69** (4):725-731.

Martinez-Torrecuadrada, J.L., Saubi, N., Pages-Monte, A., Caston, J.R., Espuna, E and Casai, J.I. (2003) 'Structure-dependant efficiency of Infectious Bursal Disease Virus (IBDV) recombinant vaccines.' *Vaccine*. **21** (23): 3342-3350.

- Matveev, S., Li, X., Everson, W and Smart, E.J. (2001) 'The role of caveolae and caveolin in vesicle dependent and vesicle independent trafficking.' *Advanced Drug Delivery Reviews*. **49** (3): 237-250.
- Maver, V., Goder, A., Bele, M., Planinsek, D., Gaberscek, M., Srcic, S and Jamnik, J. (2007) 'Novel hybrid silica xerogels for stabilisation and controlled release of drug.' *International Journal of Pharmaceutics*. **330** (1-2): 164-174.
- McCormack, W.T., Tjoelker, L.W., Barth, C.F., Carlson, L.M., Petrynick, B., Humphries, E.H and Thompson, C.B. (1989) 'Selection for B cells with productive IgL gene rearrangements occurs in the bursa of fabricius during chicken embryonic development.' *Genes and Development*. **3**: 838-847
- McGhee, J.R., Mestecky, J., Dertzbaugh, M.T., Eldridge, J.H., Hirasawa, M and Kiyono, H. (1992) 'The mucosal immune system – from fundamental concepts to vaccine development.' *Vaccine*. **10** (2): 75-88.
- Medina, E and Guzman, C.A. (2001) 'Use of live bacterial vaccine vectors for antigen delivery: potential limitations.' *Vaccine*. **19** (13-14): 1573-1580.
- Mendonça, R.Z., Arrózioa, S.J., Antoniazib, M.M., Ferreira, J and Pereiraa, C.A. 'Metabolic active-high density VERO cell cultures on microcarriers following apoptosis prevention by galactose/glutamine feeding.' *Journal of Biotechnology*. **97** (1): 13-22.
- Merritt, E.A and Hal, W.G. (1995) 'AB5 toxins.' *Current Opinion in Structural Biology*. **5** (2): 165-171.
- Messenger, G.A. (2010) 'Step-By-Step Crop Biopsy in Birds.' *Journal of Exotic Pet Medicine*. **19** (1): 87-91.
- Mestecky, J., Moldoveanu, Z., Novak, M., Huang, W-Q., Gilley, R.M., Staas, J.K., Schafer, D and Campons, R.W. (1994) 'Biodegradable microspheres for the delivery of oral vaccines.' *Journal of Controlled Release*. **28** (1-3): 131-141.
- Molina, A., Hervás-Stubbs, S., Daniell, H., Mingo-Castel, A.M and Veramendi, J. (2004) 'High-yield expression of a viral peptide animal vaccine in transgenic tobacco chloroplasts.' *Plant Biotechnology Journal*. **2** (2): 141–153.
- Minato, S., Iwanaga, K., Kakemi, M., Yamashita, S and Oku, N. (2003) 'Application of polyethyleneglycol (PEG) – modified liposomes for oral vaccine: effect of lipid dose on systemic and mucosal immunity.' *Journal of Controlled Release*. **89** (2): 189-197.
- Muir, W.I., Bryden, W.L and Husband, A.J. (2000) 'Immunity, vaccination and the avian intestinal tract.' *Developmental and Comparative Immunology*. **24** (2-3): 325-342.
- Muller, H., Islam, M.R and Raue, R. (2003) 'Research on infectious bursal disease – the past, the present and the future.' *Veterinary Microbiology*. **97** (1-2): 153-165.
- Nagamoto, T., Hattori, Y., Takayama, K and Maitani, Y. (2004) 'Novel Chitosan particles and chitosan-coated emulsions inducing immune response via intranasal vaccine delivery.' *Pharm. Res*. **21**(4), 671-674.
- Nahapetion, A., Thomas, J and Thilly, W. (1986) 'Optimization of environment for high density Vero cell culture: Effect of dissolved oxygen and nutrient supply on cell growth and changes in metabolites.' *Journal of Cell Science*. **81**: 65-103.

Neutra, M.R., Frey, A and Kraehenbuhl, J-P. (1996) 'Epithelial M cells: Gateways for mucosal infection and immunisation.' *Cell*. **86** (3): 345-348.

Newell, D.G., Koopmans, M., Verhoef, L., Dilizer, E., Aidara-Kane, A., Sprong, H., Opsteegh, M., Langelaar, M., Threfall, J., Scheutz, F., van der Giessen, J and Kruse, H. (2010) 'Food-Bourne diseases: The challenges of 20 years ago still persist while new ones continue to emerge.' *International Journal of Food Microbiology*. 139: s3-s15.

Nikolic, D and Piguët, V. (2010) 'Vaccines and Microbicides Preventing HIV-1, HSV-2 and HPV Mucosal Transmission.' *Journal of Investigative Dermatology*. **130**: 352-361.

Niemann, H., Petoukhov, M., Hartlein, M., Moulin, M., Gherardi, E., Timmins, P., Heinz, D and Svergun, D. (2008) 'X-ray and Neutron Small-Angle Scattering Analysis of the Complex Formed by the Met Receptor and the *Listeria monocytogenes* Invasion Protein InIB.' *Journal of Molecular Biology*. **377** (2): 489-500.

Ohmura, M., Yamamoto, M., Tamiyama-Miyaji, C., Yuki, Y., Takeda, T and Kiyano, H. (2005) 'Nontoxic Shiga Toxin Derivatives from *Escherichia coli* Possess Adjuvant Activity for the Augmentation of Antigen-Specific Immune Responses via Dendritic Cell Activation.' *Infection and Immunity*. **73** (7): 4088-4097.

Ohmura-Hoshino, M., Yamamoto, M., Yuki, Y., Takeda, Y and Kiyano, H. (2004) 'Non toxic Stx derivatives from *Escherichia coli* possess adjuvant activity for mucosal immunity.' *Vaccine*. **22** (27-28): 3751-3761.

Olsnes, S. (2004) 'The history of ricin, abrin and related toxins.' *Toxicon*. **44** (4): 361-370.

Oshop, G.L., Elankumaron, S., Vakharia, V.N and Heckert, R.A. (2003) 'In ovo delivery of DNA to the avian embryo.' *Vaccine*. **21**: 1275-1287.

Otzen, D.E. (2002) 'Protein Unfolding in Detergents: Effect of Micelle Structure, Ionic Strength, pH and Temperature.' *Biophysical Journal*. **83** (4): 2219-2230.

Pajot, P. (1976) 'Fluorescence of Proteins in 6-M Guanidine Hydrochloride A Method for the Quantitative Determination of Tryptophan.' *European Journal of Biochemistry*. **63** (1): 263-269.

Panayiotou, M and Freitag, R. (2005) 'Influence of the synthesis conditions and ionic additives on the swelling behaviour of thermo-responsive polyalkylacrylamide hydrogels.' *Polymer*. **46** (18): 6777-6785.

Pande, A.H., Scaglione, P., Taylor, M., Nemeç, K.N., Tuthill, S., Moe, D., Holmes, R.K., Tatulian, S.A and Teter, K. (2007) 'Conformational Instability of the Cholera Toxin A₁ Polypeptide.' *Journal of Molecular Biology*. **374** (4): 1114-1128.

Patel, G.B., Agnew, B., Deschatelets, L., Fleming, L and Sprott, G. (2000) 'In vitro assessment of archaeosome stability for developing oral delivery systems.' *International Journal of Pharmaceutics*. **194**: 39-49.

Patel, G. B., Zhou, H., Ponce, A and Chen, W. (2007) 'Mucosal and systemic immune responses by intranasal immunization using archaeal lipid-adjuvanted vaccines.' *Vaccine* **25** (51): 8622-8636.

- Peek, L.J., Middaugh, C.R and Berkland, C. (2008) 'Nanotechnology in vaccine delivery.' *Advanced Drug Delivery Reviews*. **60** (8): 915-928.
- Pina, D.G and Johannes, L. (2005) 'Cholera and Shiga toxin B-subunits: thermodynamic and structural considerations for function and biomedical applications.' *Toxicon*. **45** (4): 389-393.
- Pockel, A (1891) 'Surface tension.' *Nature*. **43**: 437-439.
- Pollok, B.A and Heim, R. (1999) 'Using GFP in FRET-based applications.' *Trends in Cell Biology*. **9** (2): 57-60.
- Puu, G., Artursson, E., Gustafson, I., Lundstrom, M and Jass, J. (2000) 'Distribution and stability of membrane protein in lipid membranes on solid supports.' *Biosensors and Bioelectronics*. **15** (1-2): 31-41.
- Quere, P and Girard, F. (1999) 'Systemic adjuvant effect of cholera toxin in the chicken.' *Veterinary Immunology and Immunopathology*. **70** (1-2): 135-141.
- Rautenschlein, S and Haase, C. (2005) 'Differences in the immunopathogenesis of infectious bursal disease virus (IBDV) following in ovo and post hatch vaccination of chickens.' *Veterinary Immunology and Immunopathology*. **106** (1-2): 139-150.
- Rautenschlein, S., Samson-Himmelstjerna, G and Hasse, C. (2007) 'A comparison of immune responses to infection with virulent infectious bursal disease virus (IBDV) between specific pathogen-free chickens at 12 and 28 days of age.' *Veterinary Immunology and Immunopathology*. **115** (3-4): 251-260.
- Rautenschlein, S., Yeh, H-Y., Njenga, M.K and Sharma, J.M. (2002) 'Role of intrabursal T cells in infectious bursal disease virus (IBDV) infection: T cells promote viral clearance but delay follicular recovery.' *Archives of Virology*. **147** (2): 285-304.
- Rezaei, M. A. (2006) 'Preparation and evaluation of chitosan nanoparticles containing diphtheria toxoid as new carriers for nasal vaccine delivery in mice.' *Arch. Razi Inst*. **61**:13-25.
- Richardson, S.C.W., Kolbeb, H.V.J and Duncan, R. (1999) 'Potential of low molecular mass chitosan as a DNA delivery system: biocompatibility, body distribution and ability to complex and protect DNA.' *International Journal of Pharmaceutics*. **178** (2): 231-243.
- Rigaut, G., Sheuchenko, A., Rutz, B., Wilm, M., Mann, M and Seraphin, B. (1999) 'A generic protein purification method for protein complex characterisation and proteome exploration.' *Nature Biotechnology*. **17**: 1030-1032.
- Rigby, S.P., Fairhead, M and van der Walle, C.F. (2008) 'Engineering Silica Particles as Oral Drug Delivery Vehicles.' *Current Pharmaceutical Design*. **14** (18): 1821-1831.
- Rodenberg, J., Sharma, J.M., Belzer, S.W., Nardgren, R.M and Naqi, S. (1994) 'Flow Cytometric Analysis of B Cell and T Cell Subpopulations in Specific Pathogen-Free Chickens Infected with Infectious Bursal Disease Virus.' *Avian Diseases*. **38**: 16-21.
- Rodriguez-Lecompte, J.C., Nino-Fong, R., Lopez, A., Markham, R.J.F and Kilenge, F.S.B. (2005) 'Infectious bursal disease virus (IBDV) induces apoptosis in chicken B cells.' *Comparative Immunology and Infectious Diseases*. **28** (4): 321-337.
- Sadek, S and Ghandehari, H. (2012) 'Transepithelial transport and toxicity of PAMAM dendrimers: Implications for oral drug delivery.' *Advanced Drug Delivery Reviews*. **64** (6): 571-588.

- Sala, F., Rigano, M., Barbante, A., Basso, B., Walmsley, M and Castiglione, S. (2003) 'Vaccine antigen production in transgenic plants: strategies, gene constructs and perspectives.' *Vaccine*. **21** (7-8): 803-808.
- Sant, S., Tao, S.L., Fisher, O.Z., Xu, Q., Peppas, N.A and Khademhosseini, A. (2012) 'Microfabrication technologies for oral drug delivery.' *Advanced Drug Delivery Reviews*. **64** (6): 496-507.
- Sameti, M., Bohr, G., Kumar, M., Kneuer, C., Bowsky, V., Nacken, M., Schmidt, H and Lehr, C.M. (2003) 'Stabilization by freeze-drying of catatonically modified silica nanoparticles for gene delivery.' *International Journal of Pharmaceutics*. **266** (1-2): 51-60.
- Sambury, Y., Angelis, I., Ranaldi, G., Scarino, M., Stammati, A and Zucco, F. (2005) 'The Caco-2 cell line as a model of the intestinal barrier: influence of cell and culture-related factors on Caco-2 cell functional characteristics.' *Cell Biology and Toxicology*. **21** (1): 1-26.
- Sandvig, K. (2001) 'Shiga toxins.' *Toxicon*. **39** (11): 1629-1635.
- Sandvig, K., Bergan, J., Dyve, A.B., Skotland, T and Torgersen, M.L. (2010) 'Endocytosis and retrograde transport of Shiga toxin.' *Toxicon*. **56** (7): 1181-1185.
- Sandvig, K and Deurs, B. (2002) 'Transport of protein toxins into cells: pathways used by ricin, cholera toxin and Shiga toxin.' *FEBS Letters*. **529** (1): 49-53.
- Sandvig, K and Deurs, B. (2005) 'Delivery into cells: lessons learned from plant and bacterial toxins.' *Gene Therapy*. **12**: 865-872.
- Schatter, A (2005) 'Consequence or coincidence? The occurrence, pathogenesis and significance of autoimmune manifestations after viral vaccines.' *Vaccines*. **23** (30): 3876-3886.
- Scheich, C., Sievert, V and Bussow, K. (2003) 'An automated method for high throughput protein purification applied to a comparison of His-tag and GST-tag affinity chromatography.' *BMC Biotechnology*. **3**:12.
- Seas, C and Gotuzzo, E. (1996) 'Cholera: Overview of epidemiologic, therapeutic and preventative issues learned from recent epidemics.' *International Journal of Infectious Diseases*. **1** (1): 37-46.
- See, Y.P., Olley, P.M and Jackowski, G. (1985) 'The effects of high salt concentrations in the samples on molecular weight determination in sodium dodecyl sulfate polyacrylamide gel electrophoresis.' *Electrophoresis*. **6** (8): 382-387.
- Senior, K. (2001) 'Biosomes: the answer to oral vaccine delivery?' *Drug Discovery Today*. **6** (20): 1031-1032.
- Schägger, H and Jagow, G. (1987) 'Tricine-sodium dodecyl sulfate-polyacrylamide gel electrophoresis for the separation of proteins in the range from 1 to 100 kDa.' *Analytical Biochemistry*. **166** (2): 368-379.
- Schmitt, J., Hess, H and Stunnenberg, H. (1993) 'Affinity purification of histidine-tagged proteins.' *Molecular Biology Reports*. **18**: 223-230.
- Sharma, J.M., Kim, I.J., Rautenschlein, S and Yeh, H.Y. (2000) 'Infectious bursal disease virus of chickens: pathogenesis and immunosuppression.' *Developmental and Comparative Immunology*. **24** (2-3): 223-235.

Shimizu, T., Sato, T., Kawakami, S., Ohta, T., Nada, M and Homabata, T. (2007) 'Receptor affinity, stability and binding mode of Shiga toxins are determinants of toxicity.' *Microbial Pathogenesis*. **43** (2-3): 88-95.

Siegall, C.B., Gawlak, S.L., Chace, D., Wolff, E.A., Mixan, B and Marquardt, H. (1994) 'Characterisation of Ribosome-Inactivating Proteins Isolated from *Bryonia dioica* and Their Utility as Carcinoma-Reactive Immunoconjugates.' *Bioconjugate Chemistry*. **5** (5): 423-429.

Singh, M., Silva, E., Schulze, S., Sinclair, D.A.R., Fitzpatrick, K.A and Honda, B.M. (2000) 'Cloning and characterization of a new theta-class glutathione S-transferase (GST) gene, *gst-3* from *Drosophila melanogaster*.' *Gene*. **247** (1-2): 167-173.

Singh, P., Prabakaran, D., Jain, S., Mishra, V., Jaganathan, K.S and Vyas, S.P. (2004) 'Cholera toxin B subunit conjugated bile salt stabilised vesicles (bilosomes) for oral immunisation.' *International Journal of Pharmaceutics*. **278** (2): 379-390.

Singh, M and O'Hagan, D. (1998) 'The preparation and characterization of polymeric antigen delivery systems for oral administration.' *Advanced Drug Delivery Reviews*. **34** (2-3): 285-304.

Simon, J.K., Maciel, M., Weld, E.D., Wahid, R., Pasetti, M.F., Picking, W.L., Kotloff, K.L., Levine, M.M and Sztein, M.B. (2011) 'Antigen-specific IgA B memory cell responses to *Shigella* antigens elicited in volunteers immunized with live attenuated *Shigella flexneri* 2a oral vaccine candidates.' *Clinical Immunology*. **139** (2): 185-192.

Skandland, S.S., Walchli, S and Sandvig, K. (2009) 'b-arrestins attenuate p38 mediated endosome to Golgi transport.' *Cellular Microbiology*. **11** (5): 796-807.

Smil, V. (2002) 'Worldwide transformation of diets, burdens of meat production and opportunities for novel food proteins.' *Enzyme and Microbial Technology*. **30** (3): 305-311.

Smith, J M., Smith, N.H., O'Rourke, M and Spratt, B G. (1993) 'How clonal are bacteria?' *PNAS*. **90** (10) 4384-4388.

Smith, P.B and Johnson, K.S. (1988) 'Single-step purification of polypeptides expressed in *Escherichia coli* as fusions with glutathione S-transferase.' *Gene*. **67** (1): 31-40.

Snyder, D.B., Vakharia, V.N and Savage, P.K. (1992) 'Naturally occurring-neutralising monoclonal antibody escape variants define the epidemiology of infectious bursal disease virus in the United States.' *Archives of Virology*. **127** (1-4): 89-101.

Song, S.W., Hidajat, K and Kawi, S. (2007) 'pH-controllable drug release using hydrogel encapsulated mesoporous silica.' *Chemical Communications*. (42): 4396-4398.

Sonna, L.A., Fujita, J., Gaffin, S.L and Lilly, C.M. (2002) 'Invited Review: Effects of heat and cold stress on mammalian gene expression.' *Journal of Applied Physiology*. **92** (4): 1725-1742.

Sørensen, H.P and Mortensen, K.K. (2005) 'Advanced genetic strategies for recombinant protein expression in *Escherichia coli*.' *Journal of Biotechnology*. **115** (2): 113-128.

Sorensen, J.G., Kristensen, T.N and Loeschake, V. (2003) 'The evolutionary and ecological role of heat shock proteins.' *Ecology Letters*. **6** (11): 1025-1037.

Shah, D and Shen, W, (2000) 'Transcellular delivery of an insulin-transferrin conjugate in enterocyte-like Caco-2 cells.' *Journal of Pharmaceutical Sciences*. **85** (12): 1306-1311.

- Spilberg, B., Llorente, A and Sandvig, K. (2007) 'Polyunsaturated fatty acids regulate Shiga toxin transport.' *Biochemical and Biophysical Research Communications*. **364** (2): 283-288.
- Stanley, A. C., Buxton, D., Innes, E. A and Huntley, J. F. (2004) 'Intranasal immunisation with *Toxoplasma gondii* tachyzoite antigen encapsulated into PLG microspheres induces humoral and cell-mediated immunity in sheep. *Vaccine* **22** (29-30): 3929-3941.
- Steele, J.H. (2008) 'Veterinary public health. Past success, new opportunities.' *Preventive Veterinary Medicine*. **86** (3-4): 224-243.
- Steffansen, B., Nielsen, C., Brodin, B., Eriksson, A.H., Andersen, R and Frokjaer, S. (2004) 'Intestinal solute carriers: an overview of trends and strategies for improving oral drug absorption.' *European Journal of Pharmaceutical Sciences*. **21** (1): 3-16.
- Stegmann, T., Kamphuisa, T., Meijerhofa, T., Goudb, E., de Haana, A and Wilschuta, J. (2010) 'Lipopeptide-adjuvanted respiratory syncytial virus virosomes: A safe and immunogenic non-replicating vaccine formulation.' *Vaccine* **28** (34): 5543-5550.
- Sternbach, G. (2003) 'The history of anthrax.' *The Journal of Emergency Medicine*. **24** (4): 463-467.
- Steri, D., Monduzzi, M and Salis, A. (2013) 'Ionic strength affects lysozyme absorption and release from SBA-15 mesoporous silica.' *Microporous and Mesoporous Materials*. **170**: 164-172.
- Stokes, C.R and Bailey, M. (1996) 'Antigen handling in the gastrointestinal lamina propria.' *Journal of Biotechnology*. **44** (1-3): 5-11.
- Strober, W. (2001) 'Trypan blue exclusion test of cell viability.' *Current Protocols in Immunology*. Doi: 10.1002/0471142735.
- Suckow, M.A., Keren, O.F., Brown, J.E and Keusch, G.T. (1994) 'Stimulation of gastrointestinal antibody to Shiga toxin by orogastric immunisation in mice.' *Immunology and Cell Biology*. **72**: 69-74.
- Sullivan, S.M. , Doukas, J., Hartikka, J., Smith, L and Rolland, A. (2010) 'Vaxfectin: a versatile adjuvant for plasmid DNA- and protein-based vaccines.' *Expert Opinion in Drug Delivery*. **7**: 1433-1446.
- Swick, A.G., Janicot, M., Cheneval-Kastelic, T., McLenithan, J.C and Land, M.D. (1992) 'Promotor-cDNA-directed heterologous protein expression in *Xenopus laevis* oocytes.' *Proceedings of the National Academy of Sciences*. **89** (5): 1812-1816.
- Tafaghodi, M., Jaafari, M. R and Sajadi Tabassi, S. A. (2006) 'Nasal immunization studies using liposomes loaded with tetanus toxoid and CpG-ODN.' *Eur. J. Pharm. Biopharm.* **64** (2): 138-145.
- Tang, F., Li, L and Chen, D. (2012) 'Mesoporous Silica Nanoparticles: Synthesis, Biocompatibility and Drug Delivery.' *Advanced Materials*. **24**: 1504-1534.
- Tang, H., Guo, J., Sun, Y., Chang, B., Ren, Q and Yang, W. (2011) 'Facile synthesis of pH sensitive polymer-coated mesoporous silica nanoparticles and their application in drug delivery.' *International Journal of Pharmaceutics*. **421** (2); 388-396.
- Thurikui, R., Grimsley, G., Scholtz, M and Pace, C. (2006) 'Hydrogen Bonding Markedly Reduces the pK of Buried Carboxyl Groups in Proteins.' *Journal of Molecular Biology*. **362** (3): 594-604.

Timasheff, S.N. (1993) 'The Control of Protein Stability and Association by Weak Interactions with Water: How Do Solvents Affect These Processes?' *Annual Review of Biophysics and Biomolecular Structure*. **22**: 67-97.

Tseng, L. P., Liang, H. J., Deng, M. C., Lee, K. M., Pan, R. N., Yang, J. C., Huang, Y. Y and Liu, D. Z. (2009) 'The influence of liposomal adjuvant on intranasal vaccination of chickens against Newcastle disease.' *Veterinary Journal*. **185** (2): 204-210.

Tsukita, S., Furuse, M & Itoh, I (2001) 'Multifunctional strands in tight junctions.' *Nature Reviews Molecular Cell Biology*. **2**: 285-293

Tuma, P and Hubbard, A. (2003) 'Transcytosis: crossing cellular barriers.' *Physiology Reviews*. **83**: 871-932.

Turner, J., Rill, B., Carlson, S., Carnes, D., Kerner, R., Mrsny, R and Madara, J. (1997) 'Physiological regulation of epithelial tight junctions is associated with myosin light-chain phosphorylation.' **273** (4): 1378-1385.

Urbanowski, J.L and Piper, R.C. (1999) 'The Iron transporter Fth1p forms a complex with the fet5 iron oxidase and resides on the vacuolar membrane.' *Journal of Biological Chemistry*. **274** (53): 38061-70.

Valet-Regi, M., Balas, F and Arcos, D. (2007) 'Mesoporous Materials for Drug Delivery.' *Angewandte Chemie International*. **46**: 7548-7558.

Vallet-Regi, M and Ruiz-Hernandez, E. (2011) 'Bioceramics: From Bone Regeneration to Cancer Nanomedicine.' *Advanced materials*. **23** : 5177-5218.

Van der Zijpp., A.J. (1999) 'Animal food production: the perspective of human consumption, production, trade and disease control.' *Livestock Production Science*. **59** (2-3): 199-206.

Van Meerloo, J., Kaspers, G and Cloos, J. (2011) 'Cell Sensitivity Assays: The MTT Assay.' *Cancer Cell Culture*. **731**: 237-245.

Vermeulen, B., Backer, P and Remon, J.P. (2002) 'Drug administration to poultry.' *Advanced Drug Delivery reviews*. **54** (6): 795-803.

Vervelde, L., Janse, E.M., Vermeulen, A.N and Jeurissen, S.H.M. (1998) 'Induction of a local and systemic immune response using cholera toxin as vehicle to deliver antigen in the lamina propria of the chicken.' *Veterinary Immunology and Immunopathology*. **62**: 261-272.

Vijayaraghavan, M., Stolnik, S., Howdle, SM., and Illum, L. (2012) 'Suitability of polymer materials for production of pulmonary microparticles using a PGSS supercritical fluid technique: Thermodynamic behaviour of fatty acids, PEGs and PEG-fatty acids.' *International Journal of Pharmaceutics*. **438**: 225-231.

Viljanena, J., Larssona, J and Broob, K.S. (2008) 'Orthogonal protein purification—Expanding the repertoire of GST fusion systems.' *Protein Expression and Purification*. **57** (1): 17-26.

Vinderola, C.E., Costa, G., Regenhardt, S and Reinheimer, J. (2002) 'Influence of compounds associated with fermented dairy products of the growth of lactic acid starter and probiotic bacteria.' *International Dairy Journal*. **12** (7): 579-589.

Vissera, N.V., Hinka, M.A., Borsta, J.W., van der Krogt, G.N.M and, Vissera, A. (2002) 'Circular dichroism spectroscopy of fluorescent proteins.' *FEBS Letters*. **521** (1-3): 31-35.

Voityuk A. A., Kummer A. D., Michel-Beyerle M. E., Rösch N. (2001) 'Absorption spectra of the GFP chromophore in solution: comparison of theoretical and experimental results.' *Chemical Physics* **269**: 83-91.

Wang, D., Xiang, J., She, R., Liu, L., Zhang, Y., Luo, D., Li, W., Hu, Y., Wang, Y., Zhang, Q and Sun, Q. (2008) 'Mast cell mediated inflammatory response in chickens after infection with very virulent infectious bursal disease virus.' *Veterinary Immunology and Immunopathology*. **124** (1-2): 19-28.

Wang, T., Jiang, H., Zhao, Q., Wang, S., Zou, M and Cheng, G. (2012) 'Enhanced mucosal and systemic immune responses obtained by porous silica nanoparticles used as an oral vaccine adjuvant: Effect of silica architecture on immunological properties.' *International Journal of Pharmaceutics*. **436** (1-2): 351-358.

Wang, T., Ming, Z., Xiaochun, W and Hung, W. (2011) 'Rab7: Role of its protein interaction cascades in endo-lysosomal traffic.' *Cellular Signalling*. **23** (3): 516-521.

Wang, W. (1999) 'Instability, stabilisation, and formulation of liquid protein pharmaceuticals.' *International Journal of Pharmaceutics*. **185** (2): 129-188.

Wang, Y., Suna, Z., Qiu, X., Lic, Y., Qina, J and Hana, X. (2009) 'Roles of Wnt/ β -catenin signaling in epithelial differentiation of mesenchymal stem cells.' *Biochemical and Biophysical Research Communications*. **390** (4): 1309-1314.

Watson, D.S., Endsley, A.N and Huang, L. (2012) 'Design considerations for liposomal vaccines: Influence of formulation parameters on antibody and cell-mediated immune responses to liposome associated antigens.' *Vaccine*. **30** (13): 2256-2272.

Webb, K.S., Mickey, D.D., Stone, K.R and Paulson, D.F. (1977) 'Correlation of apparent molecular weight and antigenicity of viral proteins: An SDS-PAGE separation followed by acrylamide-agarose electro-phoresis and immunoprecipitation.' *Journal of Immunological Methods*. **14** (3-4): 343-353.

Welzel, P. (2002) 'Investigation of adsorption-induced structural changes of proteins at solid/liquid interfaces by differential scanning calorimetry.' *Thermochimica Acta*. **382** (1-2): 175-188.

Wen, H., Guo, J., Chang, B and Yang, W. (2012) 'pH-responsive composite microspheres based on magnetic mesoporous silica nanoparticle for drug delivery.' *European Journal of Pharmaceutics and Biopharmaceutics*. In press.

Weshe, J. (2009) 'Retrograde transport of ricin.' *International Journal of Medical Microbiology*. **291** (6-7): 517-522.

White, J. (1999) 'GFP: an illuminating tool. Green Fluorescent Proteins (Methods in Cell Biology, vol.58) edited by Kevin F. Sullivan and Steve A. Kay.' *Trends in Cell Biology*. **9** (10): 420.

White, J., Johannes, L., Mallard, F., Girod, A., Grill, S., Reinsch, S., Keller, P., Tzschaschel, B., Echard, A., Goud, B and Stelzer, E.H.K. (1999) 'Rab6 Coordinates a Novel Golgi to ER Retrograde Transport Pathway in Live Cells.' *Journal of Cell Biology*. **147** (4): 743-760.

Whitmore, L. and Wallace, B.A. (2008) 'Protein Secondary Structure Analyses from Circular Dichroism Spectroscopy: Methods and Reference Databases.' *Biopolymers*. **89**: 392-400.

Wilkhu, J., McNeil, S.E., Kirby, D and Perrie, Y. (2011) 'Formulation design considerations for oral vaccines.' *Therapeutic delivery*. **2** (9): 1141-1164.

Wishnia, A and Pinder, T.W. (1966) 'Hydrophobic Interactions in Proteins; The Alkane Binding Site of b-Lactoglobulins A and B.' *Biochemistry*.

Wittmann, J.G and Rudolph, M.G. (2004) 'Crystal structure of rab9 complexed to GDP reveals a dimmer with an active conformation of switch II.' *FEBS Letters*. **568** (1-3): 23-29.

Wolf, A.A., Fujinaga, Y and Lencer, W.I. (2002) 'Uncoupling of the Cholera Toxin GM1 Ganglioside Receptor Complex from Endocytosis, Retrograde Golgi Trafficking and Downstream Signal Transduction by Depletion of Membrane Cholesterol.' *The Journal of Biological Chemistry*. **277**: 16249-16256.

Wong, W and Minchin, R.F. (1996) 'Binding and internalisation of the melanocyte stimulating hormone receptor ligand [Nle4, d-Phe7] α -MSH in B16 melanoma cells.' *The International Journal of Biochemistry & Cell Biology*. **28** (11): 1223-1232.

Yamaguchi, T., Iwata, K., Kobayashi, M., Ogawa, M., Fukushi, H and Hirai, K. (1996) 'Epitope mapping of capsid proteins VP2 and VP3 of infectious bursal disease virus.' *Archives of Virology*. **141**: 1493-1507.

Yamashita, S., Furubayashi, T., Kataoka, M., Sakane, T., Sezaki, H and Tokuda, H. (2000) 'Optimized conditions for prediction of intestinal drug permeability using Caco-2 cells.' *European Journal of Pharmaceutical Sciences*. **10** (3): 195-204.

Yan, C., Rill, W. L., Malli, R., Hewetson, J., Naseem, H., Tammariello, R and Kende, M. (1996) 'Intranasal stimulation of long-lasting immunity against aerosol ricin challenge with ricin toxoid vaccine encapsulated in polymeric microspheres. *Vaccine* **14** (11): 1031-1038.

Yates, G. T and Smotzer, T. (2007) 'On the lag phase and initial decline of microbial growthcurves.' *Journal of Theoretical Biology*. **244** (3): 511-517.

Yip., C.W., Yeung, Y.S., Ma, C.M., Lam, P.Y., Han, C.C, Zeng, F and Leung, F.C.C. (2007) 'Demonstration of receptor binding properties of VP2 of very virulent strain infectious bursal disease virus on Vero cells.' *Virus Research*. **123** (1): 50-56.

Yoshino, N., Fujihashi, K., Hagiwara, Y., Kanno, H., Takahoshi, K., Kobayashi, R., Inaba, N., Noda, M and Sato, S. (2009) 'Co-administration of cholera toxin and apple polyphenol extract as a novel and safe mucosal adjuvant strategy.' *Vaccine*. **27** (35): 4808-4817.

Zahraoui, A., Joberty, G., Arpin, M., Fontaine, J.J., Hellis, R., Tavitian, A and Louvard, D. (1994) 'A small rab GTPase is distributed in cytoplasmic vesicles in non polarised cells but co-localises with the tight junction marker ZO-1 in polarised epithelial cells.' *The Journal of Cell Biology*. **124** (1): 101-115.

Zhang-Barber, L., Turner, A.K and Barrow, P.A. (1999) 'Vaccination for control of *Salmonella* in poultry.' *Vaccine*. **17** (20-21): 2538-2545.

Zhao, W., Wu, W and Xu, X. (2007) 'Oral vaccination with liposome-encapsulated recombinant fusion peptide of urease B epitope and cholera toxin B subunit affords prophylactic and therapeutic effects against *H. pylori* infection in BALB/c mice.' *Vaccine* **25** (44): 7664-7673.

Zhou, X., Wang, D., Xiong, J., Zhang, P., Li, Y and She, R. (2010) 'Protection of chickens, with or without maternal antibodies, against IBDV infection by a recombinant IBDV-VP2 protein.' *Vaccine*. 28 (23): 3990-3996.

Zierenberg, K., Raue, R., Nieper, H., Islam, M.R., Etteradossi, N., Toquin, D and Muler, H. (2004) 'Generation of serotype 1 / serotype 2 reassortment viruses of the infectious bursal disease virus and their investigation in vitro and in vivo.' *Virus Research*. **105** (1): 23-34.

Zwietering, M.H., Jongenburger, I., Rombouts, F.M and Riet, K. (1990) 'Modeling of the Bacterial Growth Curve.' *Applied Environmental Microbiology*. **56** (6): 1875-1881.